DISCOVERY OF CRYPTIC MICROBIAL NATURAL PRODUCTS USING INDUCTION STRATEGIES AND CHARACTERIZATION OF A NOVEL BIOTRANSFORMATION PRODUCT

A Thesis

Submitted to the Graduate Faculty

in Partial Fulfilment of the Requirements

for the Degree of Master of Science

Molecular and Macromolecular Sciences

Department of Chemistry

Faculty of Science

University of Prince Edward Island

Amanda T. Sproule

Charlottetown, Prince Edward Island

December 2016

ABSTRACT

Human health has benefitted from the use of natural products since the beginning of traditional medicine. Today, the majority of approved drugs have some connection to nature whether they are genuine natural products, derivatives thereof, or synthetic compounds whose structures were inspired by these secondary metabolites. Microorganisms, particularly actinomycetes, represent an important source of bioactive natural products; they are the original source of about two-thirds of all clinically used antibiotics as well as drugs used to treat cancer, parasitic infections and other ailments.

Culturing actinomycetes under the standard conditions of the laboratory typically does not facilitate the production of all of the natural products that these organisms are genetically capable of biosynthesizing. As a result, the discovery of novel microbial natural products has diminished in recent years as the easily obtained compounds are repeatedly rediscovered. Strategies to induce the production of the unexpressed, or cryptic, natural products are therefore an important tool for natural product discovery programs, especially during present times when new antibiotics are desperately needed.

One strategy that has been used successfully many times in the past is the one strain-many compounds approach. This technique involves the systematic variation of culture conditions in order to find a set that induces production of new, cryptic natural products. Three actinomycetes, *Kitasatospora cystarginea* NRRL B-16505, *Kitasatospora griseola* NRRL B-16229 and the Prince Edward Island sediment derived strain *Streptomyces* sp. RKND004 were subjected to fermentation in 14 different media. Data analysis using LC-HRMS based metabolomics led to the discovery of terrosamycin A and B, two polyether ionophores that were selectively produced by *Streptomyces* sp. RKND004 in specific liquid media. The terrosamycins exhibited excellent antibiotic and selective anticancer properties. In addition to these compounds, this approach highlighted a number of other putatively novel, induced metabolites which are awaiting discovery.

Another strategy, co-culture, involves fermentation of two or more organisms in the same vessel in order to imitate an ecological situation and in turn, stimulate cryptic natural product production. Co-culture experiments have a lot of variables and are often difficult to reproduce. For this reason, the Kerr lab has established a more straightforward procedure called co-culture mimic in which an organism is cultured with a sterilized culture of another ecologically relevant organism. The three previously mentioned actinomycetes were subjected to ten different co-culture mimic conditions and their resulting secondary metabolism was analyzed using a similar method. Again, a list of putatively novel induced and upregulated compounds was generated for future discovery efforts.

Lastly, the co-culture mimic experiments of another Kerr lab student highlighted the production of a putatively novel compound. Subsequent collaborative scale-up efforts followed by purification and structure elucidation revealed it was a novel biotransformation product which was named PQS-GlcA. The discovery of this compound unveiled a new anti-quorum sensing mechanism which may find a useful application in the development of new therapeutics targeting bacterial infections in humans.

ACKNOWLEDGEMENTS

There are a number of people to whom I am extremely grateful for their support throughout my time as a graduate student at the University of Prince Edward Island. First, I would like to thank my supervisor Dr. Russell Kerr for the opportunity to dive in (literally!) into the world of natural products. I am so very thankful for the useful skills and unique experiences I have gained while working in your lab. Thank you also to the lab managers and senior scientists, both past and present, for their contributions and helpful advice throughout the completion of this research. Dr. Fabrice Berrué, thank you for your interest in my projects and for ensuring that I learn as much chemistry as possible during my time here. Your continued support, even from a distance, means a lot. Bradley Haltli, thank you for all of your interesting ideas, enthusiasm for my research and for all of your help learning microbiology. I am grateful to have learned many new skills from you. To Dr. Dave Overy, Dr. Hebelin Correa, Dr. Andrew Robertson and Dr. Doug Marchbank, thank you so much for always being available to offer your valued expertise.

I would like to acknowledge my supervisory committee, Dr. Russell Kerr, Dr. Fabrice Berrué and Dr. Barry Linkletter for their guidance and helpful suggestions during the completion of my research. I am also extremely grateful for financial support through scholarships and awards made available by the Department of Chemistry, the Office of Graduate Studies and the Natural Sciences and Engineering Research Council of Canada.

I am fortunate to have had the opportunity to work with many talented scientists who have contributed greatly to the research presented in this thesis. Thank you to Patricia Boland and Dr. Hebelin Correa who acquired LC-HRMS data, and to Maike Fischer who acquired NMR data. Thank you to Martin Lanteigne for performing the antimicrobial assays and Kate McQuillan for performing the cytotoxicity assays. Thank you to Dr. Andreas Decken who acquired X-ray diffraction data and performed structure refinement of terrosamycin A. Andreas, I am so very appreciative of your help with the crystal data; thank you for answering my many questions so quickly and for involving me in the process. Libang (Leon) Liang, thank you for collaborating with me for the discovery of PQS-GlcA. Hebelin, I cannot thank you enough for your help with purification and structure elucidation. Your assistance and friendship means a lot to me. Thank you also to Josh, Noelle and Nick for your training and help in the lab.

I am grateful to all of the Kerr lab graduate students and other friends who have made these past years so enjoyable both inside and outside the lab. A special thank you goes to my officemate Dr. Krista Gill; your mentorship and friendship has been invaluable. Catherine, I would not have made it through this degree without you and our adventures! To my Ontario friends (Tor, Meg, Sam) and family, thanks for making the journey to PEI to visit me! I am lucky to have people like you in my life.

Finally, thank you to my crazy family for your endless support and for encouraging me to follow my dreams even though they took me so far away from home. Mom, Marcus, Kaitlyn, Caelan and Kaycie – you have shaped me into the person I am today and I could not be happier. Mama and Papa, you have shown me such selflessness and love and I will be forever grateful for all that you have done for me. Kyle, thank you for your love, encouragement and never ending laughter. I love you all!

Dedication

For my family,

and for Nicole

TABLE OF CONTENTS

ABSTRACT ii
ACKNOWLEDGEMENTS iii
Dedication iv
TABLE OF CONTENTS v
LIST OF FIGURES viii
LIST OF TABLES x
LIST OF ABBREVIATIONS xi
CHAPTER 1 - INTRODUCTION 1
1.1. NATURAL PRODUCTS 2
1.1.1. What is a natural product? 2
1.1.2. Sources and ecological functions of natural products 10
1.1.3. Applications of natural products 14
1.1.4. Current challenges in natural product discovery 18
1.2. MICROBIAL NATURAL PRODUCTS 21
1.2.1. Benefits of using microbes as a source of natural products 21
1.2.2. Actinomycetes as a source of bioactive natural products 23
1.2.3. Polyether ionophore natural products 24
1.2.4. The role of natural products and their biotransformations in quorum sensing 32
1.3. CRYPTIC NATURAL PRODUCTS 36
1.3.1. Cryptic natural products and their importance 36
1.3.2. Traditional methods to access cryptic natural products 38
1.3.3. Co-culture methods to access cryptic natural products 41
1.4. RESEARCH GOALS 47
1.4.1. Examine the effect of varying culture media of natural product production 47
1.4.2. Examine the effect of co-culture mimic conditions of natural product production 48
1.4.3. Purify and characterize putatively new compounds from induction experiments 48
CHAPTER 2 - RESULTS AND DISCUSSION 49
2.1. THE EFFECTS OF VARYING CULTURE MEDIA ON NATURAL PRODUCT PRODUCTION AND THE DISCOVERY OF TERROSAMYCIN A AND B 50
2.1.1. Introduction 50
2.1.2. Identification of *Streptomyces* sp. RKND004 50

2.1.3. Small-scale fermentations and extractions 51
2.1.4. Data analysis and prioritization of target compounds 56
2.1.5. Large-scale fermentation and purification of terrosamycin A and B 69
2.1.6. Crystallization of terrosamycin A and analysis of X-ray diffraction data..... 69
2.1.7. Spectroscopic structure elucidation of terrosamycin A and B 75
2.1.8. Bioactivity of terrosamycin A and B 86
2.2. THE EFFECTS OF CO-CULTURE MIMIC CONDITIONS ON NATURAL PRODUCT PRODUCTION 96
2.2.1. Introduction 96
2.2.2. Preparation of stressors..... 97
2.2.3. Small-scale fermentations and extractions 100
2.2.4. Data analysis and identification of upregulated and induced compounds..... 103
2.3. PURIFICATION AND STRUCTURE ELUCIDATION OF PQS-GLCA, A NOVEL BIOTRANSFORMATION PRODUCT 113
2.3.1. Introduction 113
2.3.2. Multi-scale fermentations and extractions of *Streptomyces* sp. RKBH-B178 115
2.3.3. Large-scale fermentations and purification of PQS-GlcA and bhimamycin A and E 117
2.3.4. Structural characterization and stereochemical determination of PQS-GlcA 117
2.3.5. Bioactivity of PQS-GlcA..... 122
CHAPTER 3 - CONCLUSIONS 127
3.1. THE EFFECTS OF VARYING CULTURE MEDIA ON NATURAL PRODUCT PRODUCTION 128
3.2. THE EFFECTS OF CO-CULTURE MIMIC CONDITIONS ON NATURAL PRODUCT PRODUCTION 129
3.3. PURIFICATION AND STRUCTURE ELUCIDATION OF PUTATIVELY NEW COMPOUNDS FROM INDUCTION EXPERIMENTS..... 130
3.4. CONCLUDING REMARKS AND FUTURE DIRECTIONS 131
CHAPTER 4 - EXPERIMENTAL 133
4.1. GENERAL EXPERIMENTAL PROCEDURES 134
4.1.1. Origins and maintenance of bacteria and stressor organisms..... 134
4.1.2. Preparation of liquid media 135
4.1.3. LC-MS sample preparation and analysis..... 136
4.1.4. Characterization of target compounds..... 136

4.2. THE EFFECTS OF VARYING CULTURE MEDIA ON NATURAL PRODUCT PRODUCTION AND THE DISCOVERY OF TERROSAMYCIN A AND B 137
4.2.1. Identification of *Streptomyces* sp. RKND004 137
4.2.2. Small-scale fermentations and extractions 138
4.2.3. Data analysis and identification of target compounds 139
4.2.4. Large-scale fermentations and purification of terrosamycin A and B 140
4.2.5. Crystallization of terrosamycin A and analysis of X-ray diffraction data 141
4.2.6. Bioactivity of terrosamycin A and B 142
4.3. THE EFFECTS OF CO-CULTURE MIMIC CONDITIONS ON NATURAL PRODUCT PRODUCTION 145
4.3.1. Preparation of stressors 145
4.3.2. Small-scale fermentations and extractions 146
4.3.3. Data analysis and identification of upregulated and induced compounds 147
4.4. PURIFICATION AND STRUCTURE ELUDICATION OF PQS-GLCA 148
4.4.1. Multi-scale fermentations and extractions 148
4.4.2. Large-scale fermentations and purification of PQS-GlcA 149
4.4.3. Stereochemical determination of PQS-GlcA by Tanaka's method 150
REFERENCES 152
APPENDIX 167
6.1. Supporting information for the characterization of terrosamycin A and B 167
6.2. Supporting information for the characterization of PQS-GlcA 182
6.3. Supporting information for the characterization of bhimamycin A and E 188

LIST OF FIGURES

Figure 1.1. Biosynthetic precursors and examples of terpene natural products 4
Figure 1.2. Amino acid building blocks and examples of alkaloid natural products.....5
Figure 1.3. Starter and extender units and examples of polyketide natural products 8
Figure 1.4. Examples of well known non-ribosomal peptide antibiotics 9
Figure 1.5. Biotransformation of a toxic plant alkaloid by *Idea leuconoe* 12
Figure 1.6. The discovery of the avermectins and artemisinin 15
Figure 1.7. Category of origin of small-molecule approved drugs between 1981-2014 ...17
Figure 1.8. Timeline of discovery of new antibiotics and the current discovery void 19
Figure 1.9. Examples of polycyclic polyether antibiotics and their crystal structures 26
Figure 1.10. The three mechanisms of ion transfer by polyether ionophores.....29
Figure 1.11. Quorum sensing in Gram-negative bacteria 34
Figure 1.12. Examples of compounds discovered using the OSMAC approach.....40
Figure 1.13. Schematic of the co-culture "mimic" approach.....46
Figure 2.1. Chemical barcodes for *K. cystarginea*, *K. griseola* and *Streptomyces* sp. RKND004 58
Figure 2.2. The *K. griseola* barcode highlighting induced metabolites *m/z* 542.3230 $[M+H]^+$ and *m/z* 556.3386 $[M+H]^+$ 60
Figure 2.3. The *Streptomyces* sp. RKND004 barcode highlighting a family of induced metabolites 62
Figure 2.4. Total ion chromatogram and HRMS spectrum of the crude extract of *Streptomyces* sp. RKND004 grown in BFM7.....63
Figure 2.5. Ion intensity plot comparing the peak area of *m/z* 835.5186 $[M+Na]^+$ in each fermentation medium screened 65
Figure 2.6. Crystal structure and molecular structure showing stereochemistry of the terrosamycin A potassium salt 71
Figure 2.7. Crystal structure of terrosamycin A showing coordination and hydrogen bonds 73
Figure 2.8. Key COSY and HMBC correlations used to determine the molecular structure of terrosamycin A and B 82
Figure 2.9. Proposed mechanism for the acid-catalyzed conversion of terrosamycin B to terrosamycin A 84
Figure 2.10. Space-filling model of the crystal structure of terrosamycin A 88
Figure 2.11. Molecular structures of salinomycin, nigericin, monensin and the monensin methyl ester 91
Figure 2.12. Photograph of *C. elegans* growing on an agar plate.....99
Figure 2.13. Scatter plot showing changes in the secondary metabolome of *K. cystarginea* in response to the 10% *A. flavus* stressor 105
Figure 2.14. Example of an upregulated metabolite from co-culture mimic experiments107
Figure 2.15. Example of an induced metabolite from co-culture mimic experiments 108
Figure 2.16. Ion intensity plot comparing the peak area of PQS-GlcA in multiple scale fermentations of *Streptomyces* sp. RKBH-B178 supplemented with HHQ 116
Figure 2.17. Molecular structure of HHQ and PQS and key COSY and HMBC correlations used to determine the structure of PQS-GlcA.....121
Figure 2.18. PQS quorum sensing deactivation mechanisms 125

Figure 6.1. Extracted ion chromatograms depicting the production of terrosamycin A in certain fermentation media 167
Figure 6.2. Chromatograms of the crude extract of a large scale fermentation of *Streptomyces* sp. RKND004 in BFM3 168
Figure 6.3. +ESI-HRMS and –ESI-HRMS spectra of terrosamycin A 169
Figure 6.4. +ESI-HRMS and –ESI-HRMS spectra of terrosamycin B 170
Figure 6.5. ^{1}H NMR spectrum of terrosamycin A 175
Figure 6.6. ^{13}C NMR spectrum of terrosamycin A 175
Figure 6.7. COSY spectrum of terrosamycin A 176
Figure 6.8. HSQC spectrum of terrosamycin A 176
Figure 6.9. HMBC spectrum of terrosamycin A 177
Figure 6.10. IR spectrum of terrosamycin A 177
Figure 6.11. ^{1}H NMR spectrum of terrosamycin B 178
Figure 6.12. ^{13}C NMR spectrum of terrosamycin B 178
Figure 6.13. COSY spectrum of terrosamycin B 179
Figure 6.14. HSQC spectrum of terrosamycin B 179
Figure 6.15. HMBC spectrum of terrosamycin B 180
Figure 6.16. IR spectrum of terrosamycin B 180
Figure 6.17. Chromatograms and –ESI-MS spectrum of the crude extract of *Streptomyces* sp. RKND004 resuspended in acetonitrile 181
Figure 6.18. Chromatograms of the crude extract of Streptomyces sp. RKBH-B178 grown in ISP2 supplemented with HHQ 182
Figure 6.19. +ESI-HRMS spectrum of PQS-GlcA 183
Figure 6.20. MS^2 spectrum of PQS-GlcA 183
Figure 6.21. ^{1}H NMR spectrum (600 MHz, MeOD-d_4) of PQS-GlcA 184
Figure 6.22. ^{13}C NMR spectrum of PQS-GlcA 184
Figure 6.23. COSY spectrum of PQS-GlcA 185
Figure 6.24. HSQC spectrum of PQS-GlcA 185
Figure 6.25. HMBC spectrum of PQS-GlcA 186
Figure 6.26. ^{1}H NMR spectrum (600 MHz, DMSO-d_6) of PQS-GlcA 186
Figure 6.27. IR spectrum of PQS-GlcA 187
Figure 6.28. Chromatograms of the Tanaka reaction products to determine the configuration of the sugar moiety of PQS-GlcA 187
Figure 6.29. +ESI-HRMS spectrum of bhimamycin A 188
Figure 6.30. +ESI-HRMS spectrum of bhimamycin E 188
Figure 6.31. ^{1}H NMR spectrum of bhimamycin A 189
Figure 6.32. ^{13}C NMR spectrum of bhimamycin A 189
Figure 6.33. COSY spectrum of bhimamycin A 190
Figure 6.34. HSQC spectrum of bhimamycin A 190
Figure 6.35. HMBC spectrum of bhimamycin A 191
Figure 6.36. ^{1}H NMR spectrum of bhimamycin E 191
Figure 6.37. ^{13}C NMR spectrum of bhimamycin E 192
Figure 6.38. COSY spectrum of bhimamycin E 192
Figure 6.39. HSQC spectrum of bhimamycin E 193
Figure 6.40. HMBC spectrum of bhimamycin E 193

LIST OF TABLES

Table 1.1. Metabolites isolated from microorganism co-cultures 42
Table 2.1. Recipes for media used in OSMAC experiments 53
Table 2.2. Putatively new, induced metabolites discovered by OSMAC experiments 68
Table 2.3. ^{1}H and ^{13}C NMR data for terrosamycin A and B 77
Table 2.4. IC_{50} values for terrosamycin A and B and polyether standards against three Gram-positive pathogens 92
Table 2.5. IC_{50} values for terrosamycin A and B and polyether standards against two cancerous and two healthy cell lines.....95
Table 2.6. A summary of the ten co-culture mimic stress conditions used 102
Table 2.7. Upregulated and induced metabolites found by co-culture mimic studies.....110
Table 2.8. ^{1}H and ^{13}C NMR data for PQS-GlcA 119
Table 6.1. Crystal data and structure refinement for terrosamycin A.....171
Table 6.2. Coordination bond lengths and angles for terrosamycin A 173
Table 6.3. Hydrogen bond lengths and angles for terrosamycin A 174

LIST OF ABBREVIATIONS

Å	angstrom(s)
ACN	acetonitrile
AI	autoinducer
BFM	bacterial fermentation medium
BHI	brain-heart infusion
BLAST	Basic Local Alignment Search Tool
bp	base pair(s)
BSM	bacterial seed medium
C_{18}	octadecylsilane
CID	collision-induced dissociation
CO_2	carbon dioxide
COSY	correlation spectroscopy
CSC	cancer stem cell
Da	dalton(s)
diH_2O	deionized water
DMAP	dimethyl allyl diphosphate
DMSO	dimethyl sulfoxide
DMSO-d_6	deuterated dimethyl sulfoxide
DNA	deoxyribonucleid acid
EC_{50}	half-maximal effective concentration
ELSD	evaporative light scattering detector
ESI-HRMS	electrospray ionization mass spectrometry
EtOAc	ethyl acetate
FTIR	Fourier transform infrared spectrometry
GlcA	glucuronic acid
h	hour(s)
HCl	hydrochloric acid
HHQ	2-heptyl-4-quinolone
HIV	human immunodeficiency virus
HMBC	heteronuclear multiple bond correlation
HPLC	high performance liquid chromatography
HRESIMS	high-resolution electrospray ionization mass spectrometry
HSQC	heteronuclear single quantum coherence
IC_{50}	half-maximal inhibitory concentration
IPP	isopentenyl diphosphate
ISP	International Streptomyces Project medium
J	coupling constant
K	potassium
KOH	potassium hydroxide
LB	lysogeny broth
LC-HRMS	liquid chromatography high-resolution mass spectrometry
LC-MS	liquid chromatography mass spectrometry
LT-ELSD	low temperature evaporative light scattering detector

m/z	mass-to-charge ratio
MeOD-d_4	deuterated methanol
MeOH	methanol
min	minute(s)
MRSA	methicillin resistant *Staphylococcus aureus*
MS	mass spectrometry
Na	sodium
NaOH	sodium hydroxide
NCBI	National Center for Biotechnology Information
NGM	nematode growth medium
NMR	nuclear magnetic resonance
NRPS	non-ribosomal peptide synthetase
OSMAC	one strain-many compounds
PCR	polymerase chain reaction
PDA	photodiode array
PKS	polyketide synthase
ppm	parts per million
PQS	*Pseudomonas* quinolone signal
RP-HPLC	reversed phase high performance liquid chromatography
rpm	revolutions per minute
rpoB	beta subunit of RNA polymerase
rRNA	ribosomal ribonucleic acid
rt	room temperature
s	second(s)
THF	tetrahydrofuran
TIC	total ion chromatogram
t_R	retention time
TSA	trypticase soy agar
UHPLC-HRMS	ultra high performance liquid chromatography high-resolution mass spectrometry
UV	ultraviolet
v	volume
VRE	vancomycin resistant *Enterococci*
XIC	extracted ion chromatogram
XRD	X-ray diffraction

CHAPTER 1

INTRODUCTION

1.1. NATURAL PRODUCTS

1.1.1. What is a natural product?

Molecules that are produced by living organisms which are not required for the sustenance of life can be referred to as secondary metabolites, or natural products [1]. The relatively small compounds (> 3000 Da) are produced from primary metabolites by a broad range of living species from unicellular microorganisms to plants, insects and even mammals. Though at first the reasons for the production of these compounds were unclear, it is now understood that the biosynthesis of natural products affords an ecological and thus evolutionary advantage to the organism [2]. These compounds possess diverse and intricate structures; this structural complexity has inherently resulted in a vast scope of biological activities which have a plethora of applications. Based on their structural features arising from distinct biosynthetic origins, natural products can be sorted into four main classes.

Terpenoids represent the largest class of natural products. Their biosynthesis can begin from two separate pathways; the mevalonate pathway and the desoxyxylulose phosphate pathway [3]. Both pathways produce the activated five-carbon isoprene units dimethylallyl diphosphate (DMAP) and isopentenyl diphosphate (IPP). These units can link together to form longer chains and subsequently undergo cyclizations, rearrangements and other modifications such as oxidations or glycosylations. Depending on the number of isoprene units they contain, terpenes may be further classified as hemiterpenes (one unit, C_5), monoterpenes (two units, C_{10}), sesquiterpenes (three units, C_{15}), diterpenes (four units, C_{20}), sesterterpenes (five units, C_{25}), triterpenes (six units, C_{30}) or tetraterpenes (eight units, C_{40}). Some examples of terpenoids include the

monoterpene limonene, the sesquiterpene parthenolide, and the diterpene pseudopterosin (Figure 1.1).

Alkaloids, another large class of natural products, are typically nitrogen-containing heterocyclic compounds derived from amino acids. Despite being derived from amino acids, these metabolites are not peptides. Within this class there are many subgroups that are used to further describe the thousands of compounds labeled as alkaloids. Some examples include benzylisoquinone alkaloids including the analgesic drugs morphine and codeine produced from two equivalents of tyrosine [4]. Quinolizidine alkaloids originate from lysine and include the natural product lupinine, produced as a chemical defense mechanism in the lupin plant [5]. The illegal drug cocaine is a tropane alkaloid which, like all tropane alkaloids, contains the bicyclic tropane ring that can be formed from ornithine and arginine [6]. The most common amino acid building blocks and structures of these compounds are shown in Figure 1.2.

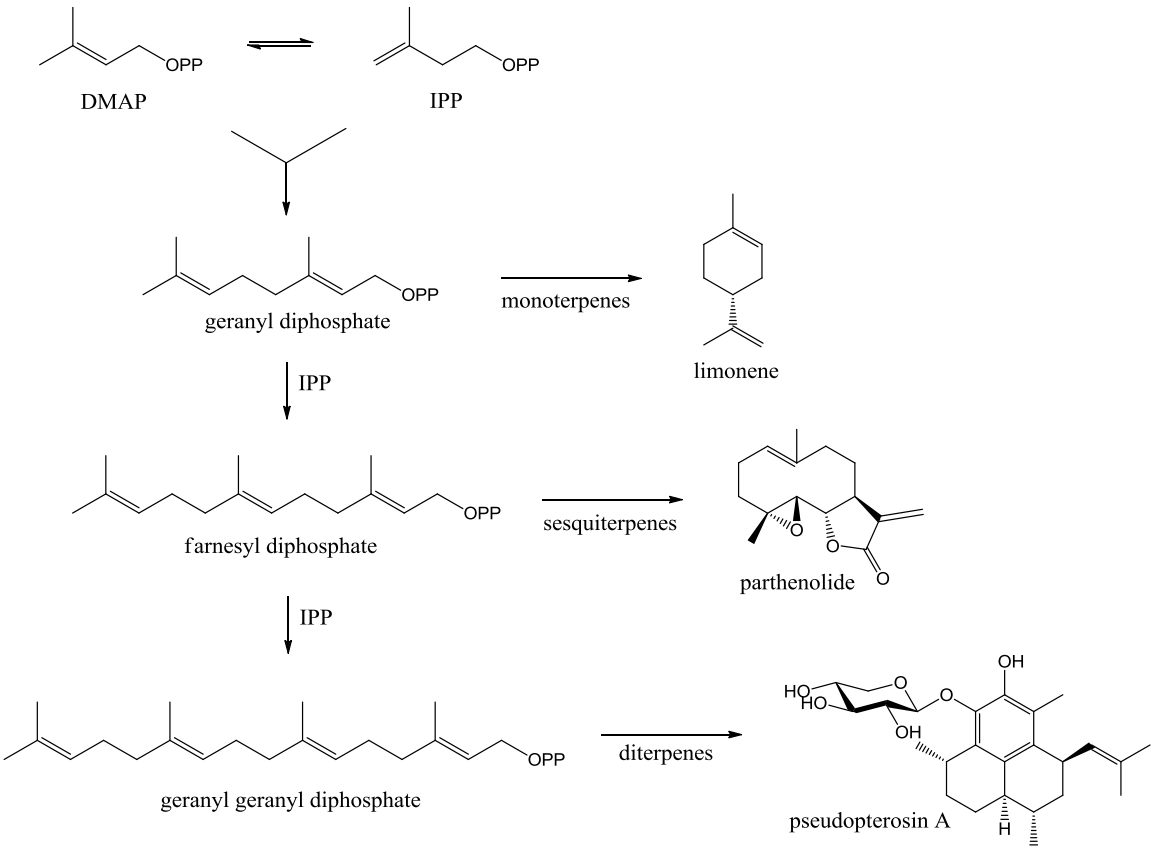

Figure 1.1. Precursors for the biosynthesis of monoterpenes, sesquiterpenes and diterpenes and examples of each illustrating structural diversity within this class.

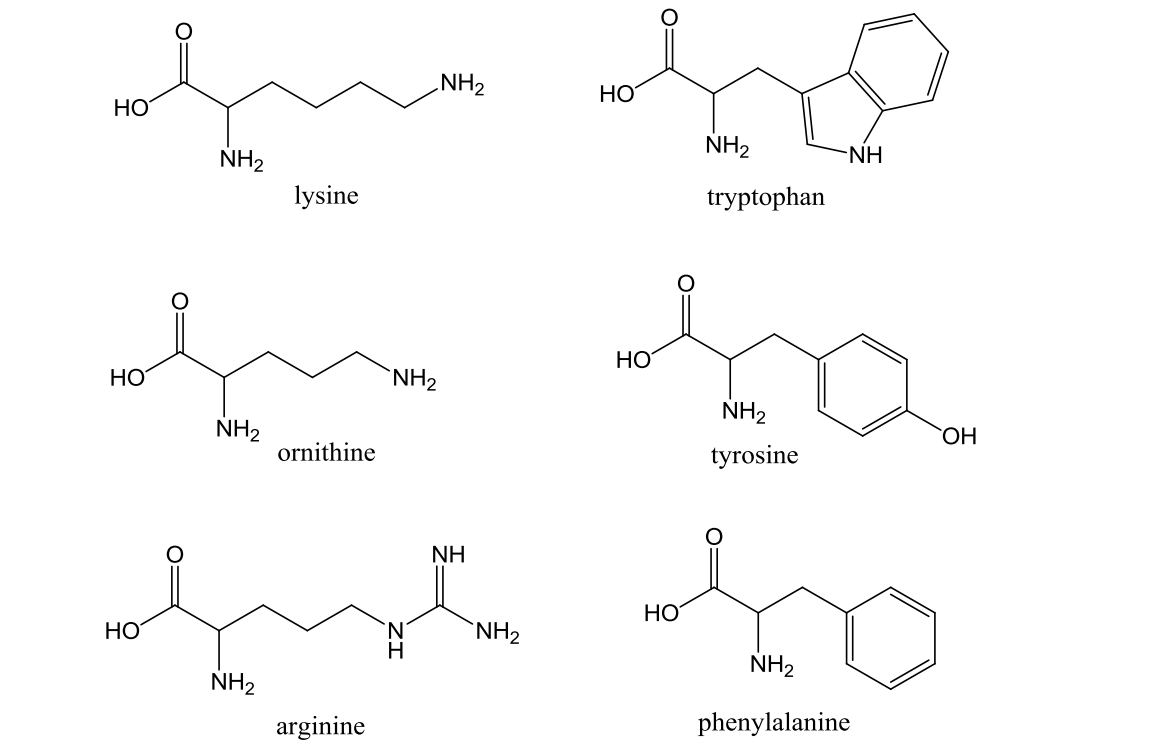

benzylisoquinone alkaloids

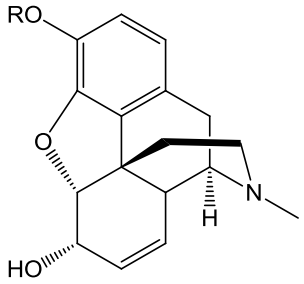

morphine (R = H)
codeine (R = CH_3)

quinolizidine alkaloids

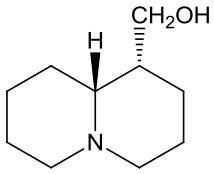

lupinine

tropane alkaolids

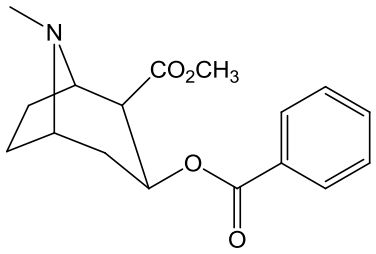

cocaine

Figure 1.2. The most common amino acid building blocks used in alkaloid biosynthesis and examples of structures belonging to the benzoisoquinone, quinolizidine and tropane subgroups.

Polyketides, which include the cholesterol lowering agent lovastatin and the antibiotics tetracycline and erythromycin (Figure 1.3), are produced via multifunctional enzymes called polyketide synthases (PKSs). Their chemical structures can be extremely diverse despite mostly containing repeating units of malonate or methylmalonate which are used as building blocks to create a long polyketide chain. The use of different starter units such as para-aminobenzoic acid or β-alanine can also contribute to structural diversity. Though they are biosynthesized through very similar pathways, the retention of oxygen-containing functionalities is what sets polyketides apart from fatty acids. There are currently three known types of PKSs. Type I PKSs contain several modules, each with its own set of protein domains which are used to complete one round of polyketide chain elongation [7]. Type II PKSs contain multiple enzymes in a large complex that harbour one set of domains which are used iteratively to lengthen the chain [8]. Type III PKSs are homodimeric and work in an iterative fashion, independent of the acyl carrier protein that is used to activate substrates in type I and II PKSs [8]. Once the polyketide chain is released from the PKS, additional structural features may arise via post-PKS tailoring steps that utilize enzymes such as oxygenases, methyltransferases, aminotransferases, glycosyltransferases and so on [9].

Finally, non-ribosomal peptides are composed of amino acids connected by peptide linkages. In contrast to proteins, non-ribosomal peptides are relatively small and are not produced using the ribosome but rather using non-ribosomal peptide synthetases (NRPSs). Like in polyketide biosynthesis, there are three types of NRPSs that act similarly to the three types of PKSs [10]. In addition to the proteinogenic amino acid building blocks used by NRPSs to produce the final natural product, non-ribosomal

peptides often contain non-proteinogenic amino acids. Tailoring steps can occur to add structural features such as sugars, hydroxyl groups and methyl groups [11]. Interestingly, there are some natural products that contain both polyketide and non-ribosomal peptide moieties. Examples of well known non-ribosomal peptides include penicillin, gramicidin and vancomycin (Figure 1.4).

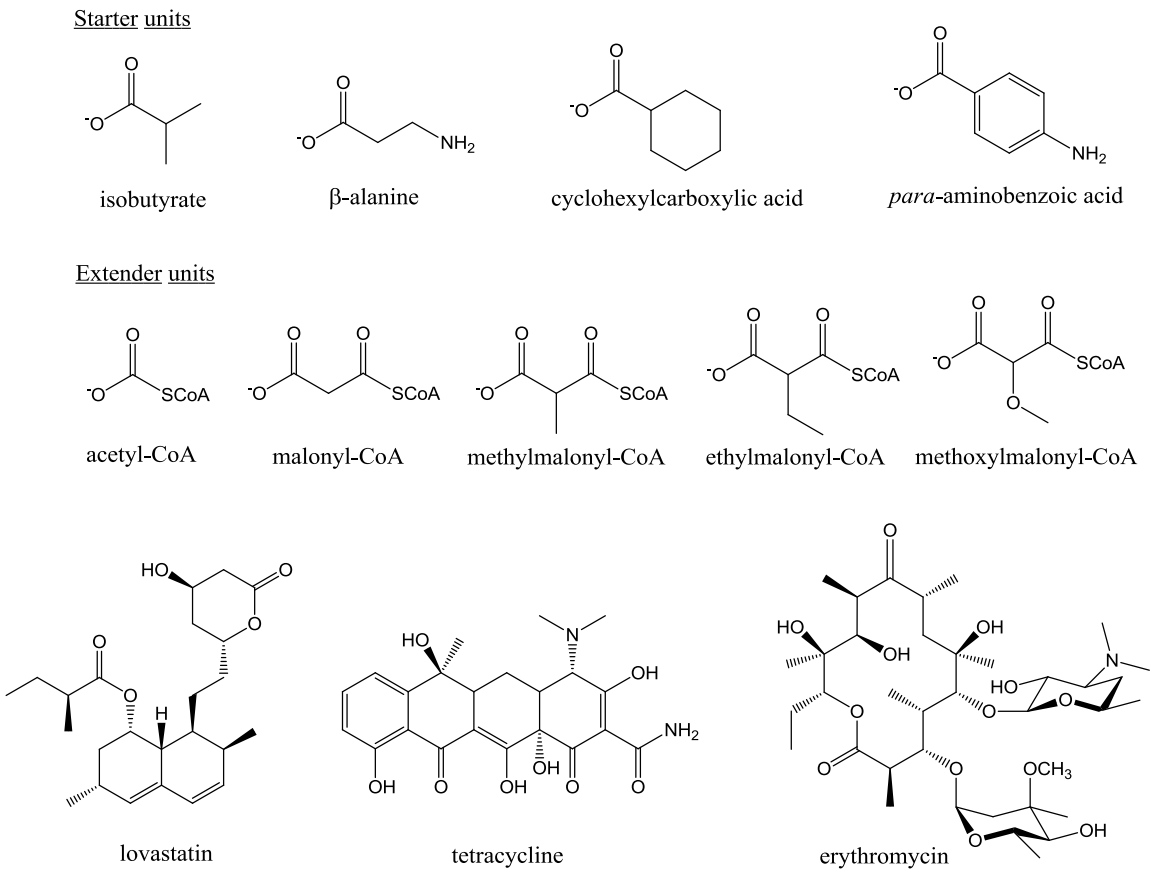

Figure 1.3. Examples of starter units and extender units commonly used in polyketide biosynthesis and the structures of three well known polyketide antibiotics.

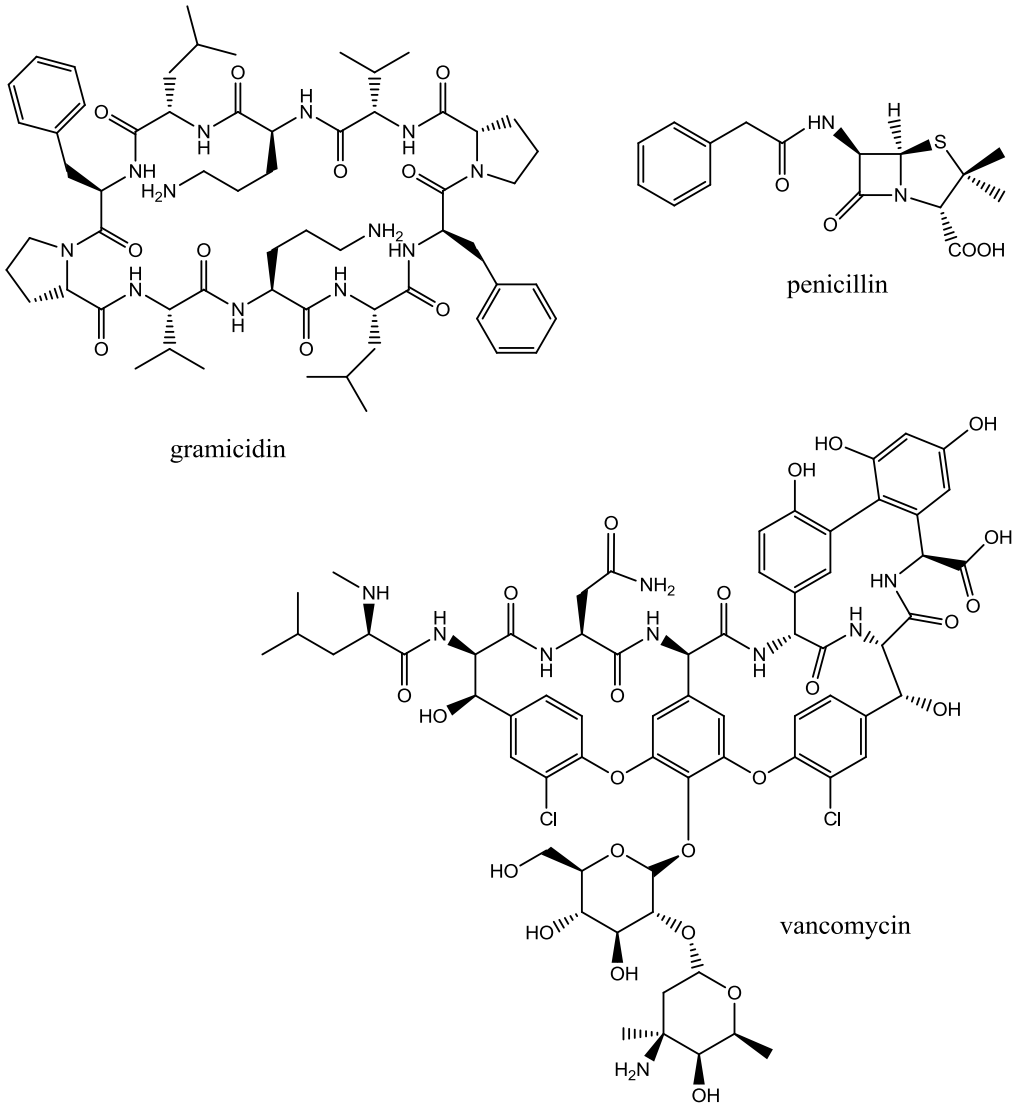

Figure 1.4. Three well known non-ribosomal peptide antibiotics showing structural diversity within this class of natural products.

1.1.2. Sources and ecological functions of natural products

Organisms from all six kingdoms of life are able to produce natural products. The structures of natural products are often complex and are energetically expensive for the producing organism to biosynthesize. For this reason, it was hypothesized that natural products must provide some sort of advantage to the producer, rather than simply being a waste product or a nonfunctional byproduct [1]. With the rise of the field of chemical ecology, the specific functions of some secondary metabolites have become apparent [12]. Organisms that lack an immune system or some kind of physical protection are often found to produce compounds that provide a chemical defense mechanism [12, 13]. There are also examples of natural products used by predatory species [14]. Furthermore, many natural products are used as intra- and interspecies chemical signals or as scavengers which can supply the producer with vital nutrients in an environment that is nutritionally deficient [15]. Despite what is currently understood about the reasons some of these compounds are biosynthesized, the ecological roles of many natural products remain unknown.

Many of the natural products known today come from plants. These compounds are often produced to defend the plant against herbivores, insects and microbial pathogens. Mentioned earlier, quinolizidines such as lupinine have a bitter taste which makes the lupin plant less desirable for consumption by herbivores than sweet lupins bred to be alkaloid-free [5]. The pepper family (Piperaceae) can produce dihydropiperine which is acutely toxic to insects that feed on the plant [16]. The cyclic triterpine ursolic acid is found in the plant *Mirabilis jalapa* as well as many herbs and fruits such as apples and cranberries. It was found to inhibit plant-associated biofilm formation of both Gram-

positive and Gram-negative bacteria [17]. As a final example, the daisy family (Asteraceae) can produce more than 750 natural products, the majority of which exhibit phototoxicity effects toward both insects and fungal pathogens [16]. Some insects have adapted to toxic metabolites and have found ways to utilize them in their own life cycles. The giant butterfly *Idea leuconoe* acquires a plant alkaloid while it feeds on leaves in its larval stage; once in its adult stage the male performs a biotransformation of this compound to produce sex pheromones that attract females (Figure 1.5) [18]. In addition to using these compounds in their own defense, natural products are also produced by plants to attract pollinators facilitating their reproduction [18]. The role of natural products in the world of plant chemical ecology is instrumental and extends far beyond these few examples.

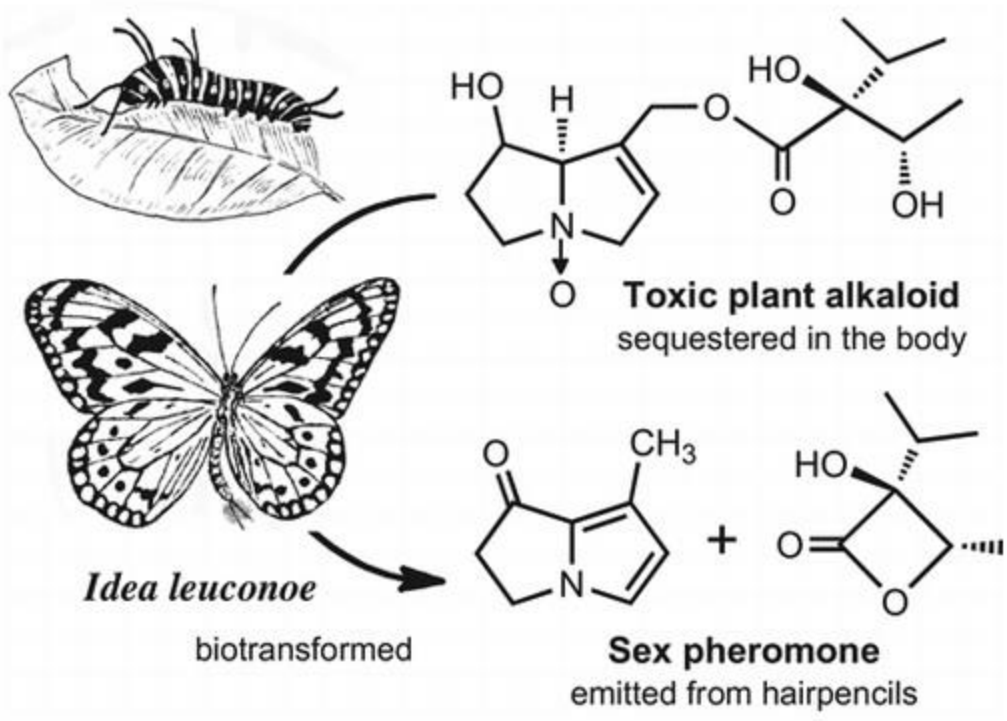

Figure 1.5. An example illustrating the vast chemical ecology of plant-derived natural products. A toxic alkaloid produced by a plant is accumulated in the body of a male butterfly in its larval stage. The male performs a biotransformation and utilizes the resulting compounds as sex pheromones to attract females. Figure created by R. Nishidia, 2014 [18].

Natural products are also produced in other terrestrial organisms. Many species, insects in particular, use their own secondary metabolites as pheromones to communicate with their colonies or alarm them of danger [19]. Reptiles such as lizards and snakes, and even mammals such as shrews and the duckbilled platypus produce venoms which help them hunt prey [20]. In the marine environment, the slow-moving cone snail hunts fish with the help of a paralyzing neurotoxin [14]. Similar to plants, sessile sponges and corals and other invertebrates in the marine environment that lack physical protection from predators are known to produce many defensive compounds. Natural products have also been isolated from larger marine animals such as squalamine which comes from the dogfish shark [21].

Ubiquitous in the environment, microorganisms have been an important source of natural products since the discovery of penicillin by Alexander Fleming [22]. Many microbes can secrete antibiotic or antifungal compounds in order to protect themselves against surrounding pathogenic microorganisms and compete for space and resources [23, 24]. The relatively new concept of quorum sensing, a regulatory system used by bacteria to communicate with themselves and their microbial neighbours involves production of natural products used as autoinducers and interspecies chemical signals [25]. Microorganisms (and plants) can also produce antifouling compounds that can inhibit the formation of microbial biofilms or attachment of plants or animals to the surface of the producer [26]. Interestingly, some natural products that were assumed to originate from a plant or animal source have turned out to be biosynthesized by a fungal or bacterial symbiont [27, 28].

1.1.3. Applications of natural products

Natural products have been used to benefit human health since the beginning of traditional medicine. Some of the earliest records describe the use of the oils from many plant species to treat a variety of ailments from a simple cold to parasitic infections and inflammation [29]. Fast forward to modern medicine and natural products remain an invaluable source of new drugs, as technology has allowed us to look at natural sources of healing at the molecular level. In 2015, the Nobel Prize in Physiology or Medicine was awarded to the discoverers of the avermectins and artemisinin. The avermectins were purified from cultures of the soil-dwelling bacterium *Streptomyces avermitilis*. A small chemical modification produced ivermectin which has nearly eradicated river blindness and elephantitis, two diseases caused by parasitic worms (Figure 1.6 **A**) [30]. The exploitation of ancient Chinese medicine for novel anti-malarial therapies led to the discovery of artemisinin from the medicinal plant *Artemisia annua* which has saved hundreds of thousands of lives in malaria infected parts of the world (Figure 1.6 **B**) [30]. These are only two examples; the structural complexity and diversity of natural products give rise to a great deal of biological activity which can be used to treat a range of other health issues including but not limited to bacterial and fungal infections, Alzheimer's disease, cardiovascular disease and many types of cancer [31].

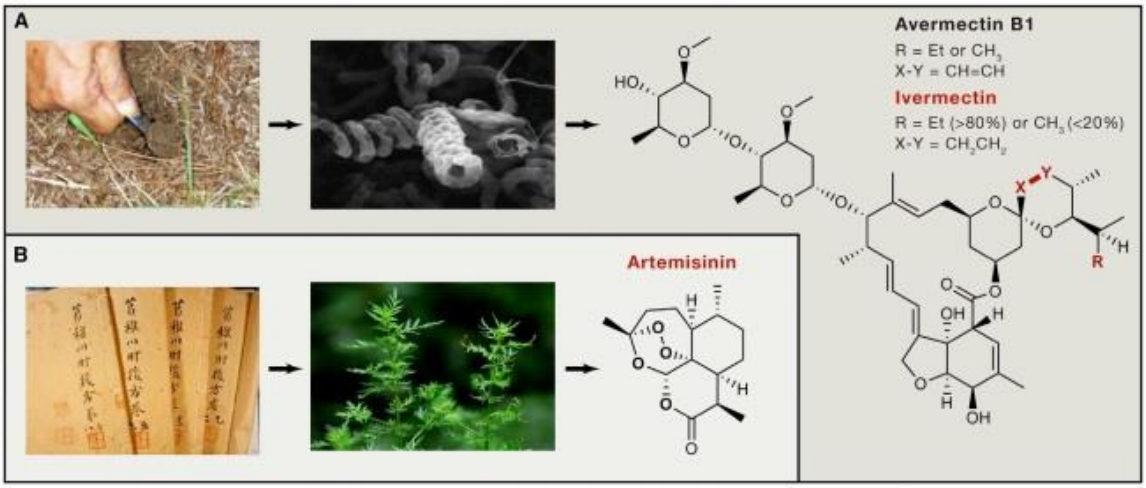

Figure 1.6. The two discoveries that were awarded the 2015 Nobel Prize in Physiology or Medicine. **A**. The anti-parasitic drug ivermectin was derived avermectin purified from cultures of the soil bacterium *S. avermitilis*. **B**. Exploitation of ancient Chinese medicine led to the discovery of the anti-malarial drug artemisinin produced by the plant *Artemisia annua*. Figure created by B. Shen, 2015 [30].

A recent survey of the sources of all small-molecule FDA-approved drugs from 1981-2014 has highlighted the importance of natural products in drug discovery (Figure 1.7) [32]. Of the 1211 approved small-molecule drugs, 35% were purely synthetic (S) while only 6% were true natural products (N). Though this seems to suggest natural products play only a nominal role in drug discovery, the categories that make up the remaining 59% of drugs are directly related to natural products. These categories include natural product derivatives (ND, 26%), botanical drugs (defined mixture) (NB, 1%), synthetic drugs that mimic a natural product (S/NM, 14%), synthetic drugs with a natural product pharmacophore (S*, 5%) and synthetic drugs with a pharmacophore that is a mimic of a natural product (S*/NM, 13%) [32]. In summary, these findings convey the important influence that nature has had on human health whether through the use of natural products themselves, or the design and synthesis of natural product-inspired drugs.

In addition to the pharmaceutical industry, natural products have also found application in the cosmeceutical and personal care industries. Less stringent testing requirements have made for a more rapid and facile process for getting a natural product to market than the clinical trials needed for approval as a drug. As active ingredients in anti-aging formulations, these products can be advertised as "natural" feeding into the current demand for organic products. There is a current trend of using marine natural products in cosmeceutical formulations, and in 2014 there were seven marine-derived natural product ingredients on the market [33]. Other applications of natural products include environmentally friendly antifouling paint to inhibit the settlement of barnacles and algae on surfaces submerged in water [34] and natural pesticides for crop protection [35], among others.

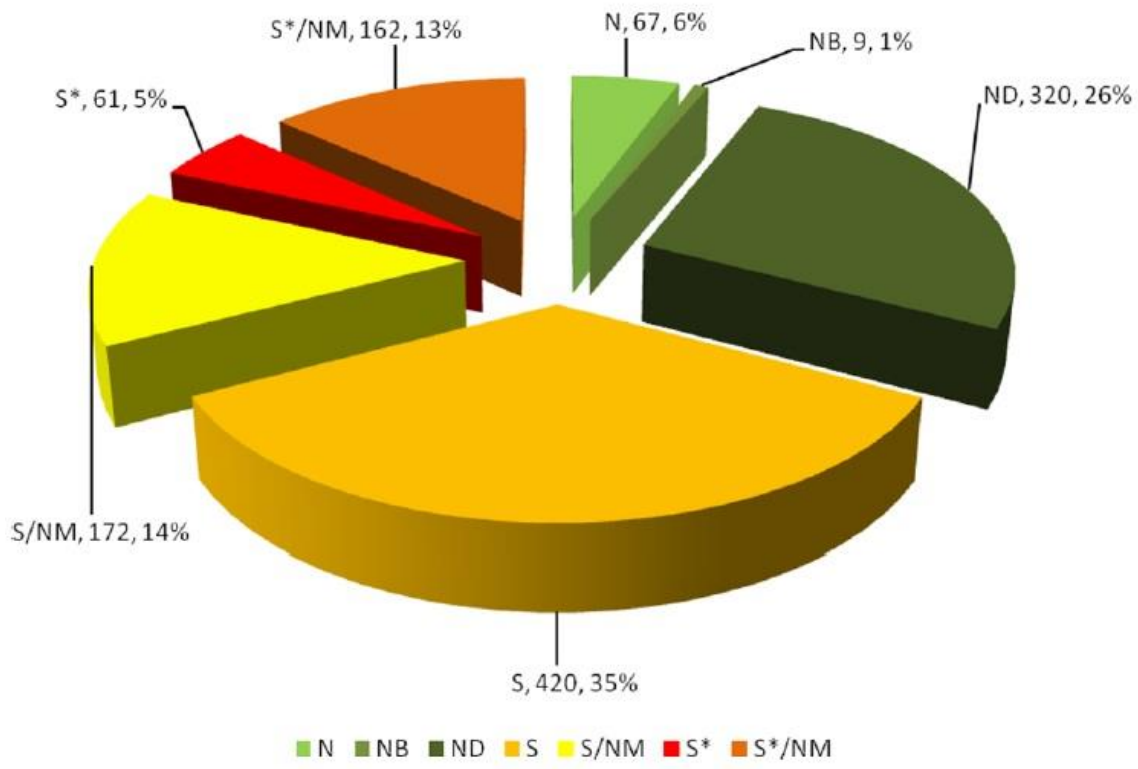

Figure 1.7. The 1211 small-molecule drugs approved between 1981-2014 categorized according to their sources. The categories include: N-natural product, NB-botanical (defined mixture), ND-natural product derivative, S-synthetic, S/NM-synthetic compound that mimics a natural product, S*-synthetic compound with a natural product pharmacophore and S*/NM-synthetic compound with a natural product pharmacophore that mimics a natural product. Figure created by D. J. Newman and G. M. Cragg, 2016 [32].

1.1.4. Current challenges in natural product discovery

One of the biggest threats currently facing human health is antibiotic-resistant bacteria. Increasingly common, infections by these superbugs are nearly impossible to treat with existing antibiotics. While we are currently experiencing a void in the discovery of novel antibiotics, new bacterial resistance mechanisms are being described on a regular basis which is leading to a global health crisis [36]. Figure 1.8 shows a timeline of the emergence of new classes of antibiotics [37]. The high rate of discovery from 1940-1960 has been termed the "Golden Age" of antibiotic discovery and occurred largely in part of the screening of many natural products, particularly microbial ones [37]. After this period, the rate of discovery dwindled as the easy-to-attain metabolites or the "low-hanging fruit" had already been picked leading to the discovery void that has been present since the 1980s. This discovery void, among numerous other reasons, has lead to the termination of natural product programs at large pharmaceutical companies despite a dire need for antibiotics. However, while the pharmaceutical industry invested in new rational drug design technologies, advancements in natural product research has addressed some of the issues of the past and now-declining pharmaceutical companies may start to turn back to natural products [38].

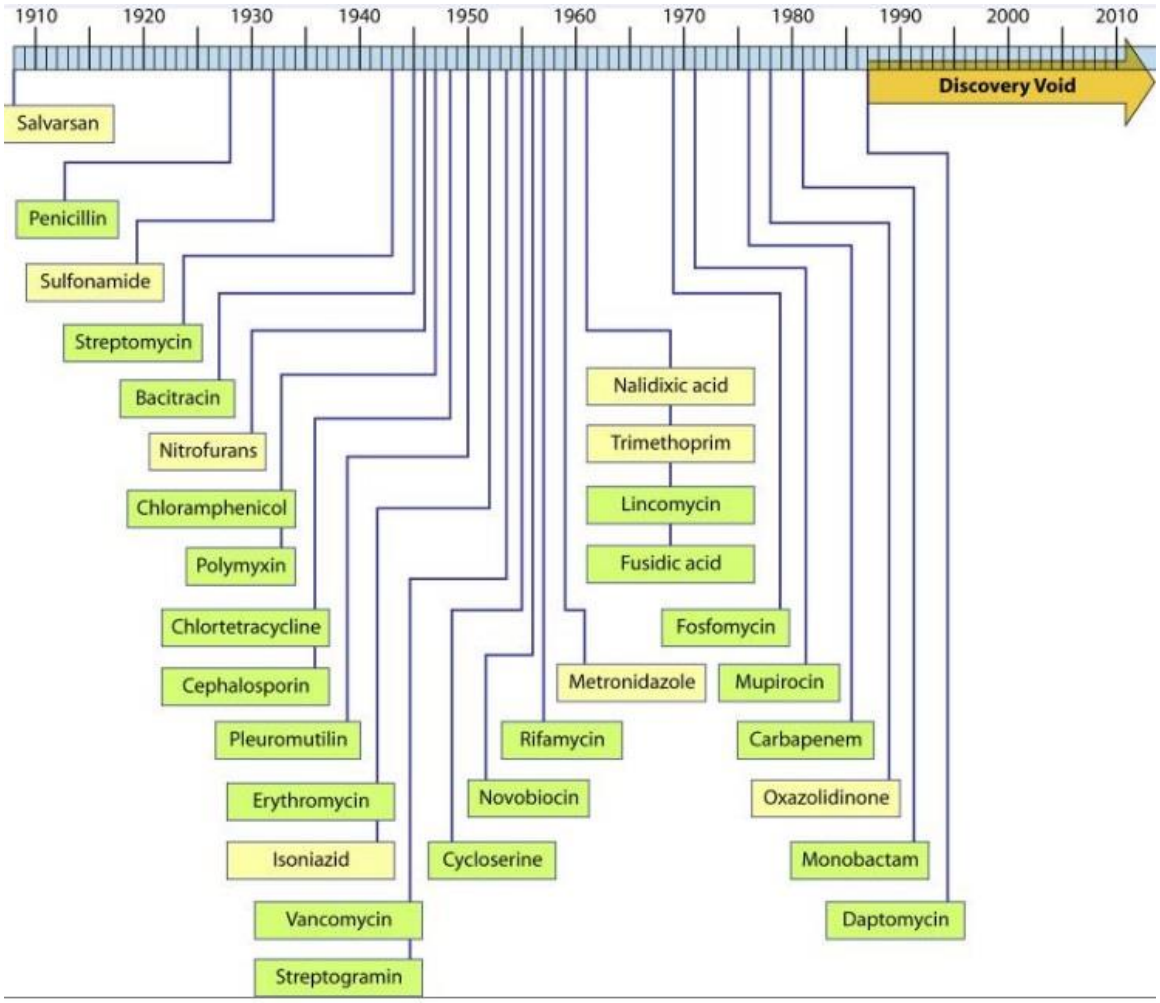

Figure 1.8. The dates of discovery of new antibiotic classes with emphasis on the discovery void that has been present since the 1980's. Figure created by L. L. Silver, 2011 [37].

An important issue facing natural product discovery programs is the accidental rediscovery of known compounds which wastes time and resources. This tends to occur when using bioassay-guided fractionation methods; samples are tested for activity, fractionated and then tested again, continuing until the active compound has been isolated. Too often, lots of time and resources are spent on this process and then structure determination reveals a compound that has previously been reported. To combat this, various dereplication techniques have been established. Dereplication, which has evolved in several different ways since its inception, is a process which attempts to improve the performance of natural product screening by rapidly identifying known chemical entities and by organizing data for prioritization of target compounds for further purification efforts [39, 40]. One way this can be achieved is using liquid chromatography-mass spectrometry (LC-MS) or nuclear magnetic resonance (NMR) spectroscopy based metabolomics techniques coupled with a comparison of compound features to existing libraries and databases [39, 41]. The resdiscovery of previously described metabolites can also be avoided by sampling from underexplored environments as biodiversity is correlated with chemodiversity. Bioprospecting in extreme environments such as the Polar regions or hard to reach marine niches has shown that these habitats are untapped sources of new natural products [42, 43, 44]. Furthermore, advances in genome mining technology has facilitated the prediction of which metabolites may be produced by an organism, guiding researchers in the direction of new compounds before any chemical extractions begin [45, 46]. Genetic information has also exposed the concept of cryptic natural products which will be discussed in Chapter 1.3.

The time-consuming nature of natural product drug discovery programs has also proven to be a challenge. Automated high-throughput screening for the early identification of putatively novel and bioactive metabolites has been an important solution in speeding up the overall process however it is a costly one. Downstream, difficulties in purification and structure elucidation of new compounds are bottlenecks in the discovery process, though high-resolution instrumentation has helped and automated isolation and structure elucidation technologies are emerging [39]. Once target compounds are isolated, the overall yields can often be extremely poor and a lack of material for any substantial biological testing is a common problem. As potential drugs make their way through the pipeline to approval, increasing quantities are required for pre-clinical and clinical trials. Synthesis or semi-synthesis may offer a solution however a complex structure could complicate these efforts. If synthesis is not an option, supply can become an issue. When drugs come from plant or animal sources, harvesting enough of the organism to provide sufficient quantities may call into question the impact on environmental sustainability raise ethical issues [47]. For this reason and others that will be discussed in the next section, the use of microorganisms as a source of natural products has been extremely important for drug discovery.

1.2. MICROBIAL NATURAL PRODUCTS

1.2.1. Benefits of using microbes as a source of natural products

Of approximately 500 000 natural products that have been described, only 10% are of microbial origin [48]. However, looking only at biologically active natural products, 47% of all known microbial natural products are active while only 7% and 3% of plant and animal derived compounds exhibit bioactivity, respectively [48]. Furthermore, 0.6% of

those bioactive microbial metabolites have been developed as drugs compared to only 0.03% of plant and 0.001% animal bioactives [48]. Despite the relatively small quantity of natural products from microorganisms that have been described, these numbers emphasize their value in the context of human health. The bioactivity of their secondary metabolites is just one of the reasons that microorganisms are quickly becoming a preferred source when searching for novel, active compounds.

The use of microorganisms as a source of natural products provides a solution to the supply issue. Ubiquitous in nature, they can be isolated from samples collected almost anywhere in the world. After being collected only once, they can be stored indefinitely and fermented on large scales to provide a continuous and sustainable supply of metabolites. Large libraries of isolates can be built over time and kept in the laboratory. It is estimated that more the 95% of the bacterial species on Earth have not yet been cultured in a laboratory and thus a very miniscule fraction of microbial species have been evaluated for natural product production [49]. With some species having the genetic capability of producing up to 50 secondary metabolites [49], microbes represent an extremely untapped resource of novel chemicals. The ability to quickly and easily sequence the whole genome of microorganisms allows insight into the metabolites they can produce. Natural product biosynthetic gene clusters can be cloned into the genomes of microbes that are easier to work with [50]. Genetic engineering can also be used to manipulate the production of different analogues designed for improved bioactivity, eliminating the need for chemical modification [50].

1.2.2. Actinomycetes as a source of bioactive natural products

Some microorganisms are better known for their production of bioactive compounds than others. Fungi are responsible for the production of about 45% of all bioactive microbial metabolites while bacteria from the order Actinomycetales of the phylum Actinobacteria account for about 39% [48]. Actinomycetes are Gram-positive filamentous bacteria that are commonly present in soil environments all over the world. Of all actinomycetes, species of the genus *Streptomyces* have been the most prolific producers and the source of about two-thirds of all clinically used antibiotics [51]. Tetracycline [52] vancomycin [53] and daptomycin [54] are all examples of streptomycete-derived antibiotics. This genus has also produced compounds used for the treatment of other medical issues such as doxorubicin and bleomycin for multiple types of cancer [55], rapamycin for the prevention of organ transplant rejection [56] or the previously discussed avermectins for parasitic infections [30]. Clinically important drugs have also been produced by actinomycetes from other genera including antibiotics such as the rifamycins produced by *Amycolatopsis* spp. [57] and erythromycin from *Saccharopolyspora erythaea* [31], or calicheamycin from *Micromonospora echinospora* which was used to treat a form of leukemia [58].

One strategy used by drug discovery programs to increase the odds of finding novel natural products is looking to rare actinomycete genera as producers. Species of rare genera are isolated less frequently than others when using conventional methods and therefore are relatively underexplored for new chemistry [59]. One such genus is *Kitasatospora* [60]. A very close relative of *Streptomyces*, *Kitasatospora* spp. are able to produce many of the same natural products and possesses many of the same genetic and

morphological characteristics [61]. There has been much debate as to the classification of this genus; *Kitasatospora* was merged with *Streptomyces* ten years after its initial description [62] but was subsequently differentiated once more just five years later [63]. *Kitasatospora* spp. are known to produce metabolites of all four main structural classes including the originally streptomycete-derived metabolites streptonigrin and bafilomycin as well as the *Kitasatospora* specific compounds setamycin and cystargin [59]. More recently, cystargamide [64] and the cystargolides [65] have been purified and characterized in our laboratory from *Kitasatospora cystarginea*, further validating the use of rare actinomycetes, specifically of the *Kitasatospora* genus, for the discovery of novel natural products.

1.2.3. Polyether ionophore natural products

One interesting group of bioactive metabolites that are produced by actinomycetes is the polycyclic polyether ionophores. These compounds are type I polyketides that always feature a carboxylic acid moiety, several tetrahydrofuran and tetrahydropyran rings and numerous hydroxyl and methyl groups [66]. Many structures possess spiroketal and cyclic hemiketal functionalities. Some structures contain ketone functional groups, and more uncommonly, amino acid and aromatic moieties. Over 120 polyether ionophores have been described [66, 67] with the majority of structure elucidation completed via X-ray diffraction analysis prior to the 2000's. Some structurally diverse examples include alborixine, calcimycin and lasalocid (Figure 1.9). Polyether ionophores are produced by only a handful of genera including mostly *Streptomyces* and *Actinomadura* spp., as well as some species of *Actinomyces*, *Dactylosporangium*, *Nocardia* and *Nocardiopsis* [68]. Though this class of compounds was first recognized in 1967, the

biosynthetic pathways that produce them have remained elusive. Generally, as for all type I PKSs, a polyketide chain is produced through a number of chain elongation steps with different extender units, and the required stereospecific reduction occurs generating the polyketide skeleton. In each of the few polyether biosynthetic pathways that have been described thus far, post-PKS tailoring steps involve epoxidation of double bonds on the polyketide chain via stereospecific epoxidase enzymes [68, 69]. The ether rings are then formed via an epoxide-opening cascade reaction catalyzed by epoxide hydrolases [70].

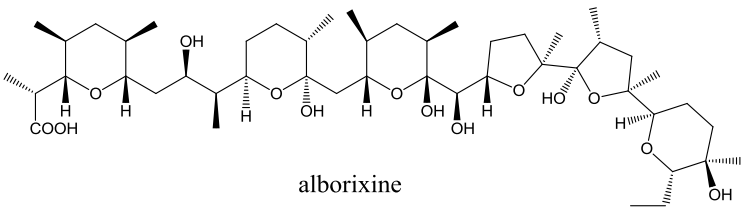

alborixine

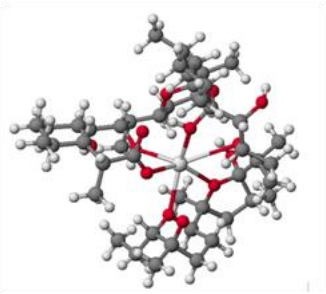

alborixine complex with sodium

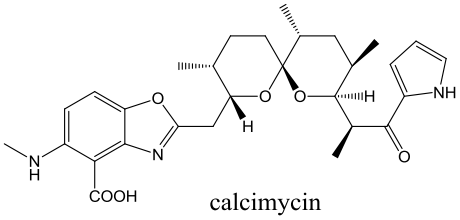

calcimycin

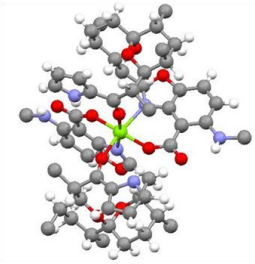

2:1 calcimycin complex with magnesium

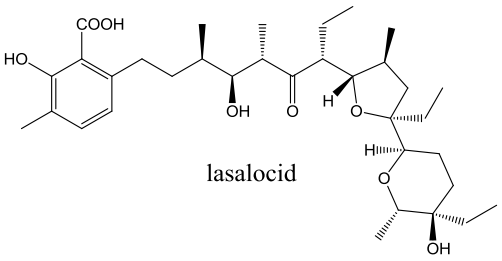

lasalocid

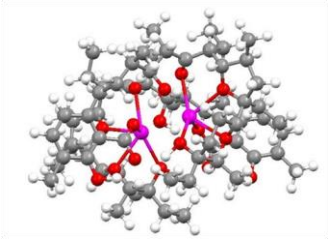

2:2 lasalocid complex with silver

Figure 1.9. The molecular structures of three polycyclic polyether ionophores with diverse structures. The crystal structures of various metal complexes of each compound are also shown. The crystal structures were obtained from the Cambridge Structural Database.

Because of their unique structures, these compounds are able to act as ionophores. In the simplest terms, ionophores are molecules which reversibly bind ions and transport them across a cell membrane. Polyethers are able to form complexes with both monovalent and divalent metal cations; the metal can coordinate to etheric and hydroxyl oxygen atoms as well as nitrogen atoms within the structure [66, 67]. In order to coordinate in this way, the polyether must adopt a three-dimensional conformation whereby it is wrapped around the metal [67]. The resulting pseudocyclic structure, often stabilized by a few intramolecular hydrogen bonds, houses the metal in a cage-like hydrophilic inner-sphere [67]. Consequently, the alkyl backbone of the polyether makes up the outer-sphere causing the entire complex to be effectively hydrophobic [67]. This property is what allows polyethers to penetrate cellular membranes resulting in tremendous biological activity. There are three mechanisms in which this can occur. Electroneutral transport (Figure 1.10 **A**) involves binding of the polyether anion ($I\text{-}COO^-$) to either a metal cation (M^+) or a proton (H^+) forming a neutral complex which can diffuse across the cell membrane [71]. The relatively alkaline cellular environment facilitates this type of transport through the deprotonation of the acid moiety on the ionophore [71]. In electrogenic transport (Figure 1.10 **B**), the polyether remains protonated and metal complexation occurs with the neutral ionophore [71]. This recently described mechanism is important when studying the effect of polyether ionophores on cancerous cells as the microenvironment of cancer cells is known to be acidic [71, 72]. Lastly, biomimetic transport (Figure 1.10 **C**) occurs with synthetically modified polyethers containing ester or amide groups rather than carboxylic acids [71]. In all three mechanisms, the general overall result is a change in the Na^+/K^+

gradient within the cell which causes an increase in osmotic pressure and swelling leading to cell death [67].

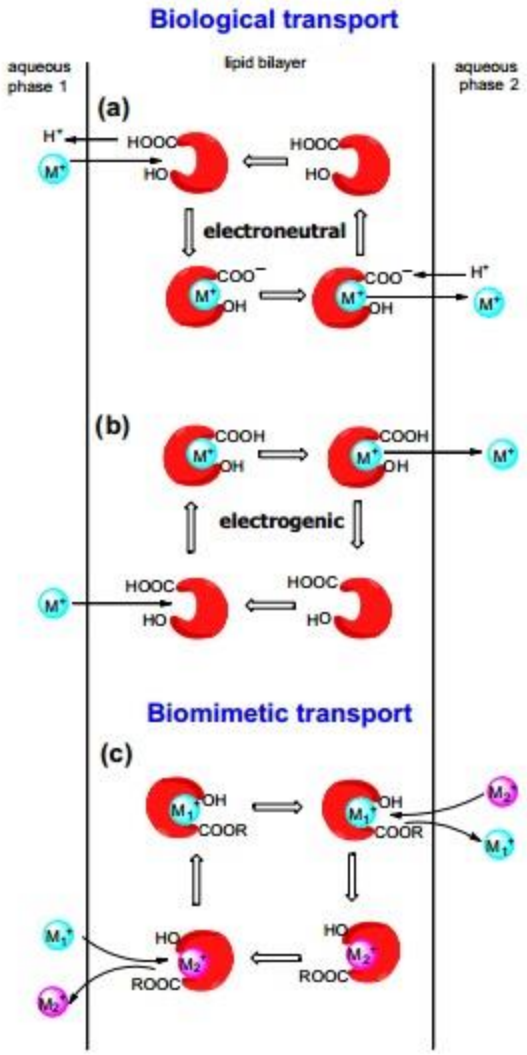

Figure 1.10. A diagram illustrating the three mechanisms in which polyether ionophores transport ions across cell membranes. Figure created by A. Huczynski, 2012 [71].

The ionophore properties of polyethers have afforded them a range of bioactivity however they are most well known for being excellent antibiotics. The complexes can easily cross Gram-positive cell membranes making them effective for treatment of various Gram-positive bacterial infections [73]. Their potency against drug resistant strains such as vancomycin-resistant enterococci (VRE) and methicillin-resistant *Staphyloccocus aureus* (MRSA) is superior to the classically used antibiotics vancomycin and oxacillin with minimal inhibitory concentrations in the low nanomolar range [74]. Most, but not all polyethers are ineffective against Gram-negative bacteria as they are unable to penetrate the lipopolysaccharide outer membrane [67, 73]. Three compounds in particular, septamycin [75], noboritomycin [76] and mutalomycin [77] are able to inhibit growth of Gram-negative pathogens at nanomolar concentrations. Fungal pathogens are more resistant to polyether ionophores, however some species are moderately sensitive to treatment [73]. Parasitic infections are very susceptible to treatment by polyethers. Half-maximal inhibitory concentrations of a number of polyethers including monensin, salinomycin, nigericin, narasin and dianemycin against chloroquine-resistant strains of the malaria-causing parasite *Plasmodium falciparum* were in the picomolar range [78, 79]. *Eimeria* spp. are parasites that cause coccidosis in cattle and poultry and are also greatly affected by these ionophores [73]. Polyether natural products have also shown promise for the treatment of viral infections, especially HIV [73]. Effects of these compounds on the cardiovascular [80], immunoregulatory [81] and central nervous systems [82] have been explored, as well as their possible use as topical anti-inflammatory [83], herbicidal [84] and anti-scarring agents [85].

Since the discovery of monensin in 1967, the anticancer activity of this family of compounds has barely been explored. Using nigericin as an example, the polyether

ionophores were mentioned as a potential new class of anticancer drugs in 1987 due to their ion exchange capabilities [86] but since then the majority of research has focused on their impressive antibiotic properties. In 2009, a large screening of 16 000 compounds for activity towards multi-drug resistant cancer cells and cancer stem cells highlighted salinomycin as having potent and selective activity which has since prompted an exponential increase of research on these compounds [87]. Thus far, studies have suggested that different polyethers have specific modes of action against different types of cancers. Salinomycin was found to activate a specific apoptotic pathway [88] while nigericin completely stops DNA synthesis by increasing intracellular pH [89], both while having a negligible effect on cells of healthy tissues. Polyethers have also been reported to have selective chemosensitizing properties; they increase the sensitivity of cancer cells to clinically used chemotherapy agents when administered together, but do not affect sensitivity to healthy cells [71, 73]. A number of polyethers are currently being evaluated for development as anticancer drugs. Salinomycin has been the most thoroughly explored to date and has seen success in pilot clinical trials for a number of cancer types [90].

Several polyether ionophores have been developed for the veterinary industry and are used worldwide. In 2012, lasalocid (Avatec®, Bovatec®), laidlomycin (Cattlyst®), maduramycin (Cygro®), narasin (Monteban®, Maxiban®), semduramycin (Aviax®), monensin (Coban®, Rumensin®, Coxidin®) and salinomycin (Biocox®, Sacox®) were marketed as antibiotics and anticoccidial agents for ruminants and poultry [71]. So far, no polyethers have been tested for use as antibiotics in humans due to their observed cytotoxicity in some mammals [71]. Only one case of acute human overexposure has been recorded which involved accidental inhalation and swallowing resulting in prolonged

weakness and pain in the extremities that was resolved after 40 days [91]. More recently, the effects of long-term low-dose exposure has revealed some negative chronic effects [92]. Development of these compounds as cancer therapeutics will shed more light on human toxicity although so far the low doses used in pilot clinical trials have shown minimal side effects [90]. Produced in large quantities by actinomycetes, polyether ionophores do not face any supply issues, and total synthesis of many members of this family has been described [93, 94]. Looking ahead, genetic screening methods are being developed in the quest to discover new polyether natural products [68].

1.2.4. The role of natural products and their biotransformations in quorum sensing

Quorum sensing is a form of bacterial communication. Some species of both Gram-negative and Gram-positive bacteria can biosynthesize and secrete secondary metabolites that act as self-signals, or autoinducers (AIs) that increase in concentration as the bacterial cell density increases [25]. When a minimum concentration of an AI is detected by the bacterium it leads to changes in gene expression which allows behavioural coordination of the entire bacterial population [25]. Figure 1.11 shows a generic diagram of quorum sensing in Gram-negative bacteria [95]. Here, the AIs are biosynthesized and secreted from the cell. When the extracellular concentration of AIs reaches a specific threshold they are detected by the cell through binding to a cognate receptor. The complex then binds to a promoter which activates gene expression. The overall result is gene regulation through quorum sensing. This phenomenon was first described in bioluminescent marine bacterium *Vibrio fischeri* that is present at high cell densities inside eukaryotic hosts like squid and fish. When a culture of this species is trapped inside of the host, it grows to a very high cell density while releasing an AI that signals

the emission of light which affords an ecological advantage to the host [96]. Quorum sensing can orchestrate a number of activities and virulence factors such as motility, sporulation, antibiotic production and biofilm formation which contribute to the pathogenicity of the bacterium [25].

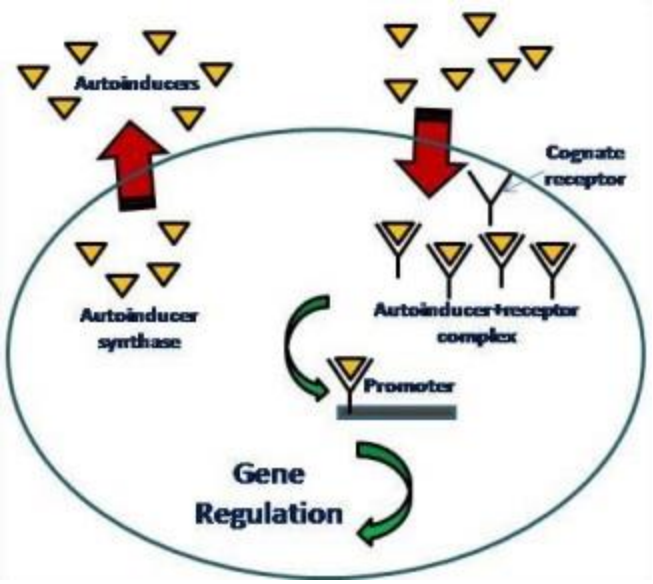

Figure 1.11. A general diagram of quorum sensing in Gram-negative bacteria. Figure created by C.-L. Koh *et al*., 2013 [95].

Currently, treatment of bacterial infections in humans and animals usually involves administering antibiotics which will inhibit the growth of the pathogen. As previously discussed, the lack of new antibiotic classes being discovered coupled with a growing number of resistance mechanisms has left society facing global health crisis. The existence of quorum sensing systems that regulate the expression of virulence factors has presented a new opportunity for treatment of infections [97]. Targeting and blocking the regulators of bacterial virulence can diminish the organism's ability to establish itself in a host thus eliminating the need for antibiotics [97]. Inhibiting the production of AIs, modifying them so they are not recognized by their receptor, or competitively binding to their receptor are three ways in which this can occur [95]. Quorum sensing antagonists can be either synthetic compounds or natural products. In addition, quorum sensing inhibition through enzymatic modification of AIs has occurred in co-cultures of two different microbes where the AIs were hypothesized to have some sort of negative effect on the foreign species [98]. It has been postulated that attenuation of virulence factors to eliminate infections will be less likely to facilitate the development of resistance mechanisms [97, 98], making this an attractive approach to treating bacterial infections.

In patients with cystic fibrosis, infection of the lungs with the Gram-negative pathogen *Pseudomonas aeruginosa* is very common. Infections are complicated by the fact that one of the virulence factors of the pathogen is biofilm formation. The formation of a biofilm provides an ideal, protected environment where the bacterial population is able to resist the action of antibiotics [99] making these infections very difficult to treat using conventional methods. The development of therapeutics based on quorum sensing

inhibition mechanisms, particularly through enzymatic modification of secreted autoinducers, is a topic of current investigation [97, 98, 99].

1.3. CRYPTIC NATURAL PRODUCTS

1.3.1. Cryptic natural products and their importance

Though the "Golden Age" of natural product discovery is behind us, some may say we are on the cusp of a second "Golden Age". Genomic sequencing technology has opened a new door in natural product discovery which has led to the exciting new world of cryptic metabolites. The genome of *Streptomyces coelicolor* A3(2) was published in 2002 [100], revealing not only the biosynthetic gene clusters responsible for the production of known metabolites, but also genes which encoded metabolites that had never been observed from this bacterium [100, 101, 102]. These seemingly inactive biosynthetic gene clusters and the metabolites that they encode can be referred to as silent or cryptic. Accessing these elusive compounds is important as novel chemistry will reveal novel bioactivity. The discovery of cryptic natural products may lead to new effective anticancer drugs or new structural classes of antibiotics which is desperately needed in present times.

Fungal cryptic natural products have been explored to some extent [102], while methods for activating silent biosynthetic pathways in bacteria are still being developed. A streptomycete genome may reveal 20-30 natural product encoding biosynthetic genes [100], yet fermentation under standard laboratory conditions typically results in just two or three natural products. If cryptic metabolites are produced, their quantities may fall below the detection limits of instrumentation used to identify them. If they are detected, there is

often not enough of the compound for purification and structure elucidation, even in large-scale cultures. Though genomic information sheds light on the presence of cryptic natural products, it does not directly convey how to upregulate or induce their production and therefore a number of different approaches are often attempted blindly. This has fortuitously resulted in the successful discovery of new cryptic natural products however alternatively, *in silico* genetic data mining can provide a more informed estimate of conditions likely to activate silent gene clusters. An example of this can be found in the induction and purification of coelichelin, one of the cryptic natural products from the previously mentioned *S. coelicolor* [103]. Analysis of the silent gene cluster predicted that it was responsible for the production of a tripeptide, which based on its structure could be a siderophore. Culturing the bacterium in an iron-deficient medium activated the coelichelin gene cluster and produced the target compound in sufficient quantities for purification. Structure elucidation revealed the compound was actually a tetrapeptide which highlighted a pitfall in the accuracy of this approach [102]. Researchers have been continuing to utilize this technology for the rapid identification and isolation of cryptic natural products, and it seems genetic mining, or genomics, is the key to success for cryptic natural product discovery of the future. When combined with advanced structure prediction informatics this approach becomes extremely powerful [104]. This being said, whole genome sequencing of large microbial libraries is not always plausible and non-specific methods of cryptic natural product induction continue to successfully unveil new compounds.

1.3.2. Traditional methods to access cryptic natural products

Induction of cryptic metabolites in a defined set of growth conditions was observed even before genome sequencing was a possibility. The biosynthesis of natural products is energetically expensive. At any given time, under a certain set of conditions, it is unlikely that an organism will spend energy producing each and every secondary metabolite it is genetically capable of [102]. Instead, natural products are produced only when needed in response to environmental situations, ultimately providing an advantage to the organism under the specific conditions [102]. High concentrations of phosphates or the addition of certain amino acids has been proposed to induce the production of previously unobserved metabolites [105]. Furthermore, antibiotic production is more commonly encountered when using a lean growth medium relatively low in nutrients as opposed to rich media. Aside from altering the composition of the culture growth media, the sudden onset of environmental stress during fermentation has produced interesting results. One good example is the induction of the jadomycins by *Streptomyces venezuelae* ISP5230 [106]. Jadomycin, a pigmented antibiotic, was discovered after an incubator malfunction caused the temperature to increase and turned cultures black in colour. It was found that the production of an analogue, jadomycin B, could be induced in response to a heat shock or by the addition of ethanol to cultures [107]. Further optimization experiments found an ideal concentration and time of addition of ethanol to yield the highest titers of the jadomycin B [107]. In addition, it was observed that the addition of different amino acids lead to the production of different analogues [107].

Examples of natural product induction that existed in the literature before the new millennium were mostly the result of serendipitous discoveries arising from random

alteration of the growth medium or culture conditions. In 2002, the idea of screening a relatively small library of microbes in a relatively large number of conditions was presented and termed the "one strain-many compounds" (OSMAC) approach [105]. Though still mostly randomized in terms of what conditions will be tested, this approach is more systematic and thorough. At the time this concept was introduced, it had been used by its inventors to successfully isolate over 100 natural products from only six producing organisms, demonstrating its impressive effectiveness [105]. This is because the OSMAC approach is not geared towards activation of one specific cryptic gene cluster as is the case for a genomics-based approach targeting one specific metabolite. By systematically varying parameters such as the culture vessel size and shape, fermentation volume, aeration, length and temperature, medium components and pH, or addition of chemical probes, the OSMAC approach is simple, inexpensive and leads to big changes in secondary metabolism. The ability of the organism to grow in the conditions to be tested is a limitation of this technique, however the infinite number of conditions that could be attempted is surely a strength.

Since its inception, the OSMAC approach has been used to upregulate and induce the production of novel cryptic metabolites from *Streptomyces* spp. One example is the discovery of the new ansamycin compound chaxamycin and the structurally rare polyketide chaxalactin from *Streptomyces* sp. C34 isolated from desert soil (Figure 1.12) [102, 108]. Initial fermentation in standard ISP2 broth afforded chaxamycin A and B, while a modified ISP2 recipe using glycerol instead of glucose produced chaxamycin C and D. Fermentation of the strain in eight more liquid media revealed three analogues of chaxalactin which were produced in connection with the presence of glycerol.

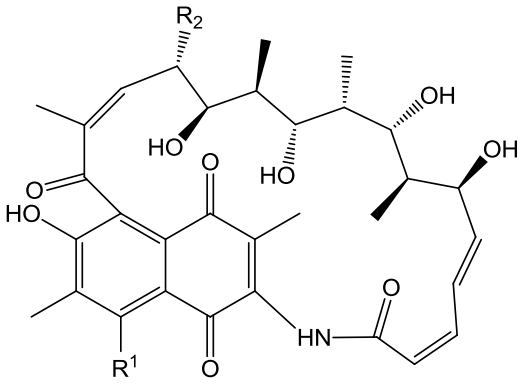

chaxamycin A: R^1 = OH, R^2 = CH_3
chaxamycin B: R^1 = H, R^2 = CH_3
chaxamycin C: R^1 = OH, R^2 = CH_2OH

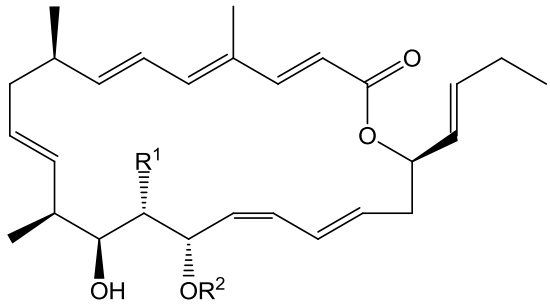

chaxalactin A: R^1 = H, R^2 = H
chaxalactin B: R^1 = OH, R^2 = H
chaxalactin C: R^1 = OH, R^2 = CH_3

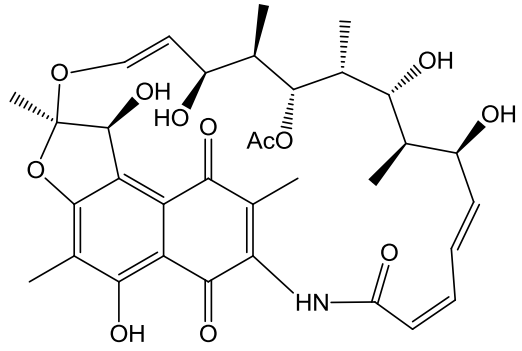

chaxamycin D

Figure 1.12. Two families of compounds discovered using the OSMAC approach. Chaxamycin A and B were produced by *Streptomyces* sp. C34 under standard laboratory culturing conditions while chaxamycin C and D, and chaxalactin A-C were induced using various modified media [108].

1.3.3. Co-culture methods to access cryptic natural products

In nature, microorganisms exist in constant interaction with other living species including other microbes, plants and animals in both terrestrial and marine environments. The relationship between microbes and other species may be symbiotic, for example a bacterium that lives within a coral that provides chemical defense in exchange for a habitat that provides ideal nutrition [109]. Alternatively, the relationships may be antagonistic which occurs in complex microbial communities that house many species competing for space and resources. The ecological stress within these microbiomes provokes a great deal of natural product production; antimicrobial metabolites and other chemical signals such as quorum sensing AIs are released into the environment and in turn can stimulate gene expression in other microbes [110]. For this reason, it is hypothesized that the production of cryptic metabolites can be induced in the laboratory by direct contact with one or more ecologically relevant "stressor" organisms and their chemical signals [110, 111]. This co-culture induction approach has been used successfully many times with fungal-fungal, bacterial-bacterial, and fungal-bacterial cultures and some examples are shown in Table 1.1 [111].

Table 1.1. Metabolites isolated from microorganism co-cultures. Table created by A. Marmann *et al.*, 2014 [111].

Co-Cultivated Microorganisms	Secondary Metabolites Reported	Reported Activity
Oyadendron sulphureoochraceum *Ascochyta pisi* *Emercillopsis minima* *Cylindrocarpon destructans* *Fusarium oxysporum*	Lateritin (k)	Cytotoxic Antifungal Antibiotic
Paraconiothyrium sp. *Alternaria* sp. *Phomopsis* sp.	Paclitaxel (k)	n.t.
Streptomyces bullii *Aspergillus fumigatus*	Brevianamide F (k)	-/-/C
	Spirotryprostatin A (k)	T/L/C
	6-Methoxy spirotrypostatin B (k)	-/L/C
	Fumitremorgin C (k)	T/L/C
	12,13-Dihydroxy fumitremorgin C (k)	T/L/C
	Fumitremorgin B (k)	T/L/C
	Verruculogen (k)	T/L/C
	11-*O*-Methylpseurotin A (k)	-/-/C
	11-*O*-Methylpseurotin A_2 (n, **19**)	-/L/C
	Ergosterol (k)	-/-/-
	Emestrin A (k)	n.t.
	Emestrin B (k)	n.t.
Aspergillus fumigatus *Streptomyces rapamycinicus*	Fumicycline A (n, 20) Fumicyline B (n, 21)	Antibiotic Antibiotic
Aspergillus fumigatus *Streptomyces peucetius*	Fumiformamide (n, 22) *NN*'-((1*Z*,3*Z*)-1,4-bis (4-Methoxyphenyl)buta-1,3-diene-2,3diyl)Di-formamide (n, 23)	Cytotoxic
Fusarium tricinctum *Bacillus subtilis*	Macrocarpon C (n, 24)	-
	2-(Carboxymethylamino)benzoic acid (n, 25)	-
	(−)-Citreoisocoumarinol (n, 26)	-
	Lateropyrone (k)	Antibiotic
	Enniatin A1 (k)	Antibiotic
	Enniatin B (k)	-
	Enniatin B1 (k)	Antibiotic
	(+)-Citreoisocoumarinol (k)	-
Tsukamurella pulmonis *Streptomyces endus*	Alchivemycin A (n, 27)	Antibiotic

n = new; k = known; n.t. = not tested; T = trypanocidal; L = leishmanocidial; C = cytotoxic; - = inactive.

Though this approach sounds relatively straightforward there are a number of decisions to be made in terms of how the experiments can be set up. Similar to random variation of fermentation conditions to induce new compounds, there is no standard way of conducting co-culture experiments. Stressor organisms can be chosen on the basis of ecological relevance in attempt to imitate an ecological situation, or they can be chosen on the basis of their pathogenicity in the hope that induced metabolites might have targeted activity towards the pathogen. Co-cultures can be performed on solid media or in liquid cultures. In liquid cultures, the microbes may be grown together or separated by a physical barrier such as dialysis tubing which allows diffusion of small metabolites into the opposing culture but avoids direct cell contact [112]. Cell-free cultures of stressors may also be used [113]. In some cases, such as the production of a red pigmented compound in a co-culture of *Streptomyces lividans* and *Tsukamurella pulmonis*, direct cell-to-cell contact was required [114]. The addition of heat-killed cultures of a stressor to a pure culture of a live strain has also been a successful method; dead cultures of *Bacillus subtilis* and *S. aureus* added to *S. coelicolor* fermentations upregulated the production of undecylprodigiosin [115]. More variables in these experiments include the media composition, as well as the time-point and concentrations in which the stressor is introduced to the live culture [116].

The co-culture approach is further complicated by a number of inherent flaws. First, fermentation conditions are limited to those in which all of the involved organisms can thrive. In the case of fungal-bacterial interactions, finding ideal growth conditions for both organisms presents a challenge. Second, the growth rates of two or more organisms in the same conditions are very difficult to control which calls into question the

reproducibility of this approach. Reproducibility is particularly important when it comes time for scale-up in order to obtain sufficient material for purification of any identified cryptic natural products. Third, without genomic data for each strain used in the experiment, it would be very difficult to identify the true producer of any cryptic natural products discovered. Finally, purification of induced natural products from extracts of co-cultures is extremely difficult as many more compounds complicate the metabolic profile.

The Kerr group has attempted to address some of these issues with the advent of a somewhat simplified standard procedure, similar to the introduction of the more systematic OSMAC approach for varying culture conditions. A number of experimental set-ups were explored to find the most convenient, reproducible parameters tailored for co-culture experiments with actinomycetes. The approach, which has been termed "co-culture mimic", involves the fermentation of an actinomycete in a medium that has been conditioned with a standardized quantity of the dead cells and secreted biomolecules of a stressor organism. More simply, aliquots of a heat-killed culture are added to the broth of a live culture. A simple schematic of this approach is shown in Figure 1.13. LC-MS based metabolomics procedures for analyzing and visualizing the results of co-culture mimic experiments have been implemented. The secondary metabolite profiles of pure control cultures versus the stressor-added culture can be directly compared to rapidly highlight natural product upregulation or induction. With only one live culture, the approach is a "mimic" of a true co-culture using two live organisms. Working with only one live culture increases the reproducibility of the resulting metabolic profiles. A set of fermentation conditions that is ideal for the producer may be chosen without any regard for the stressor, and deducing the origin of any new natural products becomes trivial.

Optimization of the best stressor concentrations and addition time points have been attempted with some success however these details vary with the specific combination of producer and stressor being evaluated. Ideally, co-culture mimic experiments will also simplify the identification of the specific chemical signals, if any, that are responsible for activating silent gene clusters in the producer. The purified signaling compounds can then be applied directly to producer cultures for an even more reproducible source of the cryptic metabolite of interest. Thus far, the co-culture mimic approach has led to the identification of numerous putatively new, induced natural products. It has also led to the unveiling of a novel and important quorum sensing inhibition mechanism which will be presented in this thesis.

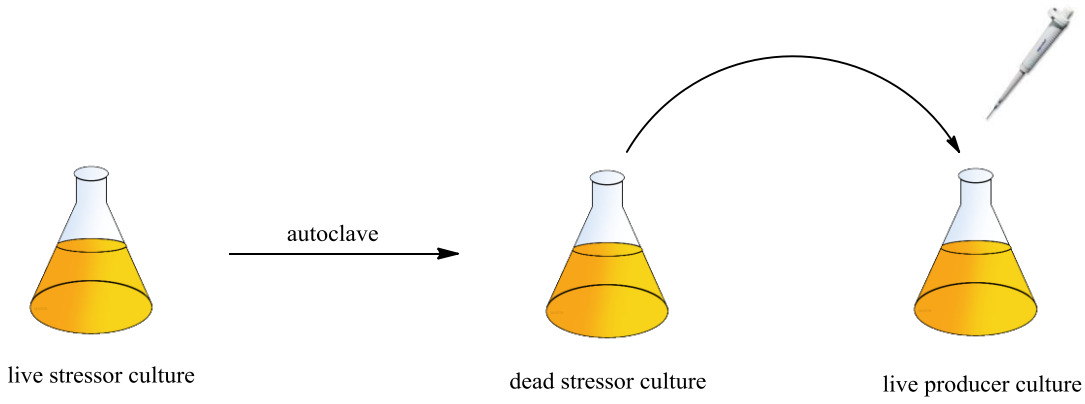

Figure 1.13. A schematic of the co-culture “mimic” approach where an aliquot of a heat-killed stressor culture is added to a live producer culture to induce cryptic natural product production.

1.4. RESEARCH GOALS

Overall, the main goal of this thesis was to identify, purify and characterize novel natural products produced by actinomycetes. Targeting cryptic natural products using well-established non-specific approaches increased the likelihood of achieving this goal. A small set of three actinomycetes were chosen on the basis of their reputation as being excellent producers of bioactive natural products. Working with a restricted set of actinomycetes, rather than a large library, increased the number of conditions that could be screened for each organism. This ultimately allowed the secondary metabolism of the three selected strains to be more thoroughly examined which is essential when searching for cryptic natural products.

1.4.1. Examine the effect of varying culture media of natural product production

The traditional approach of varying culture media to uncover cryptic natural products was applied to the three selected actinomycetes. A total of 14 different conditions were screened to increase the likelihood of achieving induction and finding new natural products. Chemical screening and dereplication via ultra high performance liquid chromatography high-resolution mass spectrometry (UHPLC-HRMS) based metabolomics revealed many changes in the secondary metabolomes of the three bacterial strains and led to the discovery of two induced metabolites, one known and one new, which exhibited both antibiotic and anticancer activity. These results will be discussed in Chapter 2.1. For convenience, LC-MS will represent UHPLC-HRMS throughout this thesis.

1.4.2. Examine the effect of co-culture mimic conditions of natural product production

Our newly developed co-culture mimic strategy was applied to the three selected actinomycetes in the continued search for novel, induced metabolites. A diverse group of stressors was chosen; the specific combinations had never before been explored thus increasing the chances of uncovering new metabolites. The effect of these conditions on natural product production was evaluated using LC-MS based metabolomics. The upregulation and induction of uncharacterized metabolites was catalogued and future work is suggested in Chapter 2.2.

1.4.3. Purify and characterize putatively new compounds from induction experiments

The co-culture mimic experiments of another student in the Kerr lab led to the identification of a compound that appeared to be induced, and the specific signal responsible for the induction was identified. In a collaborative effort, scaled-up fermentations were pursued. Purification and structure elucidation revealed the compound was not a natural product, but rather a novel biotransformation product related to quorum sensing activities. Purification and characterization of two additional metabolites was also achieved, one which exhibited upregulation in response to the specific chemical signal. The results of this collaborative project are presented in Chapter 2.3.

CHAPTER 2

RESULTS AND DISCUSSION

2.1. THE EFFECTS OF VARYING CULTURE MEDIA ON NATURAL PRODUCT PRODUCTION AND THE DISCOVERY OF TERROSAMYCIN A AND B

2.1.1. Introduction

In an attempt to activate cryptic pathways and in turn, discover new induced compounds, the secondary metabolism of three actinomycetes was examined using an OSMAC approach. Two species of the rare genus *Kitasatospora* (*K. cystarginea* NRRL B-16505 and *K. griseola* NRRL B-16229) as well as *Streptomyces* sp. RKND004, a unique strain isolated from Prince Edward Island sediment, were selected for study in order to maximize the chances of uncovering novel structures. Each strain was subjected to fermentation in 14 different types of liquid media and the resulting metabolomes were examined and compared across the different conditions. Metabolites that appeared to be induced by certain media and had no or few exact mass matches within natural products databases were prioritized for scaled-up fermentation and isolation. This approach led to the discovery of natural products which we have termed the terrosamycins, a family of polyether natural products produced by our Prince Edward Island strain which exhibited excellent antibiotic and anticancer properties.

2.1.2. Identification of *Streptomyces* sp. RKND004

The actinomycete strain labeled RKND004 was isolated by the Kerr group from a sediment sample collected in August, 2010 in Burnt River, Prince Edward Island. Preliminary phylogenetic analysis via partial 16S rRNA gene sequencing at the time of isolation revealed the strain was possibly a *Kitasatospora* species. The *rpoB* and full-length 16S rRNA gene sequences were used to further classify the bacterium. The *rpoB*

gene is a useful taxonomic marker for distinguishing between species of the closely related genera *Kitasatospora* and *Streptomyces* [117], while the 16S rRNA gene is commonly used in phylogenetic studies of bacteria as it is highly conserved among different species [118].

The *rpoB* sequence (253 bp) was compared to existing nucleotide sequences in the NCBI database using the Basic Local Alignment Search Tool (BLAST) [119]. The BLAST search revealed one *Kitasatospora* and 26 *Streptomyces* strains with 96% similarity suggesting RKND004 likely belongs to the *Streptomyces* genus. A similar search compared the 16S rRNA sequence (1471 bp) to existing bacterial 16S rRNA sequences in the database. The 16S sequence showed over 97% similarity to 12 *Streptomyces* strains, with 99% similarity to *Streptomyces yanglinensis* 1307 and *Streptomyces paucisporeus* 1412. The high degree of similarity between many 16S sequences within the genus *Streptomyces* render this technique unsuitable for differentiation at the species level [120], and thus the bacterium was identified as *Streptomyces* sp. RKND004.

2.1.3. Small-scale fermentations and extractions

Each of the three actinomycetes (*K. cystarginea*, *K. griseola* and *Streptomyces* sp. RKND004) was fermented on a small scale in 14 different liquid media (Table 2.1) in triplicate. The different media types are commonly used in the Kerr lab and were selected based on their compositional diversity and potential to stimulate production of a range of natural products. Uninoculated media blanks for each media type were included as negative controls and subjected to the same fermentation conditions. Cultures and blanks were extracted with ethyl acetate and the extracts were analyzed using LC-MS over seven

batches of analysis. Each batch began with a reserpine sample as a retention time calibration standard as well as three methanol blanks to limit carryover between samples; one before and after the reserpine standard as well as one at the end of each batch.

Table 2.1. Recipes for media used in this study.

Medium	Ingredient	Quantity (g/L Milli-Q diH_2O, unless otherwise stated)	Specified pH (± 0.2)
ISP2 [121]	yeast extract	2	-
	malt extract	5	
	dextrose	2	
BFM1* [122]	dextrin	20	-
	soluble starch	20	
	beef extract	10	
	tryptone	5	
	ammonium sulfate	2	
	calcium carbonate	2	
BFM2 [123]	soluble starch	5	-
	Pharmamedia®	5	
BFM3* [124]	magnesium sulfate heptahydrate	0.5	-
	potassium chloride	0.5	
	dipotassium phosphate	3	
	sodium chloride	5	
	nutrient agar	0.4	
	glycerol	12	
	Bacto™ soytone	5	
BFM4	toasted Nutrisoy® flour	12	6.8
	ammonium chloride	1	
	dextrose	12	
	nutrient agar	0.4	
	calcium carbonate	1	
	N-Z Amine A®	3	
BFM5 [125]	tryptone	17	7.3
	Bacto™ soytone	3	
	sodium chloride	5	
	dipotassium phosphate	2.5	
	dextrose	2.5	

BFM6	yeast extract	5	
	tryptone	5	
	iron (II) chloride tetrahydrate	0.04	
	manganese (II) sulfate monohydrate	0.00034	7.3
	magnesium sulfate heptahydrate	5	
	sodium chloride	58.44	
BFM7* [126]	potassium phosphate	1	
	dipotassium phosphate	1	
	magnesium sulfate heptahydrate	0.2	
	iron (III) chloride	0.05	
	calcium chloride dihydrate	0.02	7.3
	sodium chloride	5	
	glucose	2	
	yeast extract	2	
	olive oil	5	
BFM8* [127]	tryptone	5	
	yeast extract	1	7.6
	ferric citrate	0.1	
BFM9 [128]	yeast extract	5	
	casamino acids	0.1	
	glucose	10	
	sucrose	100	6.8
	potassium sulfate	0.25	
	magnesium chloride hexahydrate	10.2	
	MOPS sodium salt	21	
BFM10 [129]	glycerol	10	
	soybean flour	20	
	corn oil	20	
	dipotassium phosphate	1.2	
	MOPS buffer	21	7.0
	manganese (II) chloride heptahydrate	0.01	
	iron (II) sulfate heptahydrate	0.01	
	zinc sulfate heptahydrate	0.01	

BFM11 [130]	soluble starch	10	7.0
	yeast extract	4	
	tryptone	2	
	potassium bromide stock solution (20 g/L)	5 mL	
	iron (II) sulfate heptahydrate stock solution (8 g/L)	5 mL	
BFM13 [131]	yeast extract	4	-
	dextrose	2	
	sodium chloride	5	
	dipotassium phosphate	2.5	
	potassium phosphate	0.5	
BFM14 [132]	ammonium sulfate	0.39	-
	disodium phosphate	5.67	
	potassium phosphate	4.08	
	calcium chloride dihydrate	0.001	
	magnesium sulfate heptahydrate	0.197	
	manganese (II) sulfate heptahydrate	0.002	
	iron (II) sulfate heptahydrate	0.015	
	Pharmamedia®	5	

* Ingredients modified from the original recipes.

2.1.4. Data analysis and prioritization of target compounds

All raw LC-MS data were first inspected manually for any peaks that were present when the strain was grown in certain media and not in others, indicating the presence of a putatively induced metabolite. The specific strain and media producing putatively induced metabolites were noted however, due to the sheer volume of data, the software program MZmine 2 [133] was employed as a data mining tool to assess the results in greater detail. The data for each strain was processed separately due to limitations on the number of files the program can handle at one time.

Raw data was imported into MZmine 2 and processed in a similar manner as previously described by the Kerr group 41 with some additions. First, the mass detection intensity threshold was set to 1E4 to ensure that the *m/z* peaks detected were from genuine metabolites and not part of the noise. Chromatograms for each file were created and deconvoluted into individual peaks and low-intensity isotopes were removed. Normalization of the data within each sample was achieved using the maximum peak intensity method; the area of each peak within the sample was divided by the area of the largest peak within the same sample, allowing comparison of the production of any one metabolite relative to others in the same sample across each different condition screened. The lists of peaks present in each sample were joined into a single aligned peak list. Gap filling was performed in order to ensure the inclusion of peaks that may have been detected in some scans, but not in others, resulting in their undesired elimination from the list. After manual removal of peaks detected in the negative control, methanol blank and reserpine standard samples, a total of 174, 145 and 103 distinct mass features (each with

their own *m/z*, t_R and peak area) remained for *K. cystarginea*, *K. griseola* and *Streptomyces* sp. RKND004 extracts, respectively.

The resulting processed peak list was exported into Microsoft Excel resulting in a two-dimensional data matrix displaying the peak area of each defined mass feature in each sample. Using conditional formatting, cells in the spreadsheet containing a peak area greater than zero were coloured black, while those with an area equal to zero (i.e. not detected in that sample) were coloured white creating a presence-absence chemical barcode for each strain (Figure 2.1). The barcodes were used as a tool to visualize metabolites exhibiting an induction effect which may be selected for further investigation.

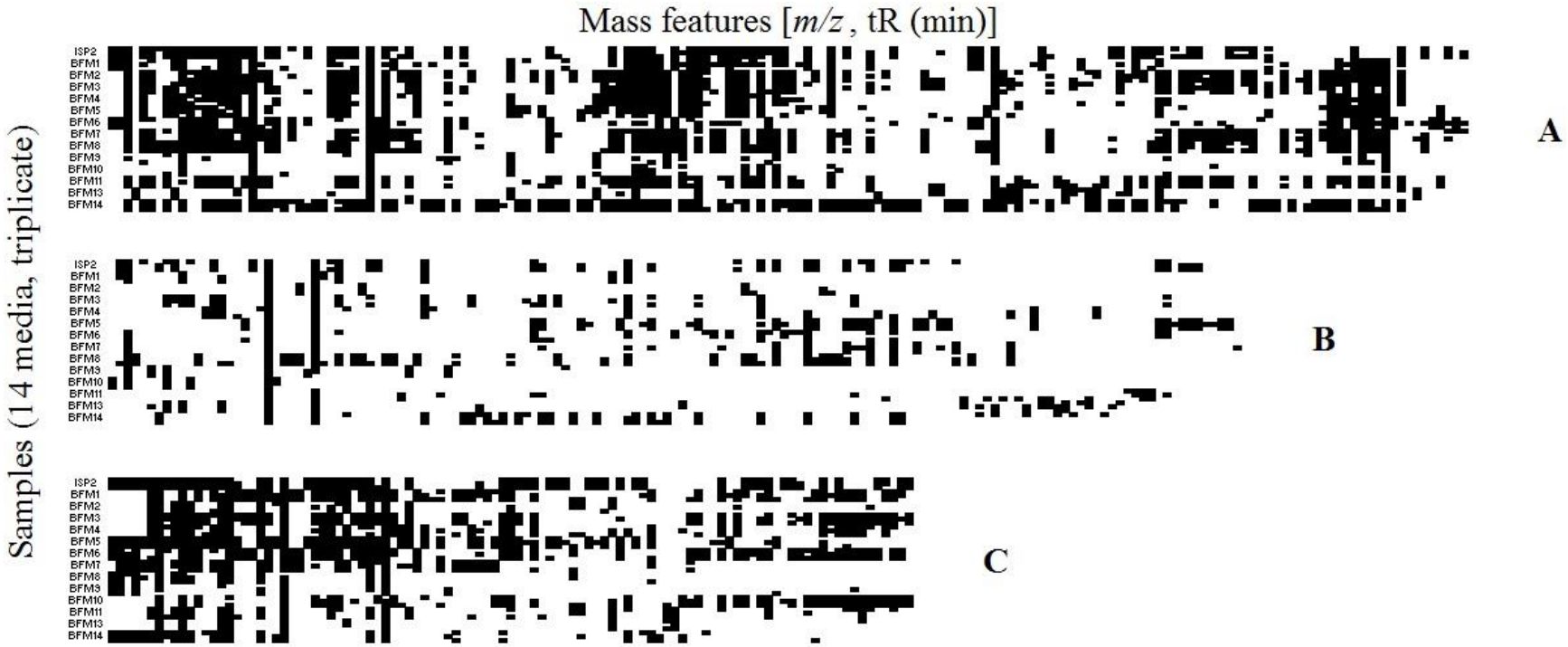

Figure 2.1. Presence-absence chemical barcodes generated by metabolomic analysis of **A**. *K. cystarginea* (174 mass features), **B**. *K. griseola* (145 mass features) and **C**. *Streptomyces* sp. RKND004 (103 mass features). Columns represent different mass features with a distinct *m/z* and t_R while rows represent different samples. Each barcode contains 42 rows; three replicates for each of the 14 media. Cells coloured in black indicate the presence of that mass feature in the sample above the defined mass detection threshold of 1E4. White cells indicate mass features that were not present above the 1E4 threshold. All three barcodes are shown for comparison and scaled to fit in one figure; cells from one barcode aligning in the same column as cells from another barcode do not indicate the presence of the same mass feature in both samples.

The barcode generated for *K. griseola* highlighted the presence of two features with a mass difference that suggested they may be analogues. The signals were located in the raw data (Xcalibur software, Thermo Scientific) and identified as the protonated adducts of two metabolites; *m/z* 542.3230 $[M+H]^+$, t_R 3.69 min and its apparent methylated analogue *m/z* 556.3386 $[M+H]^+$, t_R 3.86 min. Both compounds were produced in all replicates above the 1E4 threshold when the strain was grown in ISP2, BFM3, BFM4 and BFM14, while *m/z* 556.3386 $[M+H]^+$ was also produced consistently above the threshold when the strain was grown in BFM2, and BFM9 (Figure 2.2). These metabolites had been previously observed by former Ph. D. candidate in our lab Dr. Krista Gill, who had grown the strain in a lean production medium called 1045. When queried in both the AntiBase [134] and SciFinder databases, the exact masses of these metabolites did not match any known natural products. Additionally, our lab had sequenced the strain's genome and thus if the compounds were purified and their structures elucidated, it may be possible to attribute a gene cluster to their production. Thus, the compounds were prioritized for further investigation. Unfortunately all subsequent efforts to obtain these compounds via fermentation on multiple scales were unsuccessful as the strain produced either a very low quantity or none at all, and their identities were left undetermined.

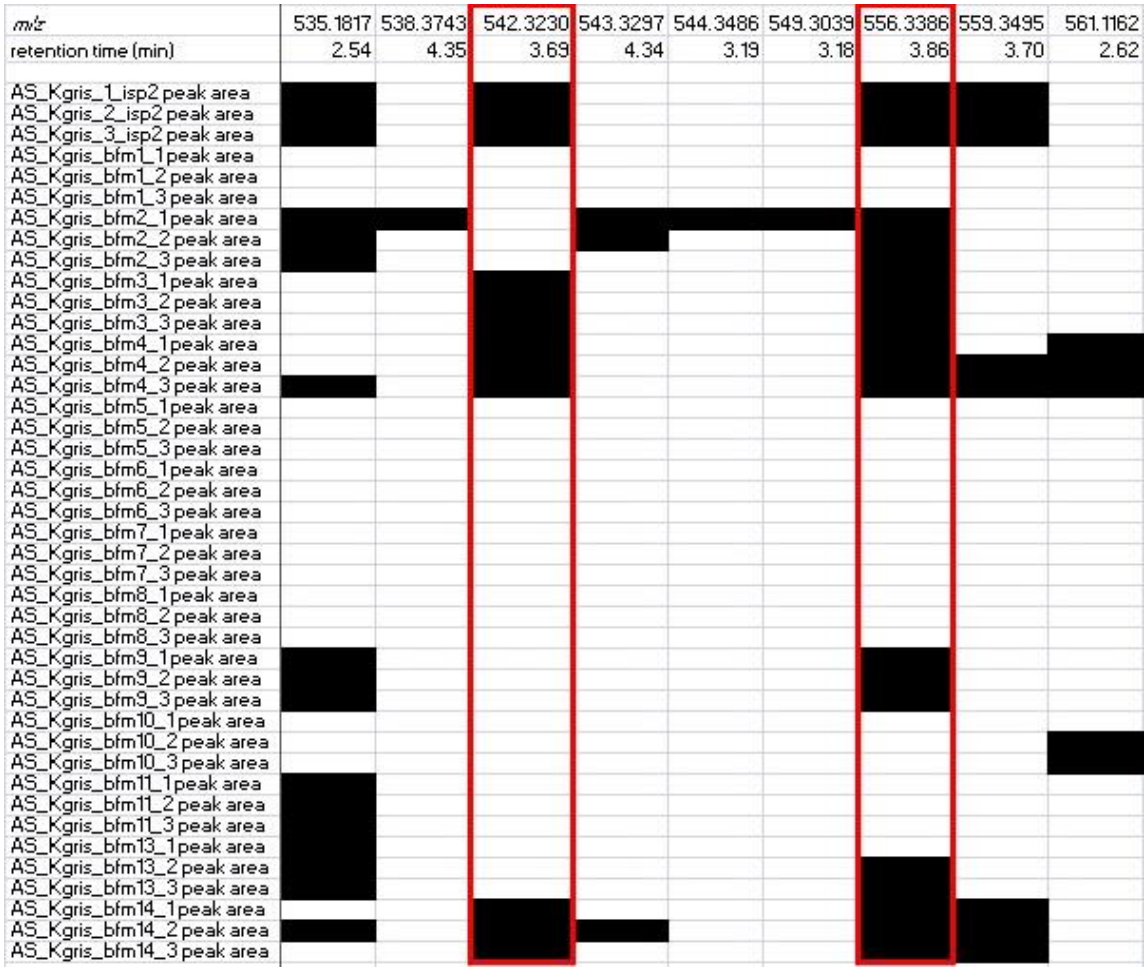

Figure 2.2. An enlarged section of the *K. griseola* chemical barcode showing the putatively induced metabolites *m/z* 542.3230 $[M+H]^+$, t_R 3.69 min and *m/z* 556.3386 $[M+H]^+$, t_R 3.86 min. Both metabolites were detected above the 1E4 mass detection threshold in all replicates when the bacterium was grown in ISP2, BFM3, BFM4 and BFM14, while *m/z* 556.3386 $[M+H]^+$ was also produced using BFM2 and BFM9.

The barcode generated for the Prince Edward Island strain *Streptomyces* sp. RKND004 revealed the presence of a number of mass features with a similar *m/z* and t_R that were detected above the threshold in the same set of conditions. Figure 2.3 shows an enlarged section of the barcode containing this family of relatively large molecular weight (*m/z* >700) pseudomolecular ions. Additionally, a large, broad peak corresponding to the presence of these compounds was observed in the LC-MS chromatograms for extracts of this strain grown only in certain media (Figure 2.4). Since natural products with large molecular weights have a higher likelihood of being novel, and since our unique Prince Edward Island strain had not yet been explored for natural product production, this family of compounds was prioritized for further study.

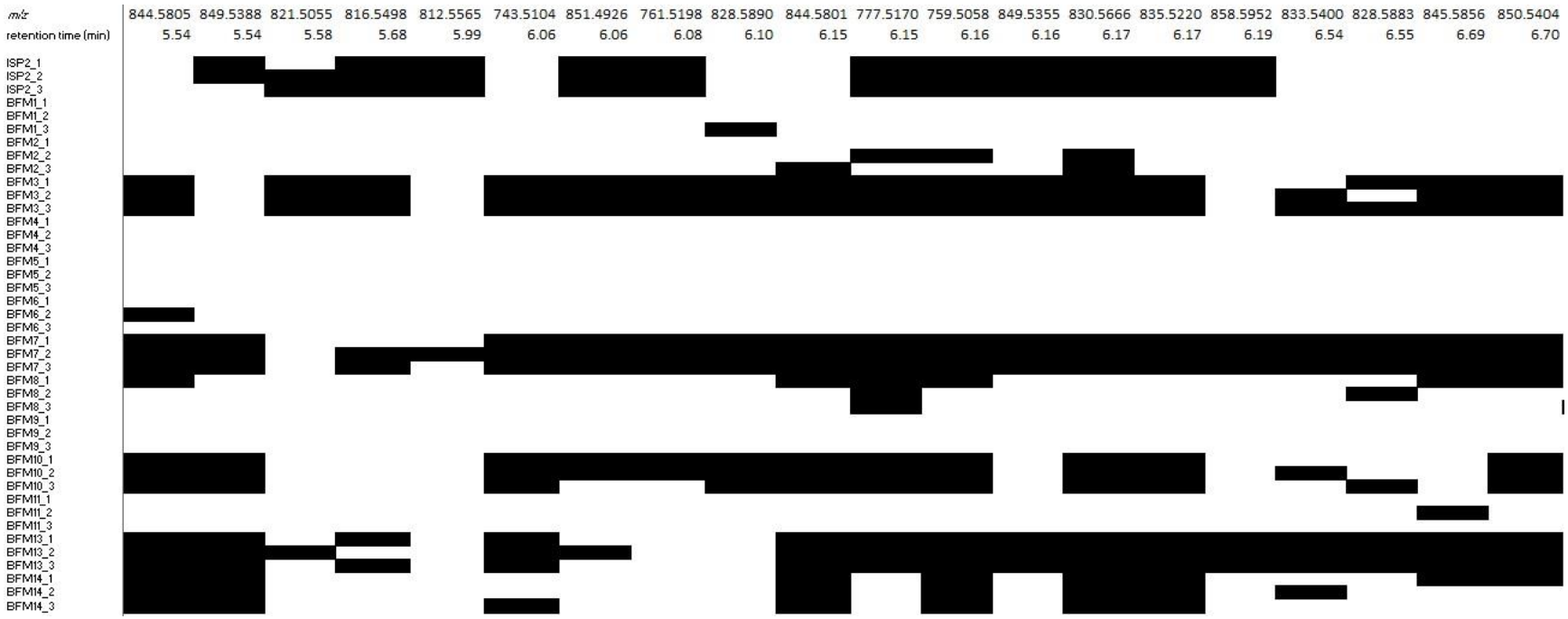

Figure 2.3. An enlarged section of the *Streptomyces* sp. RKND004 chemical barcode showing a family of relatively large molecular weight metabolites (*m/z* > 700). The compounds eluted at close retention times and were present above the 1E4 mass detection threshold in similar conditions. Generally, the production of these compounds was putatively induced when the bacterium was grown in ISP2, BFM3, BFM7, BFM10, BFM13 and BFM14.

A

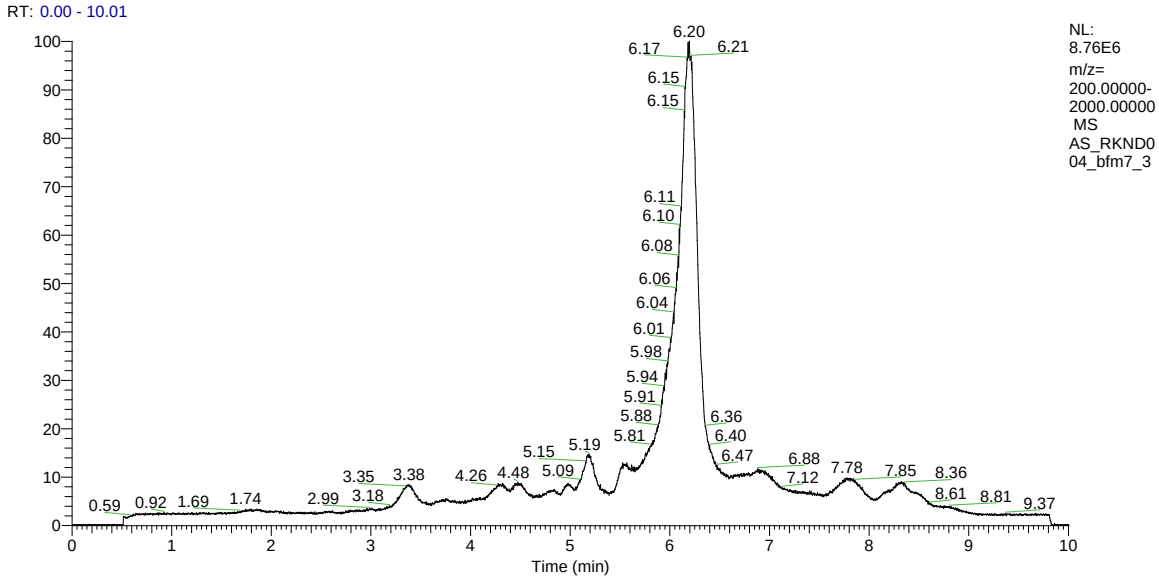

B

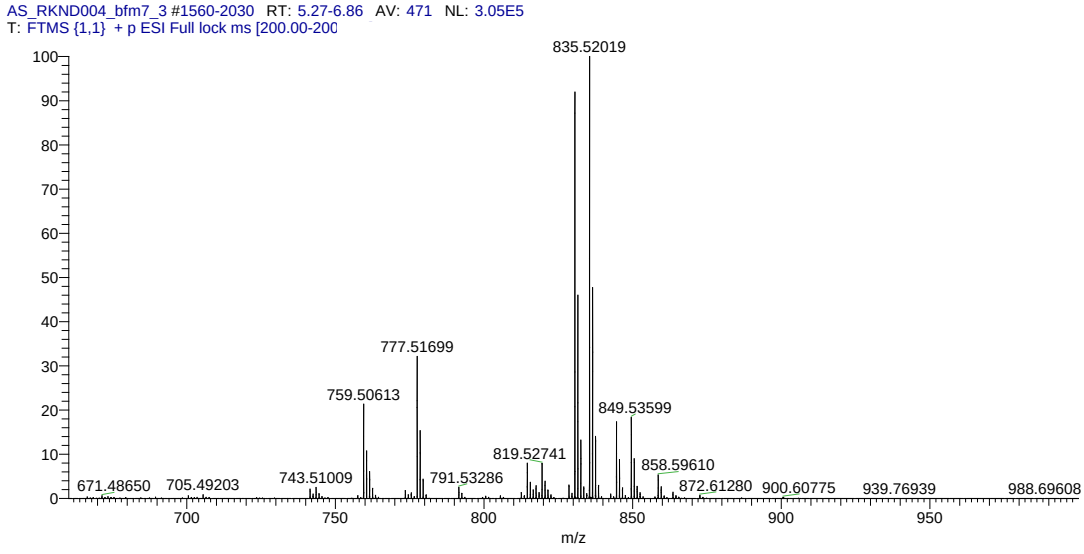

Figure 2.4. **A**. Total ion chromatogram (TIC) of the crude extract of *Streptomyces* sp. RKND004 grown in BFM7 generated using an HRMS detector with an electrospray ionization (ESI) probe in positive mode. **B**. The high-resolution mass spectrum at the retention times from 5.3-6.6 min.

The most abundant compound was identified by two pseudomolecular ions observed in the raw LC-MS data: *m/z* 830.5668 $[M+NH_4]^+$, t_R 6.20 min and *m/z* 835.5186 $[M+Na]^+$, t_R 6.20 min. To better visualize the induction effect, an ion intensity plot monitoring the intensity of the sodiated adduct was generated using MZmine 2 (Figure 2.5). Since each extract was resuspended to a concentration of 500 μg/mL prior to analysis and the data normalized with respect to the largest peak within each individual sample, the ion intensity plot compares the production of the targeted compounds relative to other metabolites in the same sample across each of the different media screened. This approach does not take into account the actual mass of the metabolites present in the sample. Alternatively, resuspension of each extract in the same volume of methanol before analysis would have allowed a direct comparison of the quantity of each target produced between samples giving an idea of which condition physically produced the most. Using the latter method however, metabolites present in extracts with a small mass may have fallen below the detection threshold in the more dilute samples and been excluded from the peak lists. To ensure the inclusion of all metabolites, the first method of normalization was used and the mass of the extracts was considered in combination with the relative production of the targets when comparing different conditions.

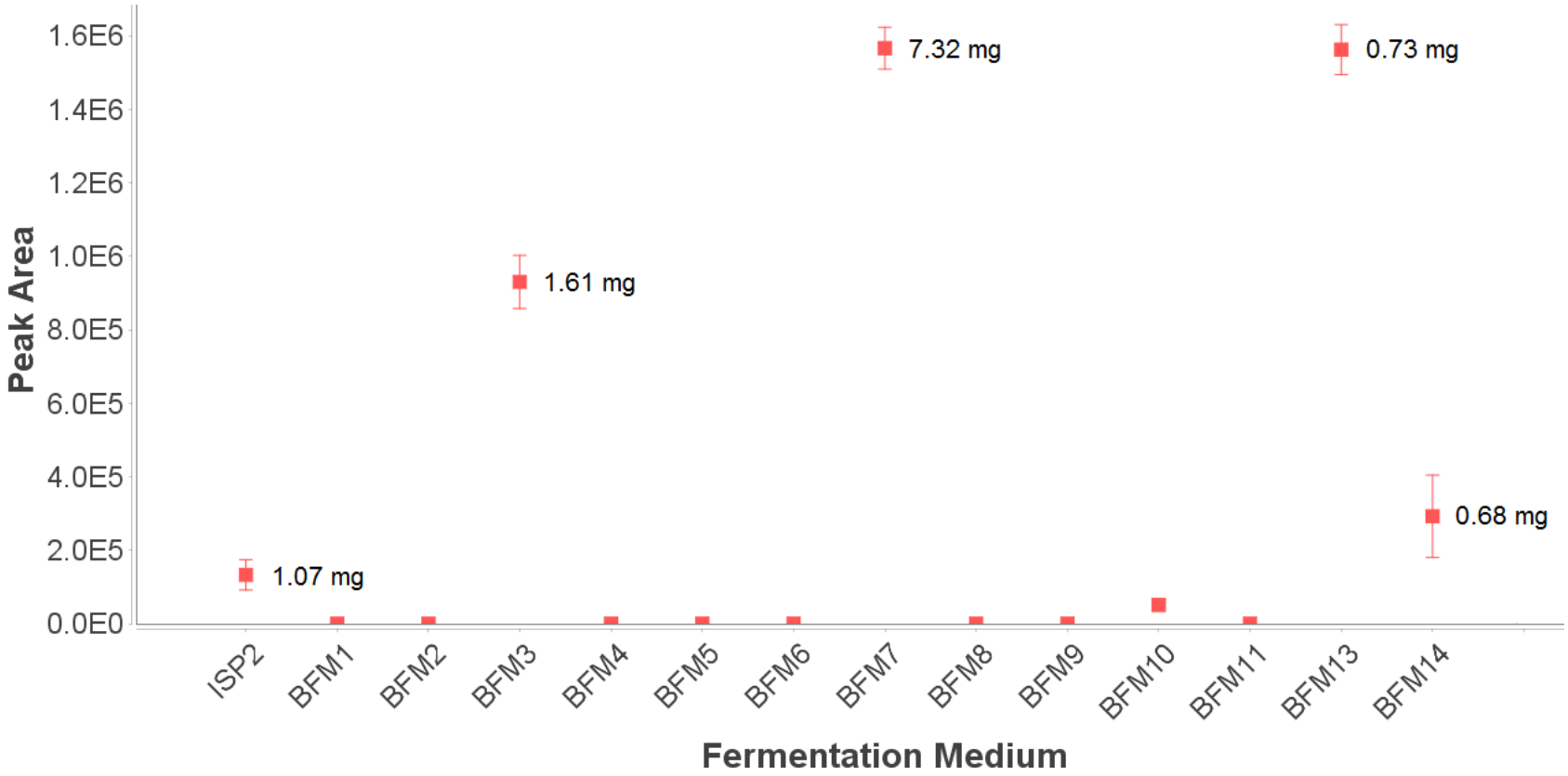

Figure 2.5. Ion intensity plot displaying the peak area of the sodiated adduct *m/z* 835.5186 $[M+Na]^+$ in each different fermentation medium. The average mass of the extracts for each condition is shown for comparison.

Figure 2.5 shows the peak area of *m/z* 835.5168 $[M+Na]^+$, t_R 6.20 min when the strain was grown in each of the different media. The compound was only present above the 1E4 mass detection threshold when *Streptomyces* sp. RKND004 was grown in ISP2, BFM3, BFM7, BFM10, BFM13 and BFM14. Extracted ion chromatograms (XICs) from the raw data monitoring the sodiated adduct confirmed that the compound was not present below the threshold in extracts from other media (except trace amounts in BFM8 and BFM4), confirming a true induction took place (Appendix Figure 6.1). Since the analysis does not take into account the physical quantity of the compound present in each condition, the average mass of the extracts were also noted in Figure 2.5. Considering this, BFM7 was the best medium to facilitate the production of this compound, however the mass of BFM7 broth extracts was artificially large presumably due to the undesired extraction of olive oil present in the media. To avoid this issue, BFM3 was chosen for future scaled-up fermentations.

In the raw data, the $[M+H]^+$ adduct (*m/z* 813.5151, t_R 6.20) was either absent or present at extremely low intensities. Lack of this signal suggested that the nature of the compound may cause the protonated adduct to be difficult to form, for example a compound containing an acid moiety. To confirm this, the samples were re-analyzed using an identical method with the instrument in negative mode which revealed *m/z* 811.5205, t_R 6.20 as the $[M-H]^-$. A query of AntiBase and SciFinder returned only one match to a compound named N664-30, a polyether ionophore compound reported only once in the literature in a patent containing minimal data [135]. Despite this one hit, the investigation of this compound was continued on the basis of the induction effect, the unique producing bacterium, the possibility that the compound may still be new and the

likelihood of finding additional analogues based on the large number of pseudomolecular ions present in the raw data.

Although two families of compounds were identified as targets for further investigation, the media study revealed many other putatively induced metabolites that have not yet been pursued. Using the chemical barcodes as an identification tool, a list of high-priority candidates for subsequent scale-up and purification was created as a starting point for future efforts to discover new, induced natural products (Table 2.2). Mass features that were present above the threshold when the strain was grown in only one of the 14 media and in all three replicates were highlighted and located in the raw data. Since the chromatograms generated using the evaporative light-scattering detector (ELSD) give the most accurate indication of the relative amounts of the metabolites present, the $[M+H]^+$ and all other abundant pseudomolecular ions for each true metabolite with a visible peak in the ELSD trace were recorded while others were eliminated from the list. Thus, the remaining metabolites were estimated to be present in sufficient quantities for purification following scaled-up fermentations. The *m/z* of the $[M+H]^+$ and $[M+Na]^+$ for each candidate was queried in AntiBase and metabolites that had close bacterial natural product hits were eliminated from the table. A total of 12 putatively new, induced natural products remained which have to potential to be purified.

Table 2.2. Summary of putatively new, induced metabolites discovered by OSMAC experiments which are produced in sufficient relative quantities for purification.

Bacterium	Medium	*m/z* $[M+H]^+$	t_R (min)	Other observed adducts	Possible analogues
K. cystarginea	BFM2	981.4763	2.79	$[M-H_2O+H]^+$; $[M+Na]^+$	
	BFM9	375.3211	2.66	$[M+Na]^+$	
	BFM9	387.3217	2.71	$[M+Na]^+$	369.3102+H_2O
	BFM9	369.3102	2.73	$[M+Na]^+$	
	BFM9	389.3385	2.74	$[M+Na]^+$	375.3211+CH_2
	BFM9	401.3375	2.82	$[M-H_2O+H]^+$; $[M+Na]^+$	387.3217+CH_2; 369.3102+2OH
	BFM9	777.5246	2.92	$[M+Na]^+$	
	BFM10	431.1340	2.30	$[M+Na]^+$	
K. griseola	BFM4	269.0809	3.13	$[M+Na]^+$	
	BFM5	300.1343	1.78	$[M+Na]^+$	
	BFM9	421.1282	3.74	$[M+Na]^+$	
	BFM14	397.3829	6.21	$[M+Na]^+$	

2.1.5. Large-scale fermentation and purification of terrosamycin A and B

The search for new and induced compounds employing the OSMAC approach using different media types lead to the discovery of *m/z* 811.5205 $[M-H]^-$, a metabolite whose biosynthesis was induced in a number of conditions. The producing bacterium *Streptomyces* sp. RKND004 was fermented on a large scale in 9 L of BFM3 broth which was shown to produce relatively large quantities of the compound. The cultures were extracted with ethyl acetate and the resulting deep-red coloured extracts were combined and fractionated by automated flash chromatography using a C_{18} stationary phase. Subsequent fractionation via automated flash chromatography with a silica stationary phase afforded 7.3 mg of **1** and 85.8 mg of **2** which were named terrosamycin A and terrosamycin B, respectively.

2.1.6. Crystallization of terrosamycin A and analysis of X-ray diffraction data

Preliminary NMR data acquired on impure samples during the purification process showed signals consistent with a polyether structure, suggesting the terrosamycins may belong to this family of natural products. Polyether natural products contain a carboxylic acid moiety and many stereocentres and thus structure elucidation is most often achieved through conversion to a salt, crystallization and X-ray diffraction (XRD) analysis of the crystal [66, 67]. Salts of **1** and **2** were prepared using sodium hydroxide and subjected to a number of different crystallization conditions in an attempt to obtain crystals suitable for XRD analysis. Crystals of the terrosamycin A salt were obtained using a slow evaporation method with acetone and diH_2O at 4 °C. XRD analysis and structure refinement was performed by Dr. Andreas Decken at the University of New Brunswick in Fredericton, New Brunswick, Canada (Appendix Tables 6.1-6.3).

The XRD analysis revealed terrosamycin A (**1**) is indeed a polyether compound. The structure features one five-membered and four six-membered heterocyclic rings containing ether linkages (Figure 2.6). As is common to all compounds in this family, a carboxylic acid functional group is located at one end of the molecule. Terrosamycin A also contains a ketone functionality as well as five hydroxyl groups, two of which are bound to carbon atoms of ether groups forming cyclic hemiketals. In addition, 11 methyl groups are found along the carbon chain. Twenty stereocentres are located within the structure and are defined in Figure 2.6 **C**. Curiously, crystallization and XRD analysis of the terrosamycin B salt resulted in an identical crystal structure. As the molecular weight was not in agreement, it was hypothesized that one of two events had taken place; the crystals obtained were due to a small amount of **1** present as an impurity in the sample, or perhaps the conditions used to prepare the salts caused a conversion of **2** to **1** prior to crystallization.

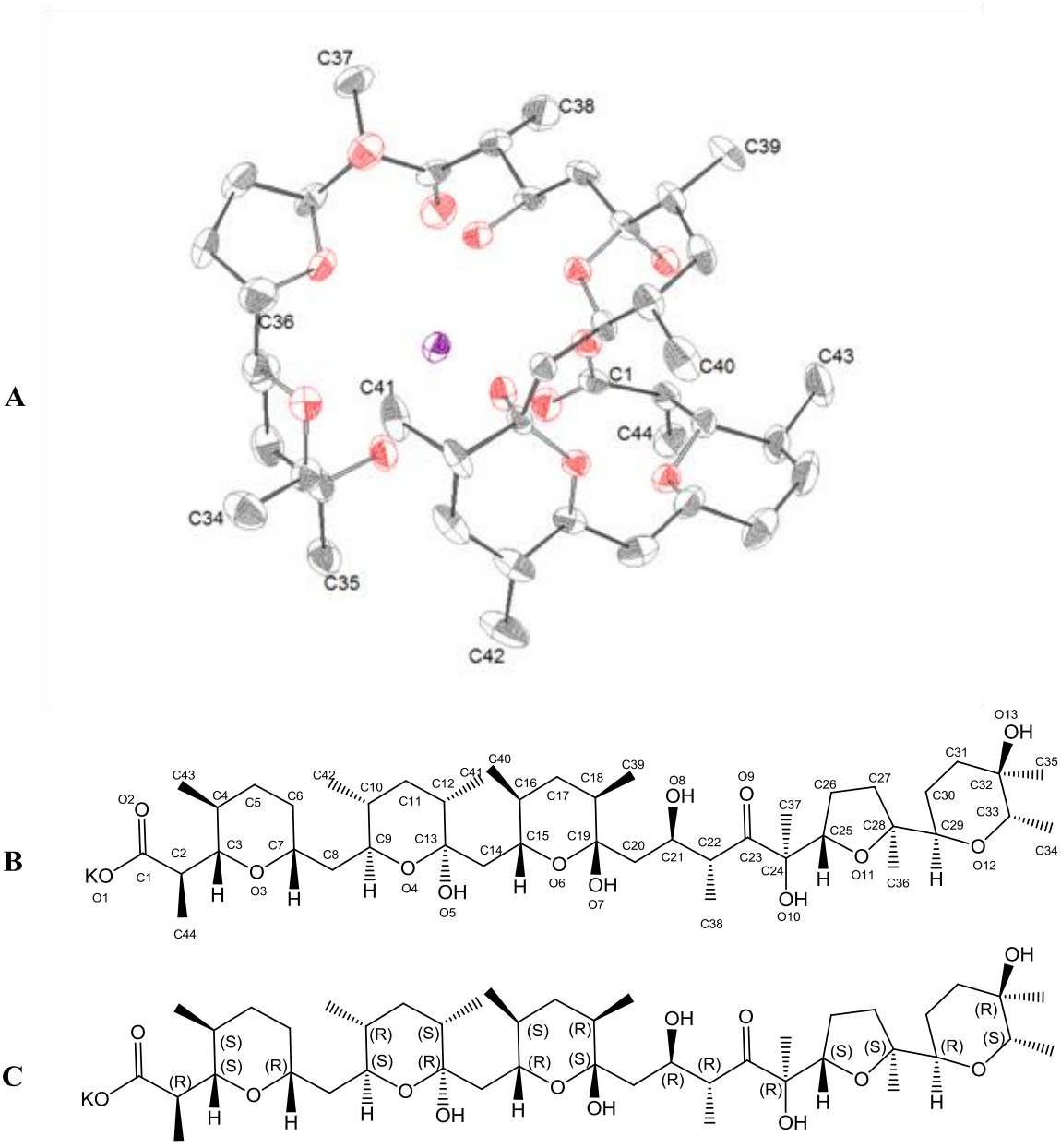

Figure 2.6. **A**. The crystal structure of the terrosamycin A potassium salt with oxygen atoms coloured red and potassium coloured purple. A second identical complex and solvent molecules were removed from the repeating unit for clarity. **B**. Molecular structure of terrosamycin A with numbering scheme used in XRD structure elucidation. **C**. Molecular structure of terrosamycin A with all stereocentres defined.

As discussed in Chapter 1, polyether natural products are known to form complexes with monovalent and divalent metal cations [66, 67] . The metals can coordinate to oxygen and nitrogen atoms within the structure causing the polyether to wrap itself around the metal. This process results in a cage-like formation with a hydrophilic inner-sphere and hydrophobic outer-sphere giving polyethers useful biological properties which will be discussed in section 2.1.8. The complexes are usually stabilized by intramolecular hydrogen bonding involving the carboxylic acid and hydroxyl groups [67]. The crystal structure of **1** shows complexation in a cage-like formation around a potassium atom. Figure 2.7 shows coordination bonds from the metal to the O1, O2, O5, O8, O9, O11, O12 and O13 atoms indicating an eightfold coordination which is typical of potassium 136. Dotted lines in Figure 2.7 depict the three hydrogen bonds (O7-H7…O1, O8-H8…O6 and C21-H21…O1) which were found within the inner-sphere and likely contribute to stabilization of the complex.

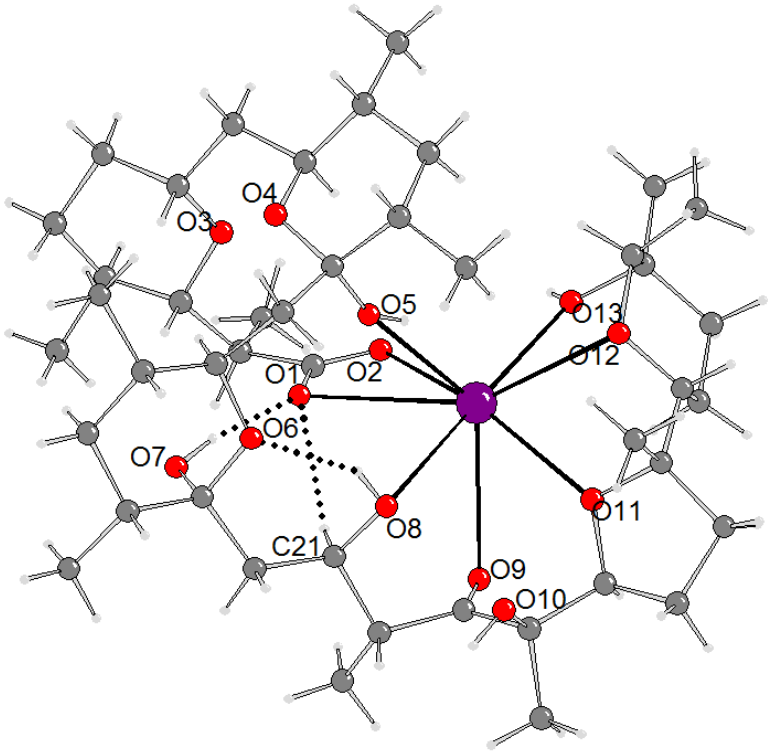

Figure 2.7. The crystal structure of terrosamycin A (**1**) showing coordination bonds (solid black) between oxygen atoms O1, O2, O5, O8, O9, O11, O12 and O13 and potassium. Three hydrogen bonds (dotted black) were found within the molecule between O7-H7…O1, O8-H8…O6 and C21-H21…O1.

The observed coordination to potassium is surprising; since the salts of these compounds were prepared using aqueous sodium hydroxide, the metal atom was expected to be sodium. The supplier of the sodium hydroxide used to prepare the aqueous solution reports the presence of trace amounts of potassium up to a concentration of 0.02%. This suggests that **1** selectively binds potassium despite a large excess of sodium. This phenomenon is not uncommon among members of the polyether family and binding studies involving numerous monovalent and divalent metal cations are often performed generating a selectivity order. Salinomycin, perhaps the most well-studied polyether antibiotic, can complex both monovalent and divalent metal cations with an affinity order of $K^+ > Na^+ > Cs^+ > Sr^{2+} > Ca^{2+} = Mg^{2+}$ [67]. Ionomycin is selective for divalent cations in the order $Ca^{2+} > Mg^{2+}$, where binding to Sr^{2+} and Ba^{2+} was insignificant [137]. Calcimycin, as the name suggests, has a high affinity for Ca^{2+} [138] but can also form a 2:1 complex with Mg^{2+}, Ni^{2+} and Zn^{2+} [139, 140, 141]. The size, shape of the cage formed around the metal, as well as the number of ligands available for coordination, is what influences the selectivity of each complex. Cations with an atomic radius that fit the cage will bind easily; smaller cations must adopt a non-optimal coordination geometry and larger ones must distort the cage in order to fit [67, 142, 143]. Interestingly, coordination to different metal cations can influence the bioactivity of the entire complex. The 2:1 salt complexes of monensin with Ba^{2+} and Mg^{2+} showed superior growth inhibition of *Mycobacterium tuberculosis* than various other monovalent and divalent cationic complexes [144]. Cationomycin forms a more stable complex with K^+ than Na^+ and was found to transport K^+ across bacterial cell membranes at a higher rate [145].

The structure of **1**, including the stereochemistry of all chiral centres, is identical to that of N664-30 which was found as a match in AntiBase and SciFinder when the exact mass of the $[M+H]^+$ and $[M+Na]^+$ adducts were queried. The compound has only been reported once before; N664-30 along with its producing strain *Streptomyces* sp. N664-30 were patented by Pfizer Inc. in 1990 [135]. The structure was determined using XRD and tentatively reported with 98% confidence causing the patent to include only a compound possessing the physical and chemical properties described. No XRD, NMR or other structural data was included in the patent. Though the authors describe possible use of the compound as an antibiotic for large farm animals and domestic pets, and as an anticoccidial agent for chickens, there is no mention of any specific bioactivity except that activity against "certain" Gram-positive and Gram-negative microorganisms was observed. Due to the lack of information included in the now expired patent, **1** and **2** named terrosamycin A and B, were further investigated in our lab. Since crystals of the terrosamycin B salt were not obtained, its structure was elucidated spectroscopically.

2.1.7. Spectroscopic structure elucidation of terrosamycin A and B

Terrosamycin A (**1**) and B **(2**) were both isolated as a colourless glass and HRESIMS analysis supported molecular formulae of $C_{44}H_{75}O_{13}$ (*m/z* 811.5205 $[M-H]^-$, Δ = 0.1 ppm) and $C_{46}H_{79}O_{13}$ (*m/z* 839.5504 $[M-H]^-$, Δ = 0.2 ppm), respectively. The molecular structure of **1** deduced from the crystal structure contains seven degrees of unsaturation accounted for by the carboxylic acid, ketone and five rings which matched the degree of unsaturation predicted by the molecular formula. The degree of unsaturation predicted for **2** was also seven suggesting similar structural features.

The NMR data for terrosamycin A (**1**) (Table 2.3) was in agreement with the crystal structure. The characteristic carboxylic carbon resonance C-1 (δ_C 183.6) and the HMBC correlations between H-2 (δ_H 2.58)/C1, H-3 (δ_H 3.66)/C-1 and H-44 (δ_H 1.08)/C-1 located the acid moiety on one end of the molecule. COSY correlations between neighbouring CH and CH_2 protons confirmed the connectivity of the carbon chain from C-2 (δ_C 44.5) through to C-12 (δ_C 30.4). Methyl groups were located along the chain by the COSY correlations H-44/H-2, H-43 (δ_H 0.87)/H-3, H-42 (δ_H 0.78)/H-10 (δ_H 1.29) and H-41 (δ_H 0.87)/H-12 (δ_H 1.49) which were further validated by the appropriate HMBC correlations. The relatively downfield chemical shifts of C-3 (δ_C 82.6) and C-7 (δ_C 75.5) indicated the presence of oxygen between them locating the ether linkage within the first six-membered ring. The chemical shifts of the alpha protons H-3 and H-7 (δ_H 3.67) were in agreement with this assignment.

Table 2.3. ^{1}H (600 MHz) and ^{13}C (150 MHz) NMR data for terrosamycin A (**1**) and terrosamycin B (**2**) in MeOD-d_4.

	terrosamycin A (**1**)				terrosamycin B (**2**)			
No.	**δ_C, type**	**δ_H, (*J*, Hz)**	**COSY**	**HMBC**	**δ_C, type**	**δ_H, (*J*, Hz)**	**COSY**	**HMBC**
1	183.6, C				178.9, C			
2	44.5, CH	2.58, dq (4.4, 7.2, 11.0)	3, 44	1, 3, 44	42.4, CH	2.64, dq (3.1, 6.8, 9.7)	3, 44	1, 3, 44
3	86.2, CH	3.66, m	2, 4	1, 2, 4, 5, 43, 44	84.4, CH	3.45, dd (3.0, 9.8)	2, 4	1, 2, 5, 43, 44
4	33.4, CH	1.51, m	3, 5b, 43	3, 5, 43, 44	33.5, CH	1.45, m	3, 5b, 43	3, 43
5	33.6, CH_2	1.47, m	4, 5a, 6	3, 4, 44	34.0, CH_2	1.53, m	4, 5a, 6a	4
		1.28, m	5b, 6b	3, 7, 43		1.21, m	5b, 6b	3, 4, 7
6	35.2, CH_2	1.86, m	5	3, 5, 7	34.1, CH_2	1.80, m	5, 7	3, 7
		1.28, m	5b, 6b, 7	7		1.27, m	5b, 6b, 7	5
7	75.5, CH	3.67, m	6a, 8	3, 6, 8, 9	75.2, CH	3.56, appt[a] (10.0)	6, 8	3, 6, 8, 9
8	39.9, CH_2	1.67, m	7, 8a, 9	7, 9, 10	41.0, CH_2	1.62, m	7, 8a	7, 9
		1.15, m	7, 8b, 9	6, 7, 10		1.34, m	7, 8b, 9	9
9	75.6, CH	3.65, m	8, 10	7, 8, 11, 42	73.6, CH	3.32, td (1.7, 3.3)	8a, 10	7, 8, 11, 42
10	37.7, CH	1.29, m	9, 11b, 42	9, 11, 42	36.6, CH	1.28, m	9, 11, 42	11
11	38.6, CH_2	1.37, m	10, 11a, 12	10, 12, 13, 41	38.4, CH_2	1.42, m	10, 11a	13, 9
		1.30, m	11b	9, 10, 12, 13, 41		1.30, m	10, 11b, 12	9, 14, 41
12	30.4, CH	1.49, m	11, 41	11, 41	36.9, CH	1.98, m	11a, 41	11, 41
13	99.8, C				101.9, C			
14	44.3, CH_2	1.82, dd (7.9, 14.8)	14a, 15	12, 13, 15, 16	38.3, CH_2	1.92, m	14a, 15	12, 13, 15, 16
		1.66, m	14b	13, 16		1.83, m	14b	12, 13, 16
15	72.9, CH	4.10, dd (8.2, 10.1)	14b, 16	13, 14, 17, 40	74.0, CH	3.38, m	14b, 16	13, 14, 17, 40
16	36.9, CH	1.40, m	15, 17, 40	13, 15, 17, 40	37.0, CH	1.48, m	15, 17b, 40	40
17	38.0, CH_2	1.48, m	17, 18	15, 16, 18, 19, 39, 40	38.0, CH_2	1.37, m	16, 17a, 18	18, 39, 40
						1.29, m	17b, 18	18, 19, 39, 40
18	40.2, CH	1.72, m	17, 39	17, 19, 20, 39	39.4, CH	1.89, m	17, 39	17, 39
19	101.3, C				102.4, C			
20	43.1, CH_2	2.08, dd (1.2, 14.1)	20a	18, 19, 21, 22	39.6, CH_2	2.08, m	20a	18, 19, 21, 22
		1.57, dd (3.2, 10.5)	20b, 21	18, 19, 21, 22		1.64, m	20b, 21	18, 19, 21, 22
21	74.9, CH	4.22, appt[a] (10.0)	20a, 22	19, 20, 22, 23, 38	72.2, CH	4.03, appt[a] (8.5)	20a, 22	18, 19, 20, 22, 23, 38
22	45.6, CH	3.5, dq (6.7, 9.8, 13.6)	21, 38	20, 21, 23, 38	47.6, CH	3.20, dq (5.5, 6.8, 13.8)	21, 38	19, 20, 21, 23, 38

23	220.7, C				217.9, C			
24	79.9, C				80.7, C			
25	84.9, CH	4.47, dd (5.6, 10.4)	26	23, 24, 26, 27, 37	84.7, CH	4.24, dd (6.0, 8.8)	26	23, 24, 26, 27, 37
26	25.8, CH_2	2.05, m	25, 26a, 27	24, 25, 27, 28	26.5, CH_2	2.01, m	25, 26a, 27	24
		1.86, m	25, 26b, 27a, 27b	24, 27, 28		1.93, m	25, 26b, 27b	24, 27
27	33.6, CH_2	2.05, m	26, 27a	25, 26, 28, 29, 36	34.8, CH_2	2.08, m	26, 27a	26, 28, 29, 36
		1.65, m	26, 27b	25, 26, 28, 36		1.63, m	26b, 27b	25, 26, 36
28	84.9, C				86.6, C			
29	74.9, CH	3.56, dd (2.3, 11.8)	30	27, 28, 30, 31, 33, 36	74.9, CH	3.40, m	30	27, 28, 30, 33, 36
30	22.0, CH_2	1.90, m	29, 30a, 31a	28, 29, 31, 32	22.8, CH_2	1.67, m	29, 30a, 31a	
		1.60, m	29, 30b, 31	28, 29, 31, 32		1.42, m	29, 30b, 31	32
31	31.8, CH_2	1.76, td (4.5, 13.5)	30a, 31a	29, 30, 32, 33, 35	32.3, CH_2	1.71, m	30a, 31a	30
		1.66, m	30, 31b	29, 30, 32, 33, 35		1.60, m	30, 31b	32, 33
32	70.3, C				70.5, C			
33	79.2, CH	4.08, q (6.5, 13.7)	34	29, 31, 32, 34, 35	78.8, CH	3.72, q (6.6, 13.5)	34	29, 34, 35
34	16.1, CH_3	1.23, d (6.9)	33	32, 33	15.5, CH_3	1.19, d (7.3)	33	32, 33
35	27.2, CH_3	1.11, s		31, 32, 33	26.5, CH_3	1.03, s		31, 32, 33
36	26.3, CH_3	1.22, s		27, 28, 29	23.3, CH_3	1.12, s		27, 28, 29
37	21.2, CH_3	1.10, s		23, 24, 25	21.5, CH_3	1.23, s		23, 24, 25
38	15.0, CH_3	0.99, d (6.4)	22	21, 22, 23	15.5, CH_3	1.12, d (6.7)	22	21, 22, 23
39	17.0, CH_3	0.91, d (6.9)	18	17, 18, 19, 20	16.8, CH_3	0.88, d (6.5)	18	17, 18, 19, 20
40	18.8, CH_3	0.84, d (6.4)	16	14, 15, 16, 17	19.0, CH_3	0.86, d (6.5)	16	14, 15, 16, 17
41	17.2, CH_3	0.87, d (6.7)	12	10, 11, 12, 13, 14	17.1, CH_3	0.87, d (6.2)	12	10, 11, 12, 13, 14
42	18.0, CH_3	0.78, d (6.2)	10	9, 10, 11	18.3, CH_3	0.79, d (5.5)	10	9, 10, 11
43	17.5, CH_3	0.87, d (6.7)	4	3, 4, 5, 6	17.9, CH_3	0.84, d (6.8)	4	3, 4, 5, 6
44	10.7, CH_3	1.08, d (7.2)	2	1, 2, 3	9.6, CH_3	1.08, d (7.6)	2	1, 2, 3
45					47.6, CH_3	3.14, s		13
46					49.1, CH_3	3.27, s		19

[a]appt indicates an apparent triplet.

The two HMBC correlations H-11 (δ_H 1.30)/C-13 (δ_C 99.8) and H-41/C-13, and the lack of a C-13 cross peak in the HSQC spectrum suggested that C-13 was a quaternary carbon attached to C-12. Similar to the first ring, the second ether linkage was assigned between C-9 (δ_C 75.6) and C-13 based on the characteristic ether carbon chemical shifts and the alpha proton H-9 (δ_H 3.65). The HMBC correlations H-14 (δ_H 1.66)/C-13 and H-15 (δ_H 4.10)/C-13 showed attachment of the continuing polyether chain to C-13. Compared to C-9, the quaternary C-13 resonance was further downshifted which suggested the attachment of an electron withdrawing group. The XRD data confirmed this was a hydroxyl group revealing the first of two cyclic hemiketal functionalities.

Again, COSY correlations between neighbouring CH and CH_2 protons extended the carbon chain from C-14 (δ_C 44.3) to C-18 (δ_C 40.2) and the positions of two more methyl groups were established using the H-40 (δ_H 0.84)/H-16 (δ_H 1.40) and H-39 (δ_H 0.91)/H-18 (δ_H 1.72) correlations. Like C-13, C-19 (δ_C 101.3) was determined to be quaternary as no cross peak was observed in the HSQC spectrum at that resonance. The HMBC correlations H-17 (δ_H 1.48)/C-19, H-18/C-19 and H-39/C-19 connected C-18 to C-19. The second cyclic hemiketal functionality was revealed based on the C-15 (δ_C 72.9) and C-19 resonances, HMBC correlations H-20 (δ_H 1.57)/C-19 and H-21 (δ_H 4.22)/C-19 and confirmation of a hydroxyl group at C-19 based on XRD data.

COSY correlations H-20/H-21 and H-21/H-22 (δ_H 3.50) implied connectivity of C-20 to C-21 and C-21 to C-22 (δ_C 45.6). The downshifted resonances of C-21 and H-21 indicated attachment of an electron withdrawing group at C-21 which was confirmed to be a hydroxyl group by XRD. Another methyl group was placed at C-22 as a result of the COSY correlation H-22/H-38 (δ_H 0.99). The ketone was located at C-23 (δ_C 220.7) using

HMBC correlations H-21/C-23, H-22/C-23 and H-38/C-23. The HMBC correlation H-37 (δ_H 1.10)/C-23 suggested the presence of a methyl group on the carbon attached to the ketone at C-23. The lack of any COSY correlations for H-37 implied the methyl group may be attached to a quaternary carbon. An HMBC correlation between the methyl protons and a quaternary carbon, H-37/C-24 (δ_C 79.9) confirmed this attachment. Extending the chain, the HMBC signals H-25 (δ_C 4.47)/C-23 and H-25/C-37 (δ_C 21.1) showed connectivity between C-24 and C-25 (δ_C 84.9). As C-24 was a quaternary carbon with a relatively downshifted resonance, a hydroxyl group was assumed to be attached and again this was confirmed by XRD.

Connectivity of C-25 to C-26 (δ_C 25.8) and C-26 to C-27 (δ_C 33.6) was established by COSY correlations H-25/H-26 (δ_H 1.86) and H-26/H-27 (δ_H 1.65). The HMBC correlations H-26/C-28 (δ_C 84.9) and H-27/C-28 showed attachment of C-27 to C-28 and the HSQC data suggested C-28 was quaternary. Again, based on the downfield chemical shifts of the carbons and alpha protons, an ether linkage was located between C-25 and C-28 closing the five-membered ring. The HMBC correlation H-36 (δ_H 1.22)/C-28 located a methyl group on C-28, and the H-29 (δ_H 3.56)/C-28 and H-36/C-29 correlations connected C-28 and C-29. COSY correlations H-29/H-30 (δ_H 1.60) and H-30/H-31 (δ_H 1.66) extended the carbon chain by confirming connection between C-29 and C-30 (δ_C 22.0), and C-30 and C-31 (δ_C 31.8). It was determined that the quaternary carbon C-32 (δ_C 70.3) was attached to C-31 due to observed HMBC correlations H-30/C-32 and H-31/C-32. An HMBC correlation H-35 (δ_H 1.11)/C-32 connected a methyl group to C-32, and the correlations H-35/C-33 (δ_C 79.2) and H-33 (δ_H 4.08)/C-32 established connectivity between C-32 and C-33. The remaining methyl group was attached to C-33

on the basis of the COSY correlation H-33/H-34 (δ_H 1.23). The downshifted resonances of C-29 and C-33 and their associated protons H-29 and H-33, as well as the HMBC correlations H-29/C-33 and H-33/C-29 placed the last ether linkage and closed the final ring. Finally, the downfield shift of the quaternary carbon C-32 revealed the remaining hydroxyl group was attached at this position.

The NMR data for terrosamycin B (**2**) (Table 2.3) revealed similar signals and correlations with the exception of two additional resonances; C-45 (δ_C 47.6) and C-46 (δ_C 49.1) and their corresponding protons H-45 (δ_H 3.14) and H-46 (δ_H 3.27) which had chemical shifts characteristic of methoxy groups. Their locations were confirmed by two HMBC correlations H-45/C-13 and H-46/C-19. The presence of two cyclic ketal functionalities rather than cyclic hemiketals was consistent with the molecular weight and predicted molecular formula for **2**. Since no XRD data was obtained, the stereochemistry of all 20 chiral centres is assumed to be the same as **1**. The key correlations used to determine the molecular structures are shown in Figure 2.8.

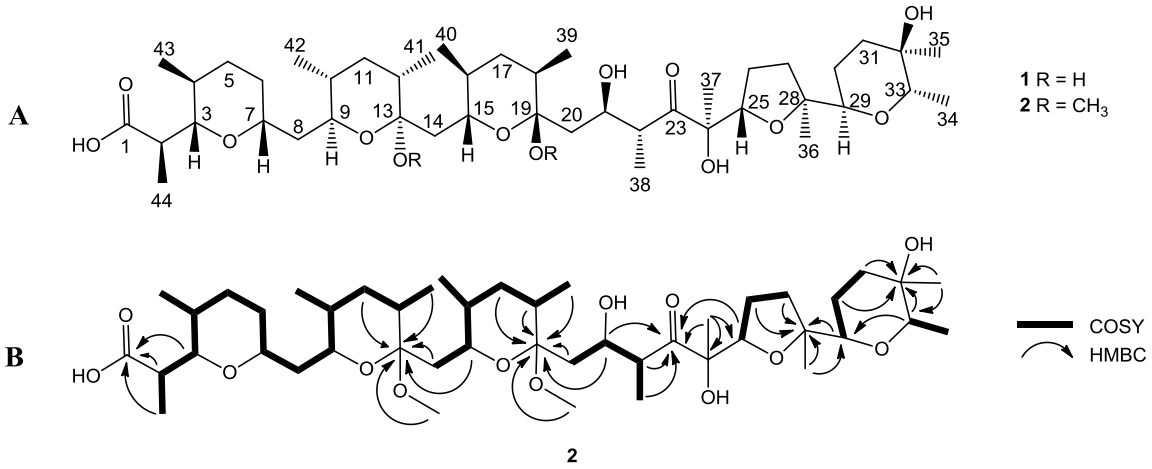

Figure 2.8. **A**. The molecular structure of terrosamycin A (**1**) and B (**2**). **B**. Key COSY and HMBC correlations used to elucidate the structure of terrosamycin B. Similar correlations were used to determine the structure of terrosamycin A.

Determination of the structure of **2** provided clarity as to why crystals of its salt were not obtained. Conversion of **1** to its potassium salt was achieved by first dissolving the compound in aqueous ethanol followed by dropwise addition of "NaOH". Dissolution of the polyether in aqueous ethanol resulted in acidic conditions due to the dissociation of the carboxylic acid. Subjecting **2** to these conditions would likely cause acid-catalyzed hydrolysis of the cyclic ketals to hemiketals [146], effectively converting **2** into **1** before the addition of NaOH (Figure 2.9). This explains why crystals from terrosamycin B samples possessed the structure of terrosamycin A. The stereochemistry at C-13 and C-19 can vary as nucleophillic attack by water may occur from either side; this offers an explanation for the broad peak for **1** observed in LC-MS chromatograms as water was used in the solvent system (Appendix Figure 6.1-6.2). Presumably, the crystal structure features the most stable enantiomers.

The conversion of ketals to hemiketals by hydrolysis is an equilibrium which occurs only under acidic aqueous conditions [147]. Thus, any time these compounds were exposed to water, an equilibrium between them was occurring. The purification of **1** and **2** involved liquid chromatography using a solvent system of water and methanol. The equilibrium typically lies in favour of hemiketal formation [147], though under these conditions it could shift toward formation of the ketal since methanol was present in relatively high concentrations. This may explain why a much higher quantity of **2** (85.8 mg) was obtained in comparison to **1** (7.3 mg) despite **1** being the most abundant compound in the crude extract (Appendix Figure 6.2).

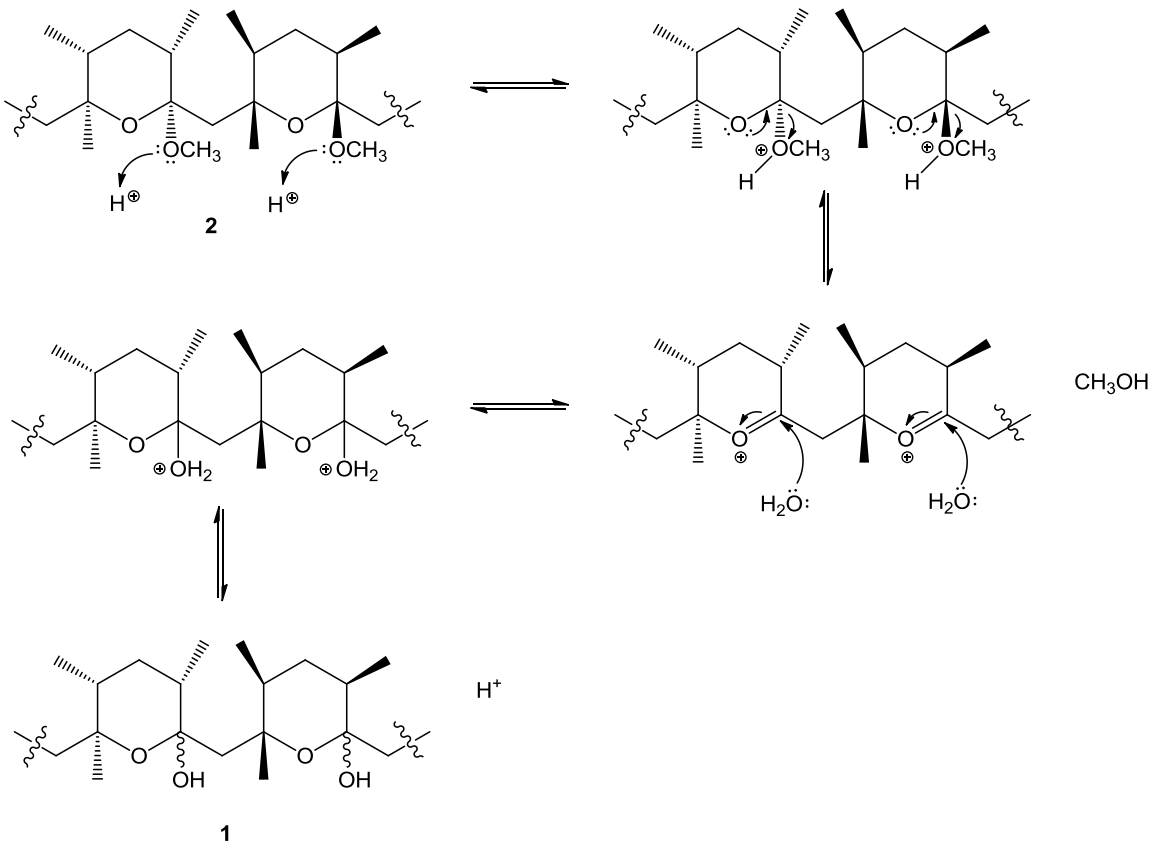

Figure 2.9. Proposed mechanism for the acid-catalyzed conversion of terrosamycin B (**2**) to terrosamycin A (**1**) under aqueous conditions.

The equilibrium that occurs between these two compounds raises questions as to whether terrosamycin B is a genuine natural product, or simply the result of methanolysis of terrosamycin A under acidic conditions with methanol. Though there are many polyether natural products that possess cyclic hemiketal functional groups [66, 67], there are few which possess cyclic ketals that have been reported. Ketal-containing derivatives of the polyether ionophores K-41 [66], X-14868B [148], maduramycin [149] and mutalomycin [77] have all been found to arise from synthetic modifications, whether performed intentionally or found accidentally. CP-70828 and CP-70228 are the only two reported compounds containing cyclic ketals that were claimed to be natural products [150]. The authors demonstrated both the purification of the compounds directly from fermentation broth and purposeful conversion between the hemiketal and ketal by treatment with methanol. This being said, it is questionable whether CP-70828 and CP70228 are genuine natural products; the use of large amounts of methanol during their purification may have caused methanolysis. To determine whether **2** was truly produced by *Streptomyces* sp. RKND004, the fermentation broth was extracted and analyzed without the use of methanol at any stage. An XIC revealed that **2** was still present in the crude extract despite never contacting methanol which suggests it is truly a natural product (Appendix Figure 6.17).

As mentioned earlier, terrosamycin A has been previously reported in a patent under the name N664-30 [135]. Since the patent leaves out many structural and biological properties, and analogue **2** is a new compound, our lab has renamed both compounds after the Prince Edward Island soil from which their producing bacterium was isolated. The name terrosamycin comes from “terra” meaning soil and “rosa” meaning red.

2.1.8. Bioactivity of terrosamycin A and B

Polyether natural products have been shown to exhibit a very wide range of biological effects including antibacterial, antifungal, antiviral and antiparasitic activities. Some members of this highly active family have also been explored for their potential as anti-cancer, anti-inflammatory and herbicidal agents [73]. Additionally, a number of polyethers possess immunoregulatory [81] or cardiovascular effects [80]. Despite all these interesting activities, polyether natural products are mostly known for their antibiotic activity against Gram-positive bacteria. As discussed in Chapter 1, they owe their potent antibiotic activity to their ability to act as an ionophore; a compound that is able to reversibly bind ions and transport them across cell membranes. Crystal structures determined from XRD studies have shown that these polyether ionophores wrap themselves around metal cations and bind via coordination of the oxygen atoms [66, 67]. The resulting complex is cage-like with the hydrophilic oxygen atoms comprising the inner-sphere. The inner-sphere is contained by the surrounding polyether hydrocarbon chain which renders the entire complex hydrophobic [67]. A space-filling model of the crystal structure of **1** is shown in Figure 2.10 illustrating this effect. Oxygen atoms can barely be seen in the centre of the complex and are essentially covered by the alkyl chain. These lipophilic complexes can easily penetrate the cell membrane of Gram-positive bacteria via three separate mechanisms [71]. Cell death arises as a result of the neutral metal-bound complex transporting cations into the cell which disrupts the Na^+/K^+ gradient causing the cell to swell and burst [67]. A small number of polyethers have shown activity towards Gram-negative pathogens [75, 76, 77], however in general, the lipopolysaccharide outer

membrane of Gram-negative bacteria acts as an effective barrier against diffusion of these hydrophobic antibiotics [151].

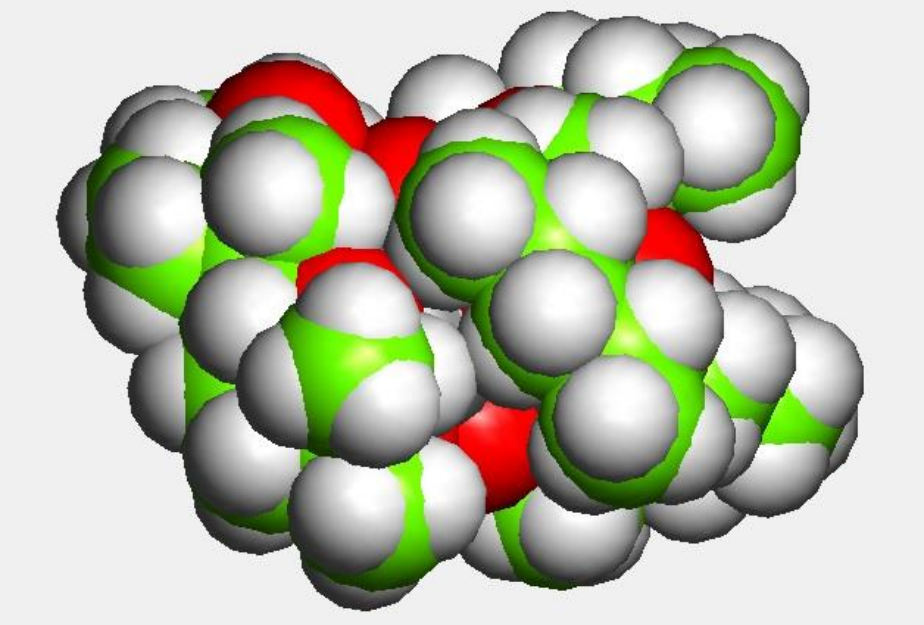

Figure 2.10. A space-filling model of the crystal structure of terrosamycin A (**1**). Oxygen atoms (red) are contained within the inner-sphere. The carbon (green) and hydrogen (white) atoms of the polyether backbone are wrapped around the hydrophilic cage rendering the complex lipophilic.

The antimicrobial activity of **1** and **2** was evaluated in a number of bioassays. For comparison, three known polyether ionophore standards were chosen and tested in parallel. Salinomycin, nigericin and monensin and its methyl ester (Figure 2.11) were selected due to the fact that they all exhibit potent antibiotic activity against Gram-positive pathogens and are among the most well-studied polyether natural products to date. Furthermore, salinomycin and monensin are currently approved and marketed in Canada as antibiotics and anticoccidial agents in cattle and poultry. The compounds were each tested against the Gram-positive pathogens methicillin-resistant *Staphyloccocus aureus* (MRSA), vancomycin resistant *Enterococcus faecium* (VRE) and *Staphylococcus warneri*, Gram-negative pathogens *Pseudomonas aeruginosa* and *Proteus vulgaris*, and the yeast pathogen *Candida albicans*. Expectedly, no activity was observed against *P. aeruginosa*, *P. vulgaris* or *C. albicans* even up to the highest tested concentration of 128 μg/mL. Only the monensin methyl ester also did not show activity in any of the Gram-positive pathogen assays. Table 2.4 shows the half-maximal inhibitory concentrations (IC_{50}) for each compound against MRSA, VRE and *S. warneri*. For each pathogen, monensin had the highest IC_{50} values of 1.54 ± 0.13, 8.32 ± 4.67 and 1.97 ± 0.18 μM, respectively indicating that other than its methyl ester, monensin was the least active in all assays. In the case of MRSA, nigericin possessed the lowest IC_{50} of 0.20 ± 0.05 μM, while **1** and **2** had similar activity to salinomycin with values of 0.53 ± 0.16, 0.34 ± 0.04 and 0.43 ± 0.11 μM, respectively. In VRE assays, **1**, **2** and nigericin had the lowest IC_{50} values of 0.58 ± 0.04, 0.51 ± 0.13 and 0.52 μM while salinomycin was slightly less potent with a value of 0.80 ± 0.24 μM. For *S. warneri*, nigericin was the most potent with an IC_{50} value of 0.29 ± 0.07, while values of 0.90 ± 0.32, 0.69 ± 0.10 and 0.88 ± 0.20 μM

implied **1**, **2** and salinomycin had similar activity. In MRSA and VRE assays, the terrosamycins, salinomycin and nigericin had lower IC_{50} values than the control compounds vancomycin and rifampicin demonstrating the potent antibiotic activity of polyether compounds.

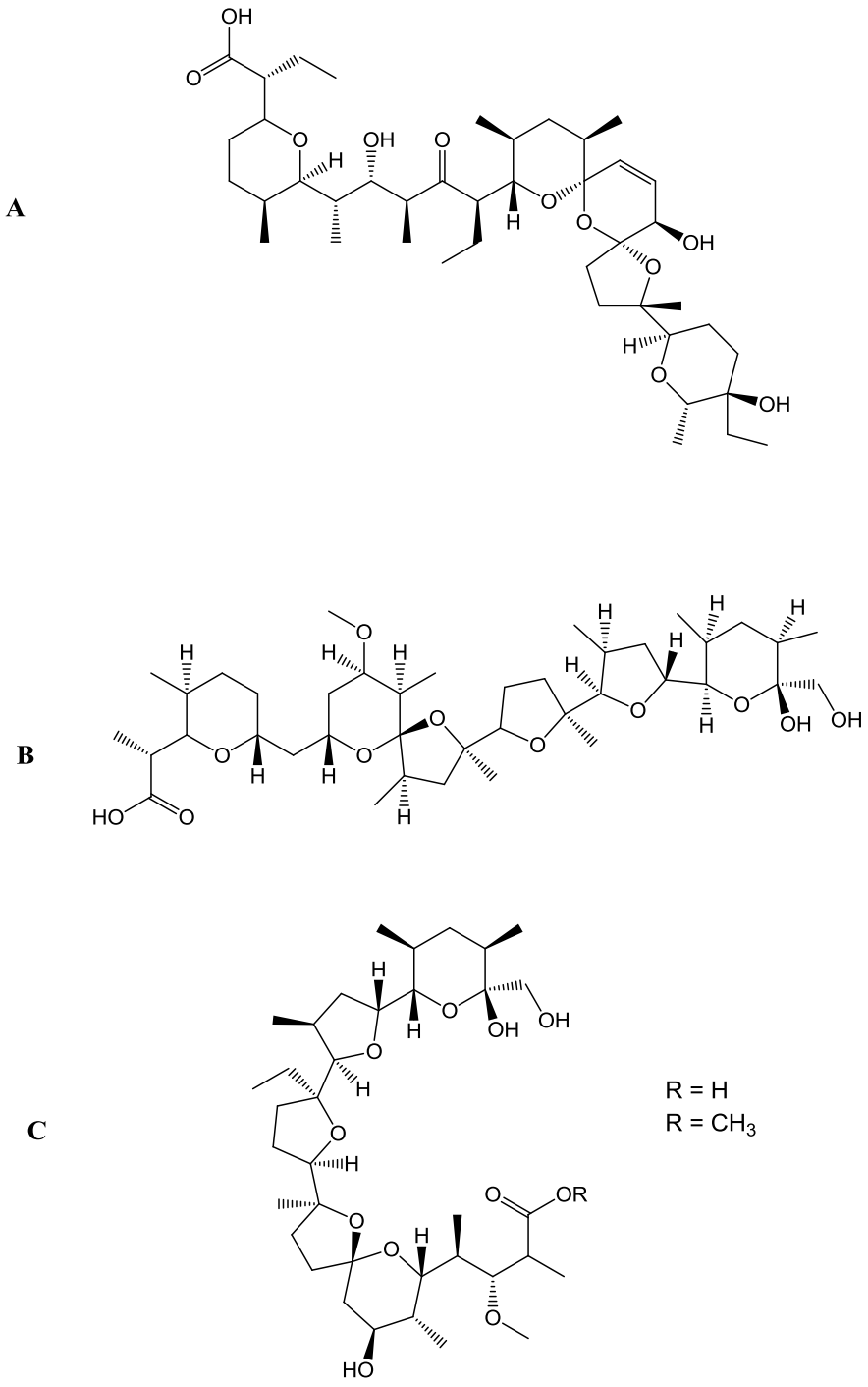

Figure 2.11. Molecular structures of **A**. salinomycin, **B**. nigericin and **C**. monensin (R = H) and monensin methyl ester (R = CH_3).

Table 2.4. Half-maximal inhibitory concentration (IC_{50}) values in μM for terrosamycin A (**1**) and B (**2**) and the polyether standards against MRSA, VRE and *S. warneri* determined from an average of six replicates.

Compound	**MRSA**	**VRE**	***S. warneri***
terrosamycin A (**1**)	0.53 ± 0.16	0.58 ± 0.04	0.90 ± 0.32
terrosamycin B (**2**)	0.34 ± 0.04	0.51 ± 0.13	0.69 ± 0.10
salinomycin	0.43 ± 0.11	0.80 ± 0.24	0.88 ± 0.20
monensin	1.54 ± 0.13	8.32 ± 4.67	1.97 ± 0.18
nigericin	0.20 ± 0.05	0.52 ± 0.07	0.29 ± 0.07
vancomycin control	0.82 ± 0.14	-	0.53 ± 0.01
rifampicin control	-	1.12 ± 0.07	-

In addition to being excellent antibiotics, polyether natural products have been the subject of recent research since the 2009 discovery of selective anti-cancer activity by salinomycin [87]. Though more work is needed to determine their specific mechanisms of action, many polyethers (including the selected standards) have exhibited potent activity against a broad spectrum of cancer cells, including multi-drug resistant cells and cancer stem cells (CSCs) [71]. Most notably, pilot clinical trials have shown the ability of salinomycin to reduce tumor volume and metastasis in four metastatic breast cancer patients as well as a metastatic ovarian cancer patient and a head and neck squamous cell carcinoma patient with no long term side effects [90]. Monensin has been identified as a potent and specific inhibitor of prostate cancer cell growth [152], while nigericin has been shown to specifically target CSCs in nasopharyngeal carcinoma and suppress metastasis in colorectal cancer [153], [154]. Furthermore, studies indicate that polyethers can increase sensitivity to chemotherapy and possible combinatory therapy is currently being explored [155].

In light of this information, **1**, **2** and our polyether standards were tested against a human breast adenocarcinoma cell line (HTB-26) and a human invasive breast ductal carcinoma cells (MCF-7). The compounds were also tested in a healthy human foreskin fibroblast cell line (BJ) and healthy *Cercopithecus aethiops* kidney epithelial cells (Vero) as an evaluation of cytotoxicity toward non-cancerous cells. Table 2.5 displays the IC_{50} values of each compound in each of the cell lines tested. All compounds tested showed a selective response toward cancerous cells as opposed to healthy cells. In the HTB-26 cell line, **2** showed the best growth inhibition with an IC_{50} value of 5.49 ± 1.23 μM, while **1** and salinomycin had a similar response with values of 10.1 ± 0.63 μM and 10.0 ± 1.21

μM, respectively. Terrosamycin B (**2**) also showed the best growth inhibition in the MCF-7 cell line with an IC_{50} value of 3.92 ± 0.42 μM, while terrosamycin A (**1**) had the next best response at 5.90 ± 1.44 μM. Although **1** had the most cytotoxicity toward healthy cells, **2** showed the least cytotoxicity in the BJ cell line and was second only to monensin in the Vero cell line. It is exciting to highlight that the activity of the terrosamycins was superior to salinomycin which has progressed to pilot clinical trials for the treatment of breast cancer, among other cancers [156]. This assay has shown that terrosamycin B in particular has a larger therapeutic window than salinomycin. These results suggest that the terrosamycins could be promising new candidates for anticancer drug development.

Table 2.5. Half-maximal inhibitory concentration (IC_{50}) values in μM for terrosamycin A (**1**) and B (**2**) and polyether standards against two breast cancer cell lines (HTB-26, MCF-7) and two healthy cell lines (Vero, BJ), determined from an average of three replicates.

Compound	**HTB-26**	**MCF-7**	**Vero**	**BJ**
terrosamycin A (**1**)	10.1 ± 0.63	5.90 ± 1.44	35.5 ± 5.87	78.5 ± 4.89
terrosamycin B (**2**)	5.49 ± 1.23	3.92 ± 0.42	93.1 ± 4.00	267 ± 27.7
salinomycin	13.0 ± 1.06	9.71 ± 2.81	78.3 ± 21.8	196 ± 2.69
monensin	10.0 ± 1.21	7.15 ± 2.13	1.12E4 ± 1.44E3	245 ± 10.6
monensin methyl ester	48.6 ± 3.28	18.2 ± 0.49	61.7 ± 6.79	127 ± 2.06
nigericin	13.2 ± 2.04	9.07 ± 3.10	60.7 ± 8.23	221 ± 10.3
doxorubicin control	3.73 ± 1.75	0.77 ± 0.09	-	-
phenoxyethanol control	-	-	12.7 ± 1.60	-
zinc pyrithione control	-	-	-	0.80 ± 0.07

Differences in the IC_{50} values provide some insight into the structure-activity relationship (SAR) of these compounds. The antimicrobial assay revealed the monensin methyl ester exhibited no activity. Further, it displayed the weakest anticancer activity in cytotoxicity assays. The lack of activity of monensin esters compared to the free acid has been observed before and suggests the carboxylic acid moiety of polyethers is important for activity [157, 158]. Though the structures of **1**, **2**, salinomycin, nigericin and monensin are quite different, they exhibited similar activities in the antimicrobial assay (with the exception of monensin displaying a slightly weaker effect against Gram-positive pathogens) and it is likely their mechanisms of action are the same. As mentioned in Chapter 1, it has been determined that different polyethers act on cancerous cells via distinct mechanisms; this is a current topic of study in which new findings are emerging regularly. For this reason, it is difficult to speculate on the SARs of these compounds in cytotoxicity assays. This being said, the slightly superior anticancer activity and less detrimental effect on healthy cells exhibited by **2** compared with **1** suggests the ketal functionalities of **2** play a role in the mechanism of action.

2.2. THE EFFECTS OF CO-CULTURE MIMIC CONDITIONS ON NATURAL PRODUCT PRODUCTION

2.2.1. Introduction

Using our newly established co-culture mimic approach, three bacterial strains were subjected to fermentation with a variety of environmentally relevant stressors and the resulting changes in natural product production were examined. The actinomycetes *K. cystarginea*, *K. griseola* and *Streptomyces* sp. RKND004 were fermented in media supplemented with a heat-killed culture of either *Aspergillus flavus* NRRL 3357, *Bacillus*

subtilis ATCC 6051 or *Mycobacterium smegmatis* ATCC 12051. A heat-killed culture of the nematode *Caenorhabditis elegans* N2 with its food source *Escherichia coli* OP50 was also used as a stressor. The stressors were added to the actinomycete cultures at different stages of the fermentation and/or in different concentrations in an attempt to find optimal conditions for an observable change in the secondary metabolism. Differences between natural product production in co-culture mimic fermentations and control cultures were visualized using scatter plots and metabolites whose production was induced or upregulated in the presence of the stressor were recorded.

2.2.2. Preparation of stressors

In naturally occurring microbial ecosystems, organisms are often forced to compete with neighboring species for resources in order to thrive. It is hypothesized that these stressful environments stimulate natural product production that is not normally observed in the luxurious conditions of axenic cultures grown in the laboratory [111]. As a result, the microbes used in co-culture studies are often chosen in an attempt to imitate a naturally occurring ecosystem. Since the producer microbes are terrestrial actinomycetes that were isolated from soil samples, a diverse group of soil-dwelling organisms were chosen as stressors for this study. Each stressor organism is known to produce a number of secondary metabolites that may potentially affect the secondary metabolism of the actinomycetes. The fungal species *A. flavus* has a cosmopolitan distribution though it is mostly found in soil environments where it is able to survive harsh conditions and in turn, out-compete its microbial neighbours for space and nutrients [159]. The bacterium *B. subtilis* is present in soil and is highly competitive through production of numerous bioactive natural products [160]. Similarly, the bacterial species *M. smegmatis* can be found

in soil and resist harsh conditions by natural product production [161]. In recent studies, the soil nematode *C. elegans* (Figure 2.12) was found to produce nematode-derived modular metabolites that serve as signals that are connected with the development and behavior of these animals [162].

Figure 2.12. A photograph of *C. elegans* growing on an agar plate taken with a dissecting microscope. The nematodes shown are in multiple different stages of growth.

The fungus *A. flavus* and two bacteria, *B. subtilis* and *M. smegmatis* were fermented in brain-heart infusion (BHI) broth on a large scale and then the cultures were killed via autoclaving. A liquid culture of the nematode *C. elegans* with its *E. coli* food source and an axenic control culture of *E. coli* (for control fermentations) were each fermented on a large scale in S medium [163] and killed by autoclaving. The cultures were each streaked onto agar plates before autoclaving and determined to be pure. After autoclaving, the cultures were streaked onto plates once more; no growth was observed which confirmed their sterilization. A control stressor for the microbial co-culture mimic experiments (to be added to control fermentations) was prepared by autoclaving uninoculated BHI broth twice consecutively. A 100-fold diluted sample of each stressor and the BHI and *E. coli* control was prepared with sterile diH_2O. The microbial stressors all contained visible biomass and the nematode stressor contained many small carcasses.

2.2.3. Small-scale fermentations and extractions

Each of the three actinomycetes (*K. cystarginea* NRRL B-16505, *K. griseola* NRRL B-16229 and *Streptomyces* sp. RKND004) was fermented on a small scale in BFM4 broth, which was chosen based on the fact that it stimulated prolific natural product production based on the previous OSMAC experiments. On the second day of the five day fermentation, the *A. flavus*, *B. subtilis* and *M. smegmatis* stressors were added to the cultures. Each actinomycete culture received an aliquot of either the concentrated or 100-fold diluted stressor which resulted in a final concentration of 10% and 0.1% (v/v), respectively. Each producer and stressor pair was performed in triplicate. Uninoculated tubes containing only BFM4 and a 10% and 0.1% concentration of the stressor were included as media blanks. Inoculated controls for each actinomycete strain were included

and received aliquots of the twice-autoclaved BHI broth at each concentration. Adding the BHI broth to the control cultures ensured any changes in natural product production of the actinomycetes could be attributed to the presence of the stressor and not the BHI broth. All culture broths and blanks were extracted with ethyl acetate and the extracts were analyzed using LC-MS over two batches of analysis, each including a reserpine instrumental control and three methanol blanks to limit carryover.

In a separate set of experiments, each of the actinomycetes was fermented on a small scale in BFM3 broth, also chosen based on the results of the previous OSMAC experiments. The *C. elegans* stressor was added to the cultures (to final concentrations of 10% or 0.1%) in triplicate at two separate time points; at the time of inoculation and on the fourth day of the five day fermentation. Uninoculated media blanks containing only BFM3 received the *C. elegans* stressor at each concentration, while inoculated controls received each concentration of sterile *E. coli* culture at the same time points. By adding the sterile *E. coli* culture to the control fermentations, any changes observed in the secondary metabolism of the actinomycetes could be attributed to the presence of the *C. elegans* stressor only and not its *E. coli* food source. All culture broths and blanks were extracted with ethyl acetate and the extracts were analyzed using LC-MS over two batches in the same manner as previous samples. In total, *K. cystarginea*, *K. griseola* and *Streptomyces* sp. RKND004 were each fermented in ten different stress conditions which are summarized in Table 2.6.

Table 2.6. A summary of the ten co-culture mimic stress conditions used in this study.

Code	Stressor organism	Fermentation Medium	Total concentration of stressor (v/v)	Addition time-point
AF1	*A. flavus*	BFM4	10%	Day 2
AF2	*A. flavus*	BFM4	0.10%	Day 2
BS1	*B. subtilis*	BFM4	10%	Day 2
BS2	*B. subtilis*	BFM4	0.10%	Day 2
MS1	*M. smegmatis*	BFM4	10%	Day 2
MS2	*M. smegmatis*	BFM4	0.10%	Day 2
CE1	*C. elegans/E. coli*	BFM3	10%	Day 0
CE2	*C. elegans/E. coli*	BFM3	0.10%	Day 0
CE3	*C. elegans/E. coli*	BFM3	10%	Day 4
CE4	*C. elegans/E. coli*	BFM3	0.10%	Day 4

2.2.4. Data analysis and identification of upregulated and induced compounds

All raw LC-MS data was processed using MZmine 2 as previously described in section 2.1.4. For experiments using the microbial stressors *A. flavu*s, *B. subtilis* and *M. smegmatis*, data was processed in three separate batches according to the producer bacterium. Data for experiments using the nematode stressor *C. elegans* was processed in a single batch. The mass detection threshold for each batch was set at 2E3 to ensure detection of genuine signals while avoiding the inclusion of noise in the data set. An aligned peak list was created for each producer with each stressor. Peaks detected in the media blanks, methanol blanks and reserpine standard samples were manually deleted. Finally, the custom database identification function was used to annotate the peak lists with the names of bacterial natural products in the AntiBase database having exact masses that matched the *m/z* of mass features in the list.

Scatter plots were used to visualize the effect of the stressor on the secondary metabolism of the producer. As an example, Figure 2.13 shows the peak area of mass features detected in *K. cystarginea* cultures when grown in the control conditions versus cultures in which the *A. flavus* stressor was added. In the scatter plot, points that lie above the x = y line have a larger peak area in the stress condition indicating upregulation of that feature. Similarly, points below the line show downregulation in response to the stressor. Interestingly, points that appear to sit along a vertical line at the left of the plot were not detected in the control conditions but were present when the producer was grown with the stressor indicating a possible induction of that feature. Since the mass detection threshold was set at 2E3 it was possible that those mass features may have still been present in controls albeit below the threshold. Furthermore, it was also possible that

those features may have been present below the threshold in the media blanks. This would mean they are not truly *K. cystarginea* metabolites, but rather a component of the media or a metabolite produced by *A. flavus* before autoclaving. Manual inspection of the raw data was therefore required to validate any findings.

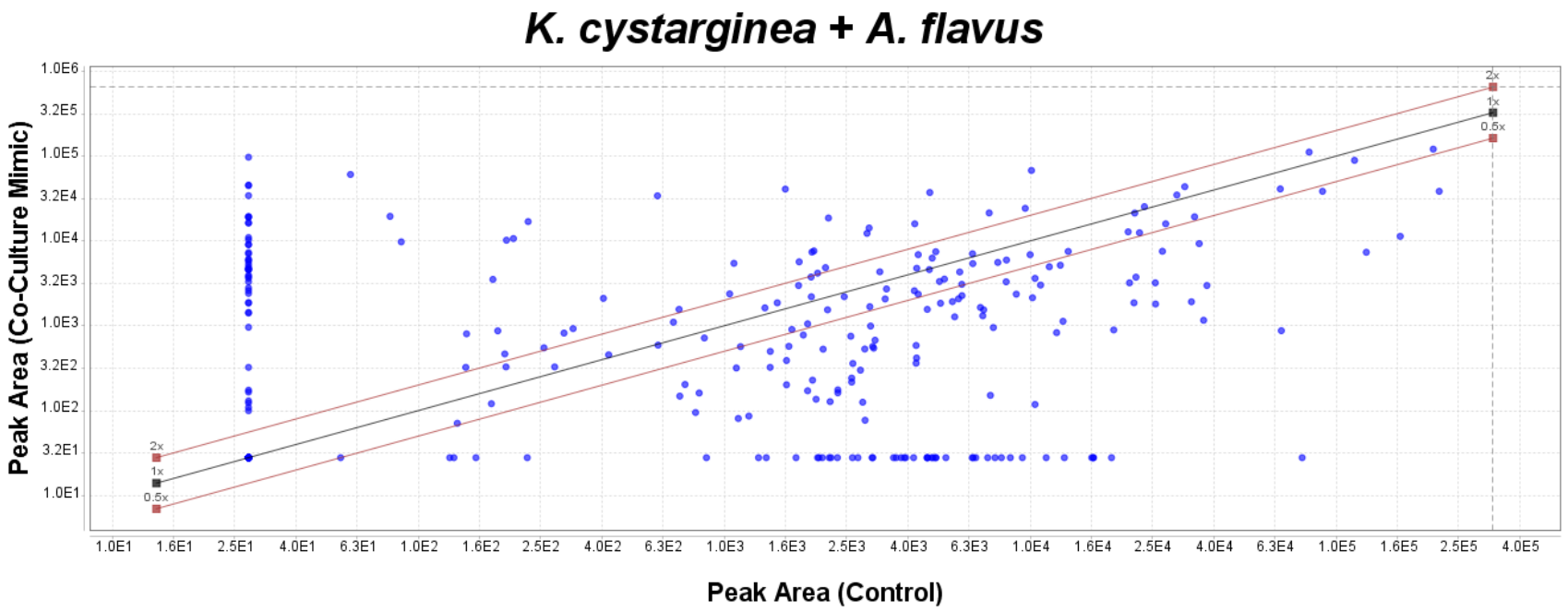

Figure 2.13. A scatter plot generated in MZmine 2 comparing the peak area of mass features detected in a *K. cystarginea* control fermentation with their peak area in fermentations with the 10% *A. flavus* stressor (AF1). Points that appear above the x = y line were upregulated while those that appear below were downregulated. Points on the far left that align vertically were not detected above the 2E3 threshold in the control but were detected in the co-culture mimic. Points that align horizontally across the bottom were detected in the control but not in the co-culture mimic.

Moving forward, the mass features present in the controls were deleted from the data sets leaving only features that appeared to be induced. Putatively induced features that were detected in each of the three replicates were further investigated; a total of 86 for all producer/stressor combinations. In Xcalibur, the features were located within the raw data and XIC plots monitoring their abundance in the appropriate samples were constructed. Those that were present in the media blank samples, as well as those that appeared to be part of the noise were disregarded. Features that were present in the controls with a smaller peak area than in the stress conditions were labeled as upregulated metabolites. Features that were absent in the controls were labeled as induced metabolites. An example of each case is shown in Figure 2.14 and 2.15 respectively.

A

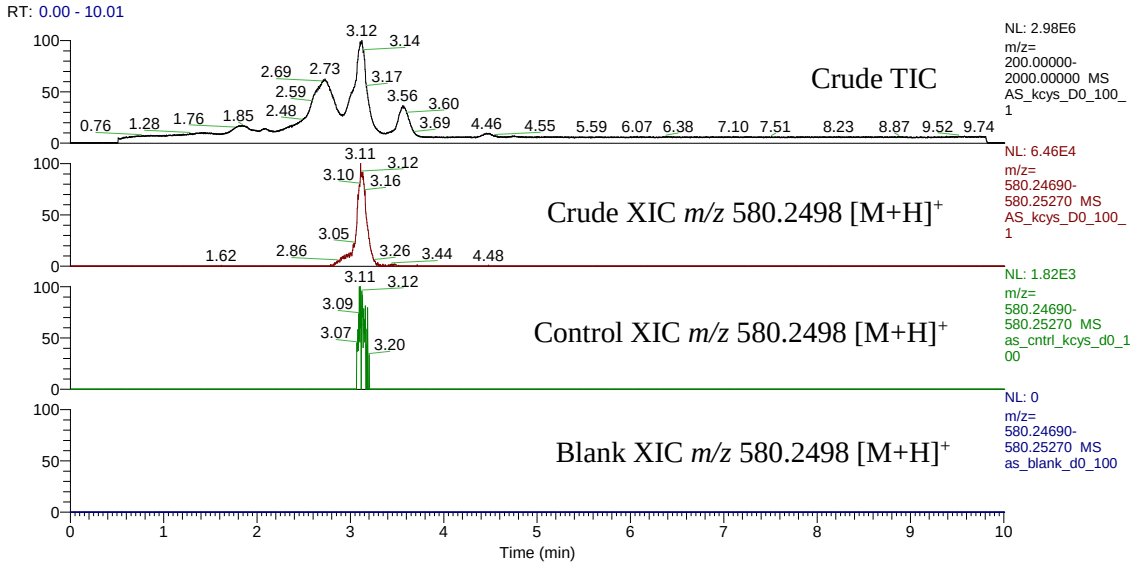

B

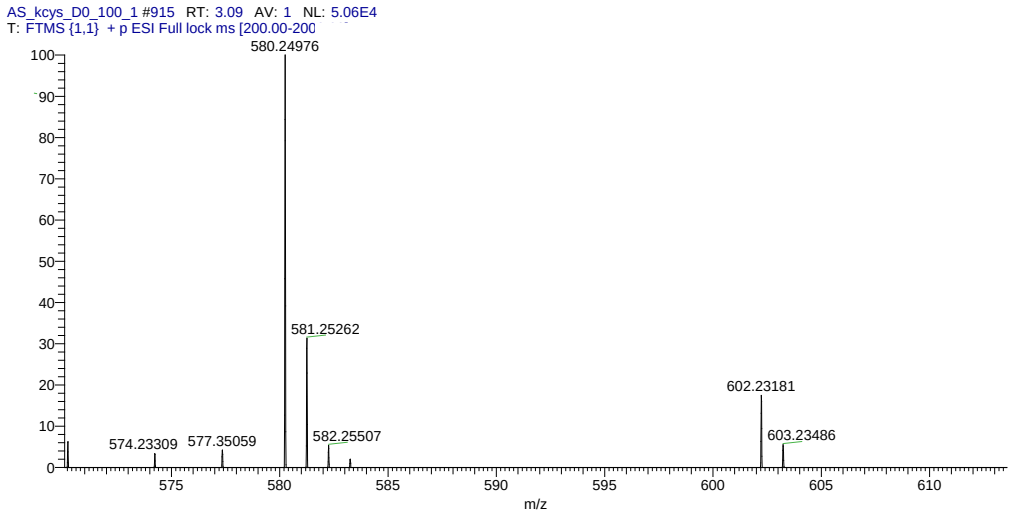

Figure 2.14. **A**. An example of an upregulated metabolite from co-culture mimic experiments. From top to bottom: TIC of the crude extract of *K. cystarginea* grown with the 10% *C. elegans* stressor (CE1) followed by the XIC of the crude extract, the 10% *E. coli* control extract and the 10% media blank extract monitoring *m/z* 580.2498 $[M+H]^+$. The metabolite was also not detected in the 0.1% blank extract. **B**. The high resolution mass spectrum of the crude co-culture mimic extract t_R 3.11 min showing the induced metabolite *m/z* 580.2498 $[M+H]^+$ and its sodiated adduct *m/z* 602.2318 $[M+Na]^+$.

A

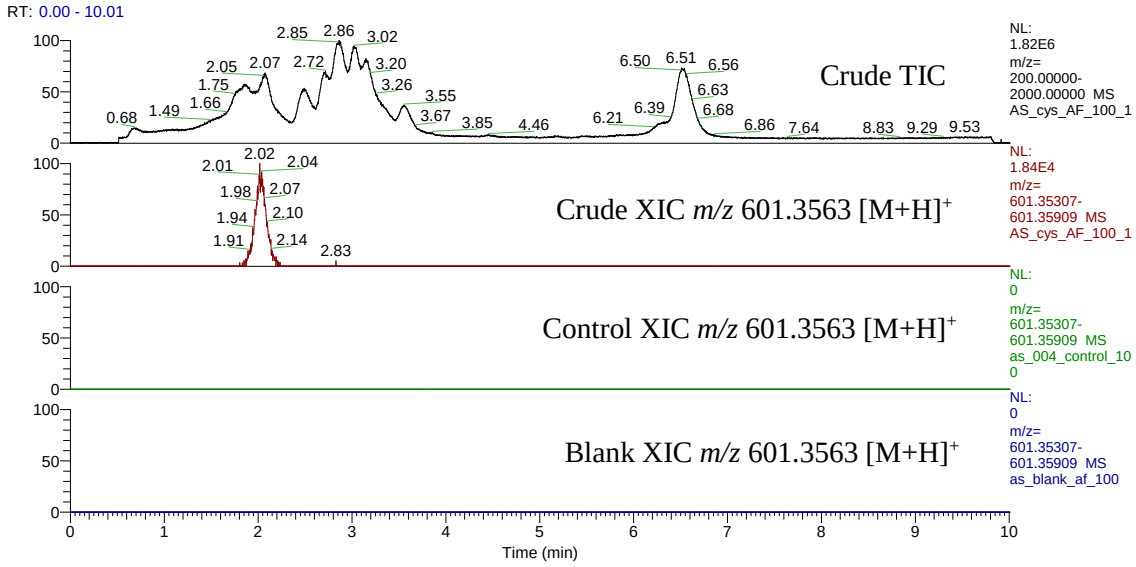

B

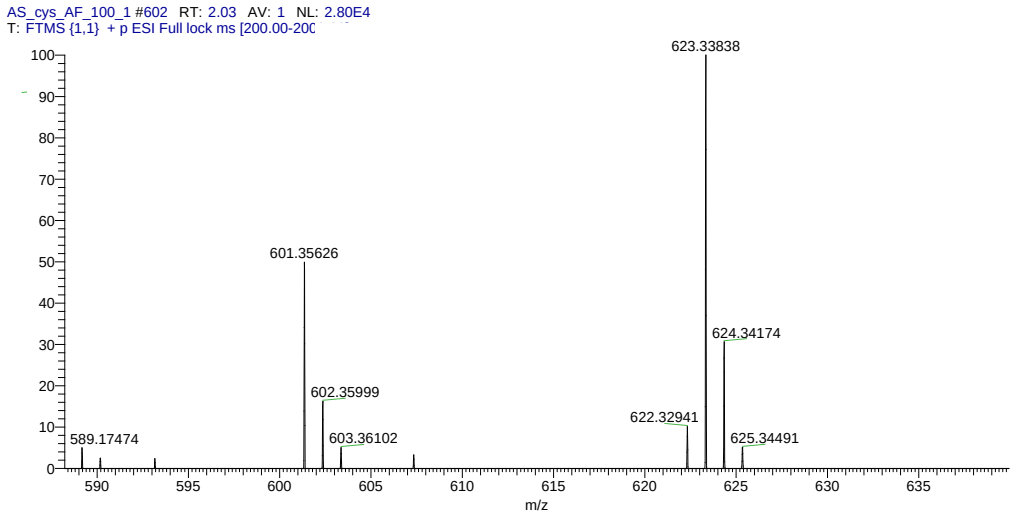

Figure 2.15. **A**. An example of an induced metabolite from co-culture mimic experiments. From top to bottom: TIC of the crude extract of *K. cystarginea* grown with the 10% *A. flavus* stressor (AF1) followed by the XIC of the crude extract, the 10% BHI control extract and the 10% media blank extract monitoring *m/z* 601.3563 $[M+H]^+$. The metabolite was also not detected in the 0.1% control or blank extracts. **B**. The high resolution mass spectrum of the crude co-culture mimic extract at t_R 2.02 min showing the induced metabolite *m/z* 601.3563 $[M+H]^+$ and its sodiated adduct *m/z* 623.3384 $[M+Na]^+$.

Table 2.7 displays the upregulated and induced compounds found in this study. The induction/upregulation of each compound listed was observed in all three replicates. A total of 19 upregulated and 14 induced metabolites were uncovered. The majority of these (eight upregulated, 13 induced) were produced by *K. cystarginea*. Six upregulated compounds were produced by *K. griseola* while five upregulated and one induced compound were produced by *Streptomyces* sp. RKND004. Although most of these compounds were found as a result of only one stressor, seven upregulated and two induced compounds were produced in response to two or more stressors. This may suggest that while the production of some metabolites was triggered by specific conditions or chemical signals, others may be produced as a generalized stress response.

Table 2.7. A list of upregulated and induced metabolites found from this co-culture mimic study.

Bacterium	*m/z* $[M+H]^+$	t_R (min)	Stressors*	Induced (I) or upregulated (U)	AntiBase hits
K. cystarginea	241.1799	3.23	AF1	I	
	289.2376	3.00	AF1	I	
	297.2039	2.81	AF1	I	
	303.2527	3.00	AF1	I	
	371.1611	2.36	AF1	I	cyclo-L-α-glutamylglycl-L-seryl-L-prolyl
	373.1969	2.30	AF1	I	
	381.1469	2.39	AF1	U	trehazolin, WS-775624A, WS-775624B
	387.2136	2.19	AF2	U	galbonolide B
	397.1945	2.22	AF2	U	2 unnamed from *Streptomyces* spp.
	443.1134	2.17	CE3	I	
	543.2915	3.45	AF1	I	
	580.2498	3.11	CE1	U	
	601.3563	2.02	AF1	I	nocardamine
	713.3986	2.82	AF2, BS2	U	
	723.4424	2.97	AF1	I	
	727.4158	2.91	BS2	U	
	741.4319	3.01	AF2, BS2	U	montanastatin
	781.4251	2.78	AF2, BS2	I	
	785.3975	3.04	AF2, BS2	U	
	795.4113	2.47	AF1	I	halomycin B
	1155.6084	3.01	AF2, BS2	I	enterocin 1071
K. griseola	229.1007	0.66	BS2	U	cyclo-(L-pro-met), caerulomycin K
	279.1509	0.72	AF2, BS2, MS1, MS2	U	oncorhyncolide
	563.1538	2.55	AF2	U	

	595.0323	2.95	AF2	U	
	691.4216	4.75	AF1, AF2, BS1, BS2, MS1, MS2	U	
	389.2323	5.06	BS2	U	
Streptomyces sp. RKND004	271.0604	2.93	AF2, BS1, BS2, MS1, MS2	U	2,5,7-trimethoxy napthoquinone, misakimycin
	567.1478	2.86	AF2, BS1	U	
	547.1006	2.95	MS1	U	
	749.1871	3.48	CE1	U	
	709.1866	3.65	CE1	U	
	635.1341	2.89	CE2	I	

*Abbreviations for stressors: AF1 - *A. flavus* 10%; AF2 - *A. flavus* 0.1%; BS1 - *B. subtilis* 10%; BS2 - *B. subtilis* 0.1%; MS1 - *M. smegmatis* 10%; MS2 - *M. smegmatis* 0.1%; CE1 - *C. elegans* 10% added at time of inoculation; CE2 - *C. elegans* 0.1% added at time of inoculation; CE3 - *C. elegans* 10% added on day 4; CE4 - *C. elegans* 0.1% added on day 4.

Most of the metabolites produced by *K. cystarginea* were a result of the fungal stressor *A. flavus*. One species of the *Aspergillus* genus, *A. fumigatus*, has been previously studied in co-culture experiments with bacteria, however in each case the induced metabolites were found to be produced by the fungus [164, 165, 166]. Since the fungal culture was sterile in these experiments, the induced compounds must be of bacterial origin. *K. griseola* and *Streptomyces* sp. RKND004 did not show a response for one preferred stressor; each of the microbial stressors elicited an upregulated compound. The *C. elegans* stressor was responsible for the induction of two metabolites (one from *K. cystarginea* and one from *Streptomyces* sp. RKND004) as well as the upregulation of two *Streptomyce*s sp. RKND004 metabolites and one *K. cystarginea* metabolite.

Although an attempt was made to find an optimal stressor concentration for natural product induction, the results indicate neither concentration elicited a better induction effect than the other in each case. In the case of the *C. elegans* stressors, an attempt was made to optimize natural product production based on the time of addition of the stressor. One induced and three upregulated compounds were identified when the stressor was added at the time of inoculation (CE1 and CE2), while one compound was induced when the stressor was added on day four of the fermentation (CE3). Based on this small set of results, addition at the time of inoculation may have resulted in a better induction effect. This may be due to the fact that the producer had more time to produce metabolites in response to the stress. Further experiments are needed to confirm these initial findings.

Since they are not produced under standard laboratory conditions, and are typically produced in low abundance, induced compounds have a high likelihood of

being novel. Furthermore, the compounds uncovered in this study had few or no hits in AntiBase. As expected, the ELSD trace in the raw data indicated that none of these metabolites were major compounds suggesting purification may be difficult. Ideally, additional experiments would be done to optimize the induction of these compounds before attempting co-culture mimic fermentations on a large-scale.

2.3. PURIFICATION AND STRUCTURE ELUCIDATION OF PQS-GLCA, A NOVEL BIOTRANSFORMATION PRODUCT

2.3.1. Introduction

The discovery of cryptic natural products through induction experiments is a current theme in the Kerr lab. In particular, development of our co-culture mimic technique began with a project started by Ph. D. student Libang (Leon) Liang. Eight actinomycetes were subjected to co-culture mimic conditions using the same group of taxonomically diverse microbial stressors described in section 2.2.2, with the addition of the Gram-negative bacterial pathogen *Pseudomonas aeruginosa*. Again, LC-MS data from extracts of the cultures was processed with MZmine 2. Heat maps were constructed to identify any upregulation or induction of the actinomycete-produced metabolites. This work led to the discovery of the metabolite *m/z* 436.1961 $[M+H]^+$ in the co-culture mimic fermentation of the sediment-derived actinomycete strain *Streptomyces* sp. RKBH B178 with the stressor *P. aeruginosa*.

Since *P. aeruginosa* is known to produce a number of quorum sensing molecules, an attempt was made to determine which, if any, specific metabolite present in the stressor was acting as a chemical signal to trigger the production of *m/z* 436.1961

$[M+H]^+$. After interpretation of LC-MS data from extracts of axenic cultures of *P. aeruginosa*, the three major metabolites produced by the stressor before autoclaving were determined to be 2-heptyl-3-hydroxy-4-quinolone (the *Pseudomonas* quinolone signal, PQS), its precursor 2-heptyl-4-quinolone (HHQ) as well as a number of rhamnolipids. These compounds have all been reported to be produced by this bacterium; PQS and HHQ are key regulators of the bacterium's quorum sensing system while rhamnolipids are an important virulence factor of the pathogen [167]. A mixture of two rhamnolipids and pure HHQ and PQS were obtained from commercial sources and added separately to axenic cultures of *Streptomyces* sp. RKBH B178. The induced metabolite was observed in cultures where HHQ and PQS were present, suggesting that these two closely related compounds were responsible for *m/z* 436.1961 $[M+H]^+$ production.

With some insight into the induction mechanism, the project moved forward toward the purification and characterization of the metabolite of interest. Fermentation on multiple scales was conducted in order to determine the best fermentation volume for production of the compound. Once an optimal volume was determined, large-scale fermentations were undertaken and purification and structure elucidation were completed revealing the new compound PQS-GlcA as a biotransformation product of the 2-alkyl-4-quinolone signals HHQ and PQS. The discovery of this compound is significant as it is connected to a novel mechanism of *P. aeruginosa* quorum sensing deactivation.

2.3.2. Multi-scale fermentations and extractions of *Streptomyces* sp. RKBH-B178

As natural product production by bacterial strains often differs based on fermentation volume or vessel shape/size [168, 169], multi-scale fermentations of *Streptomyces* sp. RKBH-B178 were undertaken in order to determine optimal conditions for production of PQS-GlcA. Since both signaling molecules induced production of the metabolite in similar quantities, fermentations were supplemented with HHQ as it was relatively inexpensive compared to PQS. Cultures of *Streptomyces* sp. RKBH-B178 with HHQ were fermented in volumes of 7 mL, 50 mL, 600 mL and 1 L. Cultures were extracted and the extracts were analyzed by LC-MS. MZmine 2 was used for data processing as previously described in section 2.1.4. An ion intensity plot monitoring the peak area of PQS-GlcA was constructed to compare production across each of the fermentation volumes (Figure 2.16). The 50 mL fermentations produced the metabolite in the largest relative quantity and thus this volume was chosen for subsequent scale-up.

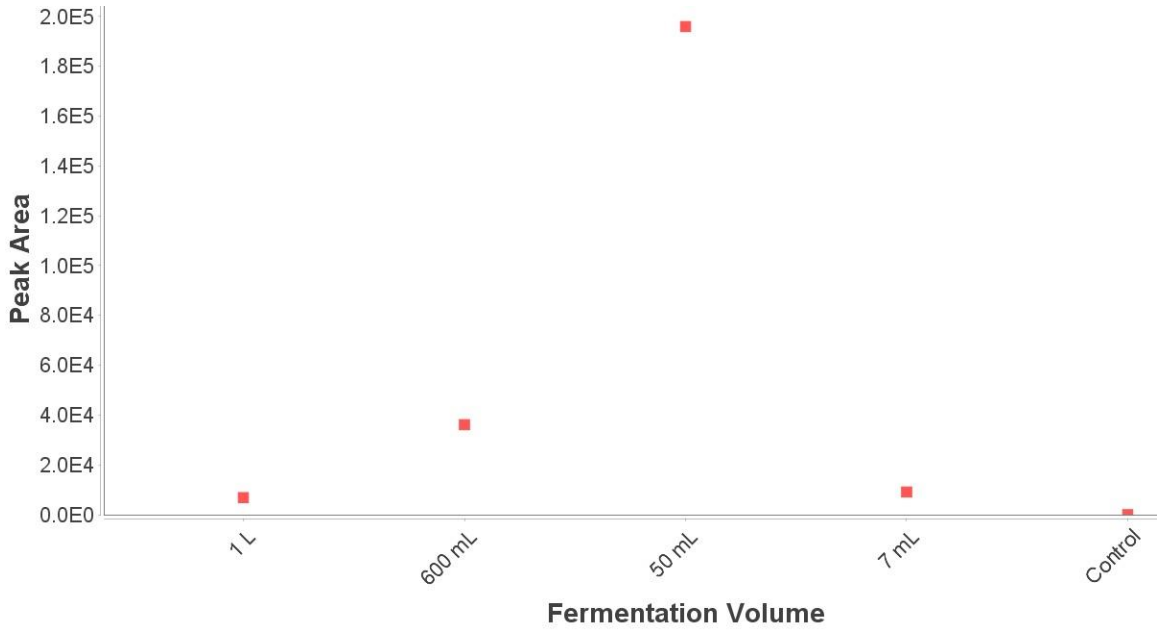

Figure 2.16. Ion intensity plot displaying the peak area of PQS-GlcA *m/z* 436.1961 $[M+H]^+$ in multiple scale fermentations of *Streptomyces* sp. RKBH-B178 supplemented with pure HHQ. PQS-GlcA was not detected in a control culture of the bacterium with no HHQ added.

2.3.3. Large-scale fermentations and purification of PQS-GlcA and bhimamycin A and E

In order to obtain sufficient material for the purification, structure elucidation and bioactivity testing PQS-GlcA, a fermentation scale-up of *Streptomyces* sp. RKBH-B178 with HHQ was performed. A total of 2.95 L was fermented in 50 mL volumes. Culture broths were extracted with ethyl acetate and the extracts were washed with water before fractionation by two successive rounds of automated flash chromatography with a C_{18} stationary phase. Fractions containing the induced metabolite were further purified by RP-HPLC with a phenyl hexyl stationary phase to yield 0.4 mg of PQS-GlcA (**3**) as a yellow oil. Two additional metabolites were purified in the process and structure elucidation through NMR spectroscopy determined their identities as the previously reported compounds bhimamycin A and E (Appendix Figures 6.29-6.40). A yield of 5.80 mg bhimamycin A and 15.92 mg of bhimamycin E were obtained after first round of automated flash chromatography. Both compounds were reported to be produced by a terrestrial *Streptomycete* [170]. Bhimamycin A was found to possess moderate activity against *B. subtilis* and *E. coli* while bhimamycin E showed selective activity only towards *S. aureus*. Interestingly, the results of co-culture mimic experiments completed by Leon Liang revealed bhimamycin A was upregulated in response to both the *P. aeruginosa* stressor and pure HHQ addition.

2.3.4. Structural characterization and stereochemical determination of PQS-GlcA

HRMS analysis of PQS-GlcA (**3**) supported a molecular formula of $C_{22}H_{30}NO_8$ (*m/z* 436.1961 $[M+H]^+$, t_R 2.74 min, Δ = 1.1 ppm) indicating eight degrees of unsaturation. The NMR data (Table 2.8) revealed the presence of four aromatic protons,

H-6 (δ_H 8.27), H-7 (δ_H 7.38), H-8 (δ_H 7.67) and H-9 (δ_H 7.61) which were assigned by interpretation of COSY correlations and the key HMBC correlations H-6/C-10 (δ_C 140.1), H-9/C-5 (δ_C 126.1), H-7/C-5 and H-8/C-10. The HMBC correlation H-6/C-4 (δ_C 174.2) allowed one of the two carbonyl resonances to be unambiguously assigned to the C-4 position. The presence of a seven carbon alkyl chain was identified using COSY and HMBC correlations suggesting that the structure of **3** was similar to HHQ and PQS. Two HMBC correlations H-11 (δ_H 3.23, 2.98)/C-8 (δ_C 152.0) and H-11/C-3 (δ_C 139.2) allowed the two remaining aromatic carbon resonances to be assigned, indicating the presence of a quinolone ring with the alkyl chain attached to the C-2 position. This assignment is in agreement with previously reported chemical shift values for both HHQ and PQS [171].

Table 2.8. ^{1}H (600 MHz) and ^{13}C (150 MHz) NMR data for PQS-GlcA (**3**) recorded in MeOD-d_4.

Position	**δ_C, type**	**δ_H, (*J*, Hz)**	**COSY**	**HMBC (H→C)**
1	NH	12.32[a], s (broad)		
2	152.0, C			
3	139.2, C			
4	174.2, C			
5	126.1, C			
6	126.3, CH	8.27, d (8.1)	7	4, 8, 10
7	124.8, CH	7.38, dd (7.5, 8.1)	6, 7	5, 9
8	133.3, CH	7.67, dd (7.5, 8.5)	7, 9	6, 10
9	119.1, CH	7.61, d (8.5)	8	5, 7
10	140.1, C			
11	30.7, CH_2	3.23, m; 2.98, m	11, 12	2, 3, 12
12	30.5, CH_2	1.75, quint (7.7)	11, 13	11, 13
13	30.5, CH_2	1.44, m; 1.37, m	12, 13, 14	12, 14
14	30.6, CH_2	1.30, m	13	13, 15
15	33.2, CH_2	1.30, m		14, 16
16	23.9, CH_2	1.32, m	17	15, 17
17	14.2, CH_3	0.90, t (6.8)	16	15, 16
1'	108.0, CH	4.68, d (7.8)	2'	3
2'	75.5, CH	3.55, dd (7.8, 8.7)	1', 3'	
3'	78.5, CH	3.48, dd (8.7, 8.7)	2', 4'	
4'	73.5, CH	3.53, dd (8.7, 9.5)	3', 5'	
5'	77.4, CH	3.57, d (9.5)	4'	6'
6'	177.0, C			

[a]Measured in DMSO-d_6

The characteristic anomeric carbon resonance C-1' (δ_C 108.0) and the HMBC correlation between anomeric proton H-1' [4.68 (d, *J* = 7.8 Hz)] and C-3 showed the presence of a carbohydrate moiety attached to the C-3 position of the quinolone ring. The glycosidic spin system H-1' – H-5' was assigned by interpretation of COSY correlations. The remaining carbonyl signal was assigned to the C-6' (δ_C 177.0) position on the basis of an HMBC correlation H-5' (δ_H 3.57)/C-6' and is consistent with the proposed molecular formula. Meanwhile, coupling constants exhibited by H-1' and H-4' [δ_H 3.53 (t, *J* = 9.3 Hz)] showed their axial relationship with neighbouring protons suggesting the presence of a *β*-glucuronic acid moiety. Tandem MS revealed fragmentation between the glucuronic acid (GlcA) moiety and the aglycone further corroborating the proposed structure (Appendix Figure 6.20). The key correlations used to determine the molecular structure are shown in Figure 2.17; structural similarity of PQS-GlcA to both HHQ and PQS suggests it is a biotransformation product resulting from glucuronidation at the C-3 position.

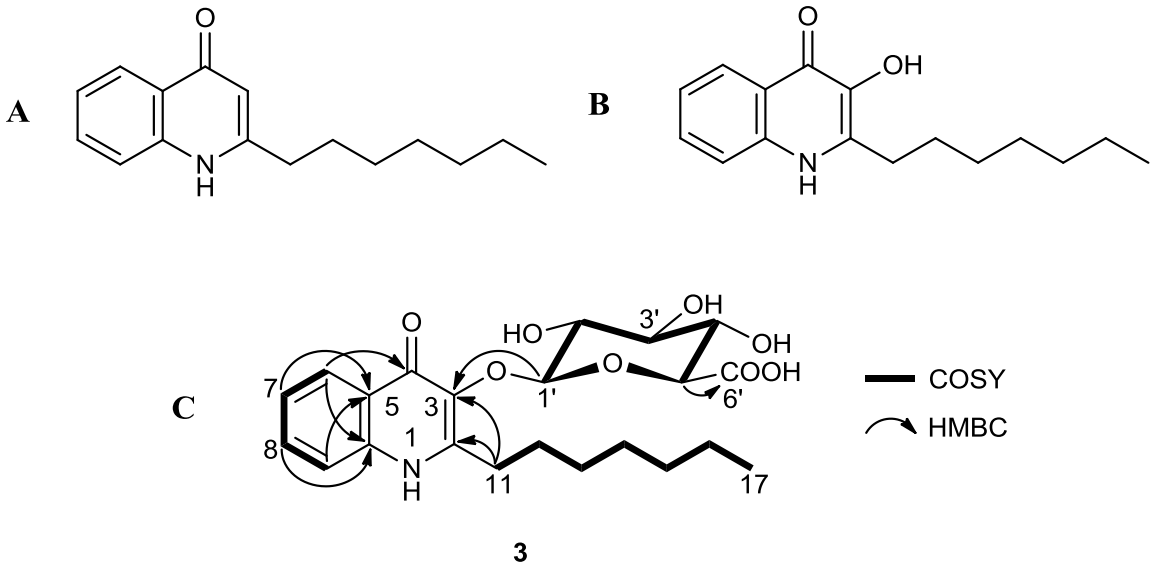

Figure 2.17. **A**. The molecular structure of HHQ. **B**. The molecular structure of PQS. **C**. The molecular structure of PQS-GlcA (**3**) with the key ^{1}H-^{1}H COSY and HMBC correlations used to determine the structure.

The configuration of the GlcA substituent was determined using a previously reported method [172, 173], which involves the reaction of D- or L-aldoses with either cysteine methyl ester enantiomer and *o*-tolylisothiocyanate yielding methyl 2-(polyhydroxylalkyl)-3-(*o*-tolylthiocarbamoyl)-thiazolidine-4(*R*)-carboxylates which are easily separated by RP-HPLC. Preparation of two thiocarbamoyl-thiazolidine derivative standards was achieved following Tanaka's protocol using D-GlcA with L-cysteine methyl ester, and D-GlcA with D-cysteine methyl ester. Purified PQS-GlcA (**3**) was subjected to acidic conditions to cleave the sugar by hydrolysis before the Tanaka reaction was performed using D-cysteine methyl ester. The reaction products were subjected to LC-MS and the retention times of the derivatives were compared by creating an XIC plotting the intensity of their exact mass (Appendix Figure 6.28). The retention times of the PQS-GlcA/D-cysteine methyl ester derivative matched exactly with the D-GlcA/D-cysteine methyl ester derivative at 25.28 min, indicating that **3** contains D-GlcA.

2.3.5. Bioactivity of PQS-GlcA

PQS is one of the four autoinducers (AI) produced by *P. aeruginosa* [167, 174]. The signal binds to the receptor protein PqsR which in turn regulates the production of PQS by inducing transcription of the *pqsA* operon [175]. This process results in the production of the precursor HHQ which can be converted to PQS by the monooxygenase PqsH [175]. The HHQ intermediate can also act as an AI by binding PqsR however it has a much lower binding affinity than PQS [176]. While HHQ can be recognized as a quorum sensing signal by some other bacterial species, PQS is an AI specific to *P. aeruginosa* [167]. Nevertheless, the presence of both of these quinolone compounds has demonstrated an ability to affect the phenotypes of different Gram-positive bacteria, Gram-negative bacteria and

pathogenic yeast [177]. Some microbes are able to avoid this phenotypic alteration by PQS. In a co-culture of *P. aeruginosa* and *Candida albicans*, the *C. albicans* signaling molecule farnesol affected the PQS quorum sensing system of the bacteria by binding to PqsR, inhibiting transcription of *pqsA* [178]. Further studies suggest that indole, a signaling compound from *E. coli*, can also inhibit PQS signaling [179].

The PQS-mediated quorum sensing of *P. aeruginosa* can also be inhibited through modification of its chemical structure. There are currently three known mechanisms of PQS deactivation; conversion to anthranilic acid by *Rhodococcus* sp. BG43 [180,] conversion to 2-heptyl-2-hydroxy-1,2-dihydroquinoline-3,4-dione (HHQD) by *Achromobacter xylosoxidans* Q19 [181] and conversion to *N*-octanoylanthranilic acid by the exogenously supplemented 1H-3-hydroxy-4-oxoquinaldine 2,4-dioxygenase Hod [182]. Each of these mechanisms involves modification of the structure at the C-3 position suggesting the substituent at this position is important for activity. To determine whether the glucuronidation of PQS at C-3 is a fourth method of inhibiting PQS quorum sensing, the activity of PQS-GlcA was evaluated by Leon Liang. The assay utilized the bioreporter strain *Pseudomonas putida* KT2440 [*pBBR-pqsR-pqsA'-'lacZ*] [183] which was not capable of producing HHQ or PQS. The strain contained a plasmid with the *psqR* gene which encoded the PqsR receptor, and the *pqsA* gene which is regulated by PqsR. The *pqsA* gene was fused to the *lacZ* reporter gene. Thus, the binding of quorum sensing-active molecules to PqsR activated the transcription of both *pqsA* and *lacZ*. Quorum sensing activity was determined by measuring the activity of the catalytically active *β*-galactosidase produced by *lacZ*.

The activity of PQS-GlcA (**3**) was compared to that of HHQ and PQS which were also tested in the assay. The half-maximal effective concentrations (EC_{50}) of PQS and HHQ were 0.03 ± 0.14 μM and 1.31 ± 0.17 μM respectively, which were comparable to a previous report [183]. The activity of **3** was much lower, with an EC_{50} value of 1.60 ± 0.01 mM. The results suggest that the glucuronidation of PQS causes inhibition of quorum sensing activity and therefore is a fourth method of PQS deactivation, performed by *Streptomyces* sp. RKBH B178. The presence of **3** in both HHQ- and PQS-supplemented cultures suggests this can be both a one- and two-step process. In order for the glucuronidation to take place in the HHQ-supplemented fermentations, *Streptomyces* sp. RKBH B178 likely has a monooxygenase isofunctional to PqsH in order to hydroxylate the C-3 position. This has also been suggested in the case of *Rhodococcus* sp. BG43 which was found to turn HHQ into PQS before deactivation by conversion to anthranilic acid [180]. Glucuronidation can then take place at the hydroxyl on C-3 by way of a glucuronosyltransferase. A schematic of the four PQS deactivation mechanisms is shown in Figure 2.18.

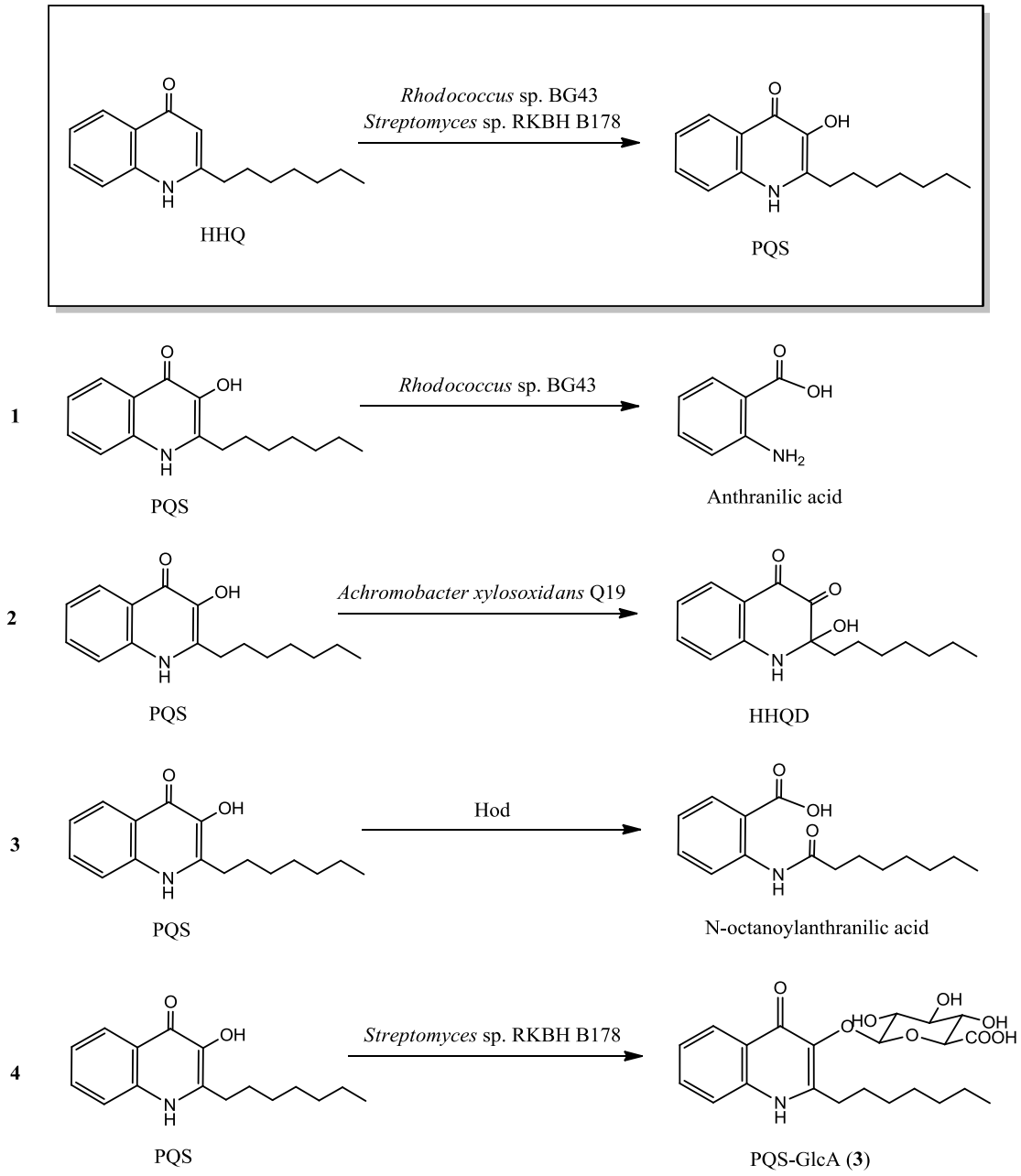

Figure 2.18. A schematic showing the biotransformation of HHQ to PQS by *Rhodococcus* sp. G43 and *Streptomyces* sp. RKBH B178 followed by the three known, and our new, PQS quorum sensing deactivation mechanisms.

As previously mentioned, glucuronidation is associated with the detoxification process. Presumably *Streptomyces* sp. RKBH B178 performs this deactivation in order to protect itself against harmful effects of HHQ and PQS, however when tested, the growth of the bacterium was not inhibited by HHQ. When evaluated for their ability to block quorum sensing in this manner, none of the 16 additional actinomycetes tested were able to biotransform HHQ into PQS-GlcA suggesting they are devoid of this glucuronosyltransferase. Though the reason for PQS-GlcA formation by *Streptomyces* sp. RKBH B178 remains unclear, the enzymatic deactivation of the *P. aeruginosa* quorum sensing molecules is a subject of current research for the development of therapeutics targeting infections in humans.

CHAPTER 3

CONCLUSIONS

3.1. THE EFFECTS OF VARYING CULTURE MEDIA ON NATURAL PRODUCT PRODUCTION

Two species of the rare genus *Kitasatospora* and a streptomycete were evaluated for natural product production in 14 different media in an OSMAC [105] approach. Metabolomics analysis via the creation of chemical barcodes allowed visualization of the effects of using different culture media for natural product production. This methodology revealed many metabolites whose production was upregulated or induced as a result of fermentation in specific media. The results indicated that the activation of otherwise "silent" gene clusters took place and successfully elicited the expression of cryptic natural products.

The Prince Edward Island sediment isolate *Streptomyces* sp. RKND004 was prioritized for further investigation based on the production of a large family of metabolites that were induced in a number of media. A comparison of the relative production levels of these compounds in each of the different media using MZmine 2 [133] allowed the selection of an optimal medium for large-scale fermentations. Two members of this family were purified and identified as polyether ionophores. Although one of the compounds had been reported once in a patent (which was lacking spectroscopic characterization and bioactivity data), its analogue was new. The compounds, which were named terrosamycin A and B, exhibited excellent antibiotic activity toward Gram-positive pathogens which was expected based on their structures. Interestingly, both analogues showed selective anticancer activity; growth inhibition of two breast cancer cell lines was observed while the growth of healthy cells was not affected to the same extent.

The antibiotic activity of the terrosamycins was comparable to a number of polyether standards which are currently used commercially as antibiotic and anticoccidial agents in veterinary medicine. The patent for terrosamycin A (formerly N664-30) was filed by the large pharmaceutical company Pfizer Inc. for use in veterinary medicine [135]. Although no clinical trial data exists for this compound and the patent has now expired, the use of the terrosamycins in this industry is still a possibility pending further *in-vitro* and *in-vivo* testing. Polyether ionophores have never been used for infections in humans because of the toxicity observed in some mammals [71] and until recently, have been completely overlooked for their treatment of human cancers [87, 71, 156]. Excitingly, the terrosamycins, particularly the new analogue terrosamycin B, exhibited better growth inhibition of cancerous cells than salinomycin which has progressed into pilot clinical trials [90]. Though these are only preliminary findings, the results suggest the terrosamycins are promising new candidates for development as anticancer agents.

3.2. THE EFFECTS OF CO-CULTURE MIMIC CONDITIONS ON NATURAL PRODUCT PRODUCTION

In the continued search for cryptic natural products, the three actinomycetes *K. cystarginea*, *K. griseola* and *Streptomyces* sp. RKND004 were subjected to co-culture mimic conditions. The experiments used a group of taxonomically diverse, yet ecologically relevant stressor organisms. Metabolomics analysis using MZmine 2 showed 86 mass features that appeared to be induced with respect to the detection threshold. Manual inspection of the raw data revealed 14 of those features were truly induced metabolites. Furthermore, 19 were upregulated metabolites. These compounds had few or

no hits in AntiBase suggesting that many of them may be both cryptic and novel natural products.

Microbial co-culture is an increasingly popular technique for the induction of cryptic natural products. The use of heat-killed cultures as a source of stress has been used in the past however the producer/stressor combinations used in this study have never before been explored in live co-cultures nor in co-culture mimics. An attempt to find optimal concentrations and addition time-points of the stressors was inconclusive; a more extensive set of optimization experiments are required. Moreover, the reproducibility of the inductions that took place should be confirmed through additional experiments before large-scale fermentations and purification of any of the metabolites is pursued.

3.3. PURIFICATION AND STRUCTURE ELUCIDATION OF PUTATIVELY NEW COMPOUNDS FROM INDUCTION EXPERIMENTS

PQS-GlcA, a new biotransformation product was isolated from fermentations of *Streptomyces* sp. RKBH-B178 supplemented with the *P. aeruginosa* quorum sensing molecule HHQ. Similar to both HHQ and PQS, PQS-GlcA is a 2-alkyl-4-quinolone, however it possesses a glucuronic acid moiety at the C-3 position. The presence of PQS-GlcA in fermentations of the bacterium with either HHQ or PQS suggested this glucuronidation can occur in both a one-step and two-step process; direct glycosylation of the hydroxyl at C-3 of PQS or hydroxylation at C-3 of HHQ followed by the glycosylation. An evaluation of quorum sensing activity of HHQ, PQS and PQS-GlcA revealed the glucuronidation is a novel method of quorum sensing deactivation; the newest of only three currently known methods. Although it is unclear why *Streptomyces* sp. RKBH-B178 is able to perform this biotransformation, this new deactivation

mechanism may find an application in the area of therapeutics targeting *P. aeruginosa* infections which is predominant in the lungs of patients with cystic fibrosis.

In addition to PQS-GlcA, the known compounds bhimamycin A and E were purified and characterized from *Streptomyces* sp. RKBH-B178 fermentations. These compounds were previously reported to be produced by a terrestrial streptomycete and possess moderate activity against some Gram-positive and Gram-negative pathogens. Interestingly, bhimamycin A showed upregulation in response to both the presence of a *P. aeruginosa* stressor and pure HHQ addition. Despite this upregulation, the compound showed no activity against *P. aeruginosa*.

3.4. CONCLUDING REMARKS AND FUTURE DIRECTIONS

Overall, all three of these studies demonstrated the validity of our approaches to unveiling cryptic natural products. Despite being perhaps the most extensively studied genus for the production of bioactive compounds, our OSMAC approach using various culture media coupled to metabolomics analysis via creation of chemical barcodes led to the discovery of the terrosamycins from *Streptomyces* sp. RKND004. Had *Streptomyces* sp. RKND004 not been subjected to fermentation in these different media, the terrosamycins may have never been discovered. Furthermore, subjecting strains from the relatively understudied genus *Kitasatospora* to a variety of culture media generated a list of high-priority, putatively novel candidate metabolites for future purification and characterization efforts. The results showed that just by simply varying the culture media, activation of cryptic gene clusters took place which exposed numerous compounds that are awaiting discovery. Though the OSMAC approach is well documented and has been

successful countless times in the past, this project has shown that it remains a useful technique and should continue to be used in natural product discovery programs.

The co-culture mimic approach coupled with metabolomics analysis also proved to be a useful technique for natural product discovery. Two separate but similar projects lead to the identification of induced metabolites, showing that the presence of dead cells and secreted biomolecules of stressor organisms triggered the activation of silent gene clusters. Though PQS-GlcA is a biotransformation product, and not a true cryptic secondary metabolite biosynthesized by the producer bacterium, bioactivity testing unveiled a novel quorum sensing deactivation mechanism that may have an important application in medicine. This finding demonstrates the validity of co-culture and more specifically, co-culture mimic experiments in quorum sensing studies. It also highlights the importance of biotransformation products and suggests that the discovery of these products may be just as interesting and useful as that of true natural products. Purification of the other induced metabolites found from these projects was not pursued and verification of their induction through additional experiments should be completed, however the list that was generated may be a starting point for future cryptic natural product discovery.

CHAPTER 4

EXPERIMENTAL

4.1. GENERAL EXPERIMENTAL PROCEDURES

4.1.1. Origins and maintenance of bacteria and stressor organisms

The bacterial strains *Kitasatospora cystarginea* NRRL B-16505 [184] and *Kitasatospora griseola* NRRL B-16229 [185] were isolated from Japanese soil and were obtained from the Agriculture Research Services Culture Collection. The strain *Streptomyces* sp. RKND004 was previously isolated by the Kerr lab from a sediment sample collected in Burnt River, Prince Edward Island in August, 2010 (46.19073° N, 62.48882° W, -43 m in depth). *Streptomyces* sp. RKBH-B178 was isolated from a sediment sample collected in Bonne Bay, Newfoundland in August, 2009. The strains were first cultured from glycerol stocks onto ISP2 or ISP3 [121] agar plates and incubated at 30 °C. Liquid seed cultures of each strain were streaked onto TSA [125] plates and incubated at 30 °C to check for purity. All plates were stored long term at 4 °C. Fresh glycerol stocks of each strain were prepared from plate cultures and stored indefinitely at -80 °C.

The fungal stressor organism *Aspergillus flavus* NRRL 3357 was obtained from the Agriculture Research Services Culture Collection. The bacterial stressors *Bacillus subtilis* ATCC 6051 and *Mycobacterium smegmatis* ATCC 12051 were obtained from the American Type Culture Collection. The strains were cultured from glycerol stocks onto ISP2 agar plates and incubated at 30 °C. Liquid cultures of each strain were streaked onto TSA plates and incubated at 30 °C to check for purity. Plates were stored long term at 4 °C. Fresh glycerol stocks of each strain were prepared from plate cultures and stored indefinitely at -80 °C.

The nematode *Caenorhabditis elegans* N2 (wild type strain) growing on an agar plate with an *Escherichia coli* OP50 lawn was obtained from the Caenorhabditis Genetics Centre (Saint Paul, MN, USA) [163]. A scraping of the *E. coli* lawn was streaked onto a fresh NGM agar plate to assess purity. A single colony from the purity plate was scraped and used to inoculate 5 mL of sterile diH_2O and vortexed for 5 seconds. Lawns of *E. coli* on NGM agar plates were prepared by spreading a 100 μL aliquot in a circle using a sterile L-shaped spreader and incubating overnight at 30 °C. Plates were stored long term at 4 °C. The nematodes were subcultured onto new *E. coli* lawns using the chunking method: a sterile spatula was used to excise a 1 cm^2 section of agar containing many nematodes and the chunk was set on top of a new lawn [163]. The plates were left at rt for four to six days before subculturing onto a fresh plate with an *E. coli* lawn to maintain the nematodes [163]. Soft agar freezing solution was used to prepare stocks of *C. elegans* to be stored at -80 °C indefinitely [163].

4.1.2. Preparation of liquid media

Recipes for liquid media used in these experiments are listed in Table 2.1. All ingredients were purchased from Sigma-Aldrich, Fisher Scientific, VWR, EMD Millipore or BD unless otherwise stated. Media was prepared using Milli-Q quality diH_2O from a Milli-Q Millipore Biocel water purification system. The pH was adjusted as required using 1 M NaOH or 1 M HCl. After preparation, the media were sterilized by autoclaving at 122 °C and 16 psi for 20 min. Media for small scale fermentations and seed cultures were prepared and sterilized in flasks and then transferred aseptically into sterile 25 × 150 mm culture tubes containing 4 to 6 glass beads, while media for large scale fermentations were prepared and sterilized directly in the appropriate fermentation

vessels as indicated. The purity of each culture was assessed after each seed fermentation by streaking the broth onto a TSA plate with a sterile inoculation loop. Purity plates were incubated at 30 °C for several days and checked periodically for contamination.

4.1.3. LC-MS sample preparation and analysis

Fermentation extracts were resuspended in MeOH to a concentration of 500 μg/mL and a 10 μL aliquot was analyzed by UHPLC-HRMS using Accela Thermo Scientific equipment. A Core Shell 100 Å C_{18} column (Kintex, 1.7 μm 50 × 2.1 mm) and a flow rate of 500 μL/min was used. The solvents used were diH_2O with 0.1% formic acid (solvent A) and ACN with 0.1% formic acid (solvent B). Each sample was eluted with a linear solvent gradient from 5% to 100% solvent B over 4.8 min. This was followed by an isocratic elution at 100% solvent B for 3.2 min. Following each run, the system was then returned to the starting conditions over 3 min. Eluent was detected by HRESIMS using an Exactive Orbitrap mass spectrometer monitoring at *m/z* 190-2000 in positive mode, a Sedex 80 low temperature-evaporative light scattering detector (LT-ELSD), and a photodiode array (PDA) detector monitoring at 200-600 nm. Reserpine at a concentration of 25 μg/mL in MeOH was used as an instrumental control for each batch of analysis. Three MeOH blanks were also included in each batch; one at the beginning of the batch, one after the reserpine control and one at the end of the batch following the experimental samples.

4.1.4. Characterization of target compounds

Optical rotations were measured on a Rudolph Autopol III polarimeter using a 50 mm microcell (1 mL). Infrared spectra were recorded on a Thermo 6700 FTIR spectrometer using a SMART iTR attenuated total reflectance accessory. NMR spectra

were obtained on a 600 MHz Bruker Avance III NMR spectrometer equipped with a cryoprobe. Chemical shifts (δ) are reported in ppm and were referenced to the MeOD-d_4 residual peaks at δ_H 3.31 ppm and δ_C 49.15 ppm. Multiplicities were reported using the abbreviations s (singlet), d (doublet), t (triplet), appt (apparent triplet), q (quartet), dd (doublet of doublets), dq (doublet of quartets), td (triplet of doublets) and m (multiplet). Coupling constants (*J*) were reported in Hz. UHPLC-HRMS data was recorded using Accela Thermo equipment with MS-ELSD-PDA detection as described in the previous section. Tandem MS spectra were recorded on a Thermo LTQ Orbitrap Velos mass spectrometer and were acquired by direct infusion of the samples (10 μg/mL) at 3 μL/min using an ESI source and fragmented using collision-induced dissociation (CID) at 35 eV.

4.2. THE EFFECTS OF VARYING CULTURE MEDIA ON NATURAL PRODUCT PRODUCTION AND THE DISCOVERY OF TERROSAMYCIN A AND B

4.2.1. Identification of *Streptomyces* sp. RKND004

Streptomyces sp. RKND004 was fermented in bacterial seed medium [124] (BSM) at 200 rpm and 30 °C for 72 h. Genomic DNA was isolated using a phenol/chloroform/isoamyl alcohol extraction method [186] for use as a template for PCR reactions. Primers used for amplification of the 16S rRNA gene were 27F (5'-AGAGTTTGATCCTGGCTCAG-3') and 1525R (5'-AAGGAGGTGATCCAGCC-3') [187]. Primers used for amplification of the *rpoB* gene were SRPOF1 (5'-TCGATCGGGCACATGCGGCC-3') and SRPOR1 (5'-TCGACCACTTCGGCAACCGC-3') 117. PCR was performed in total volumes of 25 μL consisting of 12.5 μL EconoTaq PLUS GREEN 2x master mix (Lucigen, Middleton, WI,

USA), 1.25 µL DMSO, 7.5 µL diH_2O, 0.5 µM of the forward and reverse primers and genomic DNA (1.25 µL of a 300 µL dilution). Thermocycler (Eppendorf Mastercycler) conditions were as follows: denaturation at 95 °C for 2.5 min, 30 cycles of 95 °C for 30 s, 57 °C for 45 s, 72 °C for 1 min, followed by a final extension at 72 °C for 5 min and held at 10 °C for storage. Amplicons were assessed for appropriate size using agarose gel electrophoresis.

Sequencing of both 16S rRNA and *rpoB* amplicons was performed by Eurofins MWG Operon (Hunstville, AL, USA). Full-length 16S rRNA gene sequencing (1471 bp) was completed using the primers 16S530R, 16S514F, 16S936R, 16S1525R, 16S1114F and 16S27F [188]. Sequencing of the *rpoB* gene (253 bp) was completed using the primers SRPOF1 and SRPOR1 117. Sequences were analyzed and edited using the software program Geneious (Auckland, New Zealand) and compared to existing sequences within the NCBI database using the Basic Local Alignment Search Tool (BLAST) [119].

4.2.2. Small-scale fermentations and extractions

Two successive seed cultures of *K. cystarginea*, *K. griseola*, and *Streptomyces* sp. RKND004 were fermented in a 10 mL aliquot of BSM (10 g/L dextrose, 4 g/L yeast extract, 0.4 g/L nutrient agar, 15 g/L soluble starch, 1 g/L calcium carbonate, 4 g/L N-Z Amine A®). A scraping of a single colony from agar plates was used to inoculate the first seed culture for each strain. After fermenting at 200 rpm and 30 °C for 72 h, a 1 mL aliquot of the first seed culture was used to inoculate the second 10 mL seed culture which was fermented under the same conditions for 48 h. A 10 mL aliquot of each production medium (Table 2.1) was then inoculated in triplicate with 300 µL of seed culture and fermented under the same conditions for five days. Uninoculated media

blanks were included as negative controls and were subjected to the same fermentation conditions. The cultures (126 tubes) and negative controls (14 tubes) were extracted by adding 10 mL EtOAc directly to the fermentation tubes and shaking at 200 rpm at rt for 1 h each time. The organic layers were removed via aspiration with a Pasteur pipette and evaporated to dryness. The extracts were resuspended in MeOH to a concentration of 500 μg/mL and 10 μL aliquots were analyzed by LC-MS over seven batches.

4.2.3. Data analysis and identification of target compounds

All raw LC-MS data was first inspected manually for major differences in secondary metabolite production as a result of different culture conditions and the mass and retention times of interesting metabolites was noted. The data was processed in three separate batches, one for each bacterium. Data for all experimental extracts and negative controls were processed as previously described by our group [41] with a number of additions. First, the Xcalibur (Thermo Scientific software) file converter was used to convert .RAW files generated by the instrument for each sample into their respective .CDF files. The .CDF files were imported into the open-source software program MZmine 2 [133]. In MZmine 2, mass detection was performed using the exact mass parameter with an intensity threshold set at 1E4, *m/z* tolerance was defined at 0.005 and t_R tolerance was defined at 0.01 min. Default settings were used for all subsequent parameters. Chromatogram building and de-isotoping was carried out as previously described [41], with the addition of a chromatogram deconvolution step between them. Linear normalization using the maximum peak intensity method was then applied; individual files were normalized by dividing the area of each peak by the area of the largest peak within that sample. Bucket alignment was performed [41] and a peak list was

generated. Gap filling using the peak finder method with default settings was applied in order ensure detection of mass features that may be present in some scans but not others. Mass features that were present in the negative controls, MeOH and reserpine samples were manually removed from the peak list. The processed peak list was exported as a .CSV file and presence-absence chemical barcodes were created using conditional formatting. Mass features with a peak area equal to zero were coloured white while those with a peak area greater than zero were coloured black. In MZmine 2, the processed peak list was used to create ion intensity plots for visualization of relative quantities of specific metabolites produced by a strain across all conditions screened. The masses of $[M+H]^+$, $[M-H]^-$ or $[M+Na]^+$ pseudomolecular ions of interesting metabolites were queried in the natural products database AntiBase [134] and the chemical database SciFinder to identify putatively novel compounds.

4.2.4. Large-scale fermentations and purification of terrosamycin A and B

Two successive seed cultures of *Streptomyces* sp. RKND004 were fermented as previously described (section 4.2.2). A total volume of 9 L (9 × 1 L in Fernbach flasks) of BFM3 was fermented with a 2.9% (v/v) inoculum from seed cultures for five days at 200 rpm and 30 °C. Each culture flask was extracted twice with 400 mL EtOAc overnight at rt and the organic layers were combined and evaporated to dryness. The resulting extract was fractionated by automated flash chromatography using a Combiflash Rf (Teledyne ISCO) system with a 43 g C_{18} column (High Performance GOLD, RediSep Rf) and eluted with a flow rate of 20 mL/min. A linear gradient from 1:9 MeOH:diH_2O to 100% MeOH over 24 min followed by 100% MeOH for 10 min was used and eluent was detected by UV at 214 and 254 nm. Fractions containing terrosamycin A and B eluted at

32.5-34.0 min and were combined and further separated via automated flash chromatography with a 12 g silica column (High Performance GOLD, RediSep Rf). The mixture was eluted at 30 mL/min with a gradient of 2:8 acetone:hexanes to 100% acetone over 18 min followed by 100% acetone for 20 min. The eluent was detected by UV at 214 and 254 nm. Terrosamycin A (**1**) and B (**2**) eluted at 3.0 min and 4.0 min, respectively.

Terrosamycin A (**1**): colourless glass; $[\alpha]^{28}_{D}$ -77 (*c* 0.25, MeOH); IR ν_{max} 3331, 2968, 2924, 1714, 1577, 1456, 1377, 1105, 1087, 1066, 1042, 1001 cm^{-1}; ^{1}H and ^{13}C NMR data see Table 2.3; (-) HRESIMS *m/z* 811.5205 $[M-H]^-$ (calcd for $C_{44}H_{75}O_{13}$, 811.52132).

Terrosamycin B (**2**): colourless glass; $[\alpha]^{27}_{D}$ -141 (*c* 1.08, MeOH); IR ν_{max} 3479, 2962, 2929, 2854, 1710, 1458, 1378, 1189, 1086, 1067, 1053, 1002 cm^{-1}; ^{1}H and ^{13}C NMR data see Table 2.3; (-) HRESIMS *m/z* 839.5504 $[M-H]^-$ (calcd for $C_{46}H_{79}O_{13}$, 839.55262).

4.2.5. Crystallization of terrosamycin A and analysis of X-ray diffraction data

Terrosamycin A was dissolved in 50% aqueous ethanol and converted to a salt by adding NaOH dropwise until the pH was higher than 11. The sample was dried under air and resuspended in 0.5 mL acetone and five drops of diH_2O. Crystals were grown using a slow solvent evaporation method at 4 °C over about one month. The mother liquor was removed via aspiration with a syringe and the crystals were sent to Dr. Andreas Decken at the University of New Brunswick in Fredericton, New Brunswick who performed XRD analysis and structure refinement. Single crystals were coated with Paratone-N oil,

mounted using a polyimide MicroMount and frozen in the cold nitrogen stream of the goniometer. A hemisphere of data was collected on a Bruker AXS P4/SMART 1000 diffractometer using ω and ϕ scans with a scan width of 0.3° and 10 s exposure times. The detector distance was 5 cm. The data were reduced (SAINT) [189] and corrected for absorption (SADABS) [190]. The structure was solved by direct methods and refined by full-matrix least squares on F^2 (SHELXTL) [191]. The acetone molecule was disordered over two positions. All non-hydrogen atoms were refined using anisotropic displacement parameters. Hydrogen atoms were included in calculated positions and refined using a riding model with the exception of hydrogen atoms of potassium (K) bound hydroxides that were found in Fourier difference maps and refined using bond distance restraints. The crystal structure was visualized using the open-source software package CRYSTALS and images were created using the built-in Cameron package.

Crystal Data for terrosamycin A (**1**): $C_{44}H_{75}KO_{13}$; fw = 889.19; monoclinic space group P2(1); unit cell dimensions a = 12.004(3) Å, b = 35.796(10) Å, c = 12.020(3) Å, V = 5015(2) $Å^3$, α = 90°, β = 103.826(4)°, γ = 90°; μ(Cu Kα) = 0.166 mm^{-1}; Z = 4; D_{calc} = 1.178 Mg/m^3; 34 113 reflections measured (1.74° ≤ 2θ ≤ 27.50°), 21746 independent [R_{int} = 0.0760], which were used in all calculations. The final R_1 was 0.0770 [$I > 2\sigma(I)$] and wR_2 was 0.1886 (all data).

4.2.6. Bioactivity of terrosamycin A and B

The antimicrobial activity of **1** and **2** was evaluated using panel of human microbial pathogens including methicillin-resistant *S. aureus* ATCC 33591 (MRSA), vancomycin resistant *E. faecium* EF379 (VRE), *S. warneri* ATCC 17917, *P. aeruginosa* ATCC 14210, *P. vulgaris* ATCC 12454 and *C. albicans* ATCC 14035.

Assays were performed by technician Martin Lanteigne of the Kerr lab according to Clinical Laboratory Standards Institute testing standards in a 96-well plate and in triplicate [192]. Terrosamycin A and B were dissolved in sterile 20% DMSO and serially diluted creating a range of twelve concentrations between 128 μg/mL and 0.0625 μg/mL. A Thermo Scientific Varioskan Flash plate reader was used to determine cell growth by measuring the optical density at 600 nm at time zero and after incubation at 37 ºC for 22 h. The change in OD_{600} was calculated, percentages of microorganism survival were compared to the vehicle control wells and IC_{50} values were determined. Control antibiotics used were vancomycin for MRSA and *S. warneri*, rifampicin for VRE, gentamycin for *P. aeruginosa*, ciprofloxacin for *P. vulgaris* and nystatin for *C. albicans*.

The cytotoxicity of **1** and **2** was evaluated using two healthy cell lines, human foreskin fibroblast cells (BJ, ATCC CRL-2522) and *Cercopithecus aethiops* kidney epithelial cells (Vero, ATCC CCL-81) as well as two cancer cell lines, human breast adenocarcinoma cells (ATCC HTB-26) and human invasive breast ductal carcinoma cells (ATCC MCF-7). Assays were performed by technician Kate McQuillan of Nautilus Biosciences Inc. Each cell line was grown and maintained in 15 mL of Eagle's Minimal Essential Medium in T75 cm^2 cell culture flasks with the exception of HTB-26 cells which were grown in Dulbecco's Modified Eagle's Medium/Nutrient Mixture F-12 Ham. All growth media was supplemented with 10% fetal bovine serum, 100 μU/mL penicillin and 0.1 mg/mL streptomycin; the growth medium for MCF-7 cells was also supplemented with 0.01 mg/mL human recombinant insulin. All cell cultures were incubated at 37 °C in a humidified atmosphere with 5% CO_2 and culture media was refreshed every two to three days. The cells were not allowed to exceed 80% confluency.

At 80% confluency the cells were counted and diluted in their respective growth medium without addition of antibiotics. Aliquots of 90 μL were added to a microwell plate at a density of 1×10^4 cells/well for Vero and HTB-26 cells and 5×10^3 cells/well for BJ fibroblast and MCF-7 cells. The plates were incubated at 37 °C with 5% CO_2 for 24 h to allow cells to adhere to the plates prior to treatment. The vehicle DMSO was used to dissolve **1** and **2** and was present at a final concentration of 1% in each of the wells. A dilution series was prepared for each cell line using the respective growth medium and 10 μL aliquots of each was added to the respective plate in concentrations ranging from 128 μg/mL to 1 μg/mL in triplicate. Positive control wells contained only the growth medium and DMSO, negative control wells contained the growth medium, DMSO and cells and positive treated controls contained the growth medium, cells and a concentration range of either zinc pyrithione (BJ fibroblast), phenoxyethanol (Vero), or doxorubicin (HTB-26 and MCF-7). All plates were incubated at 37 °C with 5% CO_2 for 24 h (BJ fibroblast, Vero) or 72 h (HTB-26, MCF-7). Following incubation, alamarBlue® was added to each well at a concentration of 10% (v/v). Fluorescence was measured at 560 nm excitation and 590 nm emission using a Thermo Scientific Varioskan Flash plate reader at time zero and 4 h after treatment with alamarBlue®. The change in 590 nm emission reading was used to calculate percent cell viability after each treatment relative to the negative controls. The IC_{50} values of **1** and **2** for each cell line was calculated using GraphPad Prism 6.0 using a nonlinear regression dose response, variable slope model and standard deviation was calculated based on triplicate measurements.

4.3. THE EFFECTS OF CO-CULTURE MIMIC CONDITIONS ON NATURAL PRODUCT PRODUCTION

4.3.1. Preparation of stressors

Two successive seed cultures of the fungal stressor *A. flavus* and the bacterial stressors *B. subtilis* and *M. smegmatis* were fermented in a 10 mL portion of BHI [193] broth (premix, BD). A scraping of a single colony from the agar plates was used to inoculate the first seed culture for each bacterial strain, while a 1 cm^2 section of agar was excised and used to inoculate the first seed culture of *A. flavus*. After fermenting at 200 rpm and 30 °C for 72 h, a 1 mL aliquot of the first seed culture was used to inoculate the second 10 mL seed culture which was fermented under the same conditions for 48 h. A volume of 500 mL of BHI broth in Fernbach flasks was inoculated with 2.5 mL of seed culture for each strain and fermented for five days at 200 rpm and 30 °C.

A large-scale fermentation of *E. coli* was completed using a scraping of a single colony from a purity plate to directly inoculate 2 L (2 × 1L in Fernbach flasks) of Lysogeny broth (LB) (premix, EMD Millipore). The culture was allowed to grow overnight at 200 rpm and 37 °C. The cells were pelleted by centrifugation (2 × 1L in sterile centrifuge tubes, 6000 rpm for 10 min) and the supernatant was removed via aspiration. Each pellet was resuspended in 50 mL S medium [163] and each was added to 200 mL S medium in 1L Erlenmeyer flasks. S medium (5 mL per plate) was used to wash four NGM agar plates containing *C. elegans* on a freshly cleared lawn of *E. coli*. The washes were collected and added to one of the two *E. coli* inoculated flasks while the other flask remained axenic to be used as a control for co-culture mimic fermentations.

Both cultures were fermented at rt and 200 rpm for 72 h. Nematode growth was monitored daily by viewing a drop of the culture under a compound microscope.

All stressor cultures were killed by autoclaving at 122 °C and 16 psi for 20 min. The fungal culture of *A. flavus* was homogenized prior to autoclaving with a hand-held blender. All cultures were checked for purity before autoclaving by streaking onto a TSA plate (*A. flavus*, *B. subtilis* and *M. smegmatis*) or NGM agar plate (*C. elegans*/*E. coli* and *E. coli*). The cultures were also streaked post-autoclaving to ensure sterilization. A 100-fold dilution of each stressor (including the axenic *E. coli* control) was prepared by adding 20 mL of the dead culture to 180 mL sterile diH_2O. A control for co-culture mimic fermentations with *A. flavus*, *B. subtilis* and *M. smegmatis* was prepared using twice-autoclaved liquid BHI medium and performing a 100-fold dilution as described above. The stressors and controls, both concentrated and dilute solutions, were stored in sterile, sealed bottles covered in aluminum foil at 4 °C.

4.3.2. Small-scale fermentations and extractions

Seed cultures of *K. cystarginea*, *K. griseola* and *Streptomyces* sp. RKND004 were inoculated from agar plates and fermented as previously described (section 4.2.2). Tubes containing 9 mL of the production medium BFM4 were inoculated with 300 μL aliquots of seed culture; 20 tubes were inoculated for each strain. Uninoculated fermentations containing only BFM4 (six tubes) were included as media blanks. All cultures and blanks were fermented at 200 rpm and 30°C for 48 h before addition of the stressors. For each strain, 1 mL of each stressor (six stressors: *A. flavus*, *B. subtilis* and *M. smegmatis* both concentrated and 100-fold diluted), was added to a culture in triplicate accounting for 18 tubes. The remaining two tubes were designated as no-stress controls; one receiving 1 mL

of twice-autoclaved BHI and the other receiving 1 mL of the 100-fold diluted twice-autoclaved BHI. Each of the six media blanks were treated with one of the six stressors. All cultures and blanks were fermented under the same conditions for 72 h further. Each of the 66 tubes was extracted as previously described (section 4.2.2). The extracts were resuspended in MeOH to a concentration of 500 μg/mL and 10 μL aliquots were analyzed by LC-MS over two batches.

Tubes containing 9 mL of the production medium BFM3 were inoculated with 300 μL aliquots of seed culture; 16 tubes were inoculated for each strain (including four control tubes). Uninoculated fermentations containing only BFM3 (four tubes) were included as media blanks. At the time of inoculation (day 0), 1 mL of either stressor (concentrated or 100-fold diluted *C. elegans*/*E. coli*) was added to a culture in triplicate accounting for six tubes. Each stressor was also added to a media blank tube. To two of the four control tubes, either concentrated or diluted axenic *E. coli* control stressor was added. All cultures and blanks were fermented at 200 rpm and 30 °C for four days. On day 4, the stressors were added in the same way to the remaining cultures, control cultures and media blanks. All tubes were fermented under the same conditions for a further 24 h. Each of the 52 tubes was extracted as previously described (section 4.2.2). The extracts were resuspended in MeOH to a concentration of 500 μg/mL and 10 μL aliquots were analyzed by LC-MS over two batches.

4.3.3. Data analysis and identification of upregulated and induced compounds

Raw LC-MS data was inspected manually and processed using MZmine 2 as previously described (section 4.2.2). Data for each strain grown with each stressor (each set including data from media blanks and BHI added or *E. coli* added controls) was

processed separately. The gap-filled peak list was inspected and any mass features detected in the media blanks were deleted from the entire data set. The list was annotated with possible compound identities for each mass feature by uploading the AntiBase database under the custom database search function. Scatter plots comparing mass features present in stressor-treated cultures with no-stress controls were constructed in MZmine 2. Mass features present in the controls were then deleted from the peak list leaving only putatively induced metabolites. Further, features that were not induced in all three replicates of a given condition were also deleted from the list. The 86 remaining features were located in the raw LC-MS data using XICs. Features that appeared to be part of the noise were eliminated from the list. The control and blank samples were checked for the presence of the remaining genuine metabolites and those that were present in the blanks were also removed from the list. The remaining metabolites were classified as upregulated or induced based on their presence or absence XICs of the controls (Table 2.8).

4.4. PURIFICATION AND STRUCTURE ELUDICATION OF PQS-GLCA

4.4.1. Multi-scale fermentations and extractions

Two successive seed cultures of *Streptomyces* sp. RKBH-B178 were fermented in 10 mL portions of ISP2 broth. A scraping of a single colony from the strain growing on a TSA plate was used to inoculate the first seed culture. After fermenting at 200 rpm and 30 °C for 24 h, a 1 mL aliquot of the first seed cultures were used to inoculate the second 10 mL seed cultures which were fermented under the same conditions for 48 h. A 3% (v/v) aliquot of seed culture was used to inoculate 118 tubes containing 7 mL ISP2 broth, two 250 mL Erlenmeyer flasks containing 50 mL ISP2 broth, one Fernbach flask

containing 600 mL ISP2 broth and one Fernbach flask containing 1 L ISP2 broth. All cultures were fermented at 200 rpm and 30 °C for 48 h before addition of HHQ (3.38 μg of HHQ per mL of fermentation broth). Fermentations continued for 72 h. Two media blanks in tubes were included as negative controls; one for ISP2 and one for ISP2 with added HHQ. A positive control containing ISP2 inoculated with *Streptomyces* sp. RKBH-B178 was also included. Cultures in tubes were extracted twice with 7 mL EtOAc at 200 rpm and rt for 1 h. Larger scale cultures were extracted twice with EtOAc at rt and swirled by hand periodically for 1 h; cultures in 250 mL flasks were extracted with 50 mL and cultures in Fernbach flasks were extracted with 600 mL. The extracts were resuspended in MeOH to a concentration of 500 μg/mL and 10 μL aliquots were analyzed by LC-MS in one batch.

4.4.2. Large-scale fermentations and purification of PQS-GlcA

A large-scale fermentation was completed by Ph. D. student Libang Liang. Two successive seed cultures of *Streptomyces* sp. RKBH B178 were fermented for 72 h each as previously described (section 4.2.2). A total volume of 2.95 L (59 × 50 mL in 250 mL flasks) of the production medium ISP2 was fermented with a 3% (v/v) inoculum from seed cultures and 25 μM HHQ for 6 days at 200 rpm and 30 °C. Each culture flask was extracted twice with 50 mL EtOAc for 1 h at rt and 200 rpm and the organic layers were combined, washed twice with diH_2O in a separatory funnel and evaporated to dryness.

The resulting extract was fractionated by automated flash chromatography using a Combiflash Rf (Teledyne ISCO) system with a 43 g C_{18} column (High Performance GOLD, RediSep Rf) and eluted with a flow rate of 40 mL/min. A linear gradient from 1:9 MeOH:diH_2O to 100% MeOH over 21 min followed by 100% MeOH for 5 min was used

and eluent was detected by UV at 250 and 280 nm. Fractions containing PQS-GlcA (**3**) eluted at 15.0 – 17.5 min and were combined and further separated via subsequent automated flash chromatography using a 13 g C_{18} column (High Performance GOLD, RediSep Rf) with a flow rate of 30 mL/min. An isocratic elution of 1:1 diH_2O:ACN for 6 min was used, followed by a steep gradient to 100% ACN over 1 min and held at 100% ACN for 2.5 min. The eluent was detected by UV at 254 and 278 nm. PQS-GlcA eluted at 0.8 min.

PQS-GlcA (**3**) was purified by RP-HPLC with a Luna 110 Å phenyl hexyl column (5 µm, 250 × 10.00 mm, Phenomenex). An isocratic elution with 55% diH_2O with 0.1% formic acid (solvent A) and 45% ACN with 0.1% formic acid (solvent B) over 15 min was used, followed by a linear increase to 100% solvent B over 1 min and held at 100% solvent B for 10 min. The eluent was monitored by ELSD and UV at 238 and 321 nm. PQS-GlcA eluted at 8.9 min.

PQS-GlcA (**3**): yellow oil; $[\alpha]^{30}_{D}$ -252 (*c* 0.04), MeOH); λ_{max} 239, 231 nm; IR ν_{max} 3278, 2929, 2814, 2188, 2036, 1611, 1517, 1352, 1115 cm^{-1}; ^{1}H and ^{13}C NMR see Table 2.8; (+) HRESIMS *m/z* 436.1961 $[M+H]^+$ (calcd for $C_{22}H_{30}NO_8$, 436.19659).

4.4.3. Stereochemical determination of PQS-GlcA by Tanaka's method

The configuration of the GlcA moiety in PQS-GlcA (**3**) was determined using Tanaka's method [172, 173]. PQS-GlcA (100 µg) was dissolved in 10 µL tetrahydrofuran (THF) and 40 µL diH_2O. Hydrolysis was performed overnight by adding 50 µL 2M HCl and incubating at 95 °C in a sealed reaction vessel. The reaction mixture was evaporated to dryness, resuspended in 50 µL of a 1 mg/mL D-cysteine methyl ester (Tokyo Chemical

Industry, Portland OR, USA) stock solution and sonicated until all particulate matter was dissolved. After incubation at 60 °C for 1 h, 0.5 µL *o*-tolylisothiocyanate (Sigma-Aldrich, St. Louis, MO, USA) (neat) was added and the reaction was mixed well and incubated again at 60 °C for 1 h. The D-D and D-L Tanaka derivative standards were prepared using a similar protocol; two additional reactions were performed with commercial D-GlcA (Sigma-Aldrich, St. Louis, MO, USA) being reacted either with D-cysteine methyl ester or L-cysteine methyl ester (Sigma-Aldrich, St. Louis, MO, USA) to yield the appropriate products. The reaction mixtures were evaporated to dryness and resuspended in MeOH to a concentration of 500 µg/mL. A 10 µL aliquot was analyzed by LC-HRMS using a Hypersil Gold 100 Å column (Thermo, 1.9 µm C_{18} 50 × 2.1 mm) with a flow rate of 400 µL/min. An isocratic elution of 87% diH_2O 0.1% formic acid (solvent A) and 13% MeOH 0.1% formic acid (solvent B) over 20 minutes was used, followed by a linear gradient to 30% solvent B over 8 min and held for 2 min. This was followed by another linear gradient to 100% solvent B over 2 min, held at 100% for 6 min, and a linear decrease to 13% solvent B over 4 min and held for 2.8 min. Eluent was detected by HRESIMS monitoring at *m/z* 190-2000 in positive mode. Retention times of the Tanaka derivatives were as follows: D-GlcA/D-cysteine methyl ester 25.28 min, D-GlcA/L-cysteine methyl ester 26.96 min, PQS-GlcA/D-cysteine methyl ester 25.28 min.

REFERENCES

1. Williams, D. H., Stone, M. J., Hauck, P. R. & Rahman, S. K., Why are secondary metabolites (natural products) biosynthesized? *J Nat Prod* **52**, 1189-1208 (1989).

2. Stone, M. J. & Williams, D. H., On the evolution of functional secondary metabolites (natural products). *Mol Microbiol* **6**, 29-34 (1992).

3. Springob, K. & Kutchan, T. M., in *Plant-derived Natural Products*, edited by Osbourn, A. E. & Lanzotti, V. (Springer-Verlag , New York, 2009), pp. 3-50.

4. Onoyovwe, A. *et al.*, Morphine Biosynthesis in Opium Poppy Involves Two Cell Types: Sieve Elements and Laticifers. *Plant Cell* **25**, 4110-4122 (2013).

5. Wink, M., in *Allelopathy: chemistry and mode of action of allelochemicals*, edited by Macias, F., Galindo, J. C., Molinillo, J. M. & Cutler, H. G. (CRC Press, Boca Raton, FL, 2003).

6. Docimo, T. *et al.*, The first step in the biosynthesis of cocaine in *Erythroxylum coca*: the characterization of arginine and ornithine decaboxylases. *Plant Mol Biol* **78**, 599-615 (2012).

7. Fischbach, M. A. & Walsh, C. T., Assembly-Line Enzymology for Polyketide and Nonribosomal Peptide Antibiotics: Logic, Machinery and Mechanisms. *Chem Rev* **106**, 3486-3496 (2006).

8. Shen, B., Polyketide biosynthesis beyond the type I, II and III polyketide synthase paradigms. *Curr Opin Chem Biol* **7**, 286-295 (2003).

9. Olano, C., Mendez, C. & Salas, J. A., Post-PKS tailoring steps in natural product-producing actinomycetes from the perspective of combinatoral biosynthesis. *Nat Prod Rep* **27**, 571-616 (2010).

10. Felnagle, E. A. *et al.*, Nonribosomal Peptide Synthetases Involved in the Production of Medically Relevant Natural Products. *Mol Pharm* **5**, 191-211 (2008).

11. Walsh, C. T. *et al.*, Tailoring enzymes that modify nonribosomal peptides during and after chain elogation on NRPS assembly lines. *Curr Opin Chem Biol* **5**, 525-534 (2001).

12. Kuhlisch, C. & Pohnert, G., Metabolomics in chemical ecology. *Nat Prod Rep* **32**, 937-955 (2015).

13. Schupp, P. J., Nietzer, S. & Rohde, S., Prevalence and Mechanisms of Dynamic

Chemical Defenses in Tropical Marine Sponges. *PLoS One* **10**, e0132236 (2015).

14. Olivera, B. M., Gray, W. R., Zeikus, R. & McIntosh, J. M., Peptide neurotoxins from the fish-hunting cone snails. *Science* **230**, 1338-1343 (1985).

15. Ghssein, G. *et al.*, Biosynthesis of a broad-spectrum nicotianamine-like metallophore in *Staphylococcus aureus*. *Science* **352**, 1105-1109 (2016).

16. Arnason, J. T. & Bernards, M. A., Impacts of constitutive plant natural products on herbivores and pathogens. *Can J Zool* **88**, 615-627 (2010).

17. Ren, D. *et al.*, Differential gene expression for investigation of *Escherichia coli* biofilm inhibition by plant extract ursolic acid. *Appl Environ Microbiol* **71**, 4022-4034 (2005).

18. Nishida, R., Chemical ecology of insect-plant interactions: ecological significance of plant secondary metabolites. *Biosci Biotechnol Biochem* **78**, 1-13 (2014).

19. Meinwald, J., Natural Products as Molecular Messengers. *J Nat Prod* **74**, 305-309 (2011).

20. Kita, M., Bioorganic Studies on the Key Natural Products form Venomous Mammals and Marine Invertebrates. *Bull Chem Soc Jpn* **85**, 1175-1185 (2012).

21. Moore, K. S. *et al.*, Squalamine: An aminosterol antibiotic from the shark. *Proc Natl Acad Sci* **90**, 1354-1358 (1993).

22. Fleming, A., On the antibacterial action of cultures of *Penicillium*, with special reference to their use in the isolation of *B. influenzae*. *Br J Exp Pathol* **10**, 226-236 (1929).

23. Wiener, P., Experimental studies on the ecological role of antibiotic production in bacteria. *Evol Ecol* **10**, 405-421 (1996).

24. Ola, A. R. B., Thomy, D., Lai, D., Brotz-Oesterhelt, H. & Proksch, P., Inducing secondary metabolite production by the endophytic fungus *Fusarium tricinctum* through coculture with *Bacillus subtilis*. *J Nat Prod* **76**, 2094-2099 (2013).

25. Miller, M. B. & Bassler, B. L., Quorum sensing in bacteria. *Annu Rev Microbiol* **55**, 165-199 (2001).

26. Qian, P. Y., Xu, Y. & Fusetani, N., Natural products as antifouling compounds: recent progress and future perspectives. *Biofouling* **26**, 223-234 (2010).

27. Gunatilaka, A. A. L., Natural Products from Plant-associated Microorganisms: Distribution, Structural Diversity, Bioactivity, and Implications of Their Occurrence.

J Nat Prod **69**, 509-526 (2006).

28. Sacristan-Soriano, O., Banaigs, B., Casamayor, E. O. & Becerro, M. A., Exploring the Links between Natural Products and Bacterial Assemblages in the Sponge *Aplysina aerophoba*. *Appl Environ Microbiol* **77**, 862-870 (2011).

29. Cragg, G. M. & Newman, D. J., Natural products: A continuing source of novel drug leads. *Biochim Biophys Acta* **1830**, 3670-3695 (2013).

30. Shen, B., A New Golden Age of Natural Products Drug Discovery. *Cell* **163**, 1297-1300 (2015).

31. Dias, D. A., Urban, S. & Roessner, U., A Historical Overview of Natural Products in Drug Discovery. *Metabolites* **2**, 303-336 (2012).

32. Newman, D. J. & Cragg, G. M., Natural Products as Sources of New Drugs from 1981 to 2014. *J Nat Prod* **79**, 629-661 (2016).

33. Martins, A., Vieira, H., Gaspar, H. & Santos, S., Marketed Marine Natural Products in the Pharmaceutical and Cosmeceutical Industries: Tips for Success. *Mar Drugs* **12**, 1066-1101 (2014).

34. Burgess, J. G. *et al.*, The development of a marine natural product-based antifouling paint. *Biofouling* **19**, 197-205 (2003).

35. Dayan, F. E., Cantrell, C. L. & Duke, S. O., Natural products in crop protection. *Bioorg Med Chem* **17**, 4022-4034 (2009).

36. Blair, J. M. A., Webber, M. A., Baylay, A. J., Ogbolu, D. O. & Piddock, L. J. V., Molecular mechanisms of antibiotic resistance. *Nature Rev Microbiol* **13**, 42-51 (2015).

37. Silver, L. L., Challenges of Antibacterial Discovery. *Clin Microbiol Rev* **24**, 71-109 (2011).

38. David, B., Wolfender, J. & Dias, D. A., The pharmaceutical industry and natural products: historical status and new trends. *Phytochem Rev* **14**, 299-315 (2015).

39. Guadencio, S. P. & Pereira, F., Dereplication: racing to speed up the natural products discovery process. *Nat Prod Rep* **32**, 779-810 (2015).

40. Hubert, J., Nuzillard, J. & Renault, J., Dereplication strategies in natural product research: How many tools and methodologies behind the same concept? *J Phytochem Rev*, 1-41 (2015).

41. Forner, D., Berrue, F., Correa, H., Duncan, K. & Kerr, R. G., Chemical dereplication of marine actinomycetes by liquid chromatography-high resolution mass

spectrometry profiling and statistical analysis. *Anal Chim Acta* **805**, 70-79 (2013).

42. Ramesha, B. T. *et al.*, Biodiversity and chemodiversity: future prospects in bioprospecting. *Curr Drug Targets* **12**, 1515-1530 (2011).

43. Liu, J. T. *et al.*, Bioactive natural products from the antarctic and arctic organisms. *Mini Rev Med Chem* **13**, 617-627 (2013).

44. Montaser, R. & Luesch, H., Marine natural products: a new wave of drugs? *Future Med Chem* **3**, 1475-1489 (2011).

45. Li, M. H. T., Ung, P. M. U., Zajkowski, J., Garneau-Tsodikova, S. & Sherman, D. H., Automated genome mining for natural products. *BMC Bioinformatics* **10**, 185 (2009).

46. Zerikly, M. & Challis, G. L., Strategies for the discovery of new natural products by genome mining. *Chem Bio Chem* **10**, 625-633 (2009).

47. Kingston, D. G. I., Modern Natural Products Drug Discovery and its Relevance to Biodiversity Conservation. *J Nat Prod* **74**, 496-511 (2011).

48. Berdy, J., Thoughts and facts about antibiotics: Where we are now and where we are heading. *J Antibiot* **65**, 385-395 (2012).

49. Demain, A. L., Importance of microbial natural products and the need to revitalize their discovery. *J Ind Microbiol Biotechnol* **41**, 185-201 (2014).

50. Pickens, L. B., Tang, Y. & Chooi, Y., Metabolic Engineering for the Production of Natural Products. *Annu Rev Chem Biomol Eng* **2**, 211-236 (2011).

51. Lucas, X. *et al.*, StreptomeDB: a resource for natural compounds isolated from *Streptomyces* species. *Nucleic Acids Res* **41**, D1130-D1136 (2013).

52. Chopra, A. & Roberts, M., Tetracycline Antibiotics: Mode of Action, Applications, Molecular Biology and Epidemiology of Bacterial Resistance. *Microbiol Mol Biol Rev* **65**, 232-260 (2001).

53. Levine, D. P., Vancomycin: a history. *Clin Infect Dis* **42**, 5-12 (2006).

54. Baltz, R. H., Miao, V. & Wrigley, S. K., Natural products to drugs: daptomycin and related lipopeptide antibiotics. *Nat Prod Rep* **22**, 727-741 (2005).

55. Orlikova, B., Legrand, N., Panning, J., Dicato, M. & Diederich, M., Anti-inflammatory and anticancer drugs from nature. *Cancer Treat Res* **159**, 123-143 (2014).

56. Saunders, R. N., Metcalfe, M. S. & Nicholson, M. L., Rapamycin in transplantation: a review of the evidence. *Kidney Int* **59**, 3-16 (2001).

57. Floss, H. G. & Yu, T. W., Rifamycin-mode of action, resistance, and biosynthesis. *Chem Rev* **105**, 621-632 (2005).

58. Bernt, K. M. *et al.*, Eradication of CD19+ leukemia by targeted calicheamicin θ. *Bioconjug Chem* **20**, 1587-1594 (2009).

59. Tiwari, K. & Gupta, R. K., Rare actinomycetes: a potential storehouse for novel antibiotcs. *Crit Rev Biotechnol* **32**, 108-132 (2012).

60. Omura, S., Takahashi, Y., Iwai, Y. & Tanaka, H., *Kitasatosporia*, a new genus of the order Actinomycetales. *J Antibiot* **35**, 1013-1019 (1982).

61. Ludwig, W. *et al.*, in *Bergey's Manual of Sytematic Bacteriology*, edited by Whitman, W. *et al.* (Springer-Verlag, New York, 2012), pp. 1-31.

62. Wellington, E., Stackebrandt, E., Sanders, D., Wolstrup, J. & Jordensen, N. O. G., Taxonomic status of *Kitasatospora* and proposed unification with *Streptomyces* on the basis of phenotypic and 16S rRNA analysis and emendation of *Streptomyces*. *Int J Sys Bacteriol* **42**, 156-160 (1992).

63. Zhang, Z., Wang, Y. & Ruan, J., A proposal to revive the genus *Kitasatospora* (Omura, Takahashi, Iwai, and Tanaka 1982). *Int J Sys Bacteriol* **47**, 1048-1054 (1997).

64. Gill, K. A., Berrué, F., Arens, J. C. & Kerr, R. G., Isolation and Structure Elucidation of Cystargamide, a Lipopeptide from *Kitasatospora cystarginea*. *J Nat Prod* **77**, 1372-1376 (2014).

65. Gill, K. A., Berrué, F., Arens, J. C., Carr, G. & Kerr, R. G., Cystargolides, 20S Proteasome Inhibitors Isolated from *Kitasatospora cystarginea*. *J Nat Prod* **78**, 822-826 (2015).

66. Dutton, C. J., Banks, B. K. & Cooper, C. B., Polyether ionophores. *Nat Prod Rep* **165-181**, 12 (1995).

67. Rutkowski, J. & Brzezinski, B., Structures and Properties of Naturally Occuring Polyether Antibiotics. *BioMed Res Int* **2013**, 1-31 (2013).

68. Wang, H. *et al.*, Genetic Screening Strategy for Rapid Access to Polyether Ionophore Producers and Products in Actinomycetes. *Appl Environ Microbiol* **77**, 3433-3442 (2011).

69. Harvey, B. M. *et al.*, Insights into Polyether Biosynthesis from Analysis of the Nigericin Biosynthetic Gene Cluster in *Streptomyces* sp. DMS4137. *Chem Biol* **14**,

703-714 (2007).

70. Jiang, C., Wang, H., Kang, Q., Liu, J. & Bai, L., Cloning and Characterization of the Polyether Salinomycin Biosynthesis Gene Cluster of *Streptomyces albus* XM211. *Appl Environ Microbiol* **78**, 994-1003 (2012).

71. Huczynski, A., Polyether ionophores-promising bioactive molecules for cancer therapy. *Bioorg Med Chem Lett* **22**, 7002-7010 (2012).

72. Huczynski, A., Janczak, J., Lowicki, D. & Brzezinski, B., Monensin A acid complexes as a model of electrogenic transport of sodium cation. *Biochim Biophys Acta* **1818**, 2108-2119 (2012).

73. Kevin II, D. A., Meujo, D. A. F. & Hamann, M. T., Polyether ionophores: broad spectrum and promising biologically active molecules for the control of drug resistant bacteria and parasites. *Expert Opin Drug Discov* **4**, 109-146 (2009).

74. Yoo, J. C. *et al.*, Production and biological activity of laidlomycin, anti-MRSA/VRE antibiotic from *Streptomyces* sp. CS684. *J Microbiol* **45**, 6-10 (2007).

75. Keller-Juslen, C., King, H. D., Kis, Z. L. & von Wartburg, A., Septamycin, a polyether antibiotic. Taxonomy, fermentation, isolation and characterization. *J Antibiot* **28**, 854-859 (1975).

76. Keller-Juslen, C., King, H. D., Kuhn, M., Loosli, H. R. & von Wartburg, A., Noboritomycins A and B, new polyether antibiotics. *J Antibiot* **31**, 820-828 (1978).

77. Fehr, T., King, H. D. & Kuhn, M., Mutalomycin, a new polyether antibiotic taxonomy, fermentation, isolation and characterization. *J Antibiot* **30**, 903-907 (1977).

78. Otoguro, K. *et al.*, Potent antimalarial activities of polyether antibiotic X-206. *J Antibiot* **54**, 658-663 (2001).

79. Otoguro, K. *et al.*, In vitro and in vivo antimalarial activities of the monoglycoside polyether antibiotic K-41 against drug resistant strains of *Plasmodia*. *J Antibiot* **55**, 832-834 (2002).

80. Gachon, P. & Moins, N., The cardivascular effects of two monocarboxylic ionophores, grisorixin and alborixin, in anesthetized guinea-pigs. *Arzneimittelforschung* **30**, 1502-1507 (1980).

81. Munir, K., Muneer, M. A., Tiwari, A., Chaudhry, R. M. & Muruganandan, S., Effects of polyether ionophores on the protective immune responses of broiler chickens against Angara disease and Newcastle disease viruses. *Vet Res Commun* **31**, 909-929 (2007).

82. Parfenova, H., Haffner, J. & Leffler, C. W., Phosphorylation-dependent stimulation of prostanoid synthesis by nigericin in cerebral endothelial cells. *Am J Physiol* **277**, 728-738 (1999).

83. Lee, S. J. *et al.*, Topical anti-inflammatory activity of dianemycin isolated from *Streptomyces* sp. MT-2705-4. *Arch Pharmacal Res* **20**, 372-374 (1997).

84. Heisey, R. M. & Putnam, A. R., Herbicidal effects of geldanamycin and nigericin, antibiotics from *Streptomyces hygroscopicus*. *J Nat Prod* **49**, 859-865 (1986).

85. Woeller, C. F., O'Loughlin, C. W., Roztocil, E., Feldon, S. E. & Phipps, R. P., Salinomycin and other polyether ionophores are a new class of antiscarring agent. *J Biol Chem* **290**, 3563-3575 (2015).

86. Rotin, D., Wan, P., Grinstein, S. & Tannock, I., Cytotoxicity of Compounds that Interfere with the Regulation of Intracellular pH: A Potential New Class of Anticancer Drugs. *Cancer Res* **47**, 1497-1504 (1987).

87. Gupta, P. B. *et al.*, Identification of Selective Inhibitors of Cancer Stem Cells by High-Throughput Screening. *Cell* **138**, 645-659 (2009).

88. Fuchs, D., Heinold, A., Opelz, G., Daniel, V. & Naujokat, C., Salinomycin induces apoptosis and overcomes apoptosis resistance in human cancer cells. *Biochem Biophys Res Commun* **390**, 743-749 (2009).

89. Margolis, L. B., Novikova, I. Y., Rozovskaya, I. A. & Skulachev, V. P., K^+/H^+-antiporter nigericin arrests DNA synthesis in Ehrlich ascites carcinoma cells. *Proc Natl Acad Sci USA* **86**, 6626-6629 (1989).

90. Naujokat, C., Fuchs, D. & Opelz, G., Salinomycin in cancer: A new mission for an old agent. *Mol Med Rep* **3**, 555-559 (2010).

91. Story, P. & Doube, A., A case of human poisoning by salinomycin, an agricultural antibiotic. *N Z Med J* **117**, 1-4 (2004).

92. Scherzad, A. *et al.*, Chronic exporsure of low dose salinomycin inhibits MSC migration capability in vitro. *Biomed Rep* **4**, 325-330 (2016).

93. Kocienski, P. J., Brown, R. C. D., Pommier, A., Procter, M. & Schmidt, B., Synthesis of Salinomycin. *J Chem Soc, Perkin Trans 1* **1**, 9-40 (1998).

94. Vilotijevic, I. & Jamison, T. F., Epoxide-Opening Cascades in the Synthesis of Polycyclic Polyether Natural Products. *Agnew Chem Int Ed Engl* **48**, 5250-5281 (2009).

95. Koh, C.-L. *et al.*, Plant-Derived Natural Products as Sources of Anti-Quorum

Sensing Compounds. *Sensors (Basel)* **13**, 6217-6228 (2013).

96. Engebrecht, J., Nealson, K. & Silverman, M., Bacterial bioluminescence: isolation and genetic analysis of functions from *Vibrio fischeri*. *Cell* **32**, 773-781 (1983).

97. Hentzer, M. & Givskov, M., Pharmacological inhibition of quorum sensning for the treatment of chronic bacterial infections. *J Clin Invest* **112**, 1300-1307 (2003).

98. LaSarre, B. & Federle, M. J., Exploting Quorum Sensing To Confuse Bacterial Pathogens. *Microbiol Mol Biol Rev* **77**, 73-111 (2013).

99. Lee, J. & Zhang, L., The hierarchy quorum sensing network in *Pseudomonas aeruginosa*. *Protein Cell* **6**, 26-41 (2015).

100. Bentley, S. D. *et al.*, Complete genome sequence of the model actinomycete *Streptomyces coelicolor* A3(2). *Nature* **417**, 141-147 (2002).

101. Nett, M., Ikeda, H. & Moore, B. S., Genomic basis for natural product biosynthetic diversity in the actinomycetes. *Nat Prod Rep* **26**, 1362-1384 (2009).

102. Zarins-Tutt, J. S. *et al.*, Prospecting for new bacterial metabolites: a glossary of approaches for inducing, activating and upregulating the biosynthesis of bacterial cryptic or silent natural products. *Nat Prod Rep* **33**, 54-72 (2016).

103. Lautru, S., Deeth, R. J., Bailey, L. M. & Challis, G. L., Discovery of a new peptide natural product by *Streptomyces coelicolor* genome mining. *Nat Chem Biol* **1**, 265-269 (2005).

104. Skinnider, M. A. *et al.*, Genomes to natural products PRedition Informatics for Secondary Metabolomes (PRISM). *Nucl Acids Res* **43**, 9645-9662 (2015).

105. Bode, H. B., Bethe, B., Hofs, R. & Zeeck, A., Big Effects from Small Changes: Possible Ways to Explore Nature's Chemical Diversity. *Chem Bio Chem* **3**, 619-627 (2002).

106. Ayer, S. W., McInnes, G., Thibault, P. & Walter, J. A., Jadomycin, a Novel 8*H*-Benz[b]oxazolo[3,2-f]phenanthridine Antibiotic from *Streptomyces venezuaelae* ISP5230. *Tetrahedron Lett* **32**, 6301-6304 (1991).

107. Doull, J. L., Singh, A. K., Hoare, M. & Ayer, S. W., Conditions for the production of jadomycin B by *Streptomyces venezuelae* ISP5230: effects of heat shock, ethanol treatment and phage infection. *J Ind Microbiol* **13**, 120-125 (1994).

108. Rateb, M. E. *et al.*, Diverse metabolic profiles of a *Streptomyces* strain isolated from a hyper-arid environment. *J Nat Prod* **74**, 1965-1971 (2011).

109. Taylor, M. W., Radax, R., Steger, D. & Wagner, M., Sponge-Associated Microorganisms: Evolution, Ecology, and Biotechnological Potential. *Microbiol Mol Biol Rev* **71**, 295-347 (2007).

110. Betrand, S. *et al.*, Metabolite induction via microorganism co-culture: A potential way to enhance chemical diversity for drug discovery. *Biotechnol Adv* **32**, 1180-1204 (2014).

111. Marmann, A., Aly, A. H., Lin, W., Wang, B. & Proksch, P., Co-Cultivation - A Powerful Emerging Tool for Enhancing the Chemical Diversity of Microorganisms. *Mar Drugs* **12**, 1043-1065 (2014).

112. Mearns-Spragg, A., Bregu, M., Boyd, K. G. & Burgess, J. G., Cross-species induction and enhancement of antimicrobial activity produced by epibiotic bacteria from marine algae and invertebrates, after exposure to terrestrial bacteria. *Lett Appl Microbiol* **27**, 142-146 (1998).

113. Miao, L. I., Kwong, T. F. N. & Qian, P. -Y., Effect of culture conditions on mycelial growth, antibacterial activity and metabolite profiles of the marine-derived fungus *Arthrinium* c.f. *saccharicola*. *Appl Microbiol Biotechnol* **72**, 1063-1073 (2006).

114. Onaka, H., Mori, Y., Igarashi, Y. & Furumai, T., Mycolic acid-containing bacteria induce natural product biosynthesis in *Streptomyces* species. *Appl Environ Microbiol* **77**, 400-406 (2011).

115. Luti, K. J. K. & Mavituna, F., Elicitation of *Streptomyces coelicolor* with dead cells of *Bacillus subtilis* and *Staphylococcus aureus* in a bioreactor increases production of undecylprodigiosin. *Appl Microbiol Biotechnol* **90**, 461-466 (2011).

116. Slattery, M., Rajbhandari, I. & Wesson, K., Competition-mediated antibiotic induction in the marine bacterium *Streptomyces tenjimariensis*. *Microb Ecol* **41**, 90-96 (2001).

117. Kim, B. J. *et al.*, Phylogenetic analysis of the genera *Streptomyces* and *Kitasatospora* based on partial RNA polymerase B-subunit gene (*rpoB*) sequences. *Int J Syst Evol Microbiol* **54**, 593-598 (2004).

118. Woo, P. C., Lau, S. K., Teng, J. L., Tse, H. & Yuen, K. Y., Then and now: use of 16S rDNA gene sequencing for bacterial identification and discovery of novel bacteria in clinical microbiology laboratories. *Clin Microbiol Infect* **14**, 908-934 (2008).

119. Altschul, S. F., Gish, W., Miller, W., Meyers, E. W. & Lipman, D. J., Blast (basic local alignment search tool). *J Mol Biol* **215**, 403-410 (1990).

120. Guo, Y., Zheng, W., Rong, X. & Huang, Y., A multilocus phylogeny of the *Streptomyces griseus* 16S rRNA gene clade: use of multilocus sequence analysis for

Streptomycete systematics. *Int J Syst Evol Bacteriol* **58**, 149-159 (2008).

121. Shirling, E. B. & Gottlieb, D., Methods for characterization of *Streptomyces* species. *Int J Syst Bacteriol* **16**, 313-340 (1966).

122. Liu, W. & Shen, B., Genes for Production of the Enediyne Antitumor Antibiotic C-1027 in *Streptomyces globisporus* Are clustered with the *cagA* Gene that Encodes the C-1027 Apoprotein. *Antimicrob Agents Chemother* **44**, 382-392 (2000).

123. Nagaoka, K. *et al.*, Azinomycins A and B, new antitumor antibiotics. I. Producing organism, fermentation, isolation and characterization. *J Antibiot* **39**, 1527-1532 (1986).

124. Graziani, E. I., Ritacco, F. V., Bernan, V. S. & Telliez, J. -B., Modified from: Phaeochromycins A-E, Anti-inflammatory Polyketides Isolated from the Soil Actinomycete *Streptomyces phaeochromogenes* LL-P018. *J Nat Prod* **68**, 1262-1265 (2005).

125. MacFaddin, J. F., *Media for the isolation - cultivation - maintenaince of medical bacteria*, 1st ed. (The Williams and Wilkins Co, Baltimore, MD, 1985).

126. Bushnell, L. D. & Haas, H. F., The Utilization of Certain Hydrocarbons by Microorganisms. *J Bacteriol* **41**, 653-673 (1941).

127. ZoBell, C. E., Studies on Marine Bacteria. I. The cultural requirements of heterotrophic aerobes. *J Mar Res* **4**, 42-75 (1941).

128. Fernandez, E. *et al.*, Identification of two genes from *Streptomces argillaceus* encoding glycosyltransferases involved in transfer of a disaccharide during biosynthesis of the antitumor drug mithramycin. *J Bacteriol* **180**, 4929-4937 (1998).

129. Maranesi, G. L., Baptista-Neto, A., Hokka, C. O. & Badino, A. C., Utilization of vegetable oil in the production of clavulanic acid by *Streptomyces clavuligerus* ATCC 27064. *World J Microbiol* **21**, 509-514 (2005).

130. Jensen, P. R., Williams, P. G., Oh, D. -C., Zeigler, L. & Fenical, W., Species-specific secondary metabolite production in marine actinomycetes of the genus *Salinispora*. *Appl Environ Microbiol* **73**, 1146-1152 (2007).

131. Moita, C., Feio, S. S., Nunes, L., Curto, M. J. M. & Roseiro, J. C., Optimisation of physical factors on the production of active metabolites by *Bacillus subtilis* 355 against wood surface contaminant fungi. *Int Biodeterior Biodegradation* **55**, 261-269 (2005).

132. Liu, X. Y., Yang, S. Z. & Mu, B. Z., Production and characterization of a C15-surfactin-*O*-methyl ester by a lipopeptide producing strain *Bacillus subtilis* HSO121.

Process Biochem **44**, 1144-1151 (2009).

133. Pluskal, T., Castillo, S., Villar-Briones, A. & Oresic, M., MZmine 2: modular framework for processing, visualizing and analyzing mass spectrometry-based molecular profile data. *BMC Bioinformatics* **11**, 395-406 (2010).

134. Laatsch, H., AntiBase Version 4.0 - The Natural Compound Identifier (2012).

135. Cullen, W. P., Oscarson, J. R., Tone, J. & Maeda, H., United States Patent No. 4908316, *Streptomyces* sp. N664-30 which produces an ionophore antibacterial agent (March 1990).

136. Thomas, M., Jayatilaka, D. & Corry, B., The Predominant Role of Coordination Number in Potassium Channel Selectivity. *Biophys J* **93**, 2635-2643 (2007).

137. Liu, C. & Hermann, T. E., Characterization of ionomycin as a calcium ionophore. *J Biol Chem* **253**, 5892-5894 (1978).

138. Smith, G. D. & Duax, W. L., Crystal and molecular structure of of the calcium ion complex of A23187. *J Am Chem Soc* **98**, 1578-1580 (1976).

139. Alleaume, M. & Barrans, Y., Crystal structure of the magnesium complex of calcimycin. *Can J Chem* **63**, 3482-3485 (1985).

140. Akkurt, M. *et al.*, Synthesis and crystal structure of the bis-calcimycin anion-Ni2+ complex. *Arkivoc* **2008**, 154-164 (2008).

141. Vila, S., Canet, I., Guyot, J., Jeminet, G. & Toupet, L., Unusual structure of the dimeric 4-bromocalcimycin-Zn2+ complex. *Chem Commun* **9**, 516-517 (2003).

142. Lindoy, L. F., Outer-sphere and inner-sphere complexation of cations by the natural ionophore lasalocid A. *Coord Chem Rev* **148**, 349-368 (1996).

143. Tsukube, H., Takagi, K., Higashiyama, T., Iwachido, T. & Hayama, N., Biomimetic membrane transport: interesting ionophore functions of naturally occuring polyether antibiotics toward unusual metal cations and amino acid ester salts. *Inorg Chem* **33**, 2984-2987 (1994).

144. Mimouni, M. *et al.*, Impact of Metal Nature on Bioactivity of Metal Chelates of Monensin Antibiotic: Synthesis and Anti-tubercular Activity of Metal-Monensin Complexes. *J Med Chem & Dr Dis* **4**, 7-11 (2013).

145. Delort, A. M., Jeminet, G. & Riddle, F. G., Ionophore properties of cationomycin in large unilamellar vesicles studied by ^{23}Na- and ^{39}K-NMR. *Chem Pharm Bull* **42**, 1618-1620 (1998).

146. Cordes, E. H. & Bull, H. G., Mechanism and catalysis for hydrolysis of acetals, ketals, and orthoesters. *Chem Rev* **74**, 581-603 (1974).

147. Carey, F. A. & Sundberg, R. J., *Advanced Organic Chemistry: Part A: Structure and Mechanisms*, 4th ed. (Kluwer Academic/Plenum Publishers, New York, NY, 2000).

148. Liu, C. *et al.*, Novel polyether antibiotics X-14868A, B, C, and D produced by a *Nocardia*. Discovery, fermentation, biological as well as ionophore properties and taxonomy of the producing culture. *J Antibiot* **36**, 343-350 (1983).

149. Ellestad, G. A. *et al.*, Chemistry of maduramicin I. Salt formation and normal ketalization. *J Antibiot* **39**, 447-456 (1986).

150. Cullen, W. P., Maeda, H., Ruddock, J. C. & Tone, J., United States Patent No. 4746650 (May 1988).

151. Guyot, J., Jeminet, G., Prudhomme, M., Sancelme, M. & Meiniel, R., Interaction of the calcium ionophore A.23187 (Calcimycin) with *Bacillus cereus* and *Escherichia coli*. *Lett Appl Microbiol* **16**, 192-195 (1993).

152. Ketola, K., Vainio, P., Fey, V., Kallioniemi, O. & Iljin, K., Monensin is a potent inducer of oxidative stress and inhibitor of androgen signalling leading to apoptosis in prostate cancer cells. *Mol Cancer Ther* **9**, 3175-3185 (2010).

153. Deng, C. C. *et al.*, Nigericin selectively targets cancer stem cells in nasopharyngeal carcinoma. *Int J Biochem Cell Biol* **45**, 1997-2006 (2013).

154. Zhou, H. M. *et al.*, Suppression of colorectal cancer metastasis by nigericin through inhibition of epithelial-mesenchymal transistion. *World J Gastroenterol* **18**, 2640-2648 (2012).

155. Liffers, S. T. *et al.*, Salinomycin increases chemosensitivity to the effects of doxorubicin in soft tissue sarcomas. *BMC Cancer* **13**, 490 (2013).

156. Zhang, G. -F., Li, C. -X., Liu, Z. -Q., Ma, S. & Chen, H. -B., Cancer stem cell targets - a review. *Eur Rev Med Phamacol Sci* **16**, 2045-2051 (2016).

157. Huczynski, A., Stefanska, J., Przybylski, P., Brzezinski, B. & Bartl, F., Synthesis and antimicrobial properties of Monensin A esters. *Bioorg Med Chem Lett* **18**, 2585-2589 (2008).

158. Lowicki, D. & Huczynski, A., Structure and Antimicrobial Properties of Monensin A and Its Derivatives: Summary of the Achievements. *BioMed Res Intl* **2013**, 1-14 (2013).

159. Scheidegger, K. A. & Payne, G. A., Unlocking the secrets behind secondary metabolism: a review of *Aspergillus flavus* from pathogenicity to functional

genomics. *J Toxicol* **22**, 423-459 (2003).

160. Vargas-Baustista, C., Rahlwes, K. & Straight, P., Bacterial Competition Reveals Differential Regulation of the pks Genes by *Bacillus subtilis*. *J Bacteriol* **196**, 717-728 (2014).

161. Ofer, N. *et al.*, Ectoine Biosynthesis in *Mycobacterium smegmatis*. *Appl Environ Microbiol* **78**, 7483-7486 (2012).

162. Schroeder, F. C., Modular Assembly of Primary Metabolic Building Blocks: A Chemical Language in *C. elegans*. *Chem Biol* **22**, 7-16 (2015).

163. Stiernagle, T., in *C. elegans: A Practical Approach* (Oxford University Press, 1999), pp. 51-57.

164. Konig, C. C. *et al.*, Bacteria induces cryptic meroterpenoid pathway in the pathogenic fungus *Aspergillus fumigatus*. *Chem Bio Chem* **14**, 938-942 (2013).

165. Rateb, M. E. *et al.*, Induction of diverse secondary metabolites in *Aspergillus fumigatus* by microbial co-culture. *RSC Adv* **3**, 14444-14450 (2013).

166. Zuck, K. M., Shipley, S. & Newman, D. J., Induced production of N-formyl alkaloids from *Aspergillus fumigatus* by co-culture with *Streptomyces peucetius*. *J Nat Prod* **74**, 1653-1657 (2011).

167. Tashiro, Y., Yawata, Y., Toyofuku, M., Uchiyama, H. & Nomura, N., Interspecies Interaction between *Pseudomonas aeruginosa* and Other Microorganisms. *Microbes Environ* **28**, 13-24 (2013).

168. Yezza, A., Tyagi, R. D., Valero, J. R., Surampalli, R. Y. & Smith, J., Scale-up of biopesticide production processes using wastewater sludge as a raw material. *J Ind Microbiol Biotechnol* **31**, 545-552 (2004).

169. Cao, Y. -X., Lu, H., Qiao, B., Chen, Y. & Yuan, Y. -Y., Comparison of the secondary metabolites in two scales of cephalosporin C (CPC) fermentation and two different post-treatment processes. *Microbiol Biotechnol* **40**, 95-103 (2013).

170. Fotso, S. *et al.*, Bhimamycin A ~ E and bhimanone: isolation, structure elucidation and biological activity of novel quinone antibiotics from a terrestrial Streptomycete. *J Antibiot* **56**, 931-941 (2003).

171. Reen, F. J. *et al.*, Structure-function analysis of the C-3 position in analogues of microbial behavioural modulators HHQ and PQS. *Org Biomol Chem* **10**, 8903-8910 (2012).

172. Tanaka, T., Nakashima, T., Ueda, T., Tomii, K. & Kouno, I., Facile Discrimination of Aldose Enantiomers by Reversed-Phase HPLC. *Chem Pharm Bull* **55**, 899-901

(2007).

173. Wang, Y. -H., Avula, B., Fu, X., Wang, M. & Khan, I. A., Simultaneous Determination of the Absolute Configuration of Twelve Monosaccharide Enantiomers from Natural Products in a Single Injection by a UPLC-UV/MS Method. *Planta Med* **78**, 834-837 (2012).

174. Lee, J. *et al.*, A cell-cell communication signal integrates quorum sensing and stress response. *Nat Chem Biol* **9**, 339-343 (2013).

175. Gallagher, L. A., McKnight, S. L., Kuznetsova, M. S., Pesci, E. C. & Manoil, C., Functions required for extracellular quinolone signaling by *Pseudomonas aeruginosa*. *J Bacteriol* **184**, 6472-6480 (2002).

176. Xiao, G., Deziel, E. & He, J., MvfR, a key *Pseudomonas aeruginosa* pathogenicity LTTR-class regulatory protein, has dual ligands. *Mol Microbiol* **62**, 1689-1699 (2006).

177. Reen, F. J. *et al.*, The Pseudomonas quinolone signal (PQS) and its precursor HHQ, modulate interspecies and interkingdom behaviour. *FEMS Microbiol Ecol* **77**, 413-428 (2011).

178. Cugini, C. *et al.*, Farnesol, a common sesquiterpene, inhibits PQS production in *Pseudomonas aeruginosa*. *Mol Microbiol* **65**, 896-906 (2007).

179. Lee, J., Attila, C., Cirillo, S. L., Cirillo, J. D. & Wood, T. K., Indole and 7-hydroxyindole diminish *Pseudomonas aeruginosa* virulence. *Microb Biotechnol* **2**, 75-90 (2009).

180. Muller, C., Birmes, F. S., Niewerth, H. & Fetzner, S., Conversion of the *Pseudomonas aeruginosa* Quinolone Signal and Related Alkylhydroxyquinolones by Rhodococcus sp. Strain BG43. *Appl Environ Microbiol* **80**, 7266-7274 (2014).

181. Soh, E. Y. *et al.*, Biotic inactiviation of the *Pseudomonas aeruginosa* quinolone signal molecule. *Environ Microbiol* **17**, 4352-4365 (2015).

182. Pustelny, C. *et al.*, Dioxygenase-mediated quenching of quinolone-dependent quorum sensing in *Pseudomonas aeruginosa*. *Chem Biol* **16**, 1259-1267 (2009).

183. Muller, C. & Fetzner, S., A *Pseudomonas putida* bioreporter for the detection of enzymes active on 2-alkyl-4 (1*H*)-quinolone signalling molecules. *Appl Microbiol Biotechnol* **97**, 751-760 (2013).

184. Kusakabe, H. & Isono, K., Taxonomic studies on *Kitasatosporia cystarginea* sp. nov., which produces a new antifungal antibiotic cystargin. *J. Antibiot.* **41** (12), 1758-1762 (1988).

185. Takahashi, Y., Iwai, Y. & Omura, S., Two new species of the genus *Kitasatosporia*, *Kitasatosporia phosalacinea* sp. nov. and *Kitasatosporia griseola* sp. nov. *J. Gen. Appl. Microbiol.* **30**, 377-378 (1984).

186. Kieser, T., in *Practical Streptomyces Genetics* (John Innes Foundation, 2000), pp. 162-170.

187. Weisburg, W. G., Barns, S. M., Pelletier, D. A. & Lane, D. J., 16S Ribosomal DNA Amplification for Phylogenetic Study. *J Bacteriol* **173**, 697-703 (1991).

188. Gontang, E., Fenical, W. & Jensen, P. R., Phylogenetic Diversity of Gram-Positive Bacteria Cultured from Marine Sediments. *Appl Environ Microbiol* **73**, 3272-3282 (2007).

189. *SAINT 7.32A* (BRUKER AXS, INC., Madison, Wisconsin, USA, 2006).

190. *SADABS 2008* (George Sheldrick, Bruker AXS, Inc., Madison, Wisconsin, USA, 2008).

191. Sheldrick, G. M., SHELXTL. *Acta Cryst* **A64**, 12-122 (2008).

192. Methods for dilution antimicrobial susceptibility-Test for bacteria that grow aerobically. *National Committee for Clinical Laboratory Standards* **CLSI document M07-A9**, Wayne, PA-9th Edition (2012).

193. Nash, P. & Krenz, M. M., in *Manual of clinical microbiology*, edited by Balows, A., Hausler, W. J., Herrmann, K. L., Isenberg, H. D. & Shadomy, H. J. (American Society for Microbiology, Washington, D.C., USA, 1991), pp. 1226-1288.

APPENDIX

6.1. Supporting information for the characterization of terrosamycin A and B

A

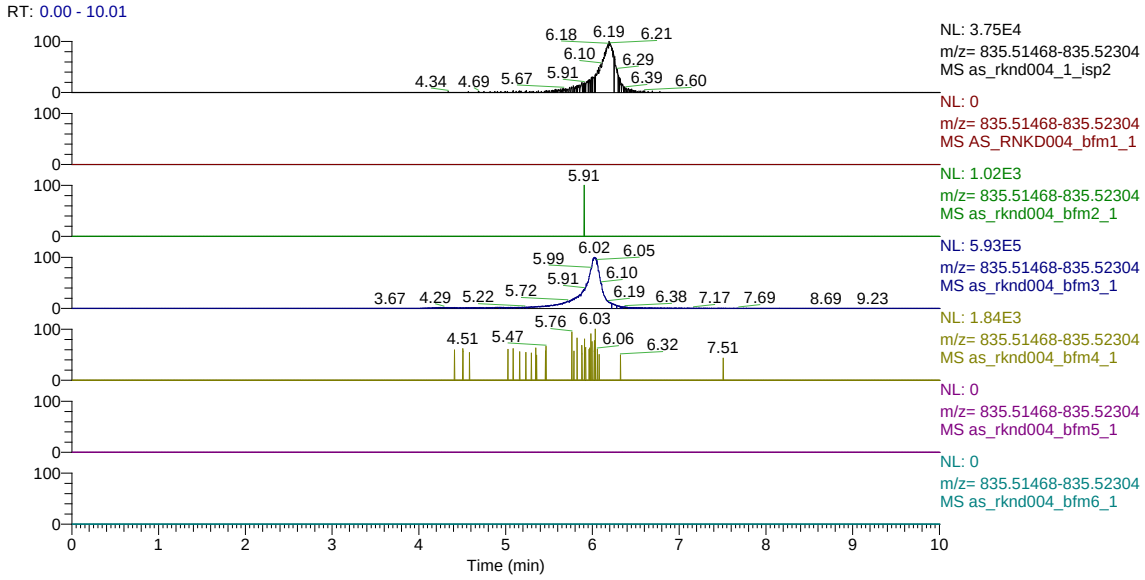

B

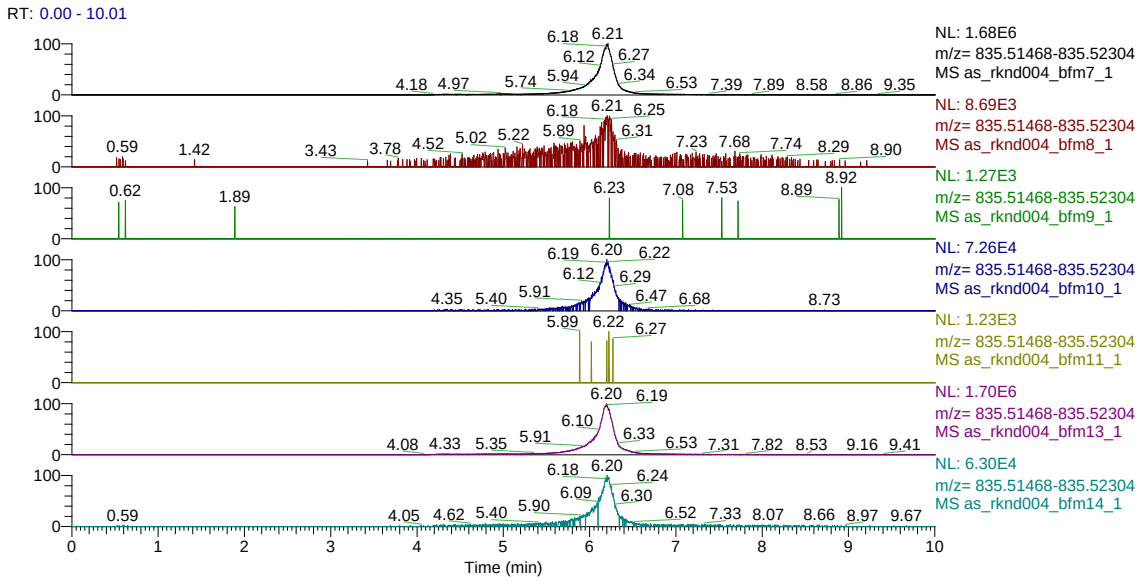

Figure 6.1. HPLC extracted ion chromatograms (+ESI-HRMS detector) monitoring *m/z* 835.5186 $[M+Na]^+$ in extracts of *Streptomyces* sp. RKND004 grown in **A**. ISP2 and BFM1 – BFM6 and **B**. BFM7 – BFM14.

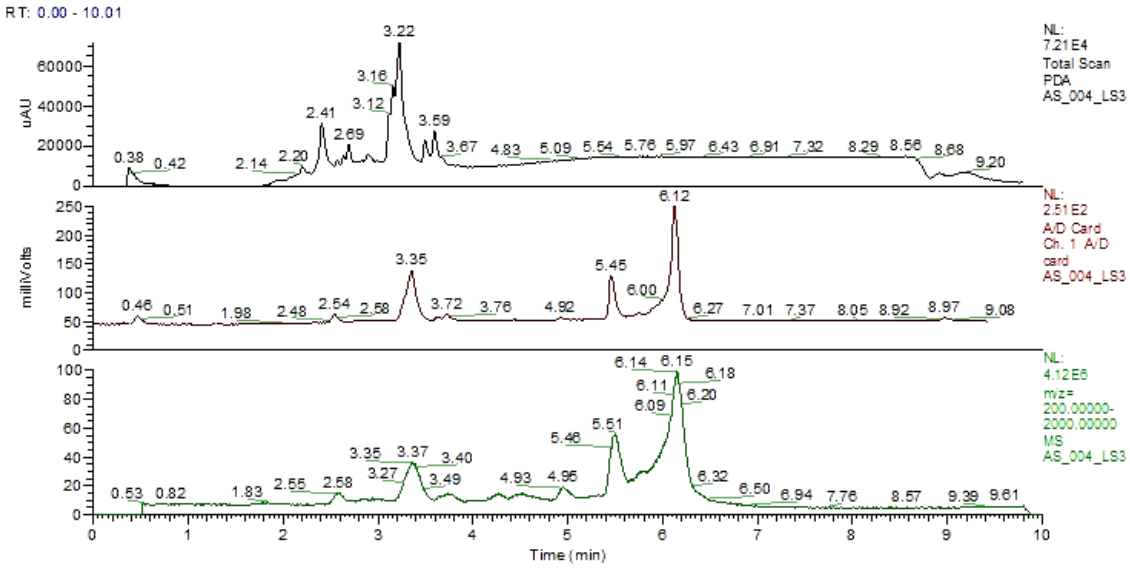

Figure 6.2. HPLC chromatograms of the crude extract of a large scale fermentation of *Streptomyces* sp. RKND004 grown in BFM3. The top chromatogram was generated using a PDA detector, the middle using an ELSD and the bottom using +ESI-HRMS.

A

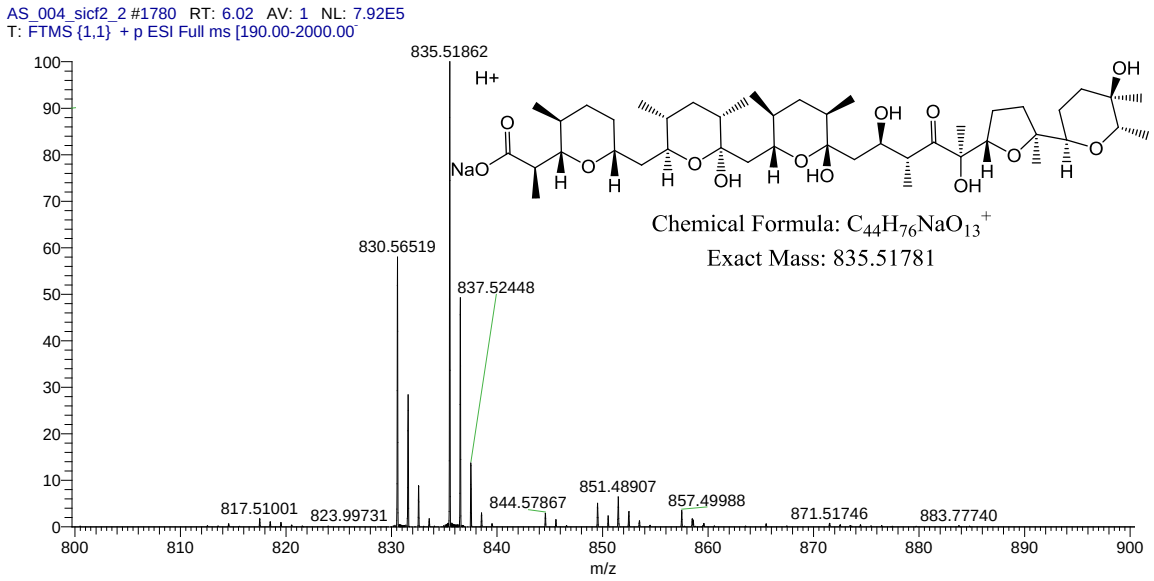

B

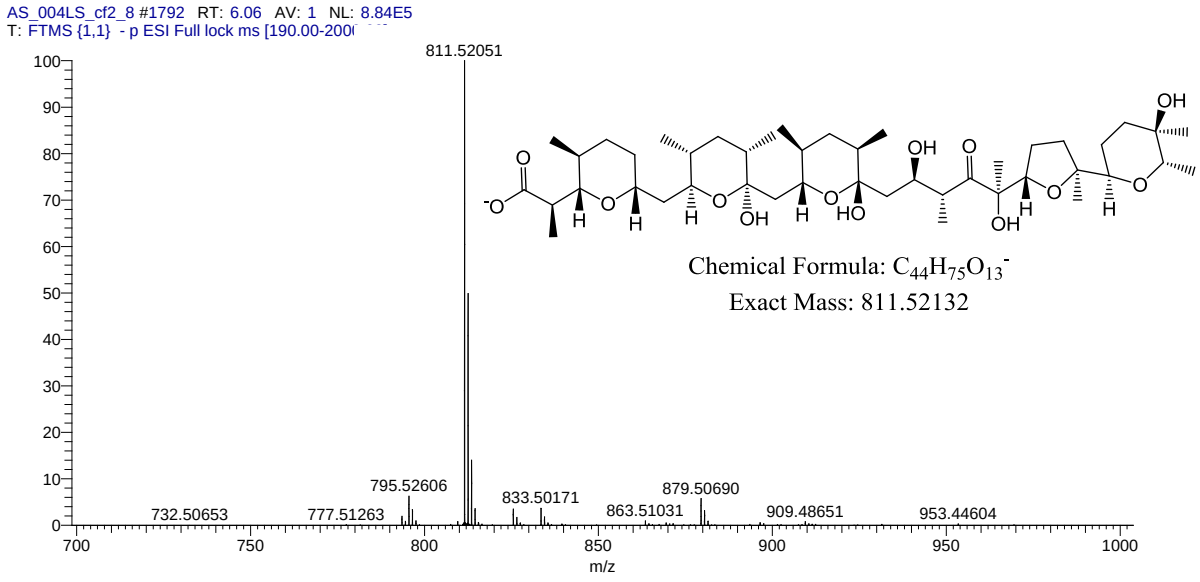

Figure 6.3. **A**. +ESI-HRMS spectrum of terrosamycin A. **B**. –ESI-HRMS spectrum of terrosamycin A.

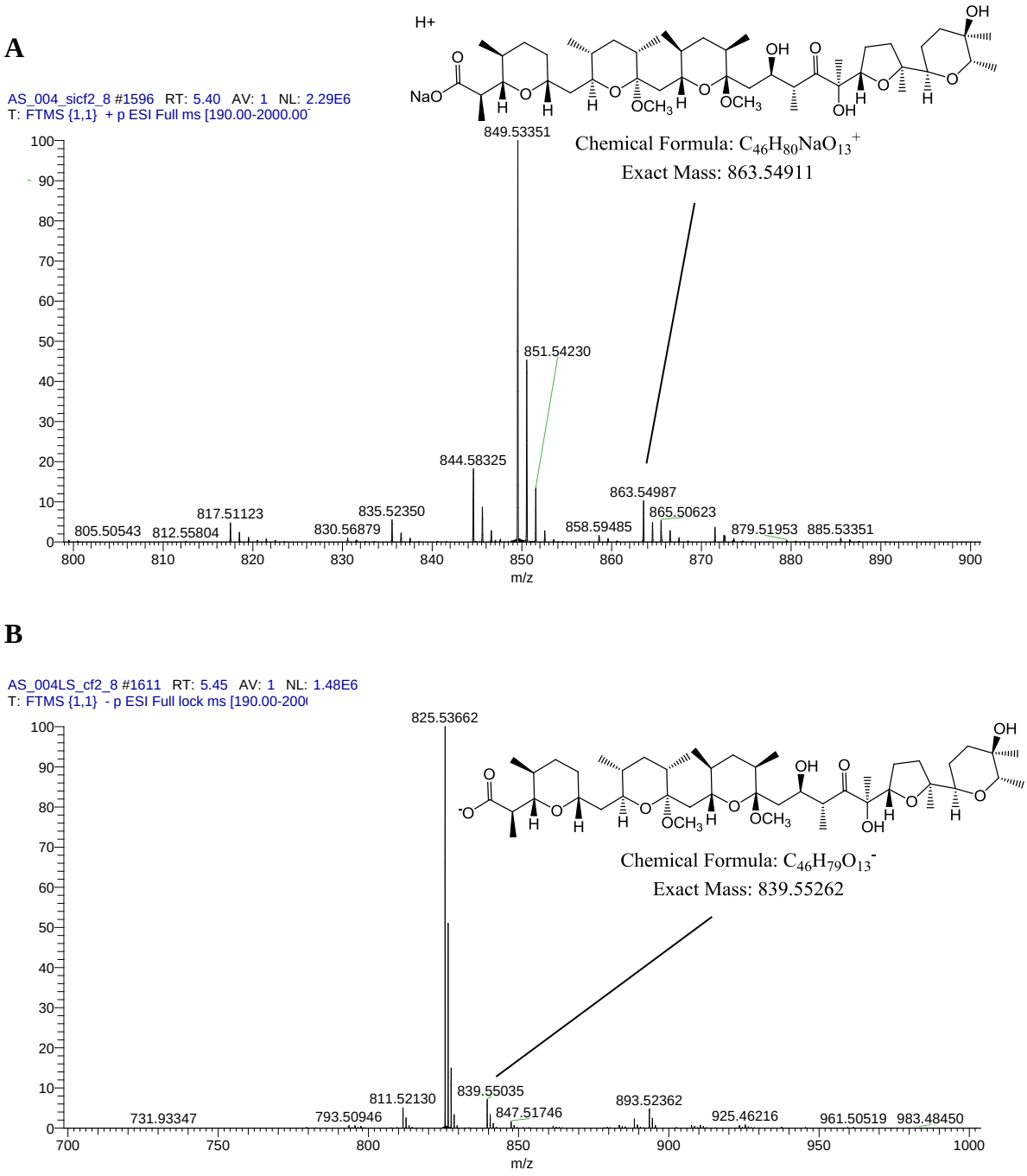

Figure 6.4. **A**. +ESI-HRMS spectrum of terrosamycin B. **B**. –ESI-HRMS spectrum of terrosamycin B.

Table 6.1. Crystal data and structure refinement for terrosamycin A.

Empirical formula	C45.50 H79 K O14
Moiety formula	$C_{44}H_{75}KO_{13}$ • ½ Me_2CO • ½ H_2O
Formula weight	889.19
Temperature	173(1) K
Wavelength	0.71073 Å
Diffractometer used	Bruker AXS P4/SMART 1000
Detector distance	5 cm
Monochromator used	Graphite
Crystal size	0.50 x 0.30 x 0.30 mm^3
Colour and habit	Colourless, block
Crystal system	Monoclinic
Space group	P2(1)
Unit cell dimensions	a = 12.004(3) Å, α = 90° b = 35.796(10), β = 103.826(4)° c = 12.020(3) Å, γ= 90°
Volume	5015(2) $Å^3$
Z	4
Density (calculated)	1.178 Mg/m^3
Absorption coefficient	0.166 mm^{-1}
F(000)	1932
θ range for data collection	1.74 to 27.50°
Completeness to θ= 25.00°	99.80%
Scan type	ω δνα ϕ
Scan range	0.3°
Exposure time	10s
Index ranges	$-15 \leq h \leq 14$, $-46 \leq k \leq 46$, $-15 \leq l \leq 13$
Standard reflections	50 frames at beginning and end of data collection
Crystal stability	No decay
Reflections collected	34113
Independent reflections	21746 [R_{int} = 0.0760]
Solution	Direct methods
Hydrogen atoms	Mixed
Absorption correction	SADABS
Max. and min. transmission	0.9520 and 0.9217
Refinement method	Full-matrix least-squares on F^2
Data / restraints / parameters	21746 / 25 / 1159
Goodness-of-fit on F2	0.997

Final R indices [I>2σ(I)]	R_1 = 0.0770, wR_2 = 0.1886
R indices (all data)	R_1 = 0.1066, wR_2 = 0.2035
Largest/mean shift/esd	0.000/0.000
Absolute structure parameter	0.04(4)
Largest diff. peak and hole	0.943 and -0.320 e.Å^{-3}

Table 6.2. Coordination bond lengths (Å) and angles (°) of terrosamycin A determined from XRD studies.

K(1)-O(13)	2.683(3)
K(1)-O(5)	2.759(3)
K(1)-O(2)	2.776(3)
K(1)-O(11)	2.828(3)
K(1)-O(8)	2.937(4)
K(1)-O(12)	2.955(3)
K(1)-O(1)	3.026(3)
K(1)-O(9)	3.028(4)
O(13)-K(1)-O(5)	108.02(12)
O(13)-K(1)-O(2)	76.93(10)
O(5)-K(1)-O(2)	80.79(10)
O(13)-K(1)-O(11)	99.94(11)
O(5)-K(1)-O(11)	121.62(11)
O(2)-K(1)-O(11)	156.58(11)
O(13)-K(1)-O(8)	170.94(10)
O(5)-K(1)-O(8)	69.45(9)
O(2)-K(1)-O(8)	110.69(9)
O(11)-K(1)-O(8)	75.07(10)
O(13)-K(1)-O(12)	58.20(10)
O(5)-K(1)-O(12)	95.17(9)
O(2)-K(1)-O(12)	131.37(10)
O(11)-K(1)-O(12)	58.75(9)
O(8)-K(1)-O(12)	112.93(9)
O(13)-K(1)-O(1)	118.21(10)
O(5)-K(1)-O(1)	54.81(8)
O(2)-K(1)-O(1)	44.26(9)
O(11)-K(1)-O(1)	141.22(9)
O(8)-K(1)-O(1)	67.98(8)
O(12)-K(1)-O(1)	148.72(10)
O(13)-K(1)-O(9)	120.42(13)
O(5)-K(1)-O(9)	130.44(10)
O(2)-K(1)-O(9)	99.55(10)
O(11)-K(1)-O(9)	61.60(10)
O(8)-K(1)-O(9)	64.21(10)
O(12)-K(1)-O(9)	118.00(10)
O(1)-K(1)-O(9)	91.18(9)

Table 6.3. Hydrogen bond lengths (Å) and angles (°) for terrosamycin A determined from XRD studies.

D-H...A	d(D-H)	d(H...A)	d(D...A)	<(DHA)
O(7)-H(7)...O(1)	0.84	1.83	2.658(4)	169.40
C(21)-H(21)...O(1)	1.00	2.38	3.170(5)	135.00
O(8)-H(8)...O(6)	0.78(6)	1.95(10)	2.643(4)	148(15)

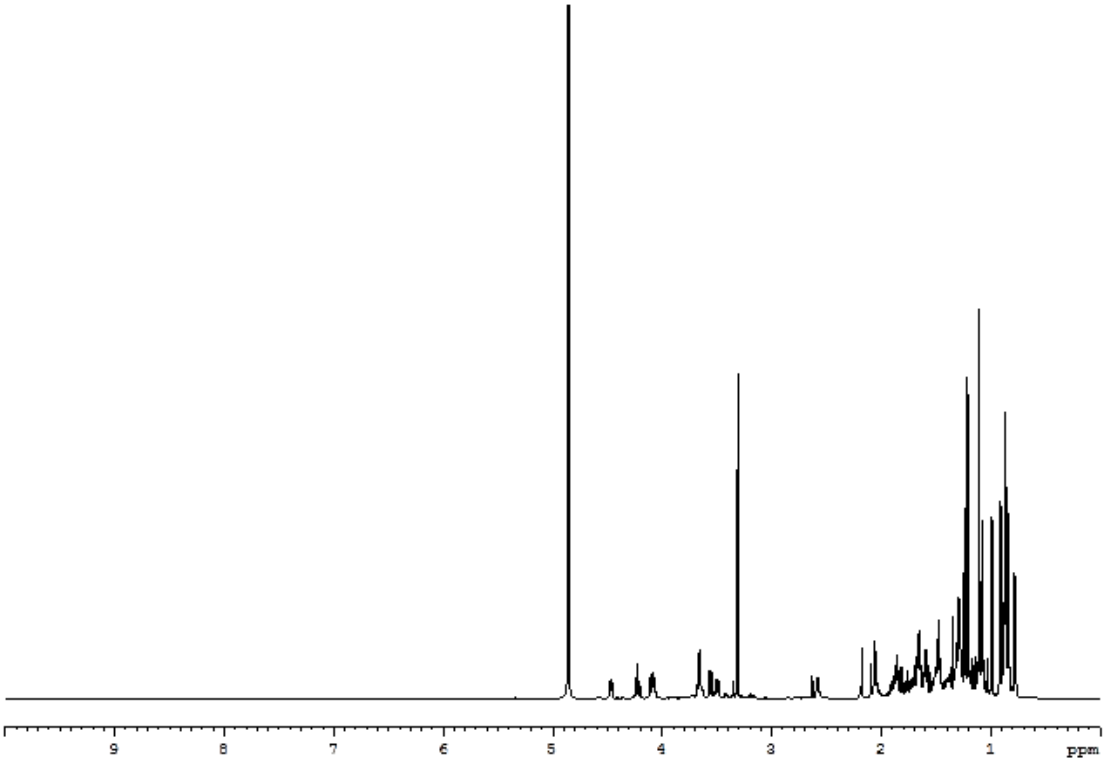

Figure 6.5. ^{1}H NMR spectrum (600 MHz, MeOD-d_4) of terrosamycin A.

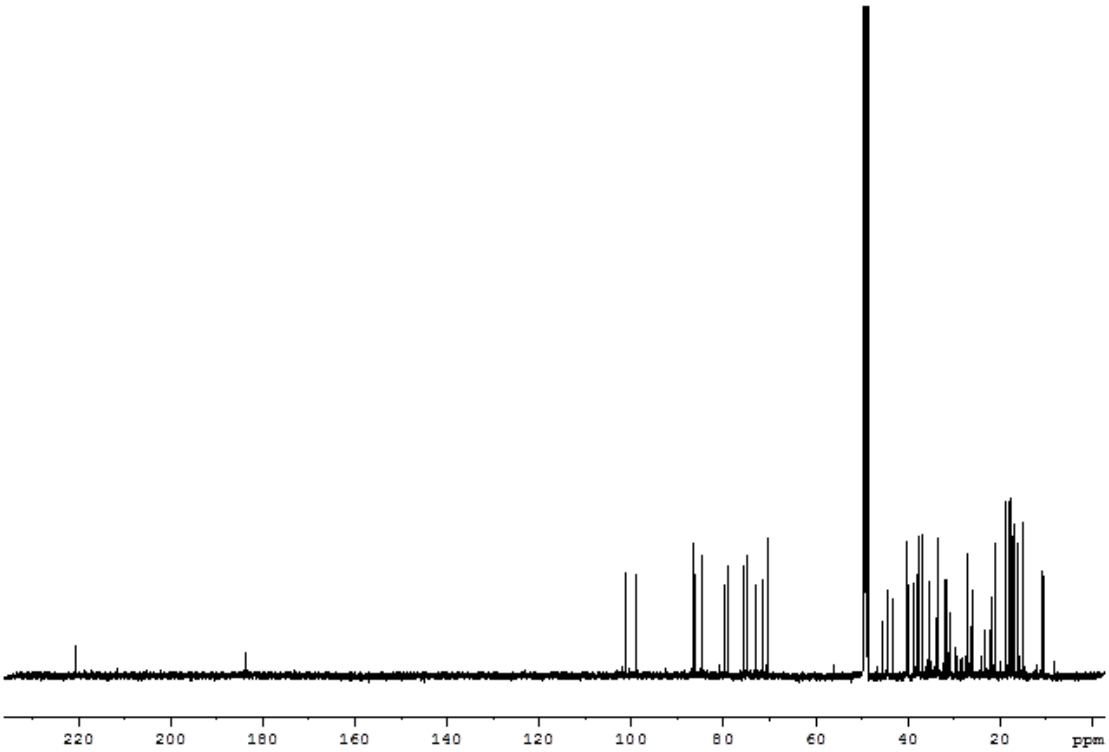

Figure 6.6. ^{13}C NMR spectrum (150 MHz, MeOD-d_4) of terrosamycin A.

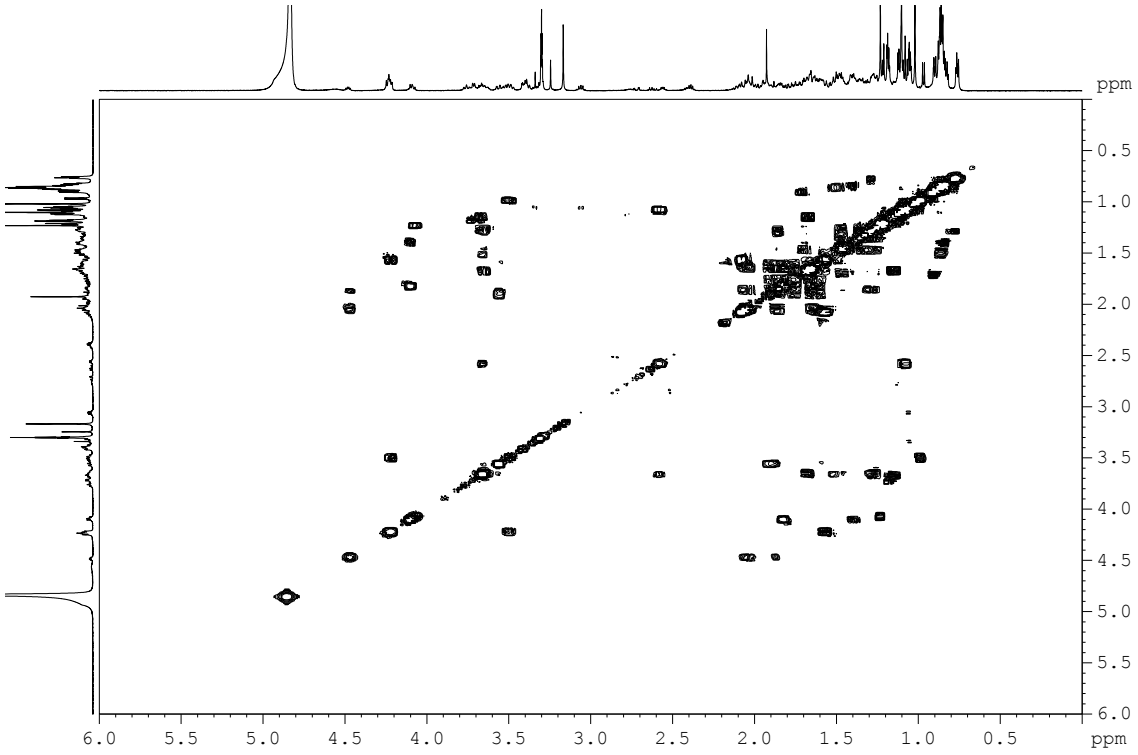

Figure 6.7. COSY spectrum (600 MHz, MeOD-d_4) of terrosamycin A.

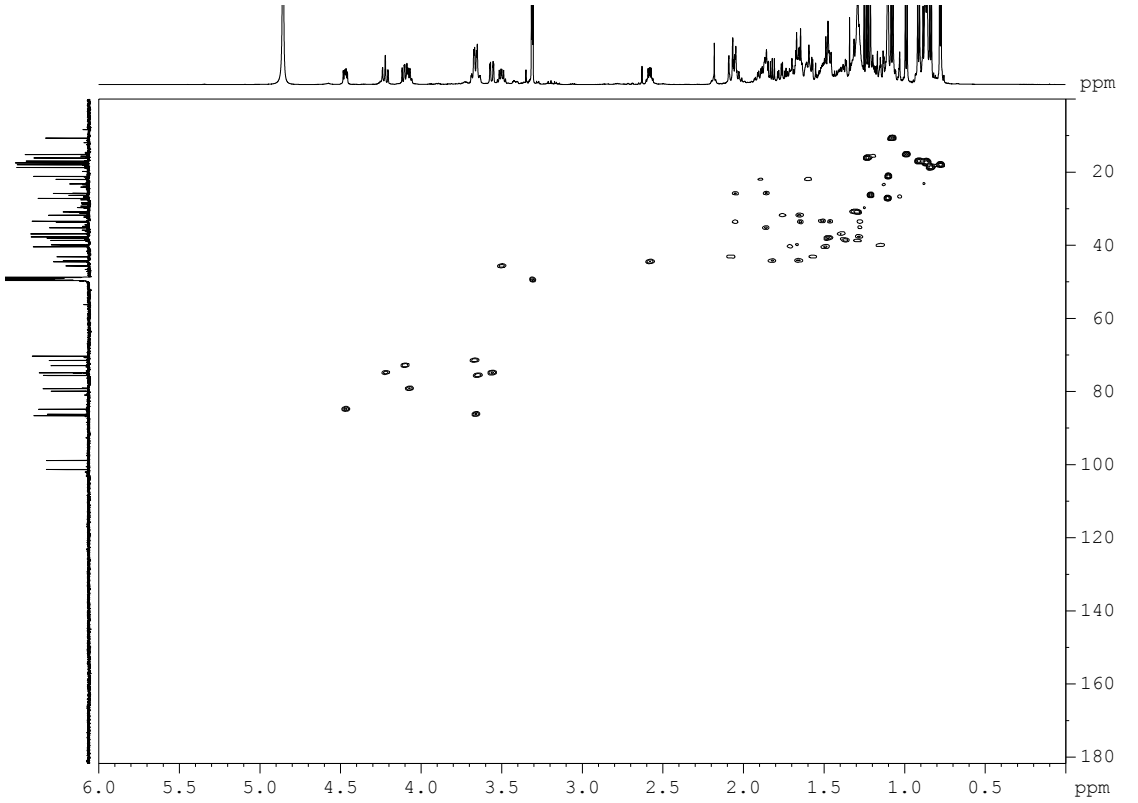

Figure 6.8. HSQC spectrum (^{1}H 600 MHz, ^{13}C 150 MHz, MeOD-d_4) of terrosamycin A.

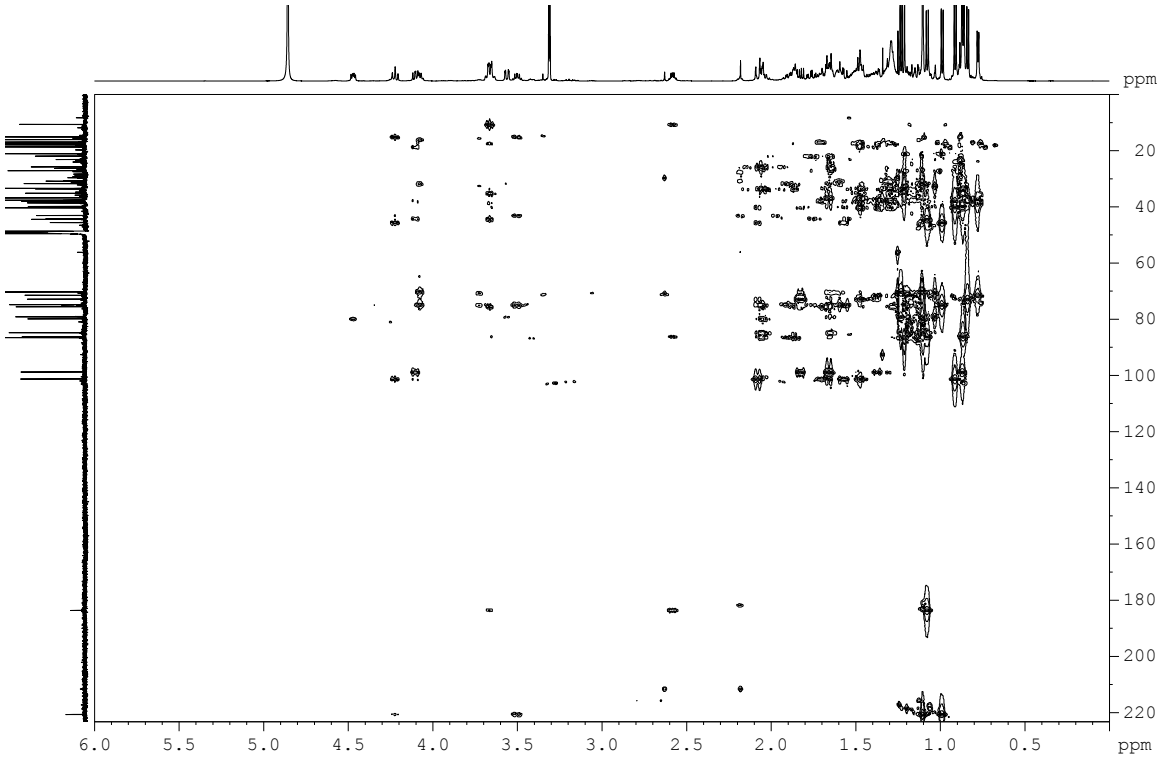

Figure 6.9. HMBC spectrum (^{1}H 600 MHz, ^{13}C 150 MHz, MeOD-d_4) of terrosamycin A.

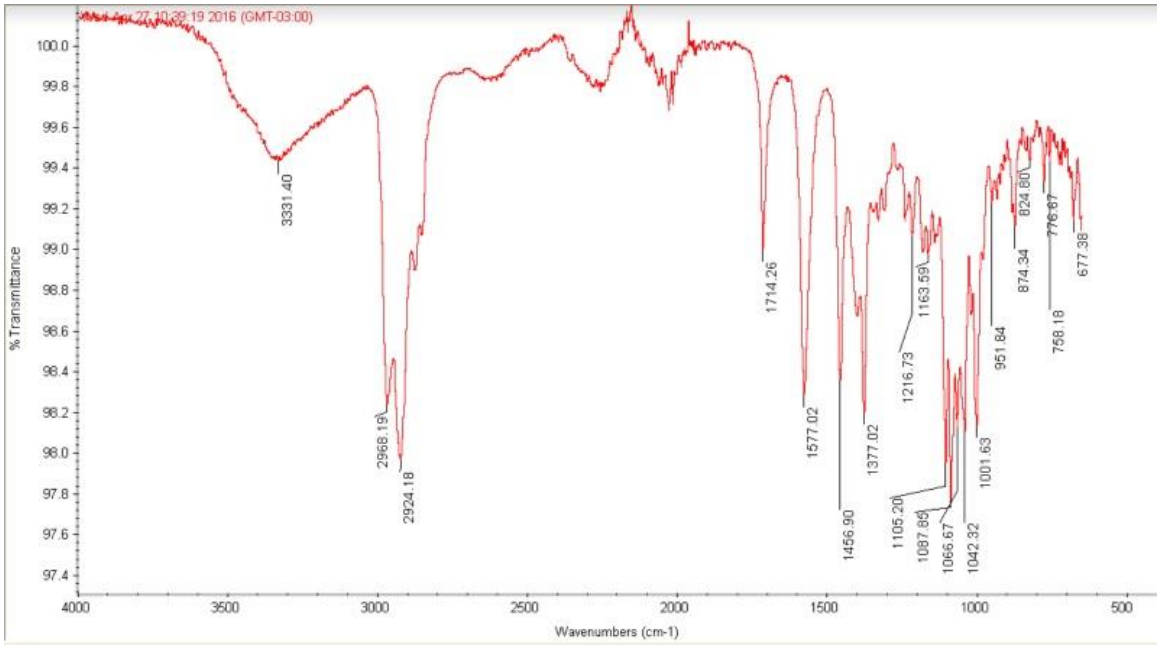

Figure 6.10. IR spectrum of terrosamycin A (MeOH, film).

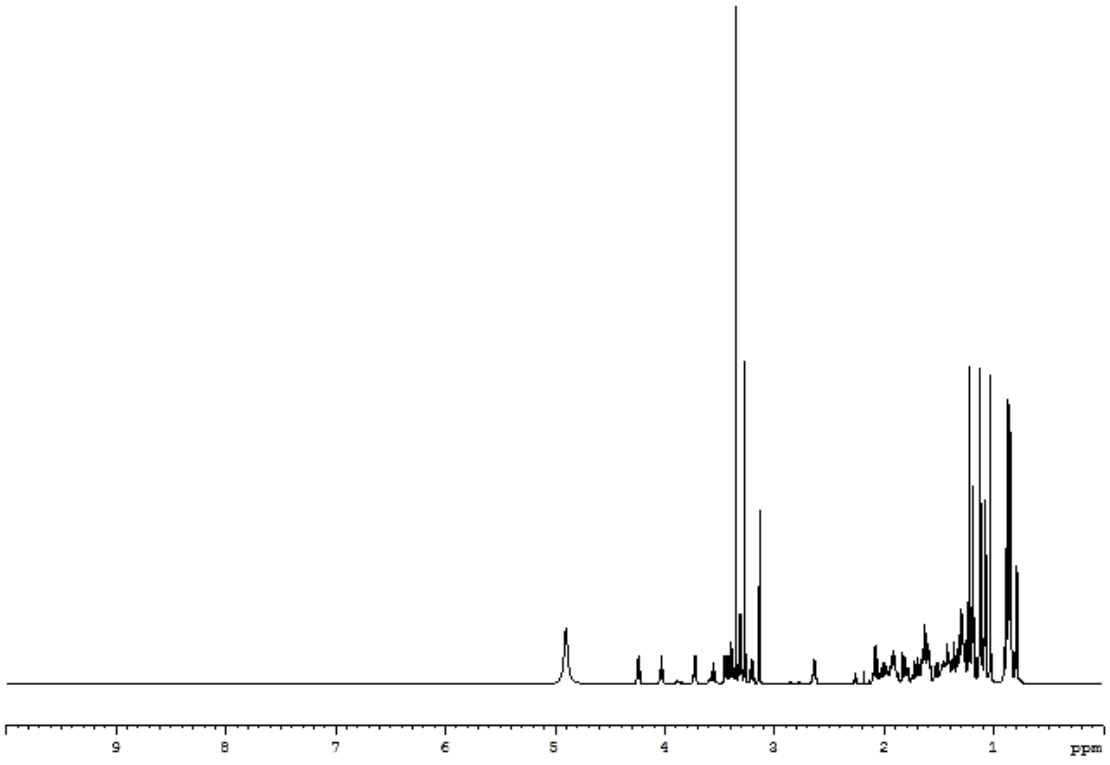

Figure 6.11. ^{1}H NMR spectrum (600 MHz, MeOD-d_4) of terrosamycin B.

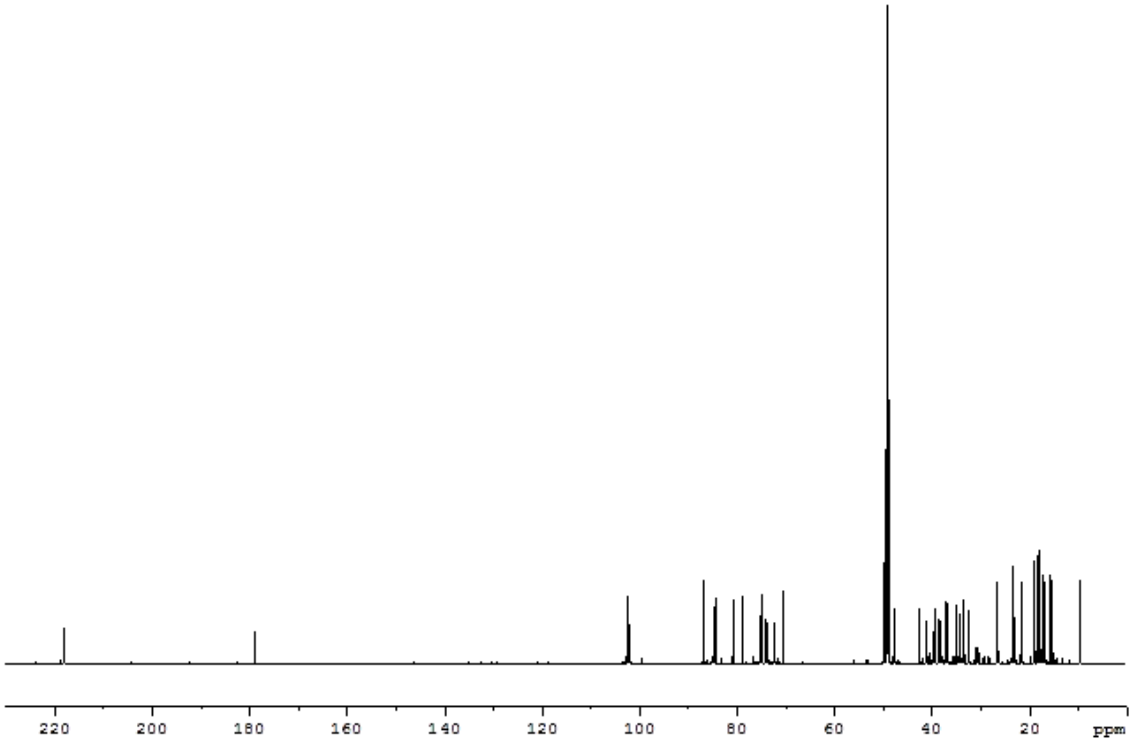

Figure 6.12. ^{13}C NMR spectrum (150 MHz, MeOD-d_4) of terrosamycin B.

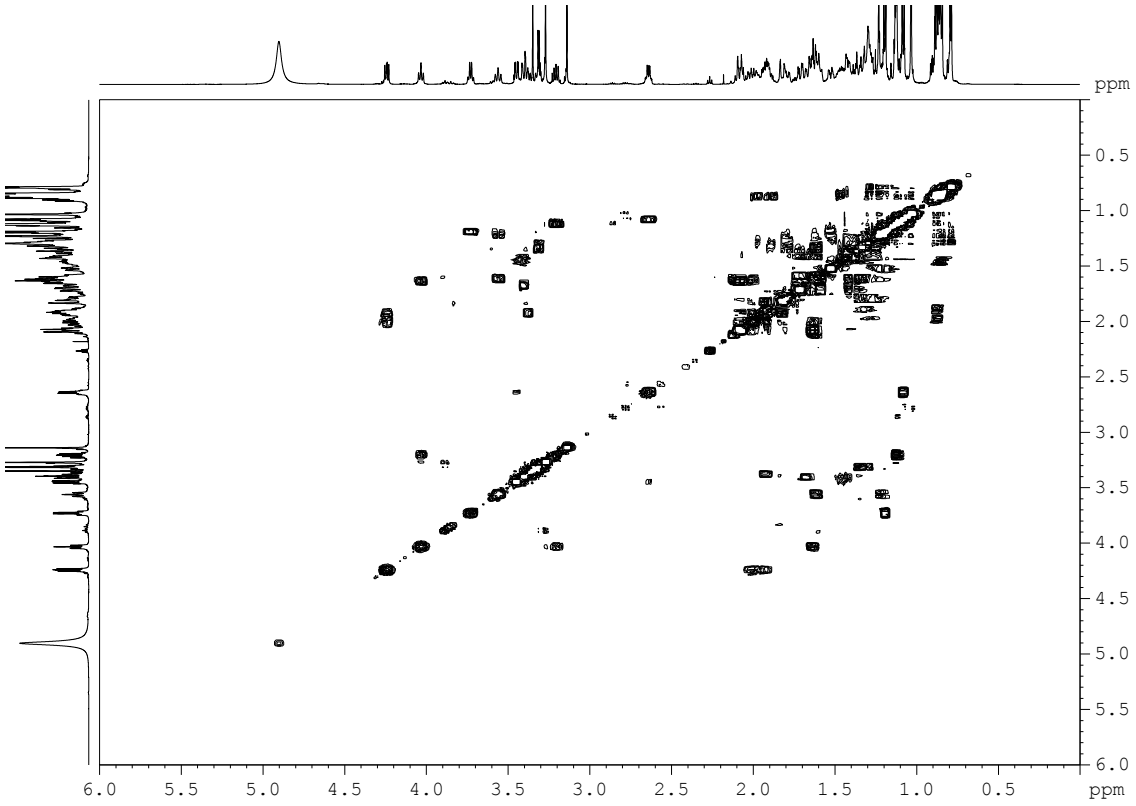

Figure 6.13. COSY spectrum (600 MHz, MeOD-d_4) of terrosamycin B.

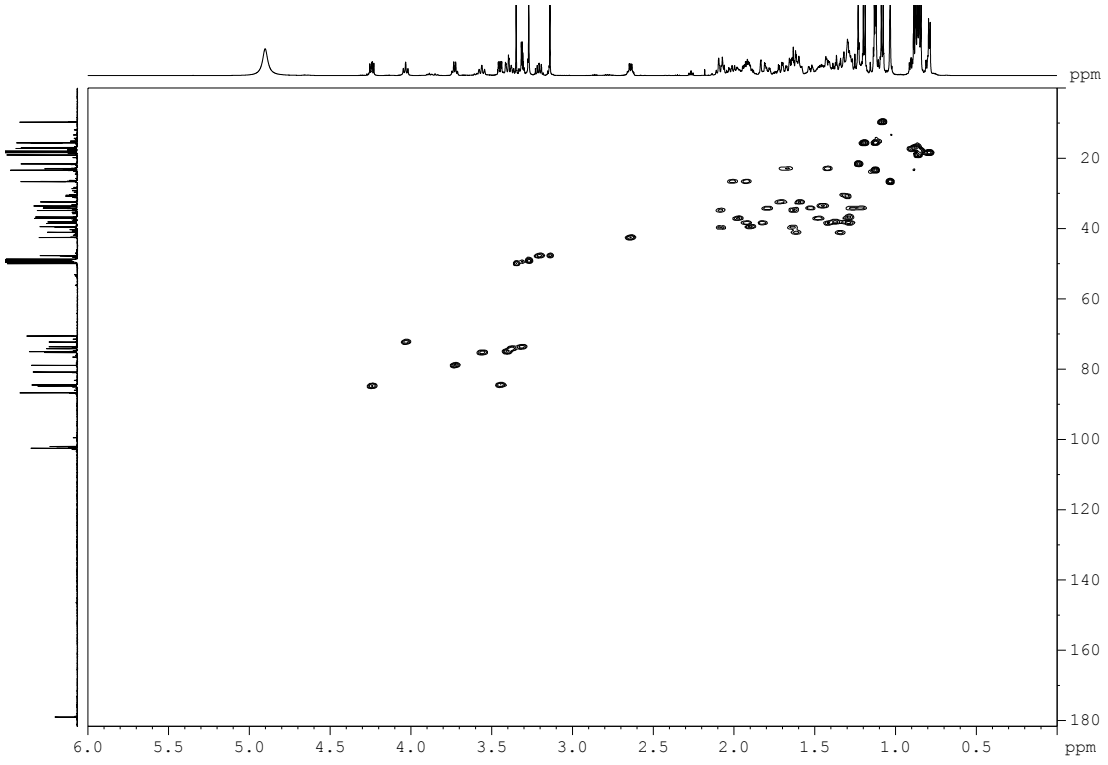

Figure 6.14. HSQC spectrum (^{1}H 600 MHz, ^{13}C 150 MHz, MeOD-d_4) of terrosamycin B.

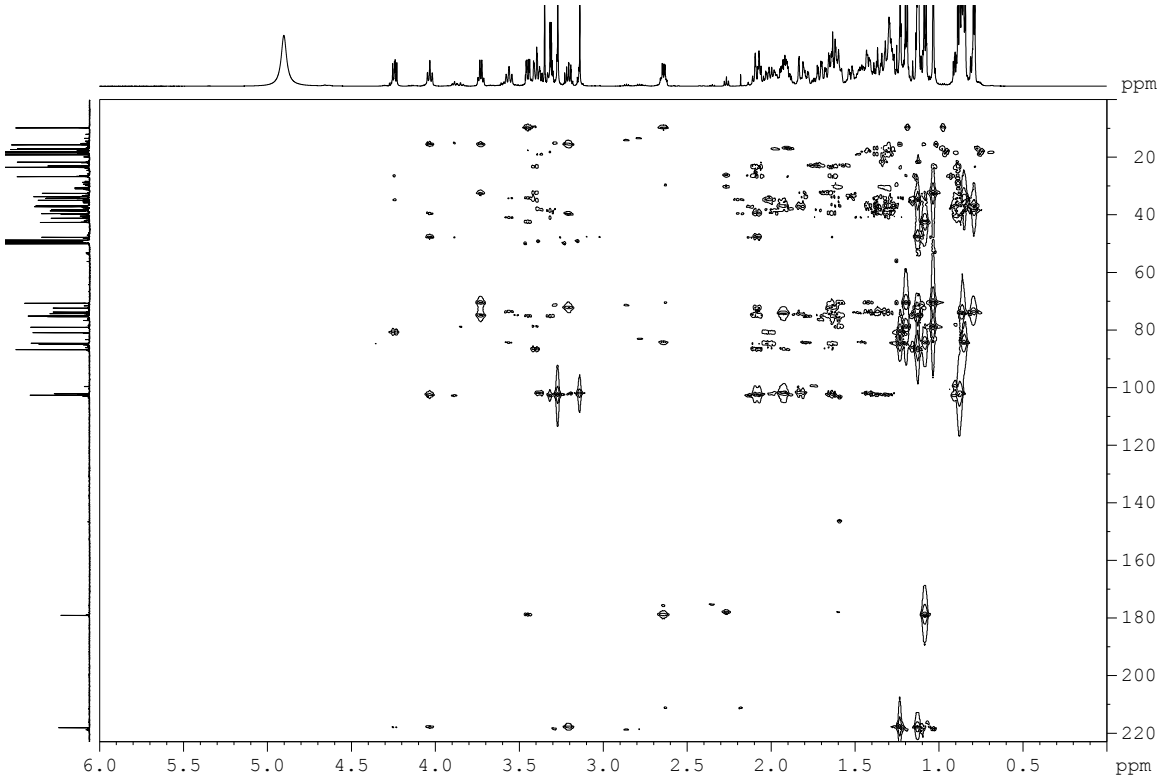

Figure 6.15. HMBC spectrum (^{1}H 600 MHz, ^{13}C 150 MHz, MeOD-d_4) of terrosamycin B.

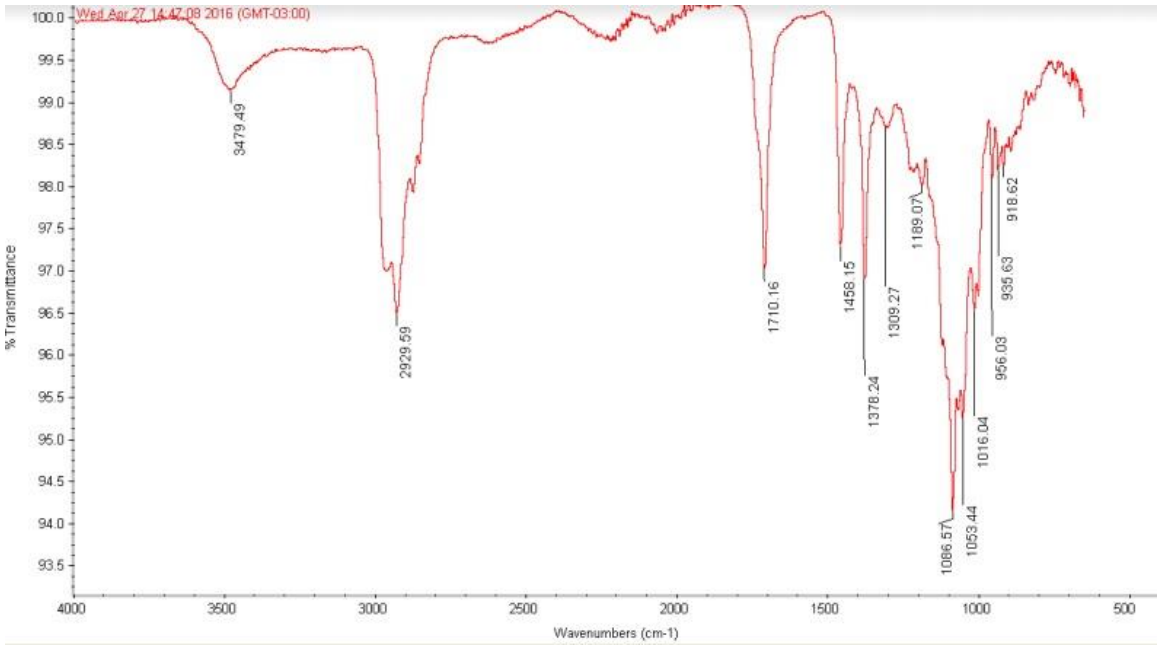

Figure 6.16. IR spectrum of terrosamycin B (MeOH, film).

A

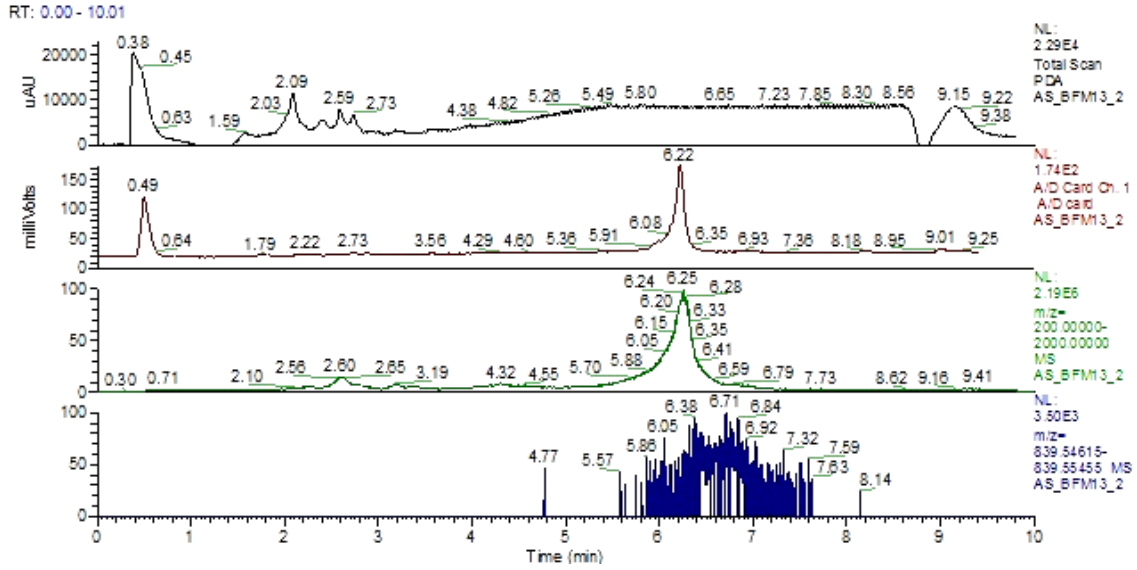

B

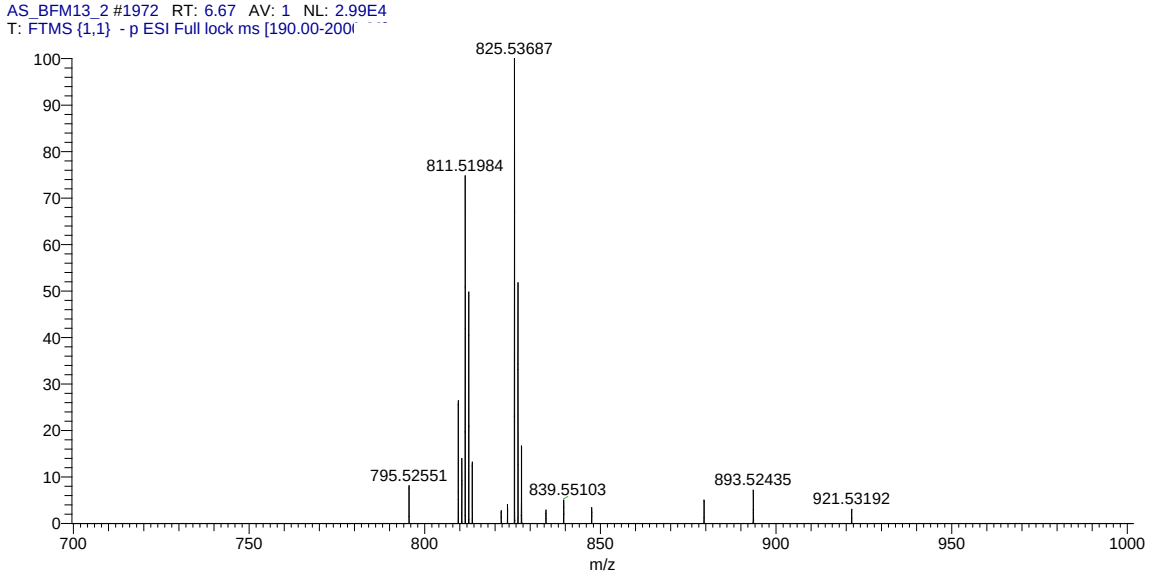

Figure 6.17. HPLC chromatograms of the crude acetonitrile extract of *Streptomyces* sp. RKND004 grown in BFM13 on small scale. The top chromatogram was generated using a PDA detector, the second using an ELSD, and the third using –ESI-HRMS. The bottom trace is an extracted ion chromatogram monitoring *m/z* 839.5504 $[M-H]^-$, showing that terrosamycin B is a genuine natural product and not the result of methanolysis during sample preparation. **B**. –ESI-HRMS spectrum of the eluent at 6.7 min.

6.2. Supporting information for the characterization of PQS-GlcA

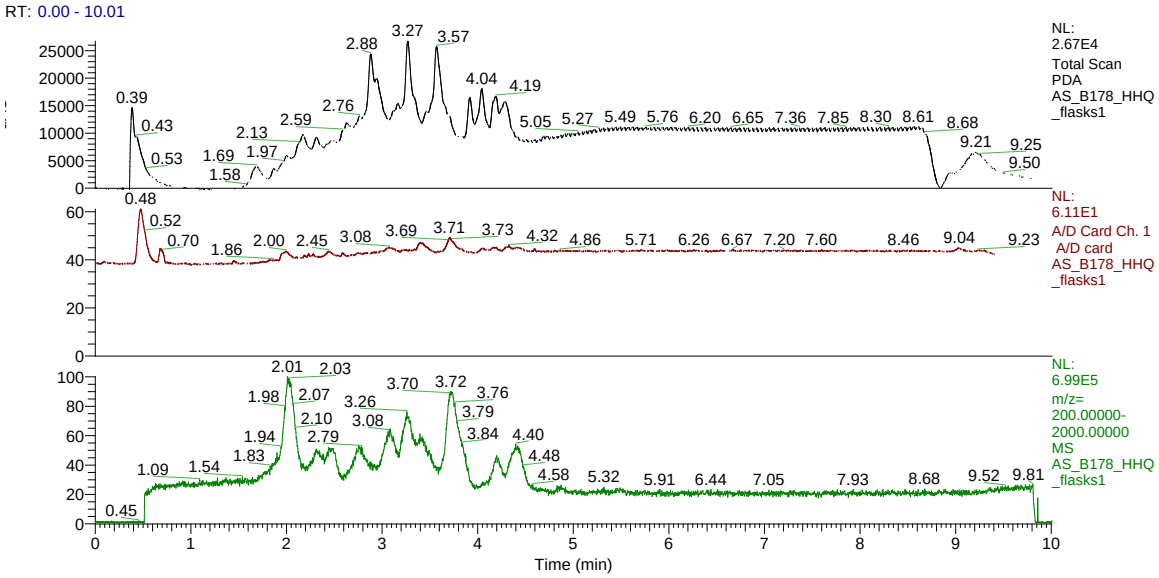

Figure 6.18. HPLC chromatogram of the crude extract of a large scale fermentation of *Streptomyces* sp. RKBH-B178 grown in ISP2 broth supplemented with HHQ. The top chromatogram was generated using a PDA detector, the middle using an ELSD and the bottom using +ESI-HRMS.

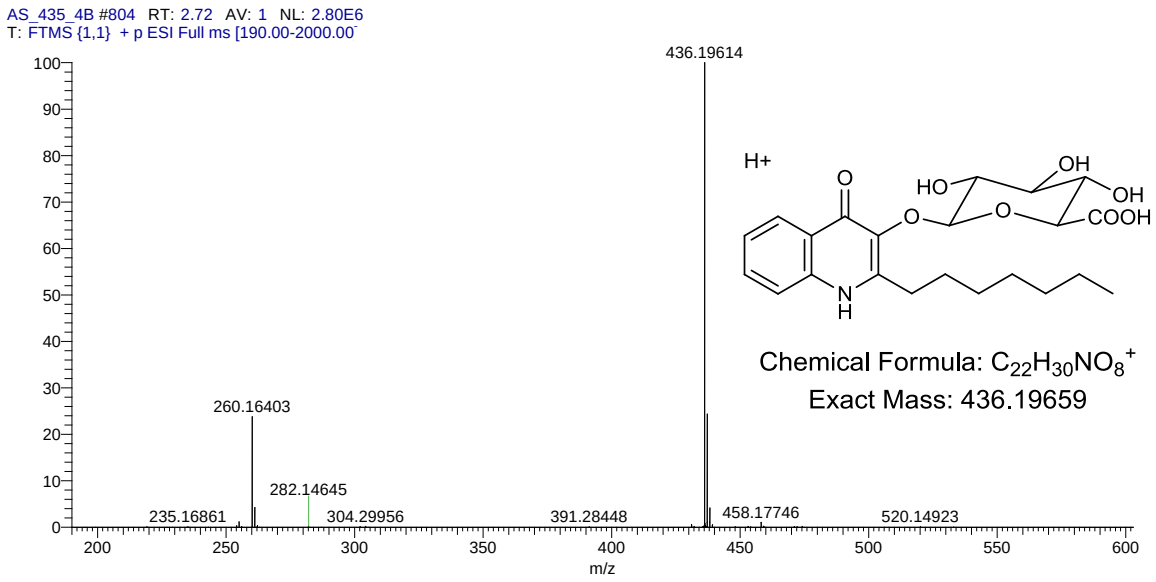

Figure 6.19. +ESI-HRMS spectrum of PQS-GlcA.

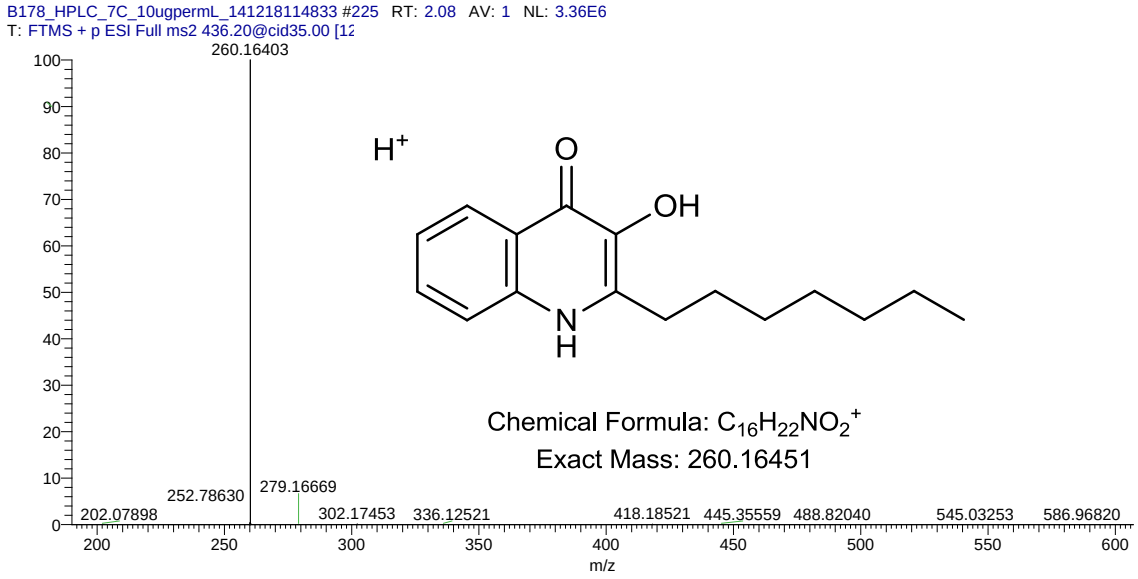

Figure 6.20. MS^2 spectrum of PQS-GlcA (parent ion *m/z* 436).

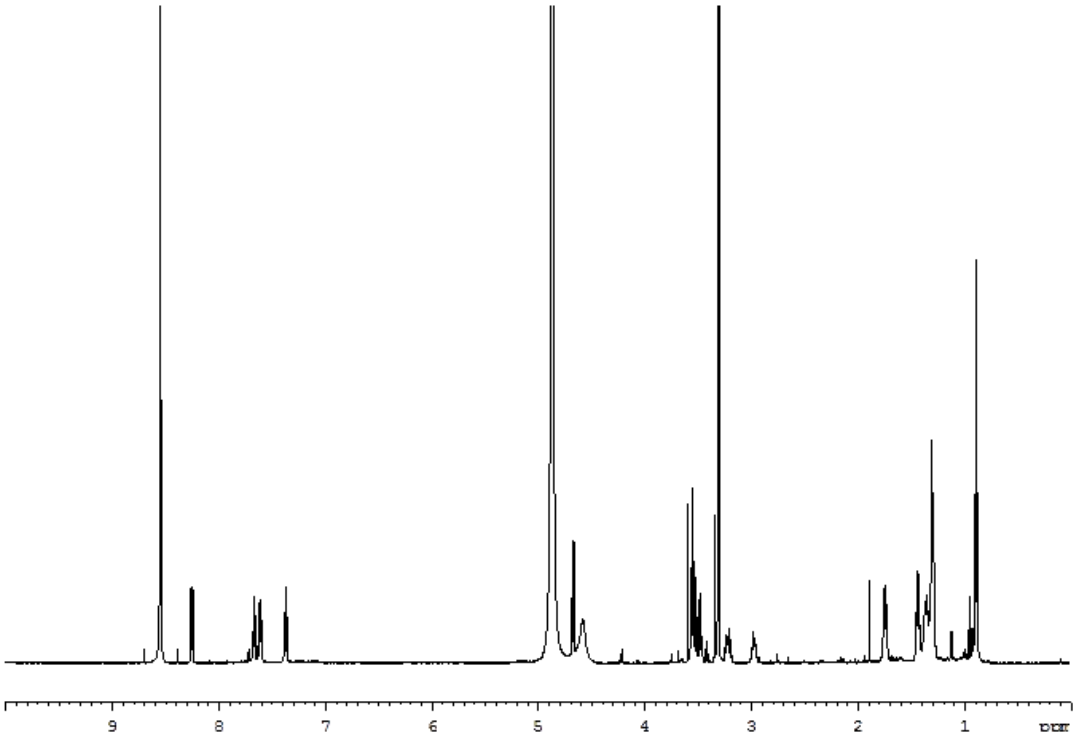

Figure 6.21. ^{1}H NMR spectrum (600 MHz, MeOD-d_4) of PQS-GlcA.

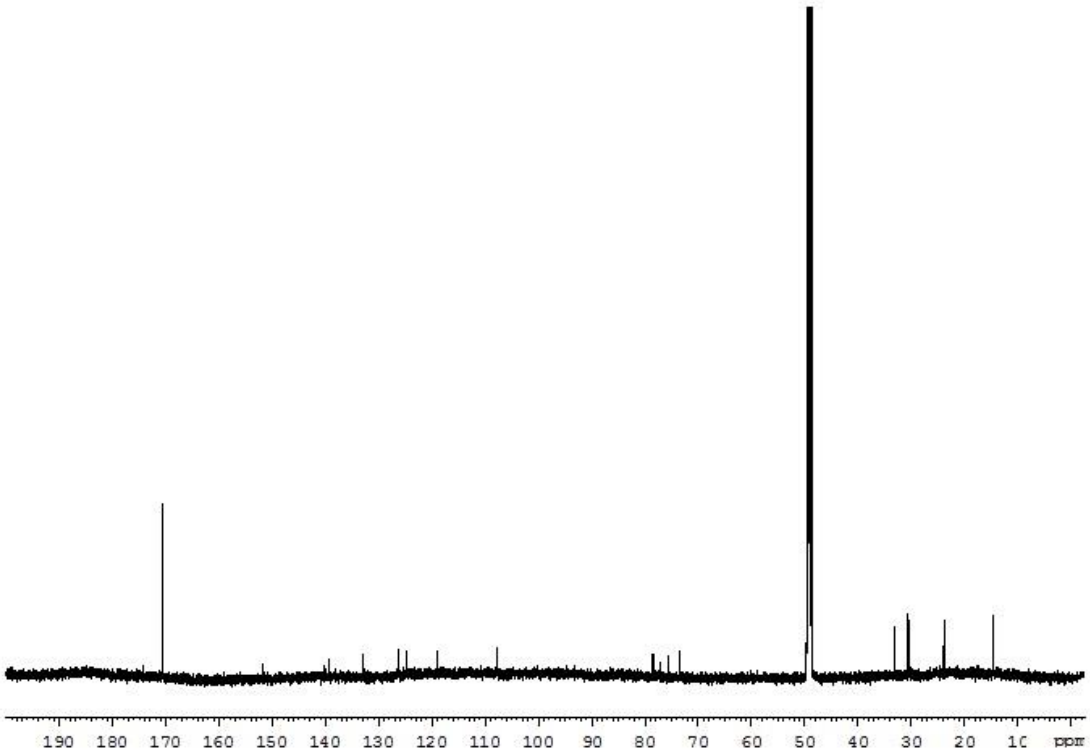

Figure 6.22. ^{13}C NMR spectrum (150 MHz, MeOD-d_4) of PQS-GlcA.

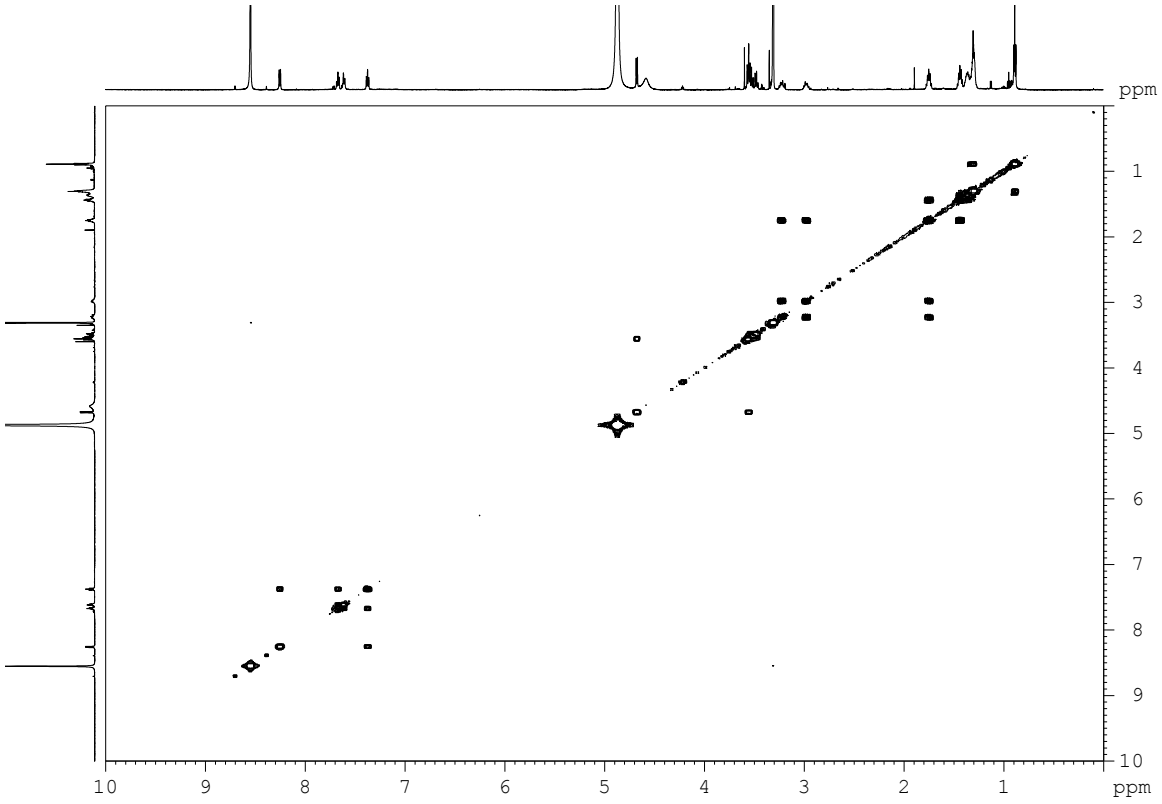

Figure 6.23. COSY spectrum (600 MHz, MeOD-d_4) of PQS-GlcA.

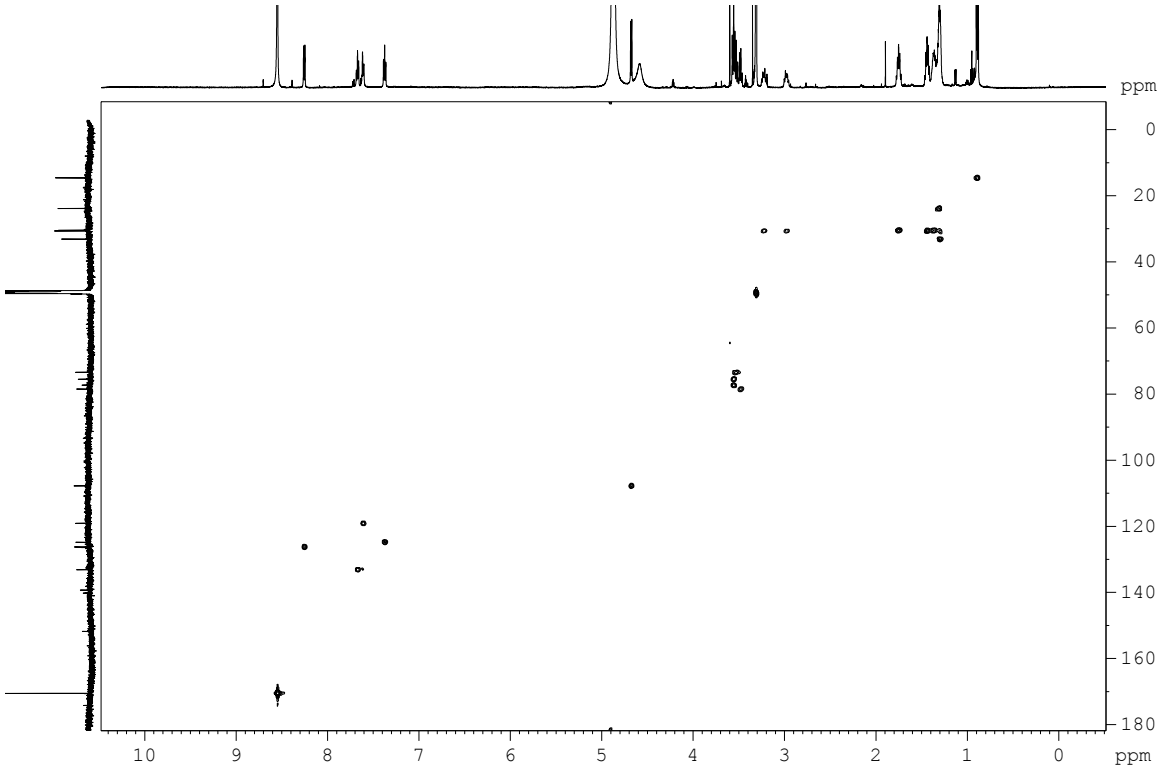

Figure 6.24. HSQC spectrum (^{1}H 600 MHz, ^{13}C 150 MHz, MeOD-d_4) of PQS-GlcA.

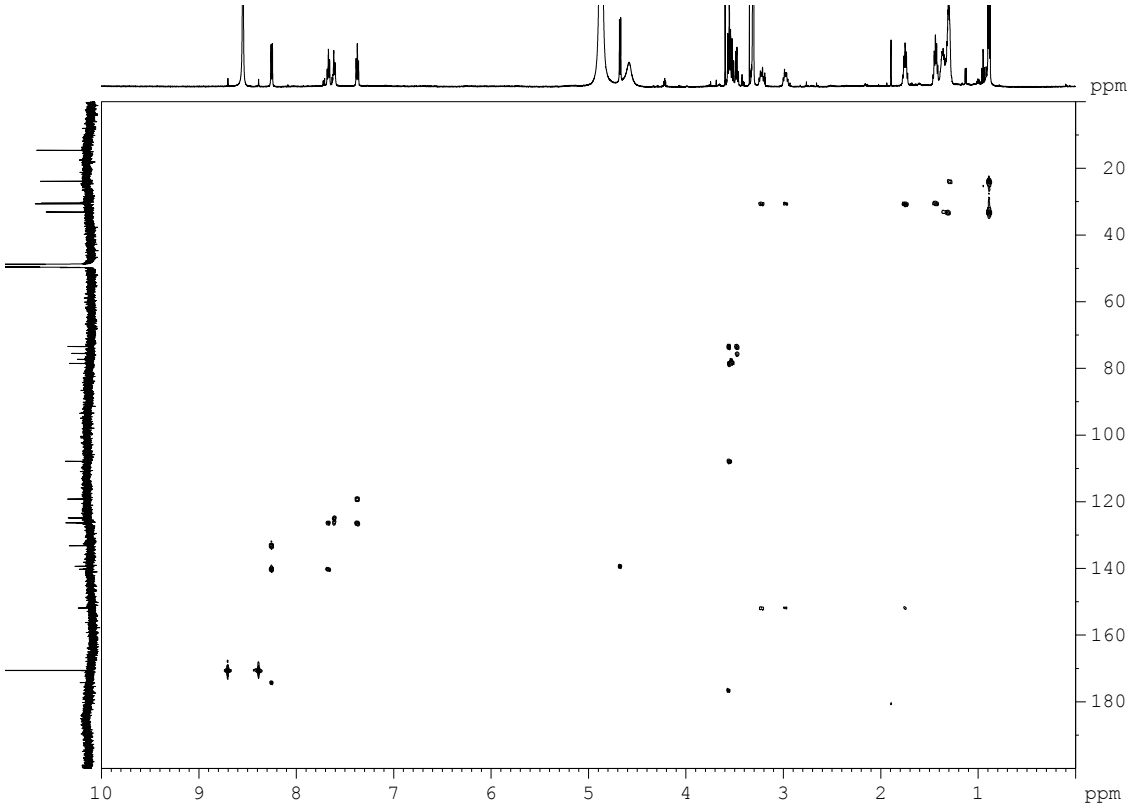

Figure 6.25. HMBC spectrum (^{1}H 600 MHz, ^{13}C 150 MHz, MeOD-d_4) of PQS-GlcA.

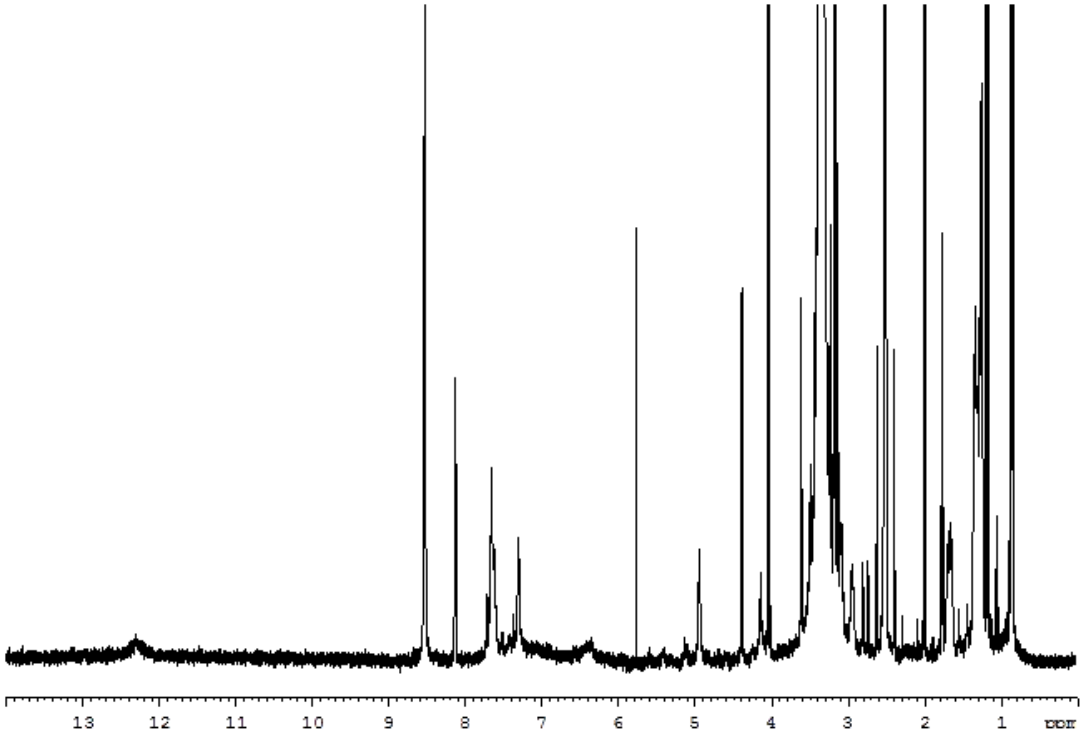

Figure 6.26. ^{1}H NMR spectrum (600 MHz, DMSO-d_6) of PQS-GlcA.

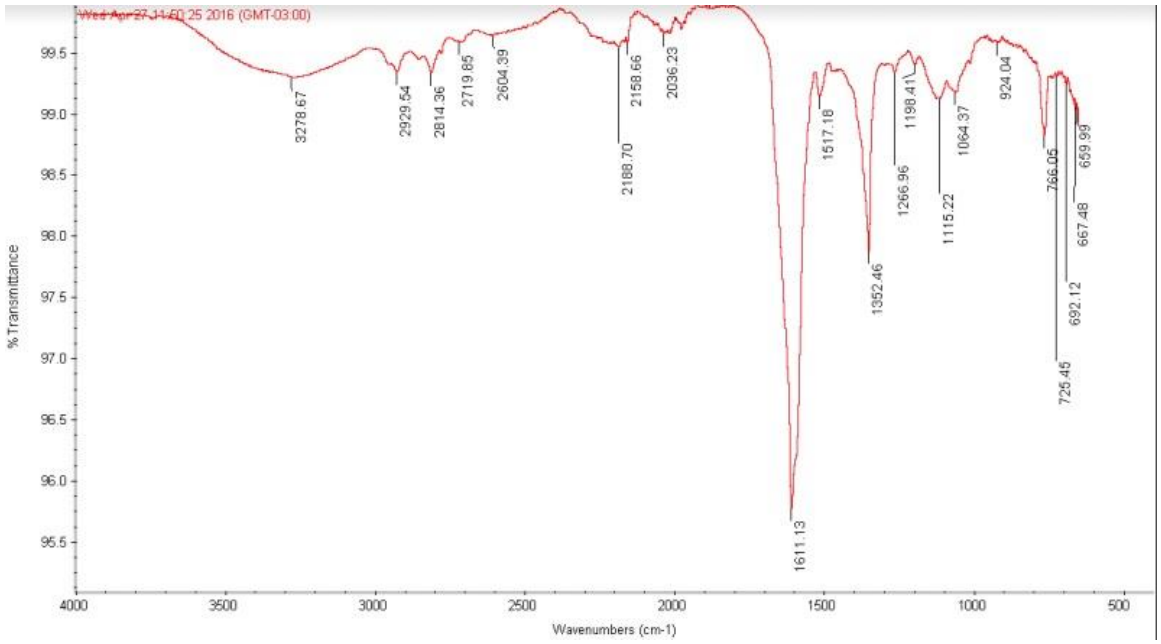

Figure 6.27. IR spectrum of PQS-GlcA (MeOH, film).

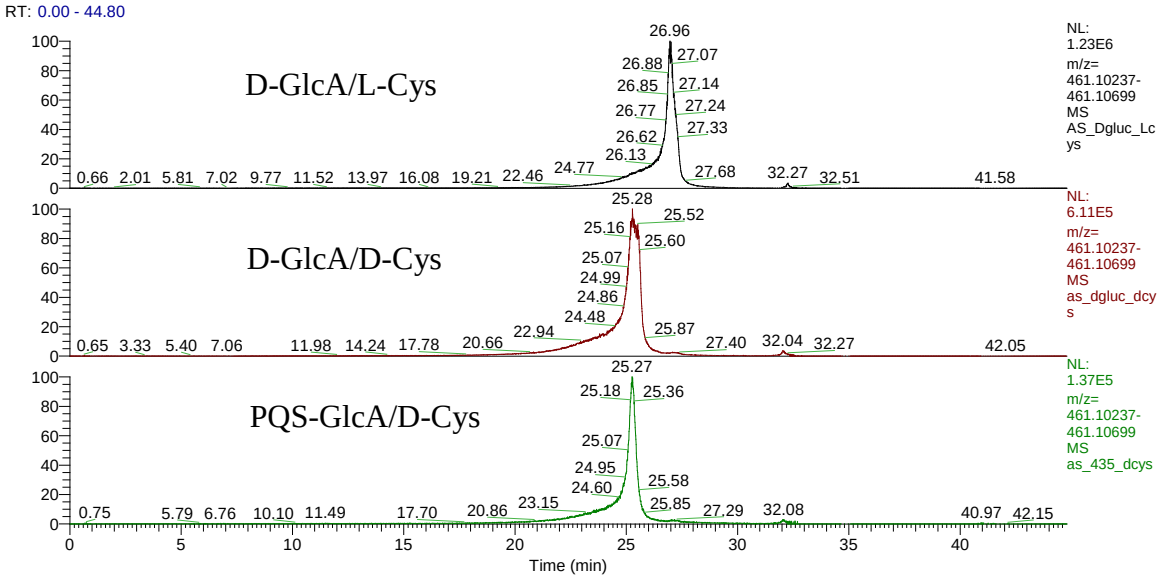

Figure 6.28. HPLC extracted ion chromatograms (+ESI-HRMS detector) of the Tanaka reaction products monitoring the exact mass of the derivatives (*m/z* 461.10468 $[M+H]^+$).

6.3. Supporting information for the characterization of bhimamycin A and E

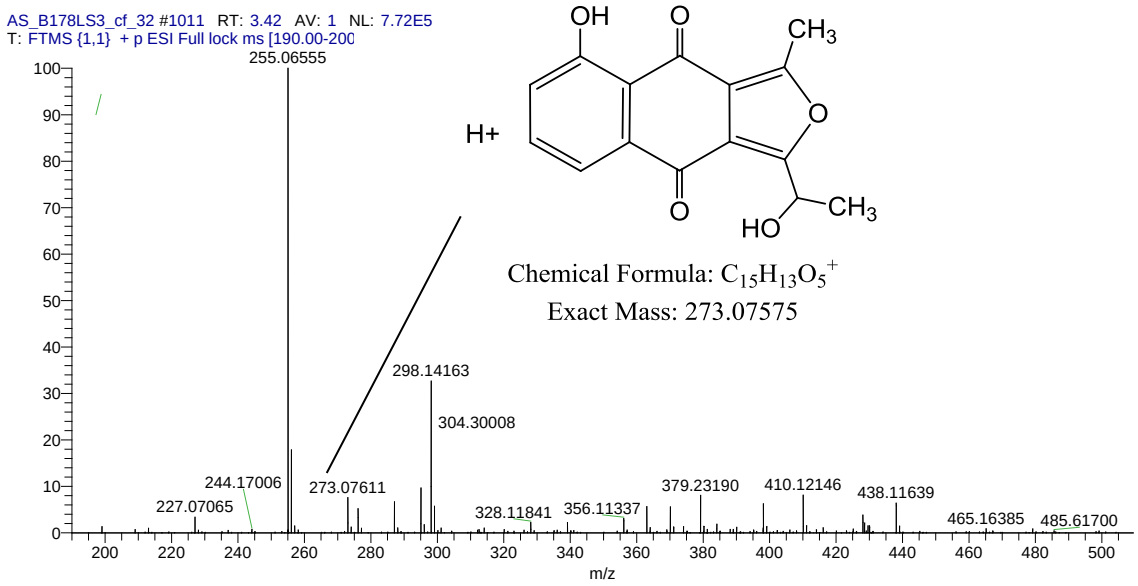

Figure 6.29. +ESI-HRMS spectrum of bhimamycin A.

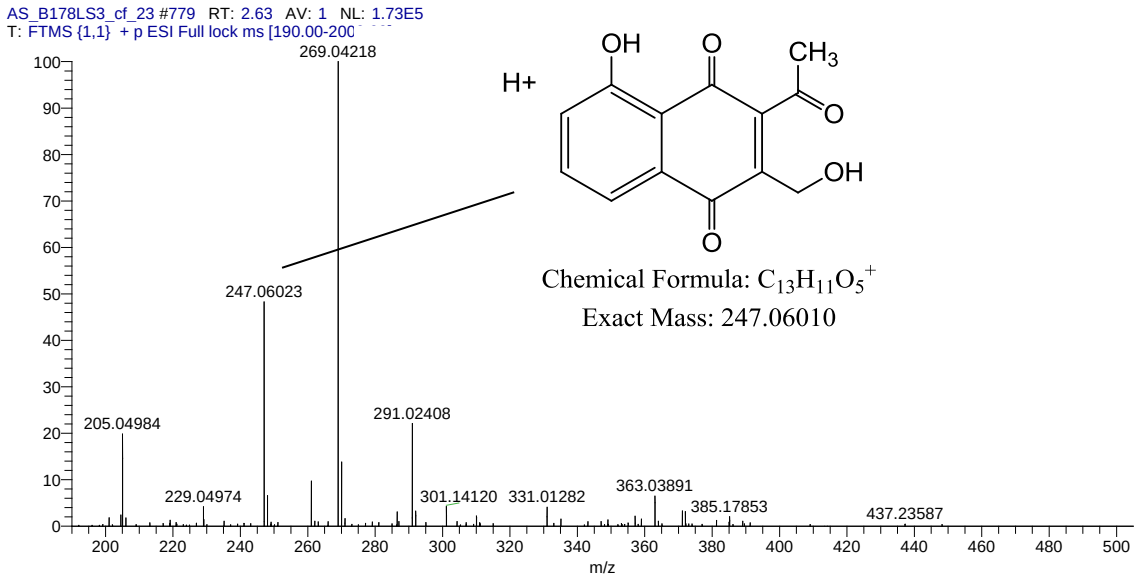

Figure 6.30. +ESI-HRMS spectrum of bhimamycin E.

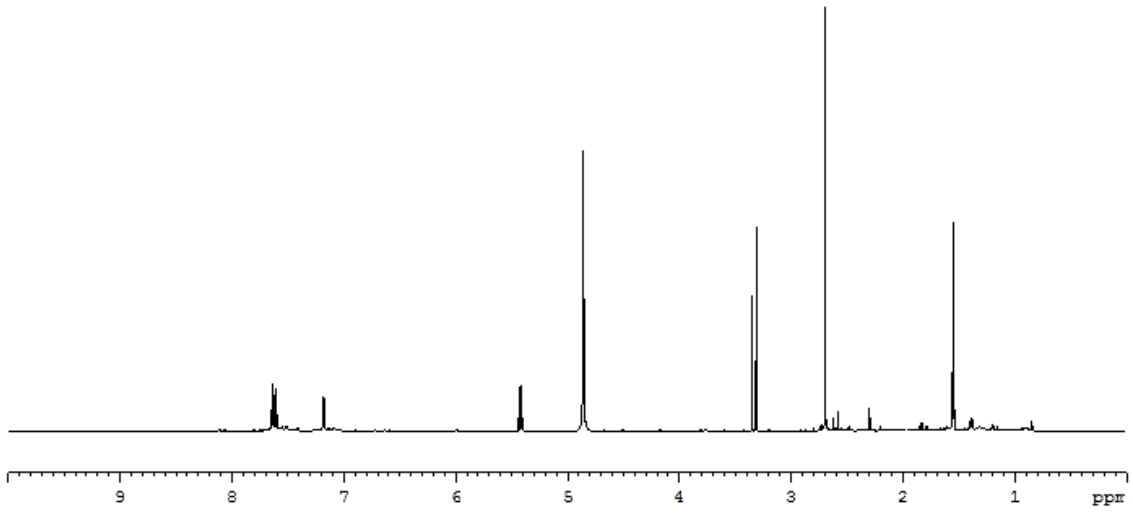

Figure 6.31. ^{1}H NMR spectrum (600 MHz, MeOD-d_4) of bhimamycin A.

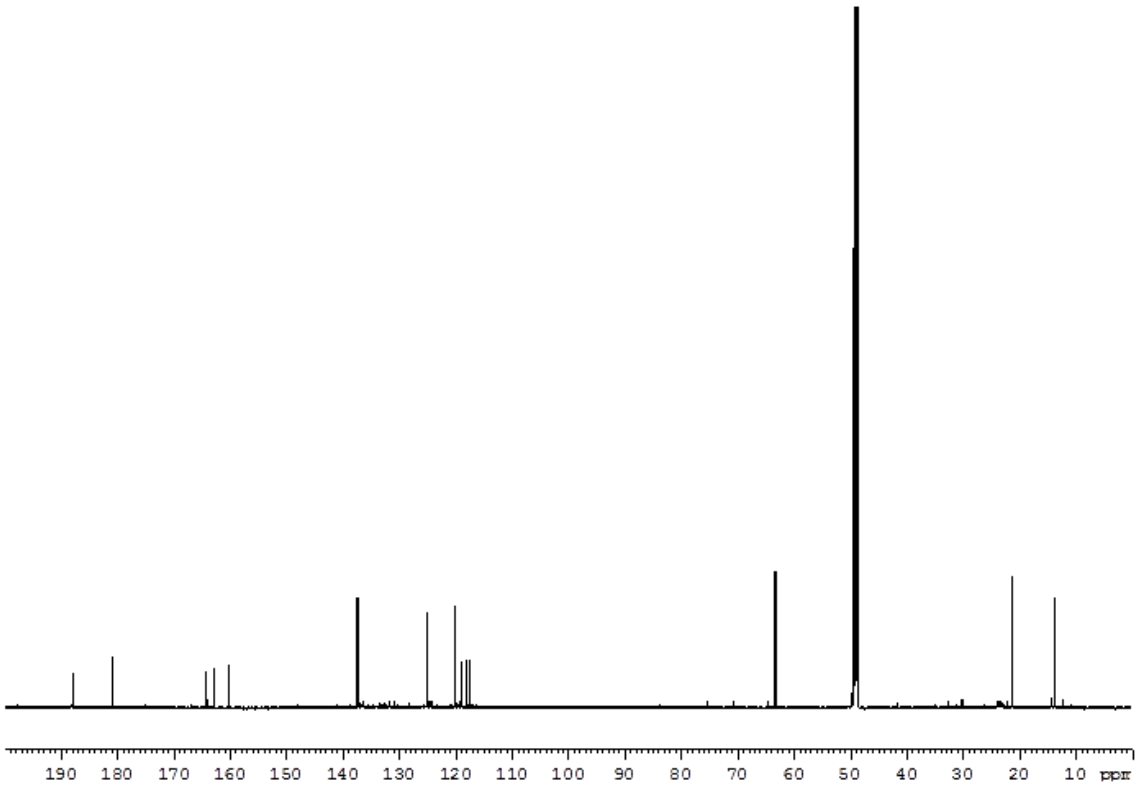

Figure 6.32. ^{13}C NMR spectrum (150 MHz, MeOD-d_4) of bhimamycin A.

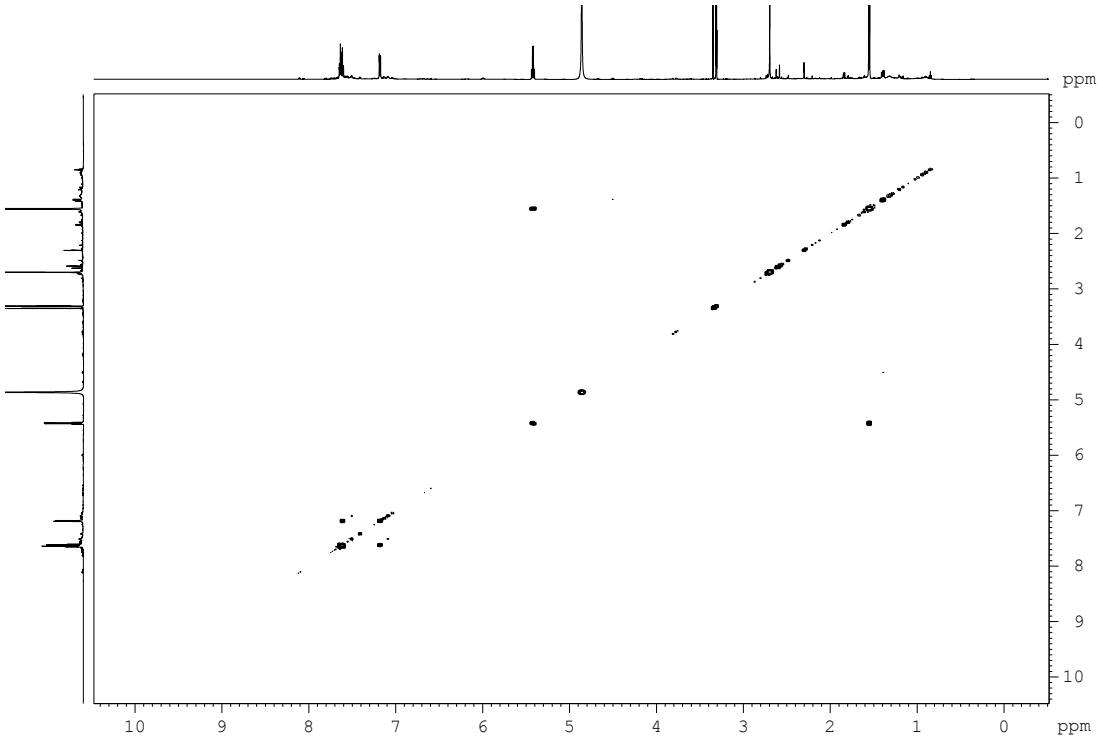

Figure 6.33. COSY spectrum (600 MHz, MeOD-d_4) of bhimamycin A.

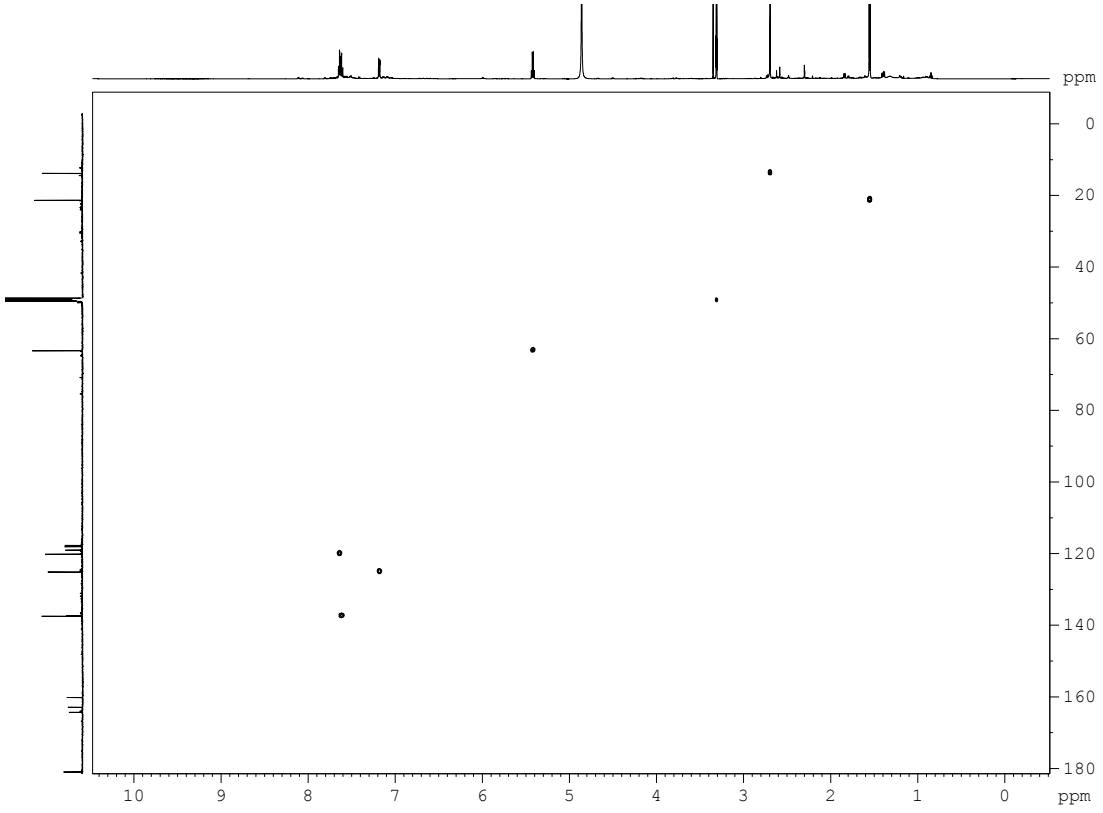

Figure 6.34. HSQC spectrum (^{1}H 600 MHz, ^{13}C 150 MHz, MeOD-d_4) of bhimamycin A.

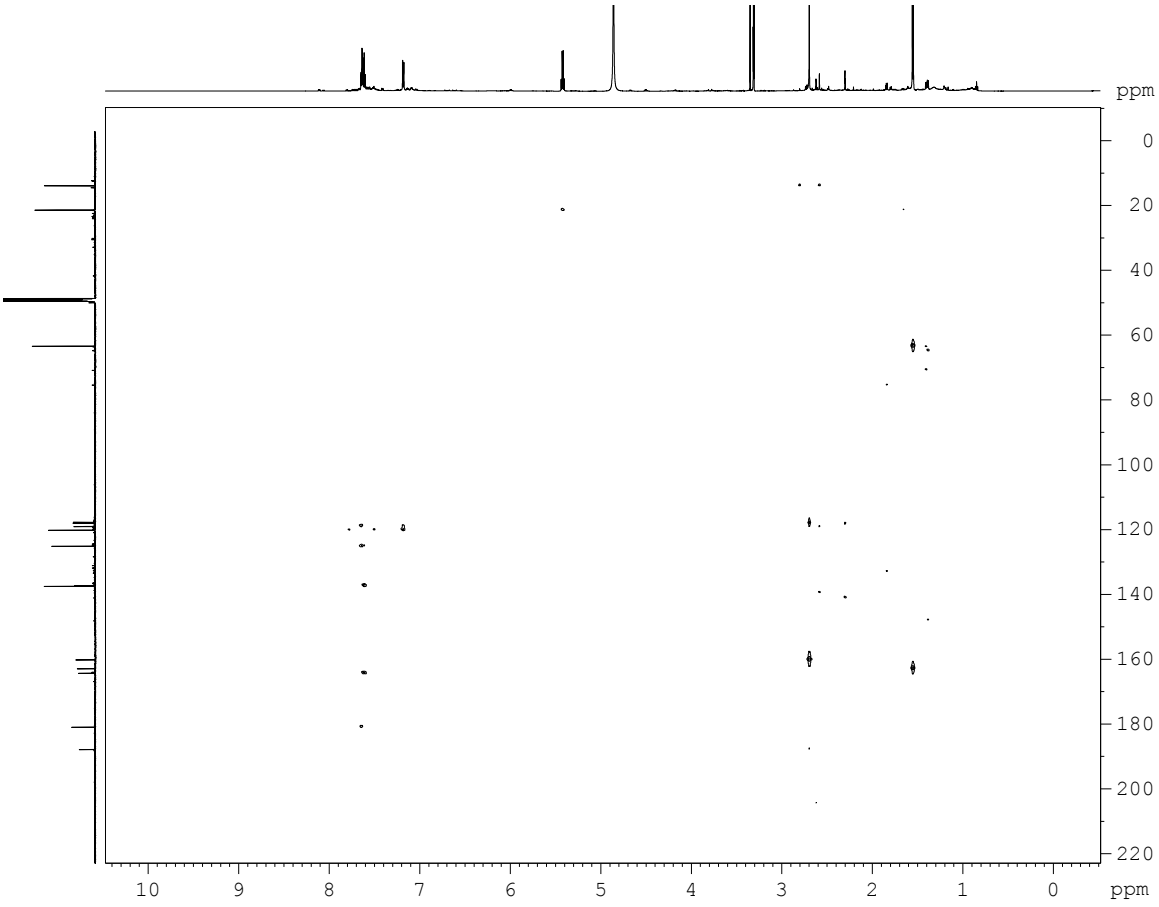

Figure 6.35. HMBC spectrum (^{1}H 600 MHz, ^{13}C 150 MHz, MeOD-d_4) of bhimamycin A.

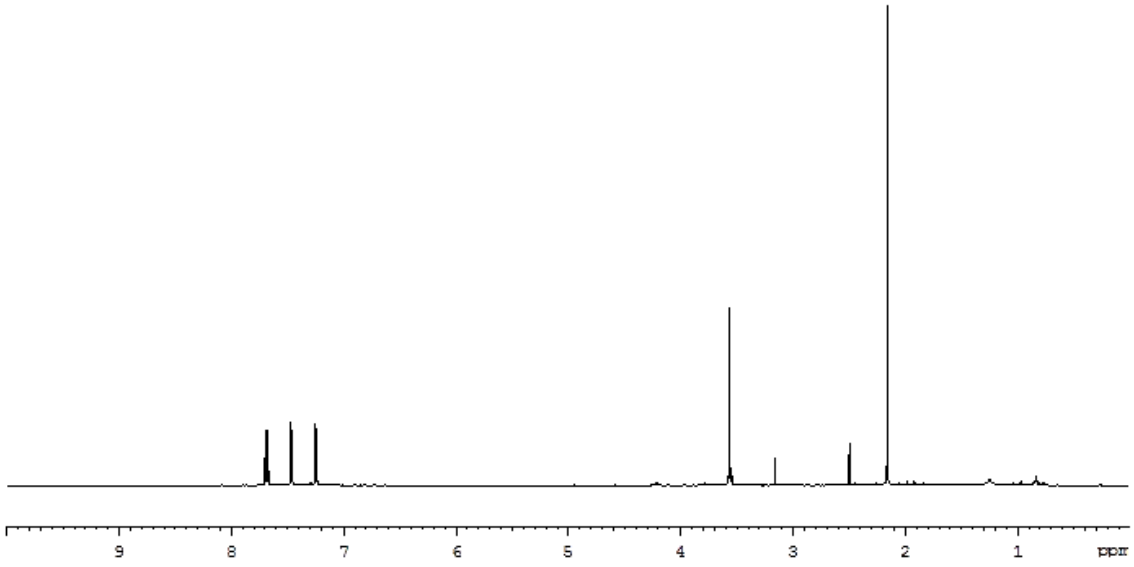

Figure 6.36. ^{1}H NMR spectrum (600 MHz, MeOD-d_4) of bhimamycin E.

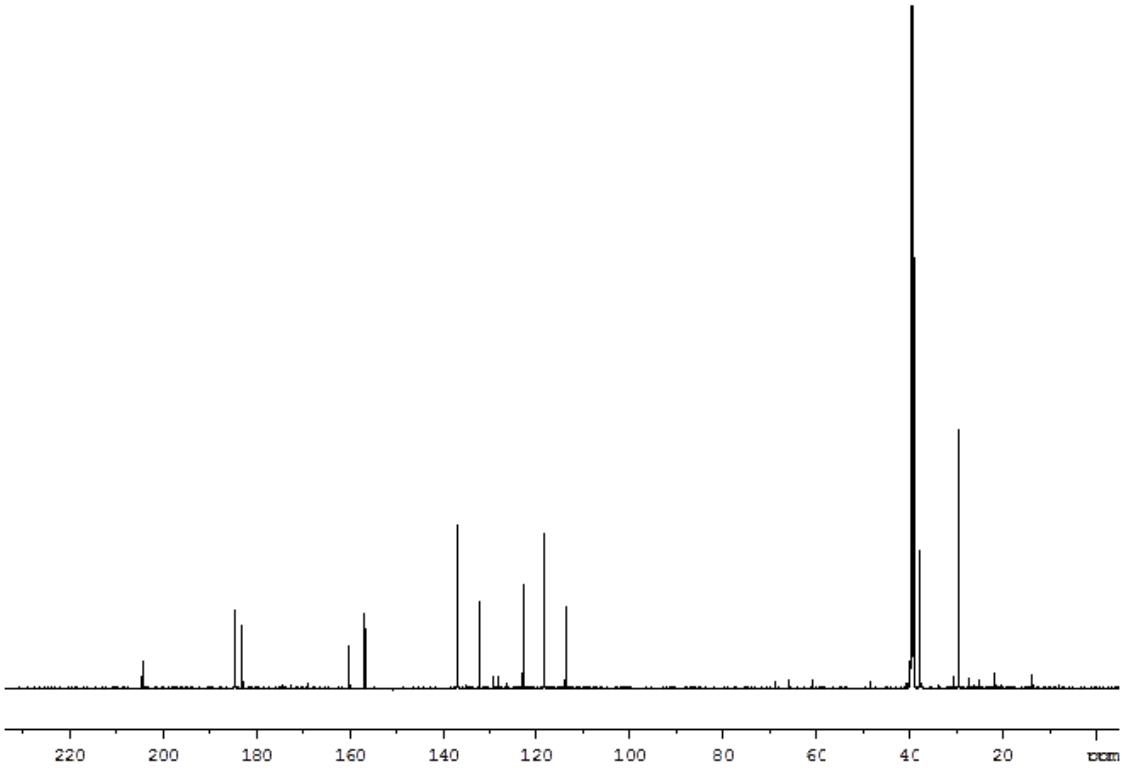

Figure 6.37. ^{13}C NMR spectrum (150 MHz, MeOD-d_4) of bhimamycin E.

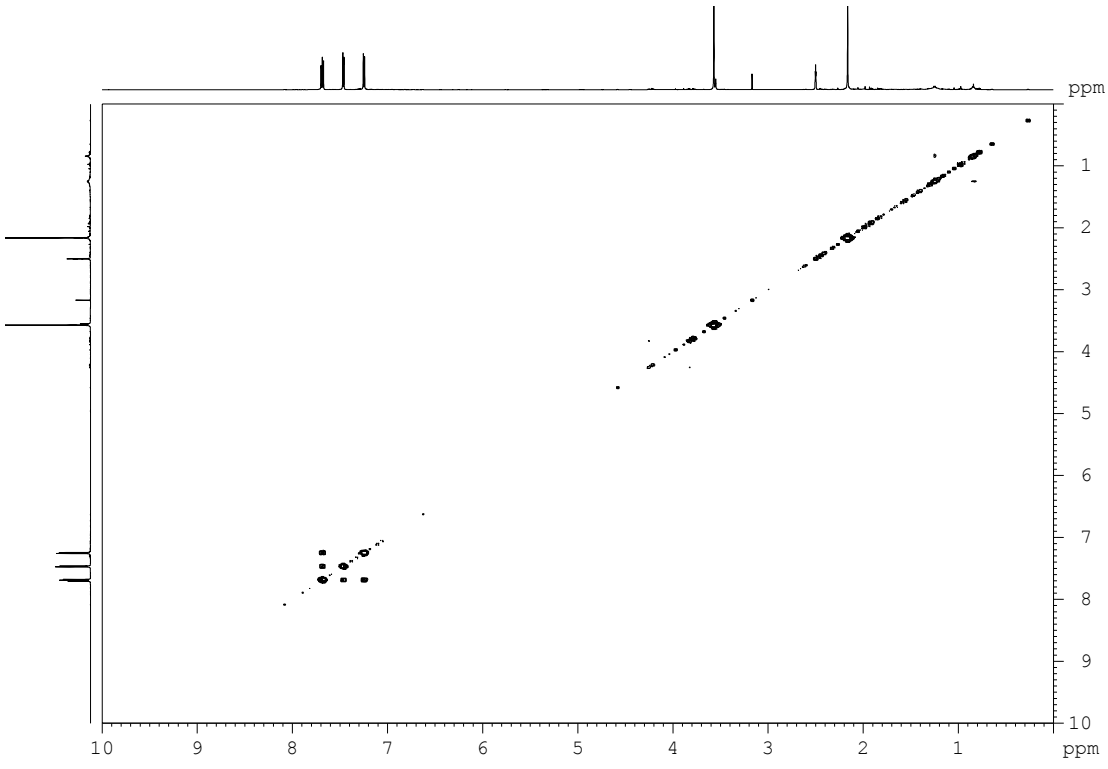

Figure 6.38. COSY spectrum (600 MHz, MeOD-d_4) of bhimamycin E.

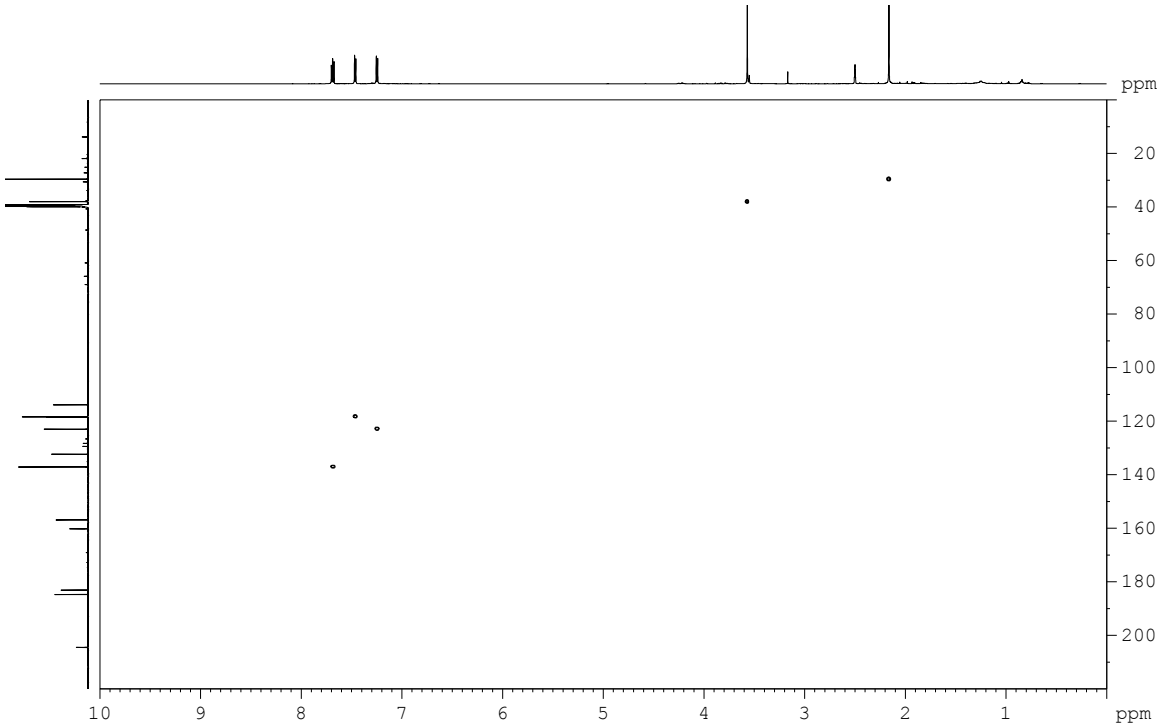

Figure 6.39. HSQC spectrum (^{1}H 600 MHz, ^{13}C 150 MHz, MeOD-d_4) of bhimamycin E.

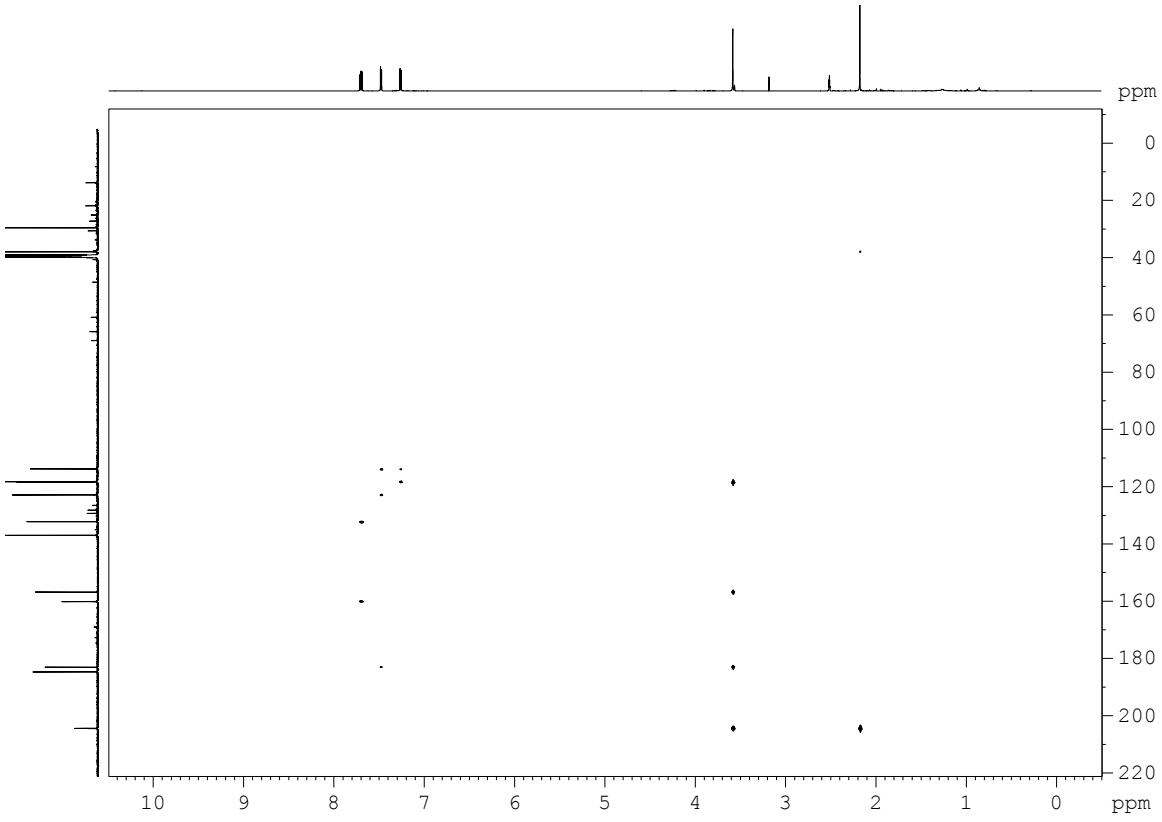

Figure 6.40. HMBC spectrum (^{1}H 600 MHz, ^{13}C 150 MHz, MeOD-d_4) of bhimamycin E.